PhD-FSTM-2021-084
The Faculty of Sciences, Technology and Medicine

DISSERTATION

Defence held on 24/11/2021 in Luxembourg

to obtain the degree of

DOCTEUR DE L'UNIVERSITÉ DU LUXEMBOURG
EN INFORMATIQUE

by

Dinh-Hieu TRAN

Born on 19 November 1989 in Gia Lai (Vietnam)

5G AND BEYOND NETWORKS WITH UAV: TRAJECTORY DESIGN AND RESOURCE ALLOCATION

Dissertation defense committee

Dr. Björn Ottersten, dissertation supervisor
Professor, Université du Luxembourg

Dr. Symeon Chatzinotas, Vice Chair
Professor, Université du Luxembourg

Dr. Miguel A. Olivares-Mendez, Chair
Professor, Université du Luxembourg

Dr. Ejder Başţuğ
Member of Technical Staff, Nokia Bell Labs

Dr. Ngo Quoc Hien
Professor, Queen's University Belfast

"Do the difficult things while they are easy and do the great things while they are small. A journey of a thousand miles must begin with a single step."

Lao Tzu
Philosopher

To my family, my friends, and my love

Abstract

Over the past few years, unmanned aerial vehicle (UAV)-enabled wireless communications have attracted considerable attention from both academia and industry due to their high mobility, low cost, strong light-of-sight communication links, and ease of deployment. Specifically, UAVs can be deployed to serve as aerial base stations (BSs), relays, power sources, etc., to support ground users (GUs) in various scenarios such as surveillance missions, search and rescue, crop monitoring, delivery of goods, data collection, emergency communications, secrecy communications, space-air-ground communications, etc. Despite many advantages, UAV-enabled communications are not without limitations. The limitations of UAVs have imposed technical restrictions on weight, size, and energy capability, thereby affecting the durability and performance of UAVs. The key goal of this dissertation is to propose and develop new frameworks and efficient optimization algorithms to solve novel challenging problems, facilitate the design and deployment of UAV-enabled communications. Consequently, these proposed algorithms can become one of the foundations for deploying UAVs in future wireless systems. Specifically, this dissertation investigates different UAV communication systems by addressing several important research problems through four emerging scenarios: 1) Design UAV trajectory based on traveling salesman problem with time window (TSPTW); 2) Full-duplex (FD) UAV relay-assisted emergency communications in Internet of Things (IoT) networks; 3) Backscatter- and cache-assisted UAV communications; and 4) Satellite- and cache-assisted UAV communications in 6G aerial networks.

In the first scenario, we provide the coarse trajectory for the UAV based on TSPTW, which has not been investigated in UAV communications yet. Concretely, we propose two trajectory design algorithms based on TSPTW, namely heuristic algorithm and dynamic programming (DP)-based algorithm, and they are compared with exhaustive search and traveling salesman problem (TSP)-based methods. Based on the feasible path obtained from proposed algorithms, we minimize the total UAV's energy consumption for each given path via a joint optimization of the UAV velocities in all hops. Simulation results show

that the energy consumption value of DP is very close to that of the exhaustive algorithm with greatly reduced complexity. Based on this work, an efficient TSPTW-based algorithm can be used as an initialized trajectory for designing a joint problem of UAV trajectory and other communications factors (e.g., communication scheduling, transmit power allocation, time allocation), which are challenges.

We then study the case of a FD UAV relaying system in IoT networks. Specifically, a UAV can be deployed as a flying base station (BS) to collect data from time-constrained IoT devices and then transfer it to a ground gateway (GW). Especially, the impact of latency constraint for the uplink (UL) and downlink (DL) transmission utilizing FD or half-duplex (HD) mode is investigated. Using the proposed system model, we aim to maximize the total number of served IoT devices subject to the maximum speed constraint of the UAV, total traveling time constant, UAV trajectory, maximum transmit power at the devices/UAV, limited cache size of the UAV, and latency constraints for both UL and DL. Next, we attempt to maximize the total throughput subject to the number of served IoT devices. The outcome of this work will motivate a new framework for UAV-aided communications in disaster or emergency communications.

Next, a novel system model that considers SWIPT, backscatter and caching in UAV wireless networks is developed. Based on this model, we aim to maximize the system throughput by jointly optimizing the dynamic time splitting (DTS) ratio and the UAV's trajectory with caching capability at the UAV. This is the first work that jointly considers wireless power transfer (WPT), caching, and BackCom in UAV communications, which provides a potential solution for a battery-free drone system that can fly for a long period in the sky to support the terrestrial communication systems.

Finally, a novel system model for effective use of LEO satellite- and cache-assisted UAV communication is proposed and studied. Specifically, caching is provided by the UAV to reduce backhaul congestion, and the LEO satellite assists the UAV's backhaul link. In this context, we aim to maximize the minimum achievable throughput per ground user (GU) by jointly optimizing cache placement, the UAV's transmit power, bandwidth allocation, and trajectory with a limited cache capacity and operation time. The outcomes of this work can provide a new design framework for Satellite-UAV-terrestrial communications that includes two tiers, i.e., the backhaul link from satellite to UAV and the access link from UAV to ground users, which imposes new challenges and was not investigated before.

Acknowledgements

First and foremost, I owe my deepest gratitude to my advisors Prof. Symeon Chatzinotas and Prof. Björn Ottersten, for their inspiring advice, motivation, and patience. During these years, they have impressed me deeply for their strong sense of professionalism and warm kindness. Without their help and guidance, this thesis would not be possible. I would like to thank the members of my Ph.D. committee, i.e., Profs. Symeon Chatzinotas, Björn Ottersten, Ejder Başţuğ, and Hien Quoc Ngo, for spending your valuable time to provide me valuable comments which have helped me to significantly enhance the dissertation's quality.

Also, I would like to thank my research collaborators sincerely: Dr. Thang X. Vu, Dr. Van Chien Trinh, Dr. Ashok Bandi, Dr. Van-Dinh Nguyen, Dr. Tan N. Nguyen, Mr. Phu X. Nguyen, Prof. Symeon Chatzinotas, and Prof. Björn Ottersten for helping me improve my technical skills, the presentation qualities of research papers, and find the right path for my Ph.D.

I would like to also thank my colleagues in SnT for encouraging me and giving me a comfortable work environment. Many thanks to Ashok, Srikan, Dung, Chien, Phuc, Tedros, Yaxiong, Anyue Wang, Anestis, Lei Lei, Ashok, Arsham, Aakash, Renato, Liz, Aakash, Praveen, Norshahida SABA, Sajad Mehrizi, Alireza Haqiqatnejad, and Sumit Gautam for their valuable comments and extensive discussions, and all the happy moments in SnT.

Last but not least, I am deeply thankful to my beloved wife Huyen, to my devoted parents, to my older sister, and my great friends for being next to me during my difficult time.

Preface

This Ph.D. Thesis has been carried out from July, 2018 to November, 2021 at the Interdisciplinary Centre for Security, Reliability and Trust (SnT), University of Luxembourg, Luxembourg, under the supervision of Prof. Symeon Chatzinotas and Prof. Björn Ottersten at SnT, University of Luxembourg, Luxembourg. The time-to-time evaluation of the Ph.D. Thesis was duly performed by the CET members constituting the supervisors at SnT, University of Luxembourg, Luxembourg and Dr. Ejder Başţuğ from Nokia Bell Labs, France.

Contents

This Ph.D. Thesis entitled *"5G and Beyond with UAV: Trajectory Design and Resource Allocation"* is divided into seven chapters. In Chapter 1, the literature review, limitations of existing works, and contributions of this thesis are described. Chapter 2 provides common knowledge about different techniques applied with UAV communications in this thesis such as full-duplex, backscatter communications, simultaneous wireless information and power transfer (SWIPT), and mobile edge caching. Chapter 3 presents a coarse trajectory design for energy minimization in UAV-enabled wireless communications with latency constraints. Chapter 4 includes the scenario where a single full-duplex UAV as an aerial base station aims to collect data from latency-constrained IoT users and then transfer it to a ground gateway. A novel backscatter- and cache-assited UAV framework is proposed and analyzed in Chapter 5, where benefits of adding backscatter communications and cache-based techniques to UAV systems are illustrated. In Chapter 6, a novel system model for effective use of LEO satellite- and cache-assisted UAV communication is proposed and studied. Finally, Chapter 7 provides concluding remarks and future research directions.

Support of the Thesis

This Ph.D. Thesis has been fully supported by the Luxembourg National Research Fund under Project FNR CORE ProCAST (Budget code: R-STR-5010-00-Z), grant C17/IS/11691338. The effort of collaborators and dissemination costs were supported by other projects, namely, FNR 5G-Sky, grant C19/IS/13713801. Additionally, the time-to-time support from SIGCOM is also gratefully acknowledged.

The major milestones of the Thesis are in-line with the timely deliverables of the CORE ProCAST (Proactive Edge Caching for Content Delivery Networks powered by Integrated Satellite/Terrestrial Backhauling: R-STR-5010-00-Z) of the University of Luxembourg. The main objective was to investigate how edge caching can prevent video traffic from congesting current communication networks. Particularly, caching at the network edge can be instrumental in reducing the long dumb pipes that move repetitive information through the core network. More importantly, hybrid satellite/terrestrial networks will be used to optimize the backhaul capacity needed for caching. This is a key element since satellite networks can deliver large amounts of delay-tolerant information with just two hops to multiple edge nodes through geocasting (broad/multicasting across large geographic areas). This will take the load off the multihop terrestrial backhaul networks which can be used to deliver the unicast broadband services that they were originally designed for.

List of Tables

List of Figures

Contents

Chapter 1

Introduction

In recent years, unmanned aerial vehicles (UAVs) or drones, have been adopted in various real-life applications from civilian (e.g., aerial photography, disaster response, rescue mission, hospital emergency care, monitoring forest fire, oil rigs, and traffic monitoring) to military (e.g., battlefield surveillance, border security, target localization, counter insurgency, tracking, crime control, and anti-terrorism arrests) [1–6]. As reported by the Federal Aviation Administration (FAA), the number of UAVs is estimated to increase about 367 folds from 2.4 million in 2022 to 880.3 million in 2038 [7]. Besides, the UAV market is expected to grow around two fold from 27.4 billion USD in 2021 to 58.4 billion USA by 2026 [8].

With the advantages in agility, mobility, swift deployment, and maneuverability, UAVs such as airships, aircraft, balloons have been widely adopted in wireless communications. Prominent examples of potential projects for UAV communications include Google Project Wing, Google Loon, Facebook Halts Aquila, and Amazon Prime Air [9–12]. For example, Google has built and tested autonomous aerial vehicles (AAVs) project termed Project Wing [9]. This project aimed to develop UAVs that could be used after a disaster, e.g., earthquakes or floods, to delivery necessary necessities to isolated areas. Facebook Halts Aquila project built a fleet of drones in the sky to beam internet to GUs [10]. In particular, these drones can stay aloft for three months using solar panels. Besides, AT&T and Qualcomm have been planning to adopt UAVs for facilitating large-scale wireless communications in 5G networks [12]. Despite many benefits, UAV communications are not without limitations due to energy, resource constraints (e.g., bandwidth, power capacity), and other technical challenges. In this chapter, we introduce an overview of the state-of-the-art research on UAV communications over the past few years. We then point out the limitations in these works, giving impetus to our contributions.

1.1 Related Works

UAV communications have been an active area of research in the past few years. In the following, we provide some advantages and potential applications of UAVs in wireless communications. Specifically, this section shows the closest works related to our main contributions in this dissertation.

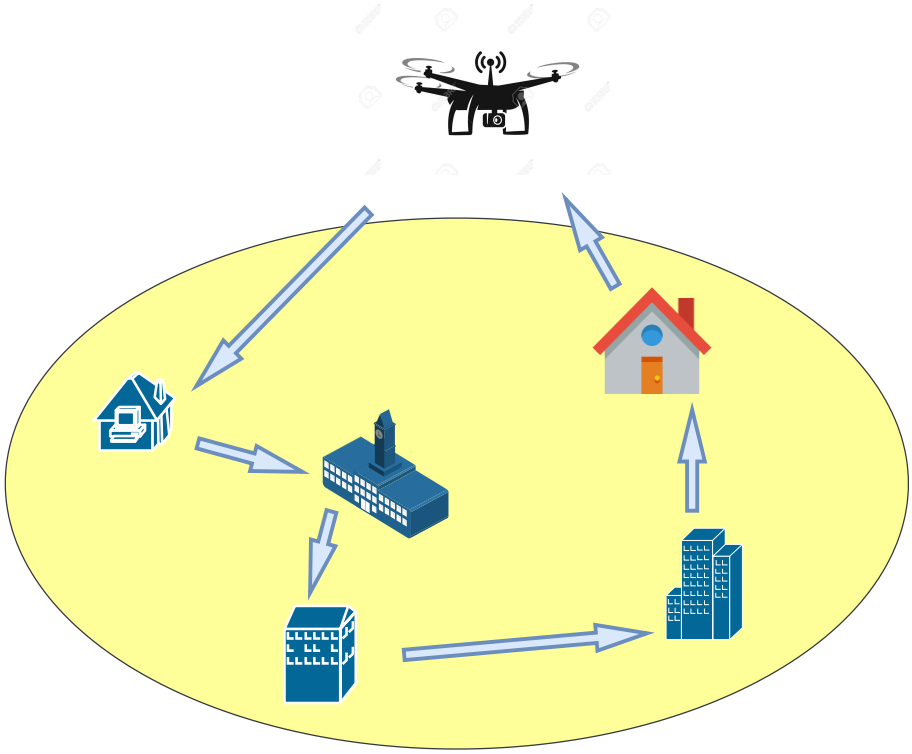

FIGURE 1.1: Traveling salesman problem in UAV communications.

1.1.1 Trajectory Design for UAV System

Unmanned aerial vehicles (UAVs) have been applied in many areas such as aerial photography and videography, mapping and surveying, reconstruction, monitoring, delivery, search and rescue, and UAV-aided communications. In these applications, planning the optimal trajectory for UAVs is a key challenge in UAV-based communication systems with limited resources, e.g., bandwidth, energy capacity. The UAV trajectory is dramatically affected by various factors such as flight time, battery capacity, GUs' demands, obstacle avoidance,

(a) Forest (b) Cave (c) City

FIGURE 1.2: 3D trajectory design in complex environments.

and authority requirements. Therefore, the UAV trajectory design has received significant attention from researchers recently [13–19].

Fig. 1.1 shows the traveling salesman problem (TSP) for path planning in UAV communications. The TSP is an NP-hard problem that finds the shortest path that visits all nodes exactly once and returns to the original depot with given locations and distance between nodes. Zeng et al. was the first to bring up the traveling salesman problem (TSP) in UAV communications [13]. Specifically, they studied the trajectory design to minimize the mission completion time in UAV-enabled multi-casting. They proposed strip-based waypoints, TSP-based, virtual base stations (VBSs) as waypoints, and optimal waypoints methods to design the trajectory of UAV for multi-casting information to GUs. Based on the TSP-based trajectory design in [13–15] investigated the energy minimization problem in wireless communications with rotary-wing UAVs Besides classic TSP, there are many other TSP-related problems such as multiple TSP [20–22] or vehicle routing problem (VRP) [23–25]. Multiple TSP is generalized of TSP, whereas multiple users travel through N nodes in the networks, then it returns the original point. The distinct point with TSP is that users can go through a node multiple times. VRP describes the problem of multiple vehicles that transfer goods to customers who require a different amount of goods. They aim to design a path to minimize cost or path length. Therefore, TSP is a special scenario of VRP. In literature, there are many intelligent algorithms proposed to solve TSP efficiently

such as genetic algorithm [26, 27], the particle swarm optimization (PSO) [28], the ant colony optimization [29–31], the neural network algorithm [32, 33], the deep reinforcement learning [34–36]. In Table 1.1, we list different efficient methods to solve the TSP.

TABLE 1.1: Listing of algorithms to solve the traveling salesman problem

Intelligent algorithms to solve TSP	**Related references**
Genetic algorithm	[26, 27, 37]
Particle swarm optimization (PSO)	[28, 38]
Ant colony optimization	[29–31]
Simulated annealing algorithm	[39]
Neural network algorithm	[32, 33]
Fuzzy Neural Network	[40]
Deep reinforcement learning	[34–36]

TABLE 1.2: Intelligent algorithms used to obtain the UAV 3D trajectory

Algorithms	**Related references**
Sampling-based algorithms	probabilistic roadmap [41],3D voronoi [42], simplified probabilistic roadmap [43], k-nearest probabilistic roadmap [44], corridor map [45], rapidly-exploring random trees [46]
Mathematic model-mased algorithms	mixed integer linear programming (MILP) [47], optimal control [48], binary linear programming (BLP) [49], non-linear programming (NLP) [50]
Node-based algorithms	Dijkstra's algorithms [51], Harmony search [48], lifelong llanning A(LPA) [52]
Multi-fusion based algorithms	PRM based optimal algorithms [41]; visibility graph node-based optimal algorithms [53]; visibility graph, Voronoi diagram, and potential field (VVP) algorithms [54]; visibility graph Geodesics algorithm [55]
Bio-inspired algorithms	shuffled frog leaping algorithm [56], genetic algorithm [57], ant colony optimization [58]

Fig. 1.2 illustrates the 3D UAV trajectory design scenarios for aerial mapping, scene exploration, urban reconstruction, surveying, and cinematography, in which many studies have been carried out recently [59–68]. A complete scene construction can offer an exact three-dimensional (3D) environment for map navigation autonomous driving, which is a foundation for real-time/ultra-low latency decision-making. Furthermore, scene reconstruction models give data sources for emergency scenarios analysis or urban planning. In [60, 61], the authors applied UAVs-enabled light detection and ranging points (LDRP)

to overcome the inherent limitations of traditional LDRP system, e.g., high-cost sensors, sparse point clouds, and this method is not suitable for high building reconstructions. Qin [62, 63] adopted a semi-global matching algorithm (SGMA) for satellite stereo images, which was rarely investigated before. In [64, 65], the authors used drones for filming missions. Huang et al. [64] proposed autonomous cinematography (ACT) system by using UAV to address the existing challenges in action movies. In particular, it is the first UAV camera system that can autonomously capture cinematic action scenes based on skeleton point movements in outdoor and indoor environments. Nageli et al. [65] proposed a new method for automatic aerial filming in turbulent and dynamic environments. In [66–68], the authors utilized UAV for mapping tasks. Yang et al. [66] deployed UAV to map along the west coast of North America to measure patchiness, dynamics, and eelgrass meadow extent in Oregon, California, Washington, and Alaska. Rokhmana et al. [67] utilized UAV in post-disaster mapping for quick rehabilitation and assessment, e.g., Merapi volcano eruption and Kelud volcano eruption in 2010 and 2014, respectively. TaoZhang et al. [68] solved the problem of how to integrate between simultaneous localization and mapping (SLAM) and UAV systems. Concretely, the authors controlled the UAV altitude to help the SLAM's direct method effectively converges and faster. Besides the applications of 3D UAV trajectory design mentioned above, 3D UAV trajectory design has also been received significant attention in UAV-enabled wireless communications. The authors in [16, 17, 19] investigated 3D trajectory by adding altitude optimization into consideration. Sun et al. [16] studied a joint 3D trajectory design, transmit power, and sub-carrier allocation for solar-powered UAV communication systems. Guo et al. [17] considered a problem of jointly optimizing 3D trajectory, UAV's charging duration, and power allocation to maximize the minimum transmission rate of all GUs. In summary, the algorithms used to obtained an efficient 3D UAV trajectory can be listed in Table 1.2.

1.1.2 Deployment of UAV for Delivering Time-Sensitive Information

Fig. 1.3 shows the applications of UAV in public safety and emergency communications. It is because the existing communication technologies are significantly dependent on the terrestrial network; interruption or failure of terrestrial base stations (BSs) due to malicious attacks or natural disasters will make communication difficulties for public safety/emergency communications. For example, in mission-critical IoT applications such as smart grids, factory automation (e.g., printing machines, packaging machines, and process automation), and intelligent transport systems (e.g., road safety highway and traffic efficiency) [69]. On the other hand, IoT devices often have limited storage capacity, and thus their generated data needs to be collected timely before it becomes worthless due to obsolete transmissions or being overwritten by incoming data. Consequently, the out-of-date gathering data may result in unreliable controllable decisions, which may ultimately be disastrous [70]. Therefore, the UAV must reach the right place at the right time.

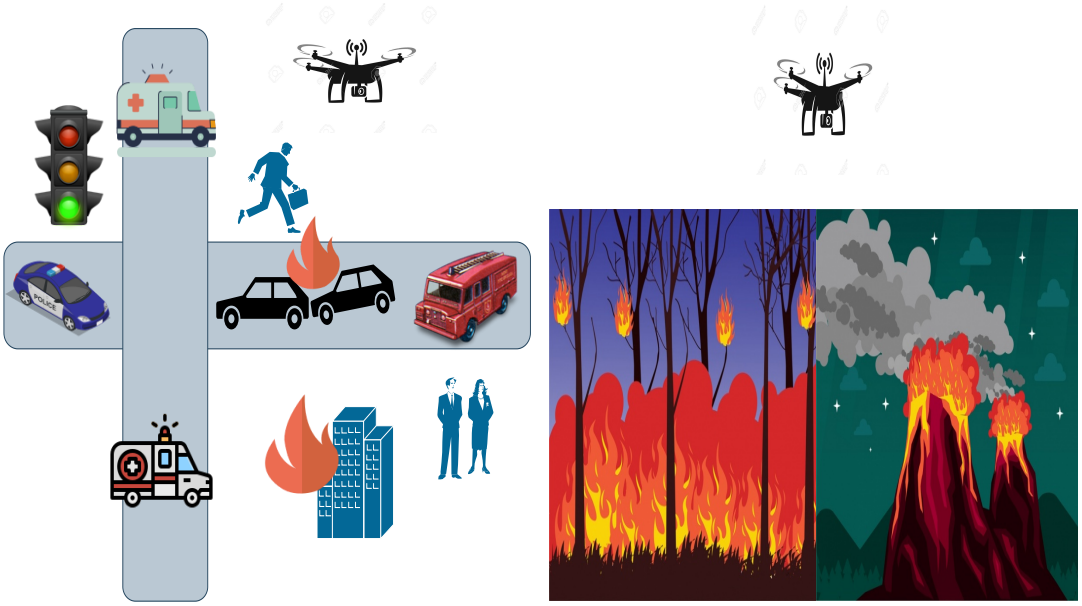

(a) Public safety. (b) Search and rescue mission in disasters.

FIGURE 1.3: UAV-enabled communications for disaster or emergency scenarios.

Recently, many studies focus on applying UAVs to overcome the above limitations [70–76]. Merwaday et al. [71] deployed UAVs as aerial base stations (ABSs) to support the backbone network in the case that the terrestrial BSs are broken or damaged after disasters or malevolent attacks. Vamvakas et al. [72] solved the resource allocation problem in UAV-aided public safety networks (PSNs), where the UAV's bandwidth can be shared with all users in the disaster areas. Anwar et al. [73] investigated the sound-based drone detection applying Mel frequency cepstral coefficients (MFCC), linear predictive cepstral coefficients (LPCC), and support vector machines (SVM). In [74], the authors proposed two UAV trajectories, termed Max-AoI-optimal and Ave-AoI-optimal, to efficiently collect data from ground sensor nodes under the impact of age of information (AoI) metric. Specifically, the Max-AoI-optimal and Ave-AoI-optimal trajectory planning minimize the age of the oldest information and the average AoI of all sensor nodes, respectively. The work in [75] studied the role of a UAV acting as a relay to minimize the average Peak AoI for a transmitter-receiver link, which was accomplished via a joint optimization of the UAV trajectory, energy spending, and the service time allocations for packet transmissions. In [76], the authors designed the UAV trajectory to minimize expired data packets in UAV-enabled wireless sensor networks (WSNs) and then applied the reinforcement learning (RL) method for the solution, which enhances the time-effectiveness and path design performance. The authors

in [70] optimized the UAV trajectory as well as service bandwidth allocation to maximize the total number of served ground IoT users, in which the UAV needed to collect data from users within their RT constraint. Different from [70, 74–76], which only studied the aspect of data collection on the UL channel, the works in [77] and [78] further studied the latency constraint on the DL channel.

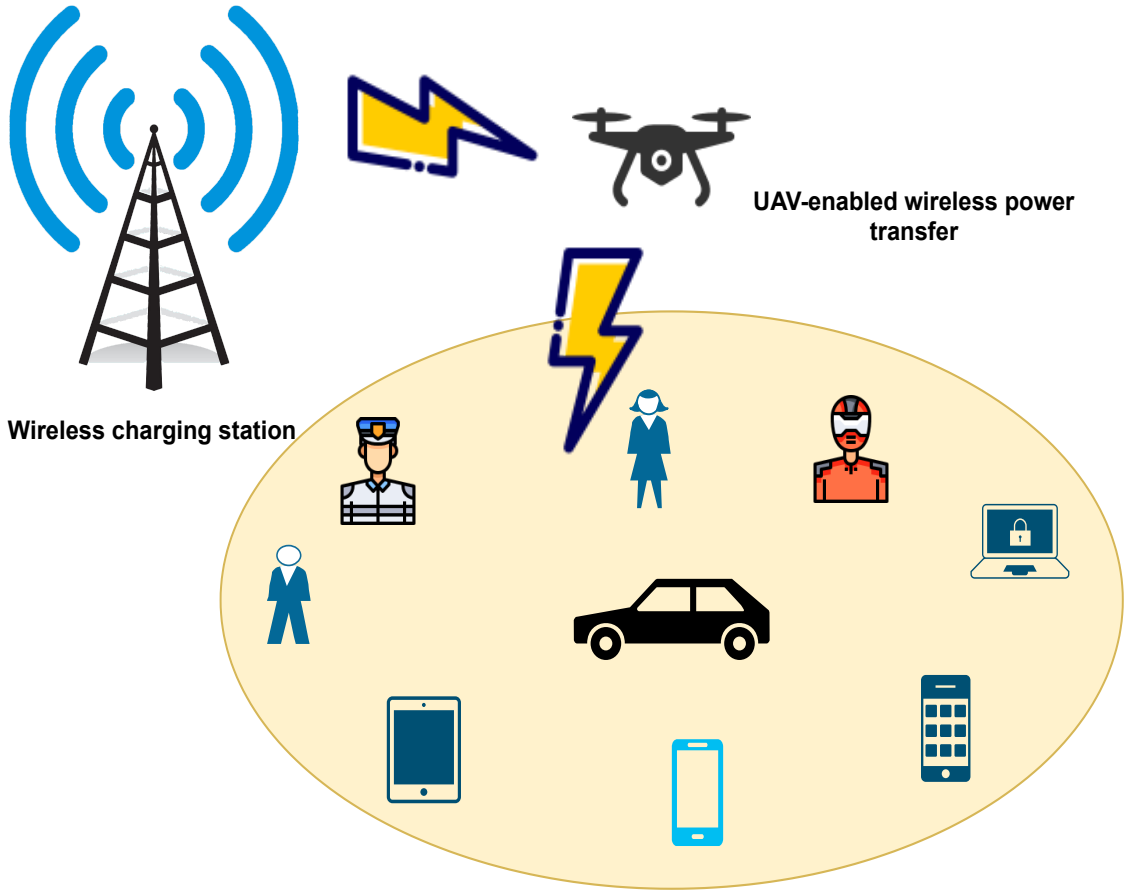

FIGURE 1.4: Wirelessly power UAV communications.

1.1.3 Wirelessly Powered UAV Communications

Fig. 1.4 shows the wirelessly powered UAV communication systems, whereas the UAV plays as a flying BS. Moreover, it can harvest energy from a wireless charging station or transfer energy to the power-limited devices on the ground. Since a restricted onboard battery is

one of the inherent limitations of the UAV, which greatly affects the UAV lifetime and performance in practice. To overcome this problem, there are some papers that investigate energy-efficient systems [79, 80]. Besides, wireless power transfer (WPT) has emerged as a promising solution to tackle this issue due to its controllability and predictability compared to other ambient source such as wind, vibration, and solar [16,81]. Thanks to the development of WPT technology that can transfer power to the user at a distance of up to 6.3 km [82], which can benefit UAV-assisted communications. Particularly, there has been reports on solutions for battery-free drone that can fly forever with wireless power [83,84]. Specifically, the demo in [84] showed that a heavy drone with peak power consumption up to 450 Watts and was powered completely wirelessly. As a research upsurge, wireless powered UAV is a hot topic that receives considerable attention from researchers [85–87]. Yin et al. [85] investigated a downlink (DL) cellular network, whereas multiple UAVs were powered by a ground charging station using save-then-transmit scheme. Jayakody et al. [86] proposed a new self-energized UAV system, where they considered an EH scheme including WPT, simultaneous wireless information and power transfer (SWIPT), and self-interference from full-duplex (FD) mode. Yan et al. [87] studied a UAV-enabled wireless sensor network (WSN) in which the UAV harvested energy from the base station (BS), then it used this harvested energy to serve multiple WSNs to maximize total energy received by all sensors.

1.1.4 UAV and Satellite in 6G Aerial Networks

Although fifth-generation (5G) wireless systems are being deployed around the world [88], the explosive growth of mobile data traffic still poses significant challenges for future networks, i.e., beyond 5G or 6G. It is predicted that individual user data rates will exceed 100 Gbps by 2030, and overall mobile data traffic will reach 5016 exabytes per month [89]. To overcome these challenges, the research community is working towards a sixth-generation (6G) system [90, 91]. Notably, the integration of satellite, aerial, and terrestrial networks is promoted as a key factor in providing high-capacity and ubiquitous connectivity for 6G [19, 90, 92].

Satellite communication (Satcom) has received considerable attention from both industry and academia due to its ability to provide wide-area coverage, e.g., telemedicine, military, satellite-assisted maritime communication, rescue missions, and disaster management system (DMS) [93–95]. Essentially, satellites are installed in geostationary earth orbit (GEO), medium earth orbit (MEO), and/or low earth orbit (LEO), which can complement and support terrestrial communication networks. Compared to its GEO and MEO counterparts, LEO Satcom operates at much lower altitudes, i.e., from 160 km to 2000 km [96], and it provides lower path losses and transmission latency. Therefore, many projects such as SpaceX, SPUTNIX, OneWeb, and Kepler plan to launch thousands of LEO satellites for providing globally seamless and high throughput communications cooperating with terrestrial communications [97]. Because of these benefits, many works have studied the hybrid

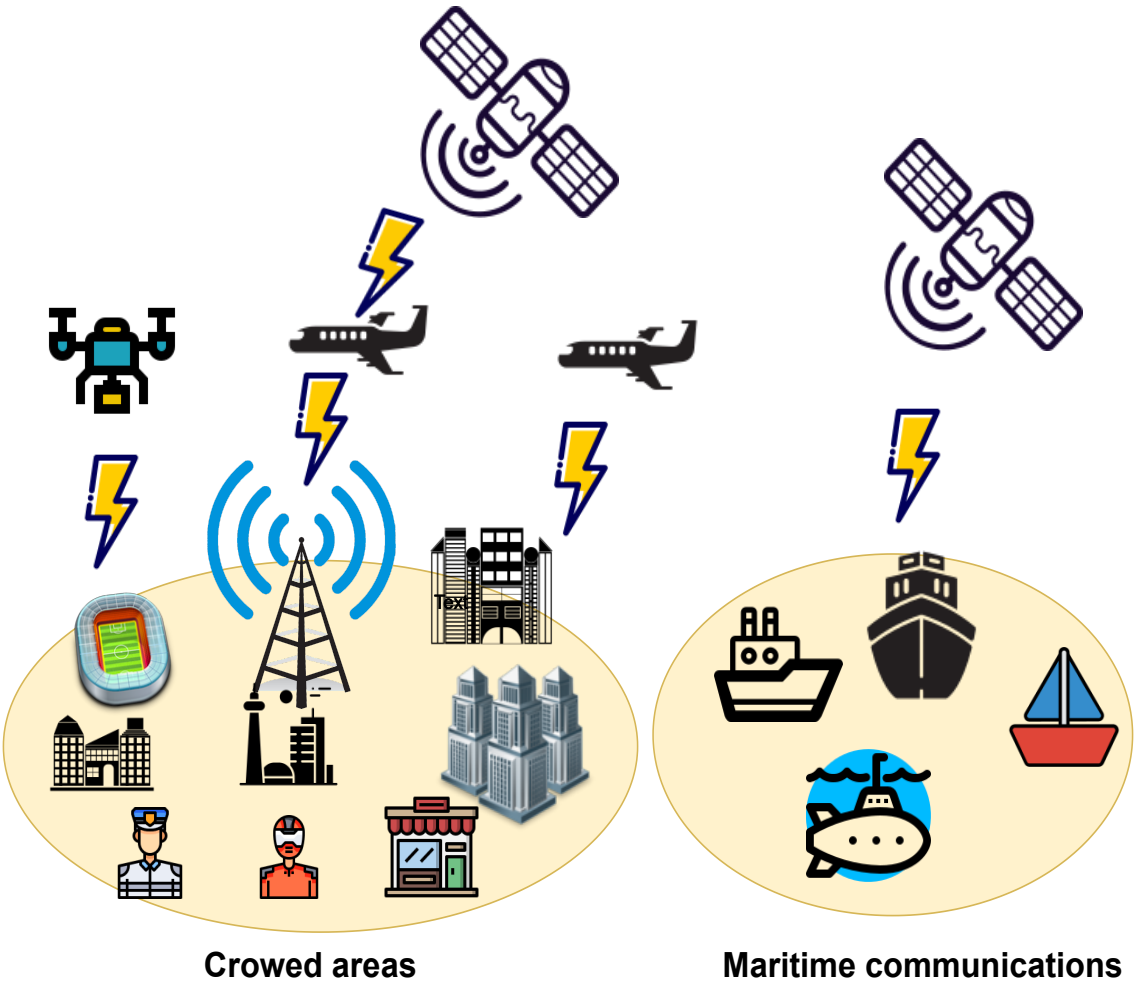

FIGURE 1.5: Satellite-Aerial-Terrestrial communications.

LEO satellite-terrestrial communication networks [98–100].

Fig. 1.5 illustrates the Satellite-UAV-Terrestrial networks in crowded areas and maritime communications. Due to its necessity, there has been a lot of research works on hybrid satellite and UAV in space-air-terrestrial communication networks to leverage the benefits of each one [101–104]. Yu et al. [101] studied the 3D channel tracking and modeling for satellite and UAV communications with LEO satellite movement and 3D trajectory design for UAV. Gu et al. [102] proposed a new system model, termed cache-enabled satellite-UAV-vehicle integrated network (CSUVIN), in which a GEO satellite and UAVs act as a cloud server and edge caching servers, respectively. Then, they proposed an energy-aware

coded caching to reduce the burden on the backhaul link. In [103], the authors investigated the outage performance for a satellite-terrestrial network, where a multi-antenna satellite communicates with a GU via the help of multiple UAVs acting as relays. Zhao et al. [104] proposed a blind beam tracking approach for satellite-UAV communications in which the UAV had a large-scale antenna array.

1.2 Limitations of Existing Works

Besides many advantages, UAV-enabled communications are not without limitations. There are still many challenges and limitations in UAV communications for future networks, i.e., 5G and beyond. This section describes disadvantages or the missing aspects or unresolved challenges in the literature, which directly motives for our thesis. In summary, the main limitations of UAV-enabled communications are given as follows:

- Despite remarkable achievements in UAV trajectory design, the aforementioned works cannot provide a full picture for UAV trajectory design. More specifically, none of the works in the literature [13–15] take the time constraints into consideration. To the best of our knowledge, there are also no other works that investigate the problem of *UAV trajectory design with latency constraints in wireless communications.*

- In the literature, there are some references that take latency requirements into consideration in UAV communications [70, 74–76, 78]. Specifically, references [70, 74–76] studied the aspect of data collection on the uplink (UL) channel, while reference [78] studied latency constraints on the downlink (DL) channel. Nevertheless, these works only investigated timely data exchange on UL or DL channel utilizing HD mode. Moreover, these works [70, 74–76, 78] have not exploited benefits of full duplex (FD) radios.

- As limited energy capacity is one of the main limitations of the UAV, it significantly affects the UAV lifetime and reduces the network performance. Owning to the development of wireless power transfer (WPT) technology that can provide power to GUs at long distances. It motives for a wirelessly powered UAV communication system in which the UAV can recharge energy in the sky. Consequently, this is a potential solution to overcome the energy limit at UAV. Nevertheless, there are only a few works in wirelessly powered UAV communications [85–87]. Therefore, this opens up a new challenge for designing an energy-efficient WPT-assisted UAV system.

- Besides many advantages, Satcom is not without limitations. One satellite can cover a very large area and thus it can improve network performance by acting as a relay or a base station (BS) to provide communication services to isolated areas, e.g., ocean, desert, severe areas. However, only ground users (GUs) are equipped with

expensive high-gain antennas to benefit from satellites. Other users within satellite coverage cannot take advantage of Satcom's broadband services since they do not have high-gain antennas [93]. Consequently, the deployment of a UAV as a relay is a potential solution to transfer information from the satellite to GUs, especially during emergency communication situations such as after disasters or in isolated areas. Recently, some noticeable achievements have been obtained for UAV-satellite communications [93, 105–107], yet the aforementioned works do not take caching into consideration. In particular, the UAV is equipped with a cache that can storage popular information during off-peak hours. Thus, it can reduce power consumption and eliminate network congestion on the backhaul link.

Based on the above limitations in UAV-enabled communications, we will describe in this thesis how to solve these technical problems. More specifically, the contributions of our thesis can be summarized in the following section.

1.3 Contributions and Outline of the Thesis

The main contribution of this dissertation is to propose effective methods to overcome limitations in trajectory design, latency-sensitive data transmission, WPT, and integration with SatComs in UAV communication networks. The details of each chapter are listed as follows:

Chapter 3 includes the scenarios in which a UAV acting as a flying base station to serve latency-sensitive GUs on the downlink. Our objective is to minimize the UAV energy consumption while satisfying the latency constraint of each GU. Main contributions of this chapter are:

- In contrast to [13–15] which adopted TSP solution as an initial feasible trajectory in their proposed alternative algorithm, we proposed three algorithms, termed exhaustive search (ES), heuristic algorithm, and dynamic programming based on traveling salesman problem with time window (TSPTW) to find a feasible set of paths satisfying the latency constraint at each GU.

- Based on feasible paths obtained from proposed algorithms, we minimize the UAV energy consumption for each given path by optimizing the UAV speeds in all hops. Then, the feasible path with lowest energy consumption and guarantee the energy budget can be selected as traveling path for the UAV.

- Our results show that the proposed algorithms significantly improve the network performance compared to the TSP-based method [13–15]. Particularly, the DP scheme can obtain closed to the ES's performance while greatly reducing the calculating time.

The outputs of this chapter are published in:

[**J1**] **D. H. Tran**, T. X. Vu, S. Chatzinotas, S. Shahbazpanahi, and B. Ottersten, **"Coarse Trajectory design for energy minimization in UAV-enabled wireless communications with latency constraints,"** in IEEE Transactions on Vehicular Technology, Sept. 2020. Doi: 10.1109/TVT.2020.3001403.

[**C1**] **D. H. Tran**, T. X. Vu, S. Chatzinotas, and B. Ottersten, **"Energy-efficient trajectory design for UAV-enabled wireless communications with latency constraints,"** in 2019 53rd Asilomar on Signals, Systems, and Computers, Pacific Grove, CA, USA, 2019, pp. 347-352. Doi: 10.1109/IEEECONF44664.2019.9048942.

In chapter 4, we propose a novel system model to investigate the UAV-assisted emergency communications in IoT networks. Due to inherently limited energy budget and storage capacity, the data generated from IoTs should be collected on time before they become useless or obsolete. This chapter proposes a novel system model in UAV relay-assisted IoT networks that further explores the impact of freshness of information for UAV-assisted in disaster or emergency communications. To the best of our knowledge, this is the first work investigating the latency constraints in uplink (UL) and downlink (DL) transmissions, which is a great challenge and has not been investigated before. The contributions of this chapter is given as follows:

- We proposed a novel UAV relay-assisted full duplex (FD) IoT system by considering time-sensitive information transmission on both DL and UL.
- In this context, we aim to maximize the number of successfully served IoT devices and the achievable throughput.
- Through simulation results, we show the superiority of the proposed method by jointly optimizing bandwidth, transmit power, trajectory with caching capability compared to benchmark ones.
- The results of chapter 4 constitute one of the first comprehensive studies on joint optimal UAV trajectory, resource allocation with caching, and latency constraints on DL and UL in IoT networks.
- The outcome of this chapter will motivate a new framework for UAV-aided communications in disaster or emergency communications.

The output of chapter 4 are published in:

[**J2**] **D. H. Tran**, V.D. Nguyen, S. Chatzinotas, T. X. Vu, and B. Ottersten, **"UAV Relay-Assisted Emergency Communications in IoT Networks: Resource Allocation and Trajectory Optimization,"** IEEE Transactions on Wireless Communications, August 2021. Doi: 10.1109/TWC.2021.3105821.

[C2] **D. H. Tran**, V.D. Nguyen, S. Gautam, S. Chatzinotas, T. X. Vu, and B. Ottersten, **"Resource Allocation for UAV Relay-Assisted IoT Communication Networks,"** to IEEE Globecom Workshops 2020 (GC Wkshps), Taipei, Taiwan, pp. 1-7. Doi: 10.1109/GCWkshps50303.2020.9367522.

In chapter 5, we consider a wireless powered UAV communication with backscatter and caching technologies. In this context, a UAV is equipped with a backscatter circuit and it acts as a relay to transfer information from a source to a destination. To overcome the energy limitation, the UAV can harvest energy from the source's RF signals using the dynamic time splitting (DTS) method and it stores a part of popular information in its cache to reduce transmit power, which helps to improve the UAV lifetime. The contributions of this chapter are:

- We proposed a novel backscatter- and cache-aided UAV relay-assisted communication network. In particular, the UAV can perform both passive and active communication to improve the network performance.
- This is the first study that constitutes one of the first comprehensive studies on SWIPT, backscatter communication (BackCom), caching, and UAV, which imposes high challenges.
- In this setup, we aim to maximize the achievable throughput at the destination subject to constraints on UAV speed, limited flight time, UAV trajectory, and DTS ratio.
- Through simulation results, we show the advantages of the proposed method compared to benchmark ones, i.e., no caching (NC), fixed DTS ratio (FTau), and fixed trajectory (FTra).

The outputs of chapter 5 is published in:

[J3] **D. H. Tran**, S. Chatzinotas, B. Ottersten, **"Throughput Maximization for Wireless Communication systems with backscatter- and Cache-assisted UAV Technology ",** submitted to IEEE Transactions on Vehicular Technology, (Major revision).

Chapter 6 presents a UAV-satellite communication model to analyze the performance of GUs served by a UAV and a LEO satellite. The proposed framework takes into account the effects of cache placement, UAV trajectory, limited resources, and limited flight time. The contributions of chapter are summarized as:

- This is the first study on maximizing the minimum throughput of GUs in LEO satellite and cache-assisted UAV communication systems.

- We build a practical system model by considering the latency time due to limited resources (i.e., limited transmit power, bandwidth, limited cache capacity, and flight time) and large distance between satellite and UAV, which is not considered before.
- From simulation results, we provide the improvement of the proposed method compared to benchmark ones, i.e., no caching capability, fixed resource allocation, and fixed trajectory.

The output of chapter 6 is published in:

[**J4**] **D. H. Tran**, S. Chatzinotas, B. Ottersten, **"Satellite- and Cache-assisted UAV: A Joint Cache Placement, Resource Allocation, and Trajectory Optimization for 6G Aerial Networks,"** submitted IEEE Open Journal of Vehicular Technology, 2021.

Finally, we conclude the dissertation and discuss about future research directions in chapter 7.

1.4 Contributions beyond thesis

During my doctoral study, I have contributed to a number of publications, which are not part of this thesis. The details are listed as follows:

Journal Papers

[**J5**] P. X. Nguyen, **D. H. Tran**, O. Onireti, P. T. Tin, S. Q. Nguyen, S. Chatzinotas, H. Vincent Poor, **"Backscatter-Assisted Data Offloading in OFDMA-based Wireless Powered Mobile Edge Computing for IoT Networks,"** IEEE Internet Things J., vol. 8, no. 11, pp. 9233-9243, 2021.

[**J6**] T. N. Nguyen, **D. H. Tran**, V. D. Phan, M. Voznak, S. Chatzinotas, B. Ottersten, and H. Vincent Poor, **"Throughput Enhancement in FD- and SWIPT-enabled IoT Networks over Non-Identical Rayleigh Fading Channels,"** IEEE Internet of Things Journal, Early accepted.

[**J7**] T. N. Nguyen, **D. H. Tran**, P. T. Tin, M. Voznak, S. Chatzinotas, B. Ottersten, and H. Vincent Poor, **"Physical Layer Security in AF-Based Cooperative SWIPT Networks with a Direct Link,"** submitted IEEE TVT (Revised).

[**J8**] P. T. Tin, T. N. Nguyen, **D. H. Tran**, M. Voznak, S. Chatzinotas, **"Performance Enhancement for Full-Duplex Relaying with Time Switching-Based SWIPT in Wireless Ad-Hoc Networks,"** Sensors, vol. 21, no. 11, p.3847, 2021.

[**J9**] T. N. Nguyen, **D. H. Tran**, V. D. Phan, M. Voznak, S. Chatzinotas, and H. Vincent Poor, **"Security-Reliability Trade-Off Analysis for SWIPT- and AF-Based IoT Networks with Friendly Jammers,"** IEEE Internet of Things Journal, submitted.

[**J10**] T. N. Nguyen, **D. H. Tran**, V. D. Phan, M. Voznak, S. Chatzinotas, and H. Vincent Poor, **"Physical Layer Security Analysis of SWIPT-Enabled Cooperative Wireless IoT Networks in the Presence of Friendly Jammer and Eavesdropper,"** IEEE Internet of Things, submitted.

[**J11**] T. N. Nguyen, **D. H. Tran**, V. D. Phan, M. Voznak, S. Chatzinotas, and H. Vincent Poor, **"Security-Reliability Trade-Off Analysis for Satellite-Terrestrial Relay Networks with Friendly Jammers,"** IEEE Transactions on Communications, submitted.

[**J12**] T. N. Nguyen, L. T. Tu, **D. H. Tran**, V. D. Phan,M. Voznak, S. Chatzinotas, **"Security-Reliability Trade-Off for Satellite-Terrestrial Relay Networks with Friendly Jammer and Imperfect CSI,"** IEEE Internet of Things, submitted.

Conference Papers

[**C3**] T. V. Chien, T. L, Thanh, **D. H. Tran**, H. V. Nguyen, S. Chatzinotas, M. Direnzo, B. Ottersten, **"Controlling Smart Propagation Environments: Long-Term Versus Short-Term Phase Shift Optimization,"** 2022 IEEE International Conference on Acoustics, Speech and Signal Processing (ICASSP 2022), submitted.

Chapter 2

Preliminaries

This chapter provides common knowledge about different techniques applied with UAV communications in this dissertation, e.g., full-duplex, backscatter communications, simultaneous wireless information and power transfer (SWIPT), and mobile edge caching. We summarize the basic concept, advantages, and why UAV communication becomes an attractive approach when integrated with these techniques. The main purpose of this chapter is to bring a broader context and to give the reader a general picture. Building on the concepts presented in this chapter, advanced designs are shown in subsequent chapters to solve specific realistic challenges.

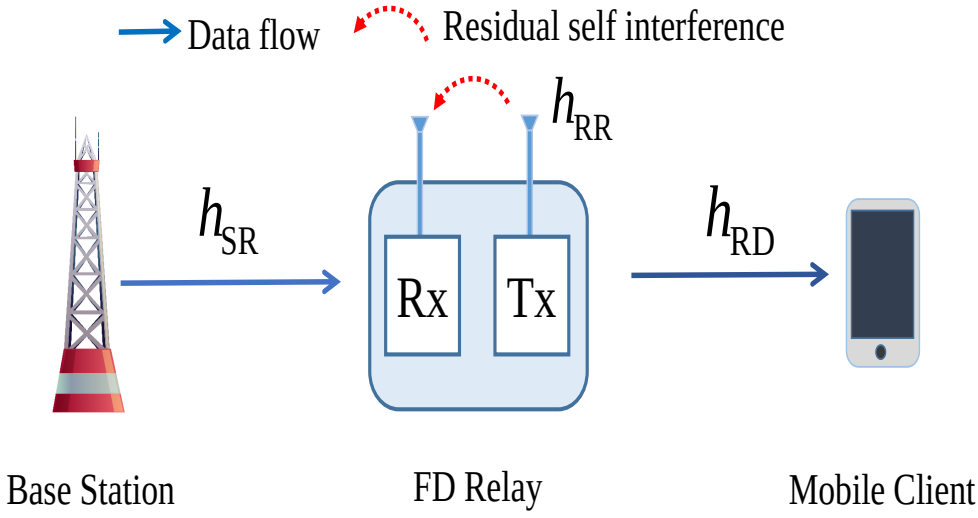

FIGURE 2.1: Two different antenna in FD communications.

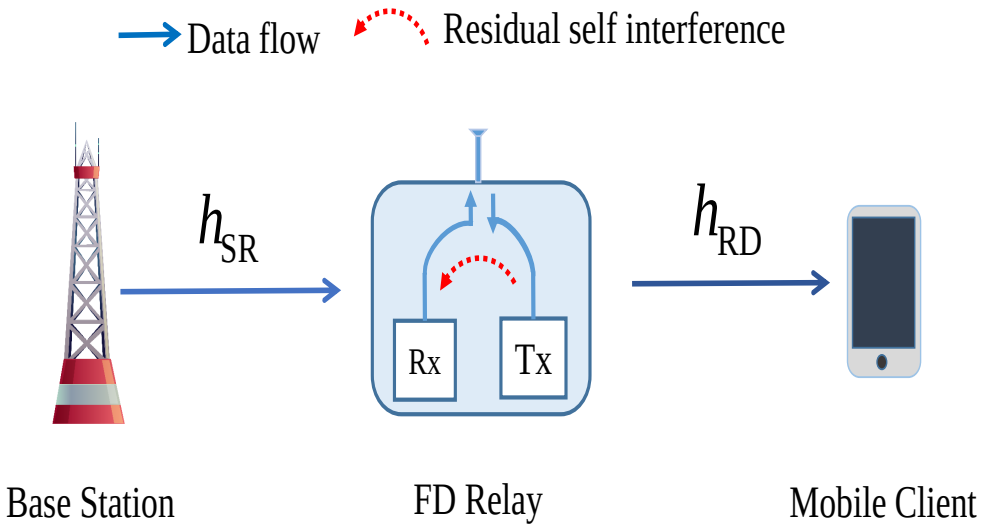

FIGURE 2.2: One antenna scenario in FD communications.

2.0.1 Full-Duplex Communications

Due to the enormous increase in mobile devices and broadband services, the spectral efficiency requirement has become a challenge for wireless communication with limited resources. As reported by Ericsson, the number of mobile users will be around 29 billion in 2022 [108]. Besides, the mobile data traffic of one user and the total mobile traffic will respectively reach 35 GB, and 300 EB at the end of 2026 [109]. Therefore, spectrum scarcity becomes a never-ending story of wireless communications. Especially when the number of users is significantly increased, such as massive machine-type communications (mMTC) in fifth-generation (5G) and beyond, a limited spectrum resource needs to cover massive data traffic and IoT users. In these scenarios, full-duplex (FD) technology has emerged as a potential solution due to its capability of doubling the energy efficiency (EE) compared to half-duplex (HD) communications. It is because FD can transmit and receive signals on the uplink (UL) and downlink (DL) simultaneously using the same frequency band. Therefore, FD can be considered as a key technology for 5G and beyond [110, 111].

The concept of FD communications has been used in at least since 1940s [112, 113]. Essentially, FD radio system can be used in two separate antennas or one antenna, as shown in Figs. 2.1 and 2.2. Self interference is the biggest challenges of FD communications and it can be overcome by using separate antennas or circulators in one antenna as shown in Fig. 2.1 or Fig. 2.2, respectively. In particular, self-interference cancellation (SIC) can be achieved to 110 dB [114] or 150 dB [115].

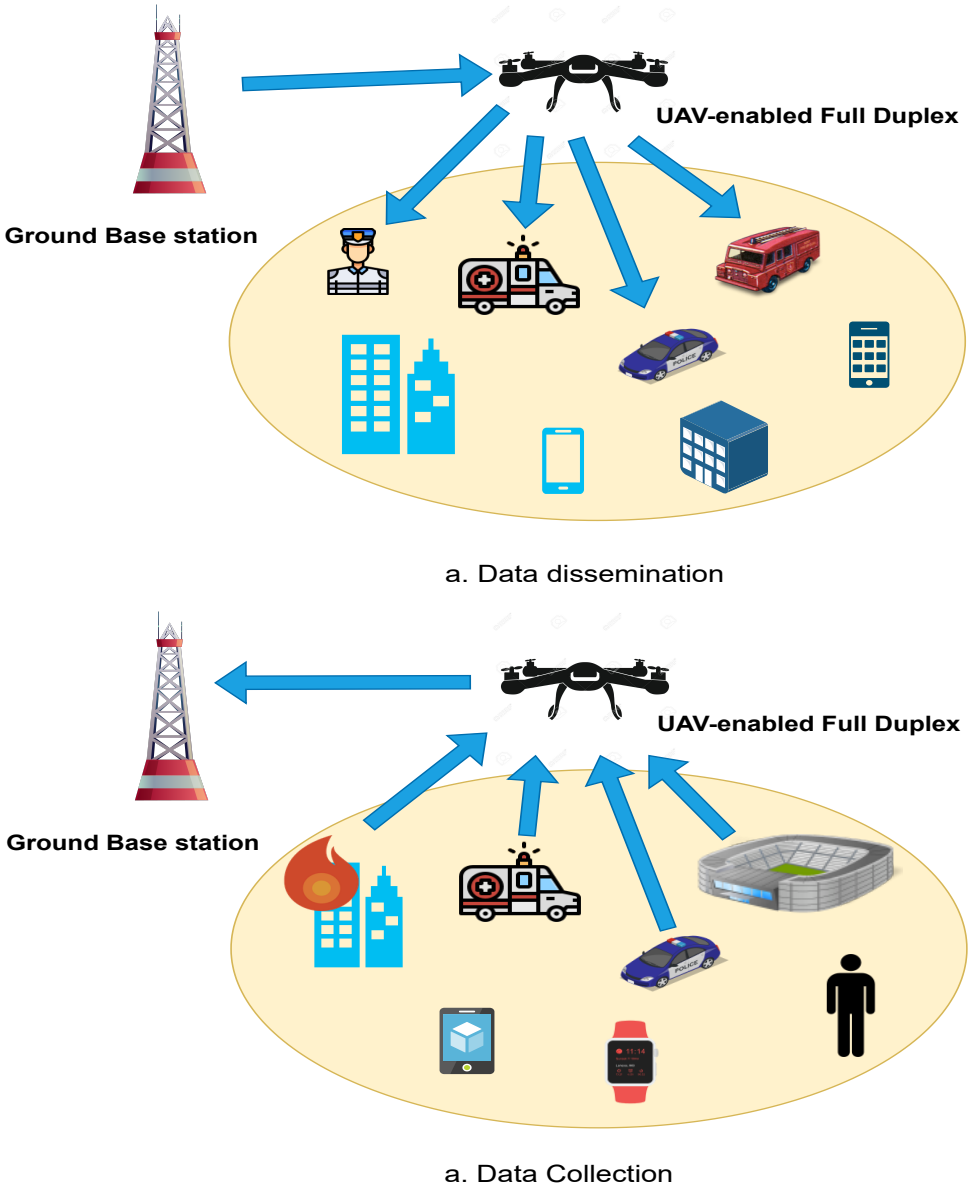

FIGURE 2.3: UAV-enabled full-duplex communication.

Owing to the development of self-interference cancellation (SIC) techniques, the advantages of the FD technique can be applied in UAV communications to improve network performance. The FD-enabled UAV communication system is motivated by realistic

communication-related applications. For instance, in content delivery networks or the age of information, when a GU requests content data, it needs to be served within a certain latency constraint. Thus, FD UAV communication helps to significantly reduce the data transmission time. Moreover, in natural disaster alert applications, the FD-enabled UAV communications help disseminate vital information to people about the incoming disaster as soon as possible, as shown in Fig. 2.3 a. Besides, in the emergency case or during the natural disaster, the out-of-date gathering data may result in unreliable controllable decisions, which may ultimately be disastrous [70]. On the other hand, IoT devices often have limited storage capacity, and thus their generated data need to be collected timely before it becomes worthless due to obsolete transmissions or being overwritten by incoming data, as shown in Fig. 2.3 b. Therefore, the FD UAV can improve the network performance in data collection process, e.g., lower latency and higher throughput. Recently, many works have investigated the integration of FD technology in UAV communications [116–122]. Haichao et al. [116] investigated the spectrum sharing problem for an FD UAV system with device-to-device communications, whereas the UAV acted as a relay to support communication between ground users. Moreover, the authors aimed to maximize the total throughput by optimizing the UAV trajectory and transmit power constraints. Gazestani et al. [117] considered FD-enabled UAVs in multi-small cell networks with imperfect self-interference cancellation (SIC). This work investigated three scenarios of maximizing the downlink (DL) rate, the uplink (UL) rate, and the sum of DL and UL rates. Wenjuan et al. [118] studied FD-enabled UAV for non-orthogonal multiple access (NOMA) communications. They aimed to minimize the power consumption on the DL and UL by jointly optimizing the resource allocation of the terrestrial users and the UAV. FD-enabled UAV network was also deployed to improve the total capacity in Millimeter-Wave networks [119]. Specifically, Lipeng et al. [119] optimized the UAV location, power allocation, and beam-forming to maximize the total throughput at the source and destination. In [120, 121], the authors applied FD-enabled UAV for IoT networks. Han-Ting et al. [120] utilized an FD rotary-wing UAV that acted as a flying base station to serve multiple IoT users (IoTU). Moreover, the UAV provided wireless power to IoT users and collect information from them when flying and hovering, respectively. Hieu et al. [121] considered a new system model for IoT networks, whereas the latency constraint was considered in both UL from IoTU to UAV and DL from UAV to ground gateway. FD UAV also brought benefits to the -intelligent reflecting surface (IRS) system [122]. Shafique et al. [122] investigated FD UAV in IRS relaying network in three scenarios, including UAV mode, IRS mode, and IRS-UAV mode to maximize the capacity and energy efficiency of the proposed systems.

2.0.2 Backscatter Communications

Stockman is the first one who introduced Backscatter communication (BackCom) for the first time in 1948 [123]. Then, this concept became a promising solution for low-powered

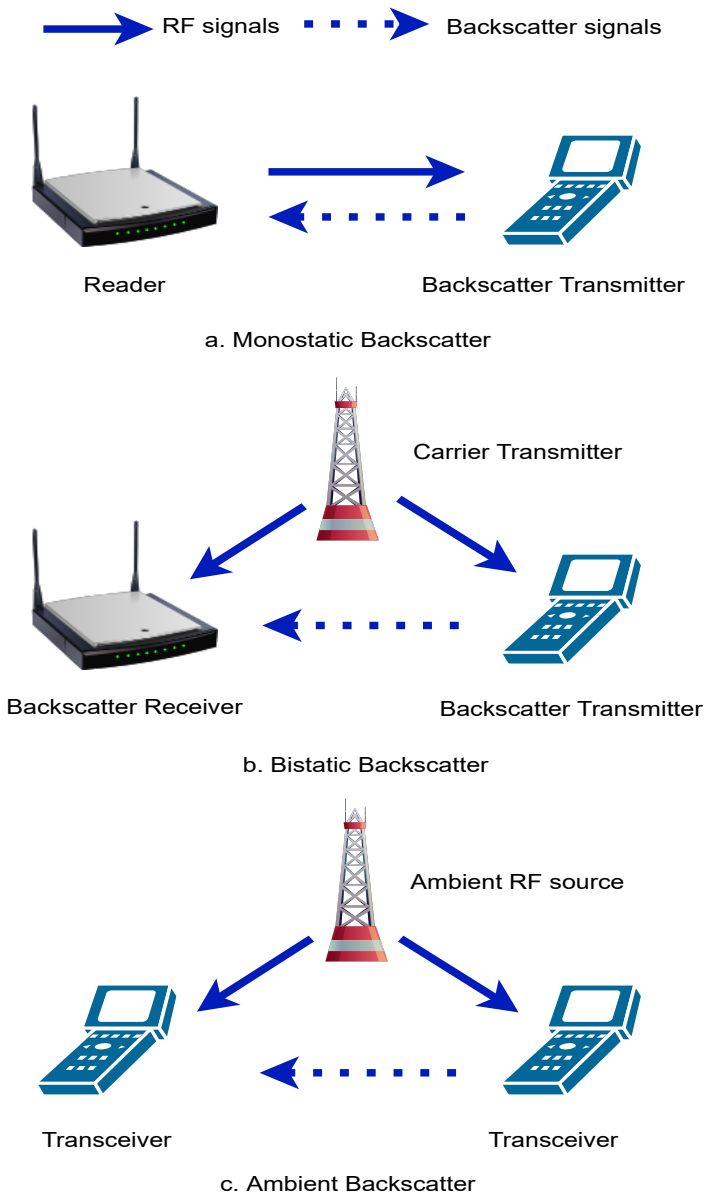

FIGURE 2.4: Models for backscatter communications.

devices since a typical backscatter circuit's power consumption is usually in the order of μW [124–126]. Moreover, BackCom has been applied widely in various aspects such as healthcare, medical telemetry, radio-frequency identification (RFID), IoT networks, etc.

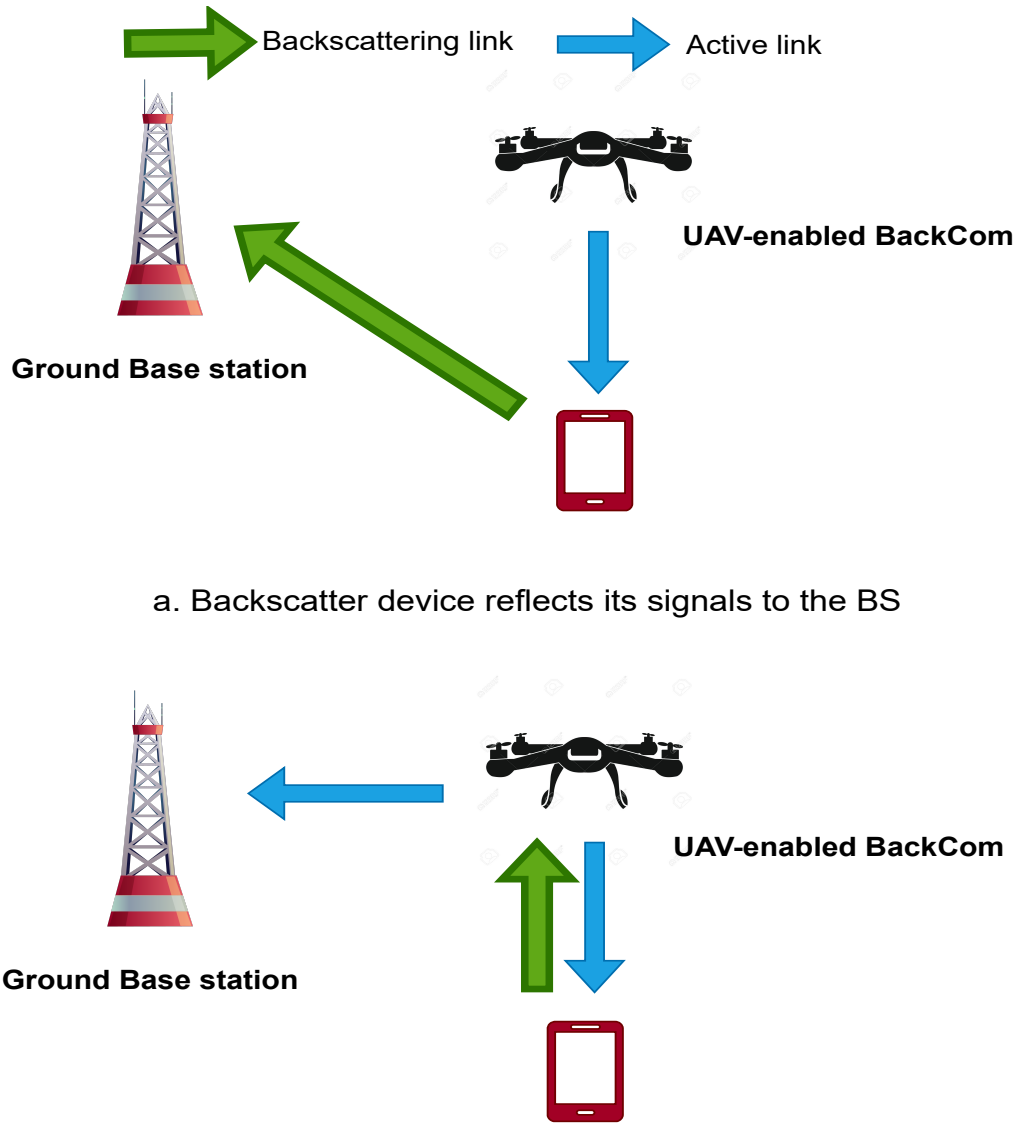

FIGURE 2.5: Models for backscatter communications.

[127, 128]. In particular, BackCom has been emerged as an ultra-power-efficient solution for massive machine-type communications (mMTC) in sixth-generation (6G) network [129, 130]. This is because BackCom allows the backscatter devices (BackDs) to harvest energy

from the ambient RF signals to maintain their operations and transfer information by reflecting the received RF signals to the receiver using intentional load impedance mismatch at the antenna.

As shown in Fig. 2.4, there are three types of BackCom, including mono-static BackCom (MoBackCom), bi-static BackCom (BiBackCom), and ambient BackCom (AmBackCom). In MoBackCom, there exists one reader and one backscatter transmitter (BackTran). The reader creates RF signals to activate the BackTran by receiving the reflecting signals from BackTran. The MoBackCom only focuses on short RFID applications. To prevent the round-trip path loss in MoBackCom, the carrier transmitter (CaTran) and backscatter transceiver (BackTranCei) are detached as in BiBackCom. Similar to BiBackCom, the CaTran in AmBackCom are also separated. Nevertheless, CaTran in AmBackCom is leveraged from ambient RF sources such as base stations, Wi-Fi access points, or TV towers.

Beyond many advantages, BackCom is not without limitations. For instance, BackCom is limited to low data rates and short-range communications [126]. Therefore, UAV can be utilized to help BackDs transfer information to the receiver due to its high mobility and flexibility [131]. In Fig. 2.5, we illustrate two main scenarios of UAV-assisted BackCom. In the first case, a UAV is deployed as a flying BS to transmit active RF signals to the BackD, then BackD can reflect its own signals to the ground BS [132]. In the second case, when the direct link between BackD to the ground BS does not exist, the UAV helps transfer backscatter's signals to the ground BS [133].

Recently, the integration of BackCom and UAV communication has received significant attention from researchers [134–138]. In [138], the authors proposed two novel schemes termed the transmit-backscatter protocol and transmit-backscatter relay protocol corresponding to the presence or absence of a direct link between backscatter user and receiver in UAV-aided BackCom networks. Yang et al. [134] considered a UAV-aided BackCom network comprising of backscatter devices (BDs) and carrier emitters (CEs) that are randomly distributed on the ground. They aimed at maximum energy efficiency (EE) by jointly optimizing the BDs' scheduling, the UAV's trajectory, and the CEs' transmit power. Farajzadeh et al. [135] proposed a novel UAV data collection in NOMA BackCom networks, where the UAV acted both as a power source and a data collector. The objective was to jointly design several backscatter devices, UAV's altitude, and backscatter coefficient to maximize the total successfully decoded bits while minimizing the UAV's flight time. The same authors in [136] studied the first work that considered UAV as an enabler to improve over-the-air computation (AirComp)'s performance. Hu et al. [137] proposed the first work that investigated secure transmissions in UAV-aided BackCom networks.

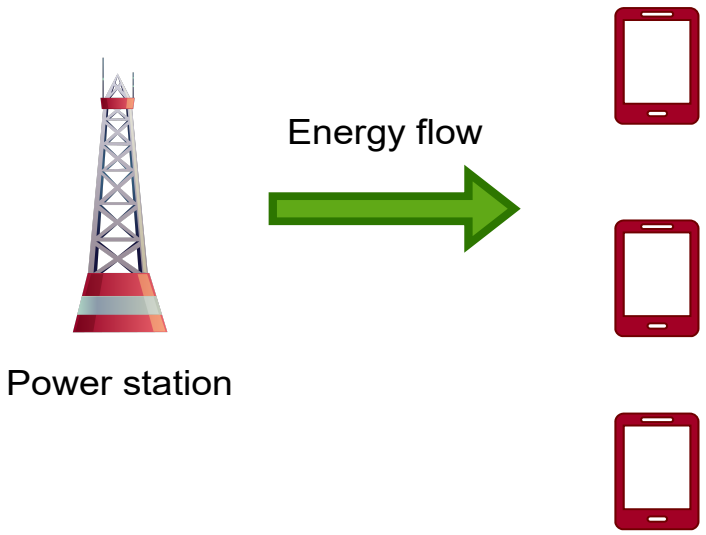

FIGURE 2.6: Wireless power transfer model.

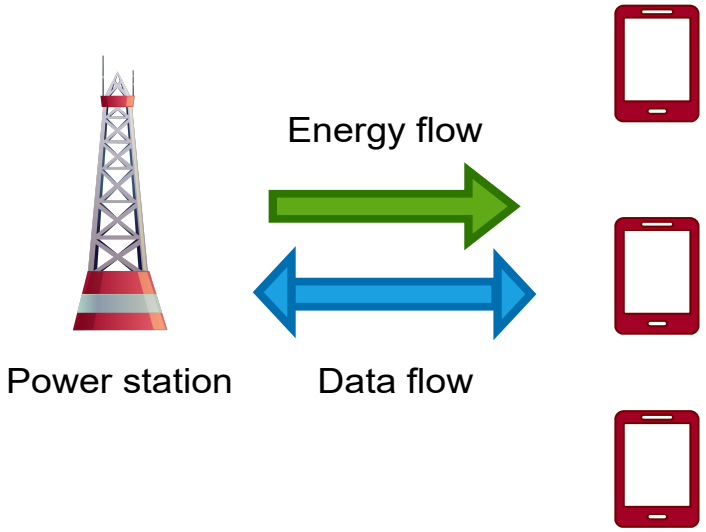

FIGURE 2.7: Simultaneous wireless information and power transfer model.

2.0.3 Simultaneous wireless information and power transfer (SWIPT)

Internet of Things (IoT) can play a key role in improving quality of life through applications such as home automation, smart cars, smart city, health care, industrial or agriculture

monitoring, augmented reality, and smart grid [139]. The number of IoT devices is estimated to reach 25 billion by 2025 [121, 140]. Moreover, there is an explosive surge of resource-intensive IoT applications such as interactive gaming, multi-view video construction, augmented reality (AR), virtual reality (VR), and face recognition, that impose stringent demands on high energy consumption due to large computation capability [141]. The constrained battery capacity of the IoT devices (IoTD) make them unsuitable for processing resource-hungry applications. Moreover, since the IoT's battery stores a finite amount of energy, it needs to be replaced or charged, which is infeasible and costly in the hazardous environments, e.g., in toxic (i.e., gas or chemical) environments. This is the reason why energy harvesting (EH) has attracted much attention in the last decade [81, 142, 143]. In particular, SWIPT plays an important pivotal role in the sixth-generation (6G) IoT networks [144, 145]. This is because a massive number of IoT devices (IoTDs) can adopt the SWIPT technique to prolong their lifetime by collecting energy from RF signals.

As illustrated in Figs. 2.6 and 2.7, RF EH techniques can be divided into wireless power transfer (WPT) and simultaneous wireless information and power transfer (SWIPT) categories. The main distinction between WPT and SWIPT is that the transmitter's RF signals carry only power in WPT, while it can carry both information and power concurrently in SWIPT. Therefore, SWIPT brings more utilities than WPT but also presents more design challenges since it needs to allocate the harvested energy and information transmission to IoT users. Varshney [146] originated the SWIPT concept and Pulkit Grover and Anant Sahai [147] extended the work to frequency-selective channels with additive white Gaussian noise (AWGN). Nevertheless, [146] and [147] only provided theoretical limits, which was impractical because the electric circuit used to harvest energy from an RF signal could not decode the carried information. To overcome the limitations in [146] and [147], Zhang and Ho [148] proposed two practical receiver designs, termed time switching (TS) and static power splitting (SPS), to schedule the wireless power transfer (WPT) and wireless information transfer (WIT) at the EH receiver.

Recently, extensive studies have been performed to investigate SWIPT with cooperative relaying communications since the SWIPT relay network can improve the communication range and provide power to energy-restricted users. Moreover, the benefits of SWIPT in communication networks have been thoroughly discussed in [82]. The SWIPT relay network can be divided into two types: time switching (TS)-based relaying [149–151] and power splitting (PS)-based relaying [152–158]. Specifically, Nasir et al. [149] proposed TS-based EH and information transmission (IT) protocols with continuous-time EH and discrete-time EH modes at the relay. They then derived the analytical expressions in terms of throughput for the proposed protocols. Focusing on the TS architecture, the authors in [150] proposed novel relaying protocols based on adaptive TS for amplify-and-forward (AF) and decode-and-forward (DF) modes. In contrast to the studies in [149] and [150], which only considered a simple static TS structure, [151] divided the total time T into N equal time slots and optimized the TS factor in all time slots. Making use of a PS-based EH

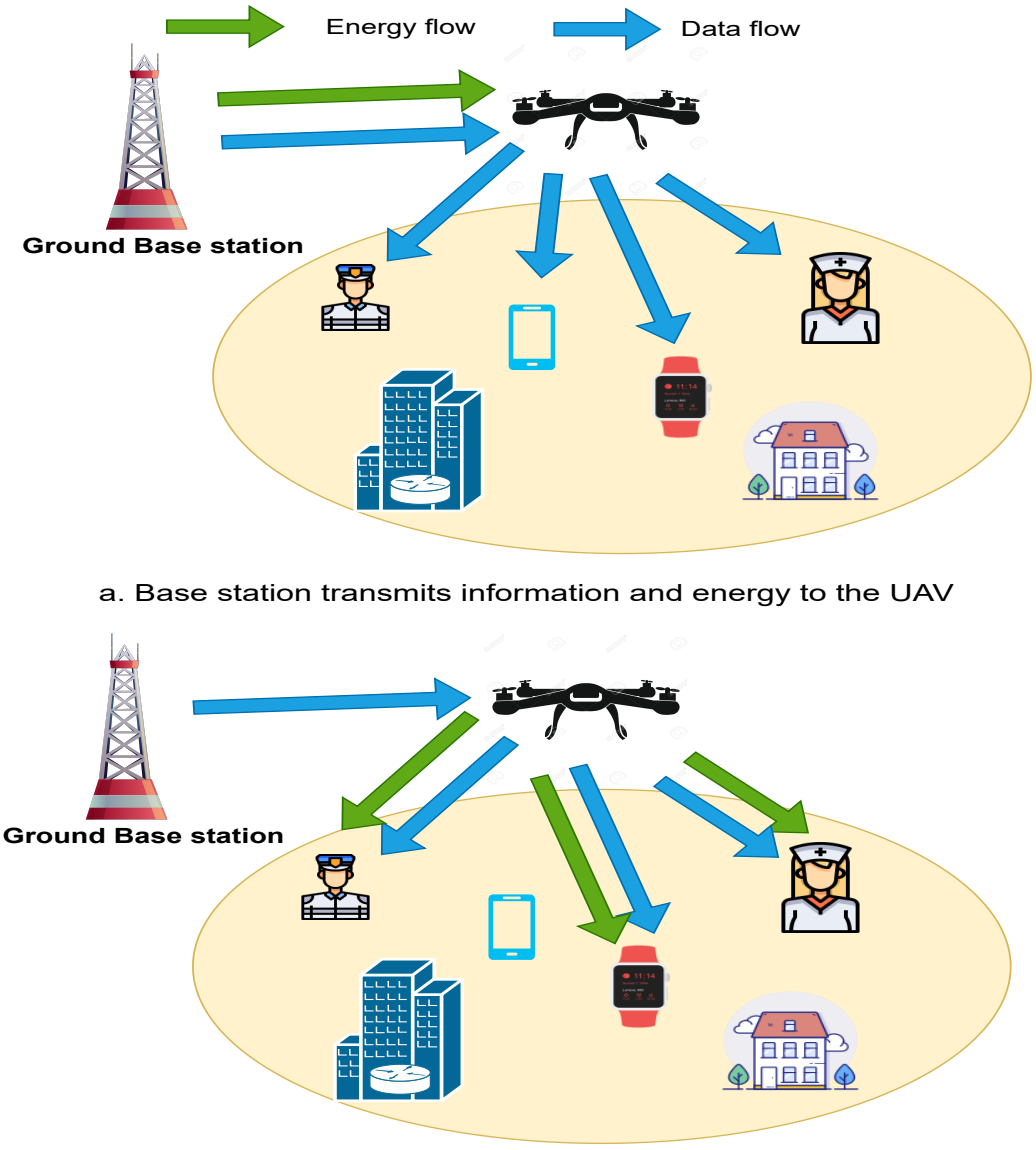

FIGURE 2.8: Integration of SWIPT and UAV in wireless communications.

receiver architecture, a novel system model in which a massive multi-input multi-output (MIMO) two-way relaying system with a PS relay was considered in [152]. By taking into account the Nakagami-m and Rayleigh fading channel, Tan et al. [153] analyzed the

performance analysis of user selection protocols with PS-based EH. Differently from [152] and [153], which only considered a static PS factor, [154] and [155] designed relay selection schemes based on an optimal dynamic PS ratio. While [152–155] only considered TS- or PS-based relaying schemes, [156] and [157] investigated a two-way half-duplex hybrid time-switching and power-splitting (HTPSR) relay network which leveraged the advantages of both TS and PS protocols. Besides, Liu et al [158] aimed to maximize the 5G and IoT transmission rate and the total power consumption by jointly optimizing time/power allocation factors and transmit powers. In [159], the authors proposed a practical non-linear EH model in SWIPT systems, where they aimed to maximize the total harvested energy at the EH receivers according to the minimum demanded signal-to-interference-plus-noise ratios at the information receivers.

Beyond many advantages, SWIPT is not without limitations. Specifically, the RF energy harvesting process works much better in the light-of-sight (LoS) data transmission compared to the non-light-of-sight (NLoS) links. By leveraging the advantages of UAVs such as mobility, flexibility, and probability of providing LoS communications, UAVs can compensate for the shortcomings of SWIPT to improve network performance. Consequently, the integration between UAV and SWIPT has attracted many attentions from researchers [86, 160–163]. As illustrated in Fig. 2.8, we present two different scenarios of the integration between SWIPT and UAV in wireless communication. In the first scenario, the ground BS can transmit both information and power to the UAV to increase the lifetime of UAV [86]. In the second scenario, a UAV acts as a flying BS to transfer both power and information to the IoTDs on the ground.

2.0.4 Mobile Edge Caching

The enormous explosion of data demand of mobile traffic, especially for videos and photos on social media networks such as Facebook, Instagram, and Youtube, has created a significant burden on wireless communication with limited resources, i.e., bandwidth, frequency, transmit power, storage capacity. As reported by Cisco, the data traffic demand will increase 500 folds in the next decade [164].

One potential solution is caching at the central cloud (CC), which stores all information at the data center or core network. Nevertheless, the CC faces many problems such as network congestion and high transmission delay due to many users connecting to the CC simultaneously and distant from users to CC, reducing system performance. To this end, Mobile Edge Caching (MEC) was recently proposed to eliminate the shortcomings of the traditional CC due to its close proximity to end-users. Consequently, MEC provides high bandwidth connectivity and comes hand-in-hand with ultra-low latency in computational offloading tasks. The architecture of caching at the CC and MEC is described in Fig. 2.9.

In Fig. 2.10, we illustrate different caching locations in cellular networks. Specifically, when user A requests for a file f, it first checks in the local storage. If user A has already

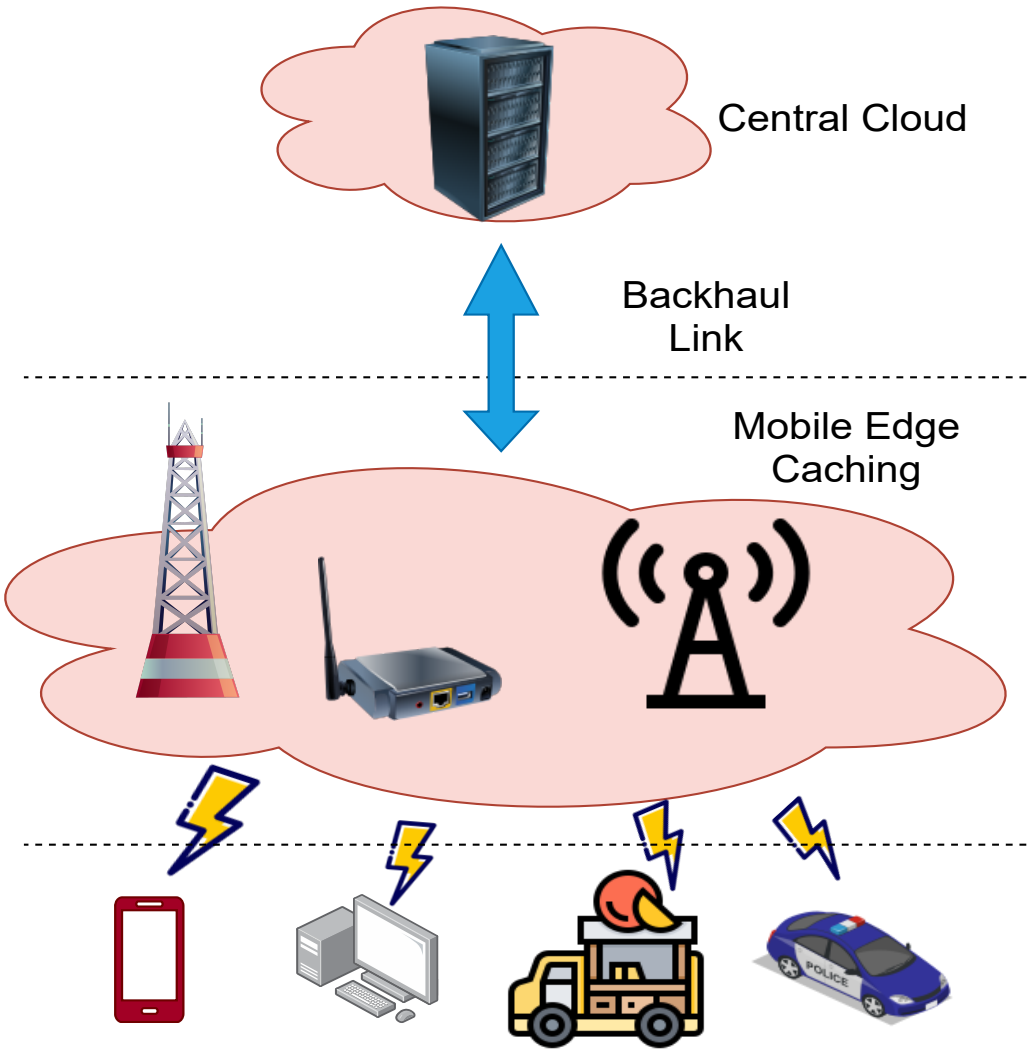

FIGURE 2.9: Caching at the central cloud and the edge networks.

cached the file f, it can be served by itself, and this scenario is local caching. Otherwise, user A can send a request to its proximity neighbors. If any user stores the requested file, it can transfer to users A, and this scenario is device-to-device caching. If both user A and its neighbors do not cache the requested file, it can send a request to the small base station (SBS). If the SBS has file f, it transmits directly to user A, and this is SBS caching. When the SBS does not cache the requested file, a request can be sent to the MBS. Then, the MBS will send file f to user A through SBS, which is MBS Caching.

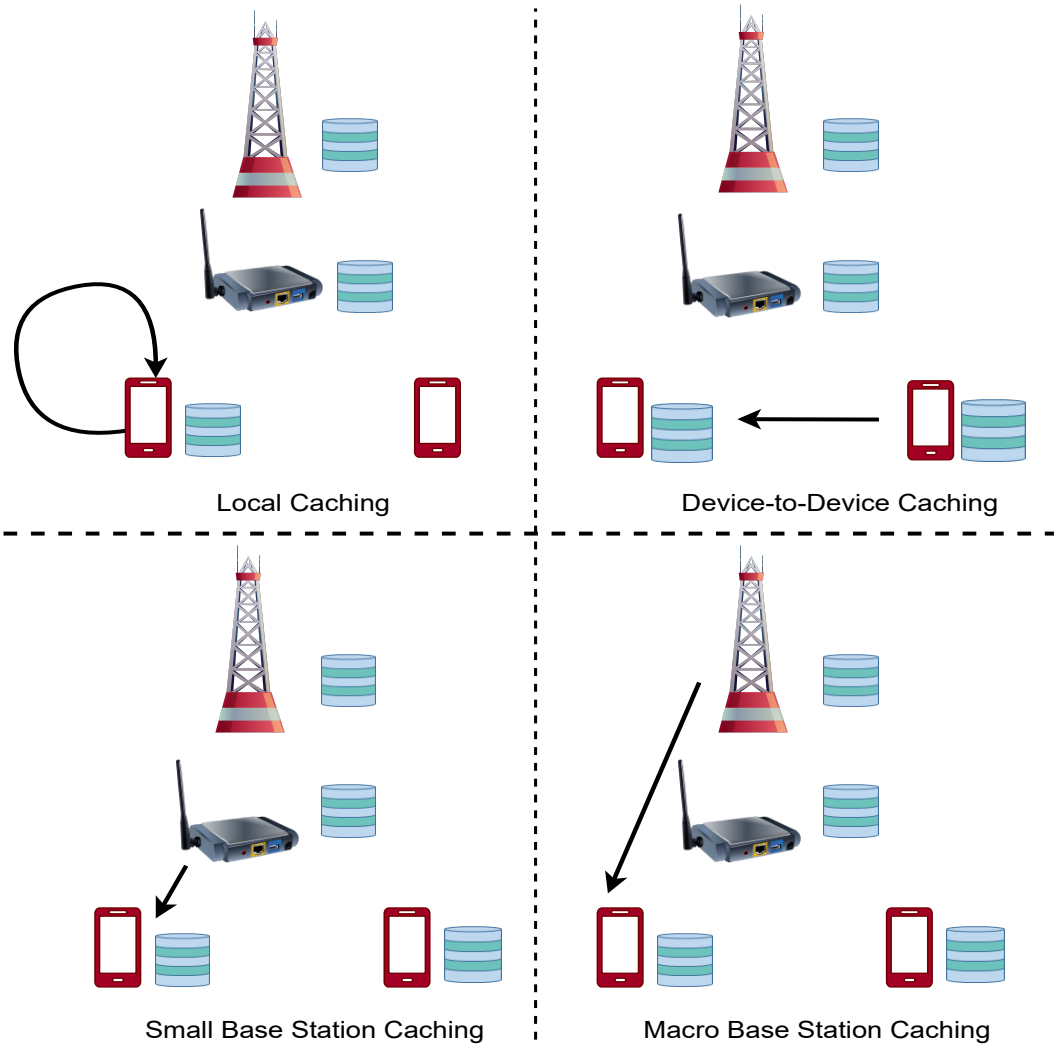

FIGURE 2.10: Different caching locations in cellular networks.

Due to the great benefit of caching, which helps to reduce congestion in the wireless network at peak times, it becomes a mainstream technology for the next generation of wireless systems, i.e., 6G networks [165, 166]. Specifically, 6G technology provides a lower delay and higher bandwidth, which can support high-speed vehicles (HPVs) to transfer a large amount of data in a short time. Nevertheless, since HPVs move faster than mobile users, they may be out of the current SBS radio transmission range. Thus, they need to shake hands between small base stations (SBSs) more often, which leads to a larger

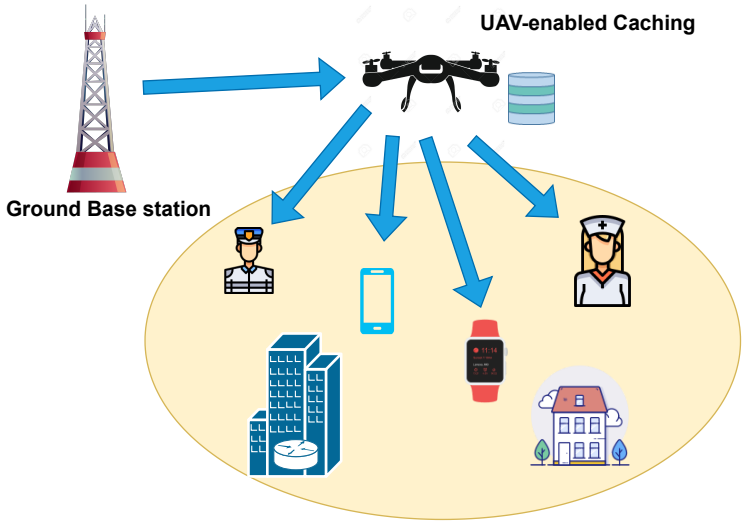

a. Cache-enabling UAV for data dissemination

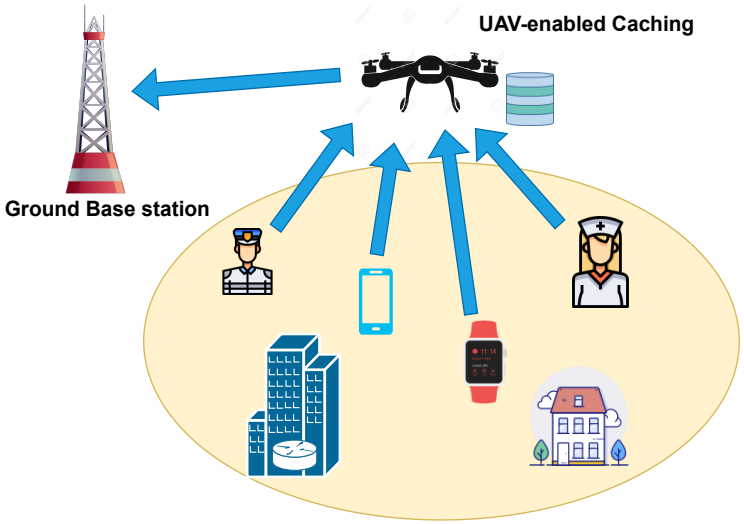

a. Cache-enabling UAV for data collection

FIGURE 2.11: Caching-enabling UAV communications.

request delay and higher packet error rates. Moreover, when the current SBS does not cache the file, it needs to send a request to the macro base station and/or to the cloud center. Caching contents at different levels, i.e., macro base stations (MBSs), SBSs, and

local cache, helps to reduce the redundant traffic load in the network and decreases data congestion [166]. Therefore, caching becomes a high promising technique for 6G in general and HPVs in particular.

Besides the advantages, caching also does not significantly improve the network condition for ground users (GUs) who do not have a good connection to the terrestrial network, i.e., terrestrial BS is overloaded or destroyed after a natural disaster or due to deep fading. In these cases, UAV is used as a relay to help transfer information to the GUs due to its fast deployment, high mobility, and LoS transmission links. The examples of UAV-enabled communication with proactive caching are illustrated in Fig. 2.11, where we show two scenarios for caching-enabling UAV communications. In the first scenario, a UAV can cache popular files during off-peak times, and it plays as a flying BSs to disseminate information to GUs. In the second scenario, a cache-enabled UAV is deployed to collect information from IoT users and transfer it back to the ground BS.

Recently, many works such as [167–171] have been devoted to cache-assisted UAV communications. Xu et al. [167] proposed a novel scheme to overcome the endurance issue at the UAV by utilizing proactive caching. Specifically, they aimed at minimizing the weighted sum of the file caching cost and the retrieval cost by jointly optimizing the UAV communication scheduling, UAV trajectory, and file caching policy. Cheng et al. [168] proposed a novel scheme to assure the secure transmission for UAV relay networks with caching capability. The learning-based approaches in cache-enabled UAV communications were investigated in [169–171]. Chen et al. [169] proposed the first work to analyze the utilization of caching in UAV communications based on conceptor-based echo state networks (ESNs). Different from existing works that focused on finite-time horizon offline trajectory design, Chai et al. [170] proposed an online trajectory and resource allocation optimization for cache-enabled UAV wireless communications. Wu et al. [171] adopted a convolutional neural network (CNN)-based deep supervised learning scheme for pushing up the decision-making speed in the highly dynamic vehicular networks.

Chapter 3

Traveling Salesman Problem with Time Windows (TSPTW)-based Trajectory Design for UAV communications

In this chapter, we design the UAV trajectory to minimize the total energy consumption while satisfying the requested timeout (RT) requirement and energy budget, which is accomplished via jointly optimizing the path and UAV's velocities along subsequent hops. The corresponding optimization problem is difficult to solve due to its non-convexity and combinatorial nature. To overcome this difficulty, we solve the original problem via two consecutive steps. Firstly, we propose two algorithms, namely heuristic search, and dynamic programming (DP) to obtain a feasible set of paths without violating the GU's RT requirements based on the traveling salesman problem with time window (TSPTW). Then, they are compared with exhaustive search and traveling salesman problem (TSP) used as reference methods. While the exhaustive algorithm achieves the best performance at a high computation cost, the heuristic algorithm exhibits poorer performance with low complexity. As a result, the DP is proposed as a practical trade-off between the exhaustive and heuristic algorithms. Specifically, the DP algorithm results in near-optimal performance at a much lower complexity. Secondly, for given feasible paths, we propose an energy minimization problem via a joint optimization of the UAV's velocities along subsequent hops. Finally, numerical results are presented to demonstrate the effectiveness of our proposed algorithms. The results show that the DP-based algorithm approaches the exhaustive search's performance with a significantly reduced complexity. It is also shown that the proposed solutions outperform the state-of-the-art benchmarks in terms of both energy consumption and outage performance.

The chapter is organized as follows. Introduction to the current state of the art is

discussed in Section 3.1. Section 3.2 introduces the system model. The energy-efficient UAV communication with path design and velocity optimization is analyzed in Section 3.3. Section 3.4 shows the simulation results. Finally, Section 3.5 provides the summary and concluding remarks of this chapter.

3.1 Introduction to TSPTW-based Trajectory Design for UAV Systems

With the proliferation of mobile devices and data-hungry applications, the next generation wireless networks are expected to support not only the unprecedented traffic increase and stringent latency but also ubiquitous coverage requirements. Although heterogeneous networks (HetNets) [172] and cloud radio access networks (C-RANs) [173,174] have shown their capability in supporting massive network traffics, their deployments are usually focused on dense areas. In less-dense areas, e.g., urban, and places where the network traffic highly fluctuates, the employment of C-RANs is economically inefficient. In such cases, the current terrestrial network architecture might suffer network congestion or be unable to support the ubiquitous coverage.

Recently, unmanned aerial vehicles (UAVs) have attracted much attention as a promising solution for improving the performance of terrestrial wireless communication networks thanks to their mobility, agility, and flexible deployment [175]. By employing a flying base station, UAVs can be deployed along with ground base stations (GBSs) to provide pervasive coverage and timely applications to ground users (GUs). Consequently, the deployment of UAVs in wireless communications has found applications in various domains, such as disaster rescue mission [176], surveillance [177], and smart farming [178]. Besides many advantages, UAV-enabled communications are not without limitation. The inherent limitations of UAVs has imposed technical restrictions on size, weight, and power capability (SWAP), which consequently affect the UAV's endurance and performance [13]. One of the major challenges in UAV deployment is to efficiently design the trajectory in order to maximize the UAV's service lifetime.

Certain efforts have recently been devoted to efficient UAV trajectory design [13,16,17, 179–184]. Yang et al. in [179] investigate the different Pareto efficiency between the optimal GU transmit power and UAV trajectory design. Phu et al. [180] use UAV as a friendly jammer to maximize the average secrecy rate of the cognitive radio network (CRN) by jointly optimizing the transmission power and UAV trajectory. Reference [13] designs the trajectory of UAV to minimize the mission completion time in UAV-enabled multi-casting systems based on the traveling salesman problem (TSP). References [181–183] study more

complicated scenarios with multiple UAVs. The authors of [181] investigate the dual-UAV enabled secure communication system via jointly optimizing the UAV trajectories and user scheduling. Reference [182] optimizes the UAV trajectory, transmit power and user scheduling to maximize the achievable secrecy rate per energy consumption unit in UAV-enabled secure communications. References [16,17,185] study more complicated UAV enabled communications systems with 3-D trajectory.

Due to the limited endurance and on-board energy of UAVs, the problem of UAV energy minimization has attracted much attention [15, 186–188]. The work [186] applies the genetic algorithm to design the trajectory with the least energy consumption to visit all BSs and return to the UAV station. Reference [187] minimizes the completion time and energy consumption problems for a fixed-wing UAV-enabled multicasting system via jointly optimizing the flying speed, UAV altitude, and antenna beamwidth. In [188], the authors consider the joint problem of the sensor nodes' wake-up schedule and the trajectory to minimize the maximum energy consumption while guaranteeing the reliability of the data collected from the sensors. Nevertheless, these works did not consider UAV's propulsion energy consumption, which is important for UAV's lifetime. In [15], the authors derive a closed-form propulsion power consumption model for rotary-wing UAVs. Then, by using this model, they aim at minimizing the total energy consumption via joint optimization of trajectory and time scheduling between GUs. Based on the energy model in [15], [188] minimizes the maximum energy consumption of all Internet-of-Things (IoT) devices while complying with the energy budget requirement.

Recently, there has been a growing research interest in applying dynamic programming (DP) in UAV-enabled wireless communications [189, 190]. The authors in [189] solve the problem of flight time minimization for data collection in a one dimensional wireless sensor networks (WSNs). More specifically, the DP algorithm is proposed to find the optimal data collection intervals of multi-sensors. In [190], the problem of optimizing the spectrum trading between macro base station (MBS) manager and UAV operators is solved. Then, the DP is adopted to find the optimal bandwidth allocation which is the most suitable for each UAV operator.

The aforementioned works have addressed the various new challenges in UAV-enabled communications, such as completion time minimization [13], energy minimization [15,186–188], and throughput maximization [185]. Moreover, efficient methods have been devised to deal with complicated optimization problems, e.g., time discretization method [17,188], path discretization method [15], block coordinate descent (BCD) in combination with the successive convex approximation (SCA) method [14], and efficient trajectory design [13]. Specifically, [13,15] and [14] have proposed a new framework to design an efficient trajectory by applying TSP solution. Basically, the TSP asks the question of finding the shortest path

that visits all users in the network and returns to the origin point which is an NP-hard problem in combinatorial optimization. Thus, a joint problem of trajectory design and other communications factors (e.g., communication scheduling, transmit power allocation, time allocation) in [14, 15] is even more challenging. In order to overcome these problems, the authors of [14, 15] are wisely using TSP solution as an initialized feasible trajectory in their proposed iterative algorithms.

To overcome the limitation in [13–15], our work studies the UAV-enabled communications systems in practical scenarios in which the GUs' transmissions are subject to some latency or requested timeout (RT) constraints. The considered system is motivated from realistic communication-related applications, e.g., content delivery networks [191] or the age of information or data collection, in which when a GU requests content data, it needs to be served within a certain RT. For example, in an emergency case or during a natural disaster, data need to be collected/transmitted promptly for evaluations/disseminations of the current situation in a given area. Concretely, the data from sensor nodes with limited storage capacity need to be collected in time for the continuous measurements before it becomes useless or being overwritten by incoming data. Besides that, the vital information must be disseminated to people about incoming disaster as soon as possible. Depending on the important role of each region, the different requested timeout values will be assigned for each area. Our goal is to design an energy-efficient UAV trajectory while guaranteeing the predefined RT constraints of all GUs. It can be seen that the considered system is clearly different from [13–15]. Therefore, the TSP-based method in those works can not be directly applied for our scenario. This motivates us to propose a new approach to solve problem of UAV trajectory design for energy minimization with latency constraints. Concretely, we propose trajectory design algorithms based on TSPTW which is a generalization of the classic TSP and has applications in many important sequencing and distribution problems [192]. The TSPTW requires that each node (or user) must be visited within a predefined time window. The time window includes start time and end time (or requested timeout) associated with each node in the network. The start time and end time define when the service at the considered node can begin and finish. The main contributions of this chapter are four-fold, listed as follows

1. Firstly, we find a feasible set of paths while satisfying the RT constraints for all GUs. In order to deal with the nature NP-hardness of the formulated problem, we propose two algorithms, namely, *DP*, and *heuristic* algorithms based on the TSPTW and they are compared with *exhaustive search* and TSP-based method [13, 15]. While the exhaustive search algorithm provides the global optimality, its exponential computation complexity might limit its applicability in practical applications. In such cases, the heuristic algorithm with a lower complexity is often considered to be a suitable replacement. However, this solution significantly decreases the performance

compared to that of exhaustive search. Thus, DP is proposed as a new algorithm to balance between exhaustive and heuristic algorithms. Especially, its performance converges to that of exhaustive at a much lower complexity.

2. Secondly, we minimize the total UAV's energy consumption for each given path in a feasible set via a joint optimization of the UAV velocities in all hops. Since the formulated problem is proved to be convex, it can be solved by using standard methods. Then, the path with lowest energy consumption which also satisfies the energy budget constraint is selected as a designed trajectory for UAV. Notably, in this chapter all the computation for path design is performed in an offline manner, i.e., prior to the UAV flight.

3. Finally, the effectiveness of the proposed algorithms is demonstrated via numerical results, which show significant improvements in both energy consumption and outage probability compared with our benchmarks [13, 15].

3.2 System Model

We consider a UAV-enabled communication system in which a UAV helps to transmit data to a set of K ground users (GUs), denoted by $\mathcal{K} \triangleq \{1, \ldots, K\}$. Due to limited access, the users can only receive data from the UAV [13, 15]. The location of GU k is denoted as $\mathbf{q}_k \in \mathbb{R}^{2\times 1}, k \in \mathcal{K}$. Let $(u_1, u_2, \ldots, u_K)$ be a permutation of $(1, 2, \ldots, K)$, and let $\mathbf{u} \triangleq [u_1\ u_2\ \cdots\ u_K]^T$ specify a trajectory of the UAV to serve all users following the path $0 \to u_1 \to u_2 \to ... \to u_K \to 0$, where 0 denotes the UAV station (or depot). It is assumed that GU k is required to be served within n_k units of time after the start of the UAV's mission. We refer to n_k as the requested timeout of GU k, for $k \in \mathcal{K}$.

3.2.1 Trajectory Design Model

In literature, there are different trajectory design models for UAV communications, e.g., Table 3.1. Basically, it can be classified into two types such as coarse (e.g., hovering-communications [13]) and fine trajectory design (e.g., fly-hover-communication (FHC) and flying-and-communication (FAC) methods in [15], virtual base station (VBS) as waypoints (VAW) and waypoints based on VBS placement and convex optimization (WVC) methods in [13]). In hovering-communications method, the UAV has to move to GU k's location and keeps hovering during the transmission period. The authors in [13, 15] utilize TSP to find the visiting order of K GUs' locations. Based on this result, the FHC method optimizes the visited locations, each for communicating with one GU, instead of hovering over each GU. The VAW is similar to FHC method, the difference is that each hovering location in VAW is for communicating with a group of GUs. In [13], FAC method, an updated version

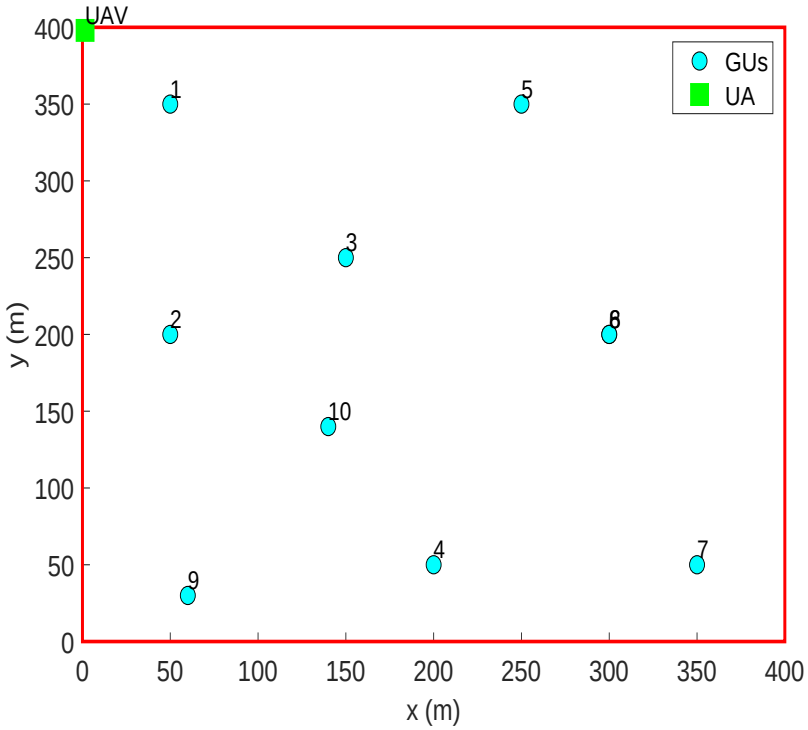

FIGURE 3.1: System model.

of FHC, is proposed in which the UAV can communicate while flying. In [15], the authors improve VAW method by proposing a more efficient waypoint (i.e., hovering point) design to reduce the traveling distance, i.e., WVC method. Based on these examples, we can conclude that the fine trajectory design can be obtained based on the coarse one.

In this chapter, hovering-communication is applied as the trajectory design model since it is a very intuitive protocol that is also easy to implement in practice. Fig. 3.1 depicts a two-dimensional Cartesian coordinate system, whereas the UAV is located at the ground station and the GUs are located in the considered area.

3.2.2 Transmission Model

The UAV's trajectory is split into $K+1$ line segments (or hops) which are represented by all connections between $K+2$ way-points on any given route. We assume that the UAV flies at a constant altitude of H (meters). Therefore, the distance traveled from GU j to

TABLE 3.1: Trajectory design methods

Name	**No. of visited GUs per 1 hovering point**	**Hovering point design**
Hovering-communications [13]	1	GU's location as hovering points
FHC [15]	1	Hovering point is within the GUs' transmission range
FAC [15]	1	Hovering point is within the GUs' transmission range and UAV transmits data when flying
VAW [13]	Multi-GUs	Hovering point is the VBS defined as the center of a group of GUs
WVC [13]	Multi-GUs	Based on VBS in VAW, they optimize the hovering point using optimization method

GU k is given by

$$l_{j\to k} = \|\mathbf{q}_j - \mathbf{q}_k\|, 0 \le j, k \le K+1, \tag{3.1}$$

where the index 0 represents the UAV station. We assume that the UAV velocity is constant during each hop but can change from hop to hop.

For $i = 1, 2, \dots K+1$, let v_i denote the UAV velocity at the i-th hop, while for $k = 1, 2, \dots, K$, τ_k stands for the transmission time needed for UAV to send the requested data stream to GU k reliably. Then, for a given trajectory signified by $\mathbf{u}$, the time for the UAV to reach the GU u_k is calculated as

$$T_k = \sum_{i=1}^{k} \left(t_{u_i} + \tau_{u_i}\right), \quad \text{for } 1 \le k \le K, \tag{3.2}$$

where $t_{u_i} \triangleq \dfrac{d_i}{v_i}$ and $d_i = l_{u_{i-1}\to u_i}$ represent the travel time and the distance in the i-th hop, respectively, for $i = 1, 2, \dots, K+1$.

We assume the channel between the GU and the UAV follows a Rician fading [193,194], where channel coefficient between GU k and UAV, h_k, can be written as

$$h_k = \sqrt{\mu_k} g_k, \tag{3.3}$$

where μ_k represents for the large-scale average channel power gain accounting for signal attenuation including pathloss and g_k accounts for small-scale fading coefficient.

In particular, μ_k can be modeled as

$$\mu_k = \mu_0 H^{-\alpha}, \tag{3.4}$$

where μ_0 is the average channel power gain at the reference distance, and α is the path loss exponent. Then, the small scale fading g_k with expected value $\mathbb{E}\left[|g_k|^2\right] = 1$, is given by

$$g_k = \sqrt{\frac{G}{1+G}}\overline{g}_k + \sqrt{\frac{1}{1+G}}\widetilde{g}_k, \tag{3.5}$$

where G is the Rician factor; $\overline{g}_k$ denotes the deterministic LoS channel component; $\widetilde{g}_k \sim \mathcal{CN}(0,1)$ denotes the Rayleigh fading channel accounting for NLoS components. Then, the maximum achievable rate between the UAV and GU k is calculated as

$$R_k = B\log_2\left(1 + \Upsilon|g_k|^2\right), \tag{3.6}$$

where $\Upsilon \triangleq \frac{P_{com}\mu_0}{H^\alpha\sigma^2}$, B is the channel bandwidth, P_{com} is the transmit power of the UAV, and σ^2 is the noise power.

As the lack of the knowledge for instantaneous channel state information (CSI) prior to the UAV's flight, the rate R_k is not exactly known. Therefore, the approximated rate for GU k is adopted, i.e., $\overline{R}_k$. Specially, $\overline{R}_k$ is chosen so that $\mathbb{P}\{R_k < \overline{R}_k\}$ remains below or equals to a target ϵ. Moreover, the outage probability that the GU k cannot successfully receive the transmitted data from UAV, i.e., $\mathbb{P}\{R_k < \overline{R}_k\}$, is expressed mathematically as follows [193]:

$$\begin{aligned}
&\mathbb{P}\{R_k < \overline{R}_k\} \\
&= \mathbb{P}\left\{|g_k|^2 < \frac{\left(2^{\overline{R}_k/B} - 1\right)}{\Upsilon}\right\} \\
&= 1 - Q_1\Big\{x_Q, y_Q\Big\} \leq \epsilon,
\end{aligned} \tag{3.7}$$

where $x_Q \triangleq \sqrt{2K}$, $y_Q \triangleq \sqrt{2\Big(2^{\overline{R}_k/B} - 1\Big)(1+G)/\Upsilon}$, $Q_1(x,y)$ is the first order Marcum Q-function. Moreover, at maximum tolerable value of ϵ, i.e., $Q_1\Big\{x_Q, y_Q\Big\} = 1 - \epsilon$, y_Q is

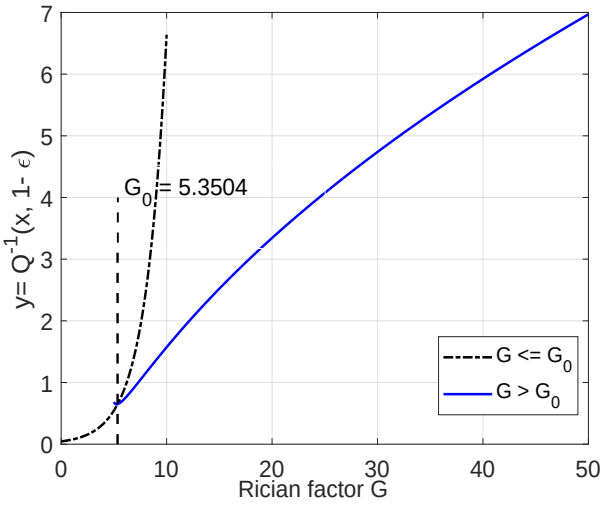

FIGURE 3.2: y_Q curves corresponding to its sub-functions, with $\epsilon = 0.001$.

defined as [193]

$$y_Q = \begin{cases} \sqrt{-2\log(1-\varepsilon)}e^{G/2}, G \leq G_0, \\ \sqrt{2G} + \dfrac{1}{2Q^{-1}(\varepsilon)} \log\left(\dfrac{\sqrt{2G}}{\sqrt{2G} - Q^{-1}(\varepsilon)}\right), \\ \sqrt{2G} + \dfrac{1}{2\sqrt{2G}}, G > G_0 \;\&\; Q^{-1}(\varepsilon) = 0, \end{cases} \tag{3.8}$$

where G_0 is the intersection of sub-functions at $\sqrt{2G} < \max[0, Q^{-1}(\epsilon)]$ and $Q^{-1}(x)$ is the inverse Q-function. Fig. 3.1 shows that G_0 can be obtained graphically based on the y_Q sub-functions.

In this chapter, since UAV hovers right above the user, we can consider a Rician channel with strong LoS component (i.e., high G factor) and $Q^{-1}(\epsilon) \neq 0$. Thus, the y_Q function can be approximated as $y_Q = \sqrt{2G} + \frac{1}{2Q^{-1}(\epsilon)} \log\left(\frac{\sqrt{2G}}{\sqrt{2G}-Q^{-1}(\epsilon)}\right) - Q^{-1}(\epsilon)$. This yields the approximated rate $\overline{R}_k$ can be expressed as:

$$\overline{R}_k = B\log_2\left(1 + \frac{{y_Q}^2\Upsilon}{2(1+G)}\right), \tag{3.9}$$

We adopt the Rician model because it can capture both LoS and NLoS links.

3.2.3 Energy Consumption Model

The energy consumption of the UAV consists of two types: propulsion energy consumption and communication energy consumption. The former measures the energy consumed to fly or hover over the UAV. The latter is used to transmit data to the GUs. In general, the energy consumption depends not only on the UAV velocity, but also on its acceleration/deceleration. Note that the energy consumption during UAV's acceleration/deceleration is ignored in [14, 15] which is reasonable for scenarios when the acceleration/deceleration speed or acceleration/deceleration duration is small. The power consumption of a rotary-wing UAV flying at velocity v is given as [15, Eq. (12)]

$$P_{\text{fly}}(v) = \underbrace{P_0\left(1+\alpha_1 v^2\right)}_{\text{bladeprofile}} + \underbrace{P_1\sqrt{\sqrt{1+\alpha_2^2 v^4}-\alpha_2 v^2}}_{\text{induced}} + \underbrace{\alpha_3 v^3}_{\text{parasite}}, \tag{3.10}$$

where $P_0 = \frac{\delta}{8}\rho s A \Omega^3 R^3$, $P_1 = (1+I)\frac{W^{3/2}}{\sqrt{2\rho A}}$, $\alpha_1 = \frac{3}{\Omega^2 R^2}$, $\alpha_2 = \frac{1}{2V_R^2}$, and $\alpha_3 = 0.5 a_0 \rho s A$. Blade profile power, parasite power, and induced power are needed to overcome the profile drag of the blades, the fuselage drag, the induced drag of the blades, respectively. Other parameters are explained as in Table I of [15].

For $i = 1, 2 \ldots, K+1$, the total energy consumption that the UAV spends on hop i is given as

$$E_i(v_i, d_i) = E_{\text{fly},i}(v_i, d_i) + E_{\text{hov},i} + E_{\text{com},i}, \tag{3.11}$$

where $E_{\text{fly},i}(v_i, d_i) = P_{\text{fly}}(v_i) \times t_{u_i} = P_{\text{fly}}(v_i) \times d_i/v_i$, $E_{\text{hov},i} = P_{\text{fly}}(v_{\text{hov}}) \times \tau_{u_i}$, and $E_{\text{com},i} = P_{\text{com}} \times \tau_{u_i}$ are the energy consumption due to flying, hovering, and communications, respectively, where $P_{\text{fly}}(v_i)$ is provided in (3.10). When UAV approaches the GU, it will fly around the GU with certain velocity v_{hov} instead of hovering directly above it to minimize the energy consumption [15]. Moreover, the energy consumption due to hovering is $E_{\text{hov},k} = P_{\text{fly}}(v_{\text{hov}}) \times \tau_k$, where $P_{\text{fly}}(v_{\text{hov}})$ and τ_k are the propulsion energy consumption due to hovering and transmission time to serve GU k, respectively. Furthermore, τ_k is computed as $\tau_k \triangleq Q_k/\overline{R}_k$, where Q_k denotes the length of the requested content in bits and $\overline{R}_k$ denotes the approximated transmission rate from the UAV to GU k. Since Q_k and $\overline{R}_k$ can be obtained prior to the UAV flight. Thus, $E_{\text{hov},k}$ is proportional to $P_{\text{fly}}(v_{\text{hov}})$ which is minimized at v_{hov} value as in Fig. 3.3.

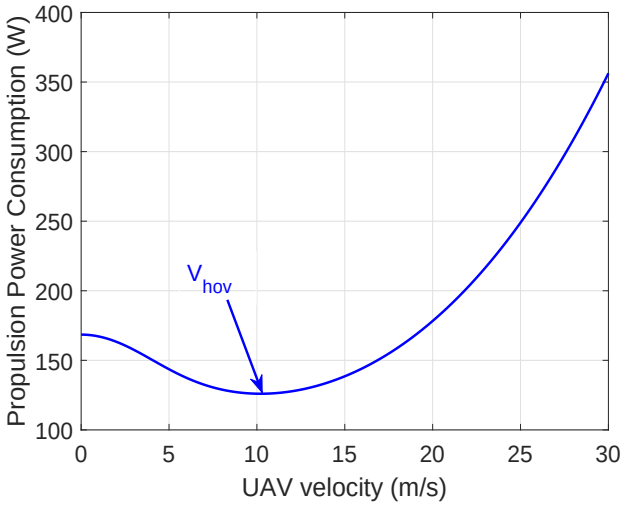

FIGURE 3.3: Propulsion power consumption versus velocity.

3.3 Energy-efficient UAV communication with path and velocity optimization

Our goal is to jointly design the path and velocities to minimize the total energy consumption while satisfying the RT constraints and energy budget for all GUs. Intuitively, we aim to find the visiting order $\mathbf{u} \triangleq [u_1, \ldots, u_K]$ and the UAV velocities which result in the smallest energy consumption. Then, the problem is formulated as

$$\begin{aligned}
\mathcal{P}_1^{\mathrm{EE}}: \min_{\mathbf{u},\{v_i\}_{i=1}^{K+1}} \quad & \sum_{i=1}^{K+1} \left(E_{\mathrm{fly},i}(v_i, d_i) + E_{\mathrm{hov},i} + E_{\mathrm{com},i}\right) \qquad (3.12)\\
\texttt{s.t.} \quad & \mathrm{C1}: \sum_{i=1}^{k} \left(\frac{d_i}{v_i} + \tau_{u_i}\right) \leq n_{u_k}, \quad \text{for} \quad 1 \leq k \leq K\\
& \mathrm{C2}: \ 0 \leq v_i \leq V_{\max}, \quad \text{for } 1 \leq i \leq K+1,\\
& \mathrm{C3}: \sum_{i=1}^{K+1} \left(E_{\mathrm{fly},i}(v_i, d_i) + E_{\mathrm{hov},i} + E_{\mathrm{com},i}\right) \leq E_{\mathrm{tot}},\\
& \mathrm{C4}: |v_{i+1} - v_i| \leq \Delta V, \forall 1 \leq i \leq K.
\end{aligned}$$

In $\mathcal{P}_1^{\mathrm{EE}}$, constraint C1 guarantees the RT requirement for the GUs which states that the maximum latency to serve GU u_k cannot exceed the predefined RT n_{u_k}, C2 requires that the flying speed of the UAV must be less than the maximum velocity $V_{\max}$, and C3

means that the total energy consumption of UAV on the considered path should not exceed the total energy budget E_{tot}. Otherwise, this is an infeasible path. C4 guarantees that the traveling speed of UAV between two consecutive hops is less than a predetermined value.

Problem (3.12) requires optimizing the path $\mathbf{u}$ and traveling velocities $\{v_i\}_{i=1}^{K+1}$ of the UAV on all hops. Note that (3.12) includes a complicated energy consumption as in C3, as well as an objective function which depends on the designed path $\mathbf{u}$. However, as the objective function is the same of the LHS in C3, we can, without loss of generality, solve $\mathcal{P}_1^{\text{EE}}$ without C3 and find the minimum total energy consumption. If this energy is less than E_{tot}, then $\mathcal{P}_1^{\text{EE}}$ is feasible and its solution is the same as the solution to $\mathcal{P}_1^{\text{EE}}$ without C3, otherwise $\mathcal{P}_1^{\text{EE}}$ is not feasible and we say *outage* has occurred.

Definition 1. *The OP is defined as $\mathbb{P}\{R_k < \overline{R}_k\}$ or the probability that no feasible path (a path that satisfies all the GUs' RT requirements and E_{tot}) is found.*

Note that even without C3, problem $\mathcal{P}_1^{\text{EE}}$ is a TSPTW, itself is already NP-hard [192]. To solve this problem, we first find the feasible set of paths (denoted as $\mathcal{U}^\star$) which satisfy constraints C1 while the hop velocities satisfy C2. Next, we will minimize the energy consumption on each given path via joint optimization of velocities over all hops. Finally, the lowest energy consumption path which satisfies the energy budget constraint C3 is chosen as the trajectory design for UAV.

3.3.1 Obtain a feasible set of paths

In this section, we introduce three solutions, namely, exhaustive search, heuristic search, and DP algorithms to obtain a feasible set of paths that satisfy constraints C1, C2 and C4. The exhaustive search gives the best solution with very high complexity. The heuristic tries to reduce the complexity but the performance also decreases. Thus, the DP is proposed as a solution to balance between exhaustive search and DP algorithms.

Specifically, the feasible set of all paths which satisfy constraints C1, C2, and C4, i.e., $\mathcal{U}^\star$, will be obtained by choosing $v_i = V_{\max}$, for $i = 1, 2, \ldots, K+1$.

The proof of this property relies on the monotonically decreasing behavior of the LHS of constraint C1 with respect to v_i, for any given i. For any $k \in \mathcal{K}$, if a path satisfies C1 with $v_i < V_{\max}$, then this path satisfies C1 with $v_i = V_{\max}$, as the LHS of C1 is monotonically decreasing in v_i, for $i = 1, 2, \ldots, K$. Also, for any $k \in \mathcal{K}$, if a path does not satisfy C1 with $v_i = V_{\max}$, then this path does not satisfy C1 with $v_i < V_{\max}$, as $\sum_{i=1}^{k} \left(\frac{d_i}{v_i} + \tau_{u_i} \right) > \sum_{i=1}^{k} \left(\frac{d_i}{V_{\max}} + \tau_{u_i} \right) > n_{u_k}$.

By considering $v_i = V_{\max}$ as above discussion, the following subsections present three proposed algorithms to find a feasible set of paths.

Algorithm 1 Exhaustive search algorithm for solving $\mathcal{P}_2^{\text{EE}}$

1: **Input:** $V_{\max}$, $\{\mathbf{q}_k, \tau_k, n_k\}_{k=1}^{K}$.
2: **Initialize**: Calculate the set $\mathcal{I}$ containing all the paths, $\boldsymbol{n_0} = [n_1, \ldots, n_K]$, $\mathcal{U} = \emptyset$, $l_{0\to k} = \|\mathbf{q}_k - \mathbf{q}_0\|, a_{0k} = \frac{l_{0\to k}}{V_{\max}} + \tau_k, k \in \mathcal{K}$, $\mathbf{a} = [a_{01}, \ldots, a_{0K}]$.
3: **if** $\mathbf{a} \leq \boldsymbol{n_0}$ **then** ▷ Check feasibility
4: **for** $m = 1 : |\mathcal{I}|$ **do** ▷ For each path $\mathbf{u}^{(m)} \in \mathcal{I}$
5: $L_k^{(m)} = \sum_{i=1}^{k} \left(\frac{l_{u_{i-1}^{(m)} \to u_i^{(m)}}}{V_{\max}} + \tau_i \right)$ ▷ Total traveling time between GUs u_{i-1} and u_i in $\mathbf{u}^{(m)}$ and data transmission time to u_i
6: **if** $\mathbf{L}^{(m)} \preccurlyeq \boldsymbol{n_0}$ **then** ▷ Check the RT constraint
7: $\mathcal{U} = \mathcal{U} \cup \mathbf{u}^{(m)}$ ▷ Update feasible paths
8: **end if** **end if**
9: **end for** **end for**
10: Find Ψ shortest feasible paths, i.e., $\mathcal{U}^\star \in \mathcal{U}$
11: **end if** **end if**
12: **Output:** $\mathcal{U}^\star$.

Algorithm 1: Exhaustive search algorithm

The principle of the exhaustive search algorithm is to visit all the paths and find Hamiltonian cycle paths [195] satisfying the RT constraint. For each path in the feasible set, we minimize the energy consumption via jointly optimizing the velocities as in Section 3.3.2. Thus, in order to reduce the computational complexity for solving (3.12), we only take Ψ feasible paths into consideration.

This problem is in a form of TSPTW problem, which can be solved by finding the minimum cost tour (Hamiltonian cycle path) starting and ending at location 0 and visiting all GUs only once [192]. The details is summarized in Algorithm 1. Firstly, we initialize all the parameters as in lines 1 and 2. More specifically, $\mathbf{q}_k$, τ_k, n_k are the location, data transmission time, requested timeout constraint of GU k, respectively; $\mathcal{U}$ is the set containing all feasible paths; $l_{0\to k}$ and a_{0k} are the traveling distance from UAV to GU k and the total time needed for UAV to finish transmitting data to GU k, respectively.

Basically, Algorithm 1 consists of two steps. In the first step, we check the RT constraint from UAV station to each GU k, as in line 3. Based on the triangle inequality constraint, if there exists any GU k which does not satisfy the RT constraint, it has no feasible path. Otherwise, we will try all $K!$ paths which visits all the GUs once, lines 4 to 9. For each path $\mathbf{u}^{(m)} \in \mathcal{I}$, we calculate the UAV traveling time from u_{i-1} to u_i and data transmission time for u_i, with u_{i-1} and $u_i \in \mathbf{u}^{(m)}$. It then compares the visit time to every GU with the corresponding RT requirements (constraint C1 in (3.12)), as in line 6. If path $\mathbf{u}^{(m)}$ satisfies the RT constraint, it will be accumulated to set $\mathcal{U}$, line 7. Thus, the complexity

Algorithm 2 Heuristic algorithm for solving $\mathcal{P}_2$

1: **Input:** $V_{\max}$, $\{\mathbf{q}_k, \tau_k, n_k\}_{k=1}^{K}$.
2: **Initialize**: $\mathbf{U} = \emptyset$, $\mathcal{I}_+ = \emptyset$, $\mathcal{I}_- = \mathcal{K}$, $l_{0\to k} = \|\mathbf{q}_k - \mathbf{q}_0\|, a_{0k} = \frac{l_{0\to k}}{V_{\max}} + \tau_k, k \in \mathcal{K}$, $\mathbf{a} = [a_{01}, \ldots, a_{0K}]$, $\boldsymbol{n_0} = [n_1, \ldots, n_K]$.
3: **if** $\mathbf{a} \leq \boldsymbol{n_0}$ **then** ▷ Check feasibility in the first hop
4: Find the closet GU having minimum RT value, i.e., $u^\star \in \mathcal{I}_-$.
5: $\mathbf{U} = \mathbf{U} \cup \{u^\star\}$ ▷ If $u^\star$ satisfy constraint C1.
6: $\mathcal{I}_+ = \mathcal{I}_+ \cup \{u^\star\}$, $\mathcal{I}_- = \mathcal{K} \setminus \{u^\star\}$
7: Repeat steps 4 to 6 until $\mathcal{I}_- = \emptyset$ or no any GU satisfying the C1 constraint.
8: **end if**end if
9: **Output:** $\mathcal{U}^\star = \mathbf{U}$.

TABLE 3.2: Illustration for Travel Time between GUs in Heuristic Algorithm

GU	0	1	2	3
0	$+\infty$	1	1.2	1.3
1	1	$+\infty$	0.5	1.2
2	1.2	0.5	$+\infty$	2
3	1.3	1.2	2	$+\infty$

of Algorithm 1 is $\mathcal{O}(K!)$ [196]. Finally, the set of Ψ feasible paths which satisfies all the RT constraints and imposes the Ψ shortest traveling time will be selected.

Algorithm 2: Heuristic algorithm

Although providing near-optimal performance, the high computation complexity of Algorithm 1 may limit its potential in realistic scenarios. In this subsection, we propose a heuristic search algorithm, which compromises the performance against complexity. The key idea behind the heuristic algorithm is to restrict the search space at each step, in which it only foresees one hop ahead when checking the RT condition. Details of the heuristic algorithm are described in Algorithm 2.

Firstly, we initialize all the parameters as in lines 1 and 2. More specifically, $\mathbf{U}$ is the feasible path; we can check other parameters as in Algorithm 1. The searching in the heuristic algorithm consists of K steps, in which it maintains two sets: a set of visited GUs and another set of GUs which have not been visited, i.e., $\mathcal{I}_+$ and $\mathcal{I}_-$, respectively. First, we check the RT constraint for the first step (or hop) as in Algorithm 1, line 3. If the RT constraint from UAV station to each GU k is satisfied, then, we select the closet GU having minimum RT value as the first visited GU into the designed path, i.e., $\mathbf{U}$ as in lines 4 to 6. Then, we continue checking a until the set $\mathcal{I}_-$ is empty. In the other hand, if there has no GUs satisfying the RT constraint at the k-th step, it is not possible to find out the

Algorithm 3 DP-based algorithm for solving $\mathcal{P}_2^{\text{EE}}$

1: **Input:** $V_{\max}$, $\{\mathbf{q}_k, \tau_k, n_k\}_{k=1}^K$.
2: **Initialize**: $\Xi_1 \triangleq \{\xi_1\}$, $\xi_1 = (\{0\}, 0)$, $C(\{0\}, 0) = 0$, $\mathcal{A} = \{a_{jk}\}$, $\mathcal{U}^\star = \emptyset$, $l_{0\to k} = \|\mathbf{q}_k - \mathbf{q}_0\|, a_{0k} = \frac{l_{0\to k}}{V_{\max}} + \tau_k, k \in \mathcal{K}$, $\mathbf{a} = [a_{01}, \ldots, a_{0K}]$, $\boldsymbol{n_0} = [n_1, \ldots, n_K]$, $\mathcal{B}_1^0 = \emptyset$,
3: **if** $\mathbf{a} \leq \boldsymbol{n_0}$ **then** ▷ Check feasibility
4: $\Xi_m = \emptyset$
5: **for** $(\mathcal{S}, j) \in \Xi_{m-1}$ **do**
6: Update $\Xi_m = \Xi_m \cup ((\mathcal{S}, j) \cup k, k)$ ▷ If $C((\mathcal{S}, j) \cup k, k) \leq n_k$ and $C((\mathcal{S}, j) \cup k, k)$ is the minimum cost of all states $((\mathcal{S}, j) \cup k, k)$
7: Update $\mathcal{B}_m^k = \{j\}$
8: **end forend for**
9: $m = m + 1$
10: Repeat steps 4 to 7 until $|\mathcal{S}| = K + 1$ or no any GU satisfying the RT constraint.
11: For each state $(\mathcal{S}, k) \in \Xi_{K+1}$, the visiting order $\mathbf{u}_\star$ is obtained by checking for backward from Ξ_{K+1} to Ξ_1 based on $\mathcal{B}_m^k$.
12: $\mathcal{U}^\star = \mathcal{U}^\star \cup \mathbf{u}_\star$
13: **end ifend if**
14: **Output:** $\mathcal{U}^\star$.

feasible path. As shown in the Algorithm 2, the fundamental operations employed in the computation are additions and comparisons. The total number of operations needed to run Algorithm 2 from steps 1 to K is $\sum_{k=2}^{K}(K-k+1) = \frac{K(K+1)}{2}$ [197, Eq. (0.121.1)]. Thus, the complexity of the heuristic algorithm is $\mathcal{O}(K^2)$, which is significantly smaller than the complexity $\mathcal{O}(K!)$ of Algorithm 1.

To make it easy to understand, we would like to give an example of heuristic algorithm. More specifically, we consider $\mathcal{K} = \{1, 2, 3\}$, $\boldsymbol{n} = \{2, 2, 5\}$ seconds, $\tau_k = 0.12$ seconds, 0 denotes the UAV station, Table 3.2 is the travel time between GUs. Firstly, the vector $\mathbf{a} = [1.12, 1.32, 1.42]$ can be determined based on the equation $a_{0k} = \frac{l_{0\to k}}{V_{\max}} + \tau_k$ as in step 2. Then, the RT constraint can be checked as in step 3. Since all GUs k satisfy the constraint C1, thus, we update the feasible path $\mathbf{U} = 1$ and $\mathcal{I}_+ = 1$ and $\mathcal{I}_- = \{2, 3\}$ as in steps 4 and 5. Next, the accumulated traveling of UAV to next GUs in $\mathcal{I}_-$ can be computed as $a_{01} + a_{12} = 1.12 + 0.62 = 1.74 < n_2$, $a_{01} + a_{13} = 1.12 + 1.32 = 2.44 < n_3$. As $a_{01} + a_{12} < a_{01} + a_{13}$, we have $\mathbf{U} = 1 \to 2$, $\mathcal{I}_+ = \{1, 2\}$ and $\mathcal{I}_- = \{3\}$. Next, we check the RT constraint to GU 3, i.e., $a_{01} + a_{12} + a_{23} = 1.74 + 2.12 = 3.86 < n_3$. Then, we can update $\mathbf{U} = 1 \to 2 \to 3$, $\mathcal{I}_+ = \{1, 2, 3\}$ and $\mathcal{I}_- = \emptyset$. Finally, we obtain the feasible path $\mathcal{U}^\star = \mathbf{U}$ as the output of Algorithm 2, as in line 8.

Algorithm 3: Dynamic programming

Although having a lower complexity, Algorithm 2 obtains a much degraded performance compared with Algorithm 1. This motivates us to propose Algorithm 3, which is based on DP method. It will be shown later that the DP-based algorithm approaches the optimal solution with a considerably reduced complexity.

Denote $G = (\mathcal{K}, \mathcal{A})$, where $\mathcal{K}$ is the set of GUs and $\mathcal{A} = \{a_{jk}\}$ is the set of the summation of travel time from GU $j \to k$ and the data transmission time to GU k, e.g., $a_{jk} = l_{j\to k}/V_{\max} + \tau_k, j \neq k$. In this chapter, since we do not consider a_{jk} with $j = k$, thus, a_{jk} will henceforth be referred to as a_{jk} with $j \neq k$. Moreover, a_{jk} is feasible if it satisfies the RT constraint, i.e., $a_{jk} \leq n_k$. As in the first step of Algorithms 1 and 2, we check the feasibility by considering the RT constraint from UAV station to GU k, as in lines 3 of Algorithm 3. Concretely, if there exists a value of a_{0k} which does not satisfy the RT constraint, a feasible path will not exist. Associate with each GU $k \in \mathcal{K}$ a time window $[0, n_k]$ and a data transmission time τ_k.

A state $(\mathcal{S}, k)$ is defined as: $\mathcal{S}$ is an unordered set of visited GUs, k is the last visited GU in $\mathcal{S}$. Define $C(\mathcal{S}, k)$ as the least cost (e.g., summation of traveling time and data transmission time to GU k) of path starting at UAV station, passing through each GU of $\mathcal{S} \subset \mathcal{K}$ exactly once, ending at GU k. Without loss of generality, we initialize the cost function C as $C(\{0\}, 0)$ equals to zero, whereas the first and second elements represent for the UAV station. The $C(\mathcal{S}, k)$ is calculated by solving the following equation [192]

$$\begin{aligned} C(\mathcal{S}, k) = \min_{(a_{jk})\in\mathcal{A}} \{&C(\mathcal{S}\backslash\{k\}, j) + C(\{j, k\}, k) | \\ &C(\mathcal{S}\backslash\{k\}, j) + C(\{j, k\}, k) \leq n_k\}. \end{aligned} \tag{3.13}$$

where $C(\{j, k\}, k) = a_{jk} = l_{j\to k}/V_{\max} + \tau_k$, $\mathcal{S} \subset \mathcal{K}, j$ and $k \in \mathcal{S}$.

We denote $\mathcal{B}_m^k$ with $k \in \mathcal{K}, m = 1, 2, \ldots, K+1$ as the set containing the last visited GU before visiting GU k in step m, as in lines 2 and 7. Specifically, when an UAV starts from ground station, there is no visited GU before this, i.e., $\mathcal{B}_1^0 = \emptyset$ as in line 2. Let Ξ_m denote the set of all feasible states $(\mathcal{S}, k)$, where $|\mathcal{S}| = m$. In order to obtain Ξ_m from Ξ_{m-1}, we do following steps. For each state $(\mathcal{S}, j) \in \Xi_{m-1}$, we consider a new state $((\mathcal{S}, j) \cup k, k)$, lines 5 to 7. This state can be added to Ξ_m iff it satisfies the RT constraint and is not yet stored, as in line 6. In the case that this state is already stored in Ξ_m, we only keep the state having minimum cost of $C((\mathcal{S}, j) \cup k, k)$, as in line 6. Let assume that there exist two states with the corresponding cost functions $C_1(\mathcal{S}, k)$ and $C_2(\mathcal{S}, k)$, respectively. If $C_1(\mathcal{S}, k) < C_2(\mathcal{S}, k)$, then, the second state will be eliminated. The goal of DP algorithm is to take all the feasible paths satisfying constraints C1 and C2. Since we only store the state with lowest value of $C(\mathcal{S}, k), k = 1, \ldots, K$ for each state $(\mathcal{S}, k)$. Thus, at the end of Algorithm 3, when $|\mathcal{S}| = K + 1$, we can achieve maximally K states $(\mathcal{S}, k) \in \Xi_{K+1}$. For each state $(\mathcal{S}, k)$, the visiting order $\mathbf{u}^\star$ is obtained by checking for backward from Ξ_{K+1} to

TABLE 3.3: Illustration for the value of $\mathcal{A} = \{a_{jk}, j, k \in \mathcal{K}, \}$ in DP Algorithm

GU	0	1	2	3
0	$+\infty$	1	1.4	1.2
1	1	$+\infty$	0.5	1.5
2	1.4	0.5	$+\infty$	2
3	1.2	1.5	2	$+\infty$

TABLE 3.4: Illustration for DP Algorithm

Ξ	$\mathcal{S}$	k	$\mathcal{B}_m^k$	$C(\mathcal{S}, k)$
Ξ_1	$\{0\}$	0	$\mathcal{B}_1^0 = \emptyset$	0
Ξ_2	$\{0, 1\}$	1	$\mathcal{B}_2^1 = \{0\}$	1
Ξ_2	$\{0, 2\}$	2	$\mathcal{B}_2^2 = \{0\}$	1.4
Ξ_2	$\{0, 3\}$	3	$\mathcal{B}_2^3 = \{0\}$	1.2
Ξ_3	$\{0, 1, 2\}$	2	$\mathcal{B}_3^2 = \{1\}$	1.5
Ξ_3	$\{0, 1, 2\}$	1	$\mathcal{B}_3^1 = \{2\}$	1.9
Ξ_3	$\{0, 1, 3\}$	3	$\mathcal{B}_3^1 = \{1\}$	2.5
Ξ_4	$\{0, 1, 2, 3\}$	3	$\mathcal{B}_4^3 = \{1\}$	3.4

Ξ_1 based on $\mathcal{B}_m^k$, as in line 10. Finally, feasible Hamiltonian cycle paths $\mathcal{U}^\star$ with $|\mathcal{U}^\star| \leq K$ is acquired at the output of DP algorithm, as in line 12.

To make it easy to understand, the DP-based algorithm is illustrated in Tables 3.3 and 3.4. More specifically, we consider $\mathcal{K} = \{1, 2, 3\}$, $\boldsymbol{n} = \{2, 2, 4\}$ seconds, 0 denotes the UAV station, Table 3.3 is the travel time between GUs. Due to the RT constraint and the condition of storing one state with minimum cost $C(\mathcal{S}, k)$, we cannot keep all states into consideration. For example, when $\mathcal{S} = 3$, we only achieve one final state, i.e., $(\{0, 1, 2, 3\}, 3)$. For the last state $\{0, 1, 2, 3\} \in \Xi_4$, we can check for backward from Ξ_4 to Ξ_1 to find the feasible path $\mathbf{u}^\star$. More specifically, from state Ξ_4, we can find out that $1 \in \mathcal{B}_4^3$ is the last visited GU before visit 3. Next, by considering the state $(\mathcal{S}, 1) \in \Xi_3$, $2 \in \mathcal{B}_3^1$ is the last visited GU before visit 1. Similarly, we check for backward until reaching UAV station 0. Finally, the visiting order $\mathbf{u}^\star$ is obtained, i.e., $\mathbf{u}^\star = \{0 \to 2 \to 1 \to 3 \to 0\}$. The complexity of the DP-based algorithm is $\mathcal{O}(K^2 \times 2^K)$ in the worst case [198]. Moreover, details of this method are described in Algorithm 3.

3.3.2 Minimization of the UAV's Energy Consumption with given path

The previous section designs the paths based on the UAV maximum speed. While this method is preferred to minimize the traveling time, it might not be energy-efficient since it over-estimates the RT constraints. In this section, we minimize total energy consumption

of the UAV via the joint optimization of UAV velocities over each given path in the feasible set $\mathcal{U}^\star$, e.g., the output of Algorithms 1, 2, and 3. The energy minimization problem is formulated as

$$\begin{aligned}\mathcal{P}_2^{\mathrm{EE}}: \min_{\{v_i\}_{i=1}^{K+1}} \quad & \sum_{i=1}^{K+1}(E_{\mathrm{fly},i}(v_i)+E_{\mathrm{hov},i}+E_{\mathrm{com},i}) \\ \texttt{s.t.} \quad & \mathrm{C1}: \ \sum_{i=1}^{k}\left(\frac{d_i}{v_i}+\tau_{u_i}\right)\le n_{u_k}, 1\le k\le K \\ & \mathrm{C2}: \ 0\le v_i\le V_{\max}, \quad i=1,\ldots,K+1. \\ & \mathrm{C3}: |v_{i+1}-v_i|\le \Delta V, \forall 1\le i\le K,\end{aligned} \tag{3.14}$$

Because $E_{\mathrm{com},i}$ and $E_{\mathrm{hov},i}$ do not depend on v_i, they can be removed from the objective function of (3.14) without loss of generality. Since function $\frac{1}{x}$ is convex in $\{v_i\}_{i=1}^{K+1}\in\mathbb{R}^+$, constraint C1 in (3.14) is convex. The most challenging is the term $E_{\mathrm{fly},i}(v_i)$.

Lemma 2. *The energy consumption $E_{\mathrm{fly},i}(v_i)$ is convex.*

Proof: From (3.10) and (3.11) we have

$$\begin{aligned}E_{\mathrm{fly},i}(v_i)=P_0d_i\left(\frac{1}{v_i}+\alpha_1v_i\right)+&P_1d_i\sqrt{\sqrt{v_i^{-4}+\alpha_2^2}-\alpha_2} \\ &+\alpha_3d_iv_i^2,\end{aligned} \tag{3.15}$$

The second derivative of $E_{\mathrm{fly},i}(v_i)$, after some manipulations, can be expressed as

$$\frac{d^2}{dv_i^2}E_{\mathrm{fly},i}(v_i)=\frac{2P_0d_i}{v_i^3}+2\alpha_3d_i+P_1d_i\beta, \tag{3.16}$$

where

$$\begin{aligned}\beta=&\frac{1}{v_i^6\sqrt{\alpha_2^2+v_i^{-4}}\sqrt{\sqrt{\alpha_2^2+v_i^{-4}}-\alpha_2}}\times \\ &\left(5-\frac{2}{1+\alpha_2^2v_i^4}-\underbrace{\frac{1}{\alpha_2^2v_i^4+1-\alpha_2v_i^2\sqrt{\alpha_2^2v_i^4+1}}}_{\beta_1}\right).\end{aligned} \tag{3.17}$$

Denote $X=\alpha_2v_i^2\ge 0$, then we can express $\beta_1=\alpha_2^2v_i^4+1-\alpha_2v_i^2\sqrt{\alpha_2^2v_i^4+1}=X^2+$

$1 - X\sqrt{X^2+1}$. Since $X\sqrt{X^2+1} \leq \frac{2X^2+1}{2}$, it yields

$$\beta_1 \geq X^2 + 1 - \frac{2X^2+1}{2} = \frac{1}{2}. \tag{3.18}$$

In addition, since $1 + \alpha_2^2 v_i^4 \geq 1$, we obtain the term in bracket in (3.17) is always greater than or equal to 1. Thus, $\beta > 0, \forall v_i$. Since P_0, d_i, α_3 are also positive, from (3.16) we conclude that the second derivative of $E_{\text{fly},i}(v_i)$ is always positive, which proves the convexity of $E_{\text{fly},i}(v_i)$.

By using Lemma 2, we observe that problem $\mathcal{P}_2^{\text{EE}}$ is convex since the objective and all constraints are convex. Thus, it can be solved by using the standard methods [199].

3.4 Simulation Results

This section provides numerical results to validate the proposed designs. The parameters are set as follows: $H = 50$ meters, $B = 2$ MHz, path loss exponent $\alpha = 2.3$, $\sigma^2 = -110$ dBm, $P_{com} = 5$ W, Rician factor G = 15 dB, UAV's coverage area is 400 m x 400 m, UAV ground station is located at (1.5m, 398m). On a more general level, we perform 1000 independent trials of Monte-Carlo simulations. In details, for each iteration, we deploy a random GUs topology distributed in the considered area, the RT constraints are uniformly ranging between $n_{\min}$ and $n_{\max}$. Moreover, the channel coefficient g_k is also regenerated for each iteration. The proposed solutions are compared with a solution in [13,15], which is based on the TSP. Specifically, since the heuristic and DP algorithms can find maximally 1 and $\Theta \leq K$ feasible paths, respectively. In order to guarantee that the exhaustive method is always an upper bound, this algorithm takes Ψ ($\Psi \geq \Theta$) shortest feasible paths while the heuristic and DP algorithms take all feasible paths into consideration.

In Fig. 3.4, we illustrate the difference trajectory designs, i.e., TSP, exhaustive search, heuristic, and DP, with $\epsilon = 0.001$, $Q_k = 50$ Mbits, $n_{\min} = 5$ seconds, $n_{\max} = 17$ seconds, $K = 7$, $E_{\text{tot}} = 100$ KJoules. For the purpose of a fair comparison, $V_{\max}$ is assumed to be sufficiently large so that all methods exists one path complying with the latency constraints. The arrows in Fig. 3.4 denote the moving direction of UAV. While the TSP always follows the shortest path and does not take latency into account, the others select the path with minimum energy consumption via optimizing the traveling velocities. Therefore, the energy consumption of TSP is higher than others. Moreover, the heuristic method selects the closet GU having minimum RT value as the next visited GU, it leads to the longer traveling distance. This explains why the energy consumption of heuristic is higher than exhaustive and DP methods. Specifically, the DP method may obtain the same trajectory design compared to that of exhaustive search. It shows the superiority of this scheme compared to other ones.

Next, we evaluate the proposed trajectory designs via the outage probability metric

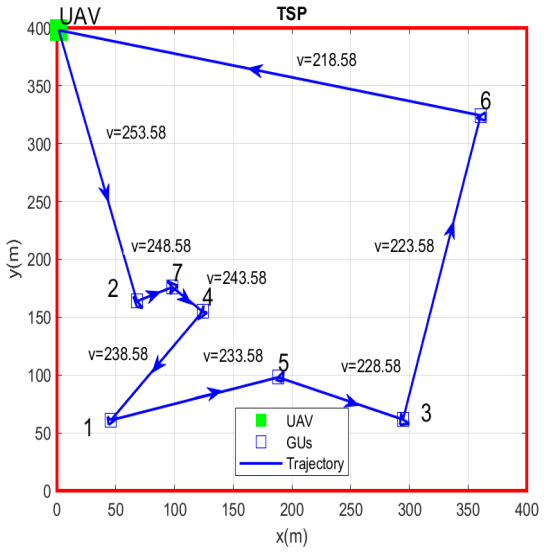

(a) Traditional TSP, $\sum_{i=1}^{K+1} E_i = 6175\ Joules$.

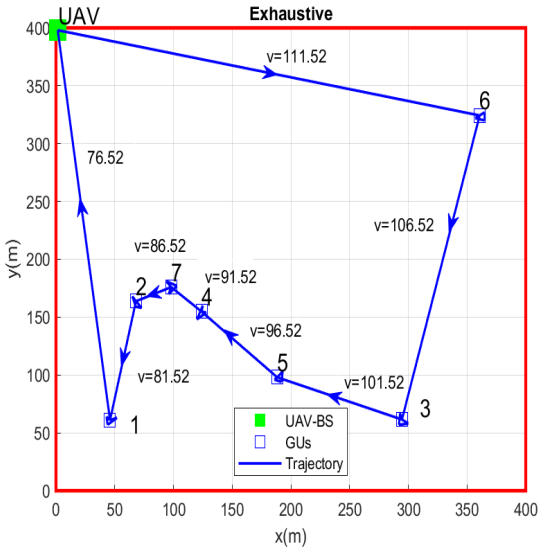

(b) Exhaustive search, $\sum_{i=1}^{K+1} E_i = 3944\ Joules$.

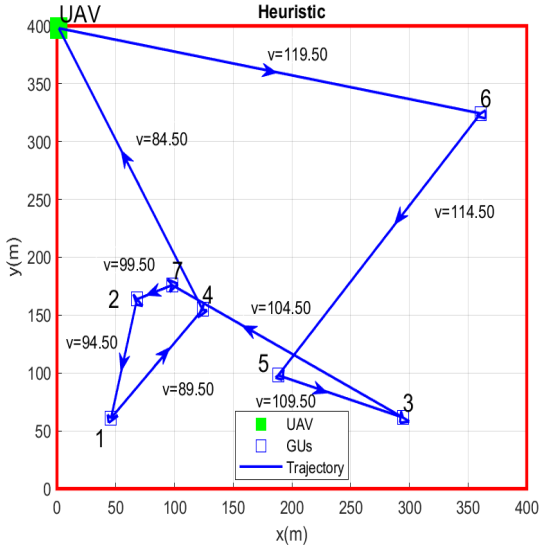

(c) Heuristic, $\sum_{i=1}^{K+1} E_i = 4484\ Joules$.

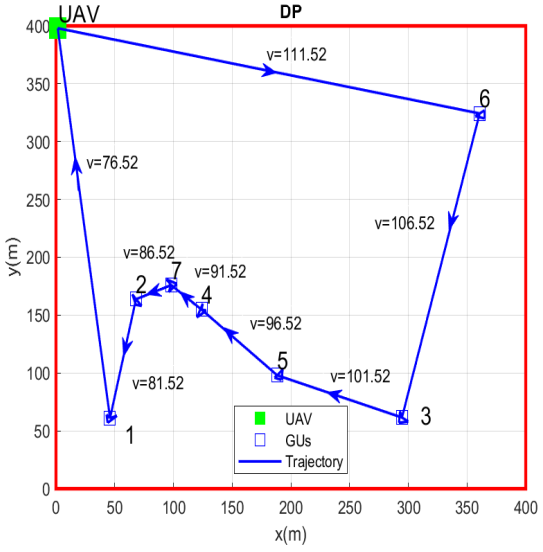

(d) Dynamic programming, $\sum_{i=1}^{K+1} E_i = 3944\ Joules$.

FIGURE 3.4: Comparison of UAV's trajectories with different path designs

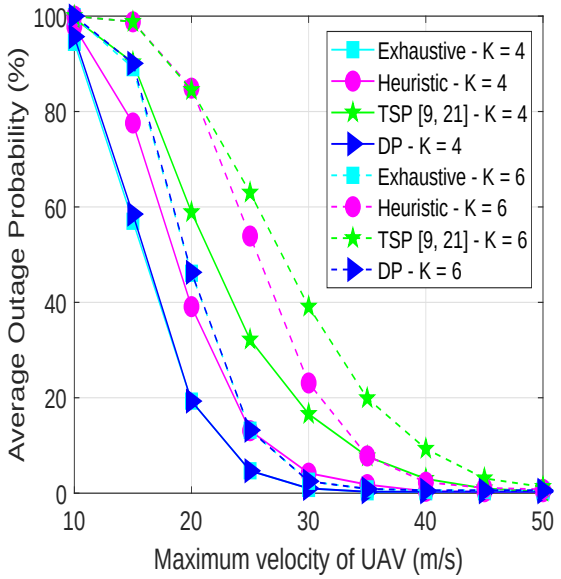

FIGURE 3.5: Average OP (%) versus $V_{\max}$ (m/s).

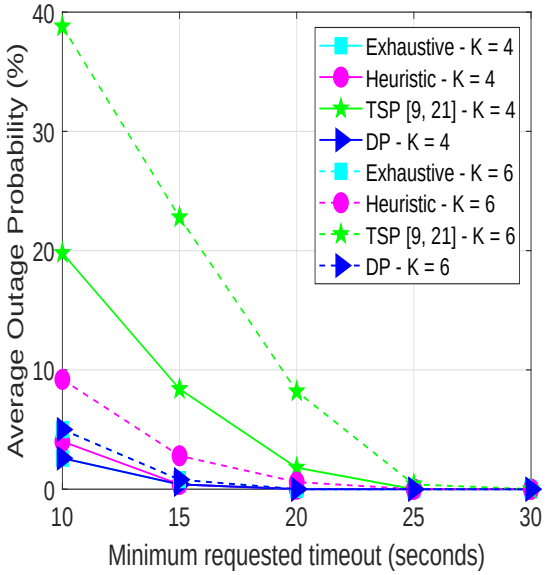

FIGURE 3.6: Average OP versus requested timeout (seconds).

(OP). Moreover, the in-feasibility also occurs if all the paths, which is obtained from Algorithm 1 (or Algorithms 2, 3), do not satisfy the energy budget constraint, i.e., C3 in (3.12). Fig. 3.5 presents the OP of the proposed algorithms and the reference as a function of $V_{\max}$ with the RT requirements n_k ranging between 22 and 60 seconds, the energy budget $E_{\text{tot}} = 500$ KJoules, $B = 3$ MHz, $\epsilon = 0.001$, $G = 15$ dB. It is shown that the proposed algorithms significantly improve the OP compared with the reference for all values of $V_{\max}$. Specifically, at $V_{\max} = 40$ m/s and $K = 6$, the exhaustive search and dynamic programing algorithms can find the trajectory that satisfies all the GUs' RT constraints with high probability and the heuristic algorithm achieves less than 1.7% OP. Whereas the reference scheme imposes 9.3% OP. The OP of all schemes can be reduced by increasing $V_{\max}$, which is because a higher $V_{\max}$ results in a lower traveling time between the GUs. Consequently, it is highly probable for the UAV to satisfy the GUs' RT.

In Fig. 3.6, the OP is presented as a function of minimum RT value $n_{\min}$ (seconds), while $n_{\max} = 65$ seconds, $V_{\max} = 45$ m/s, and $E_{\text{tot}} = 500$ KJoules, $Q_k = 10$ Mbits, $B = 3$ Mhz, $G = 15$ dB. Similar to Fig. 3.5, the DP achieves almost the same outage performance as the exhaustive search while it significantly outperforms the heuristic and reference algorithms. Specifically, at $n_{\min} = 15$ seconds and $K = 6$, the OP values of both exhaustive search and dynamic programing algorithms equal to 5% and the heuristic-based algorithm achieves less than 4.2 % OP. Whereas the reference scheme imposes 38.8% OP.

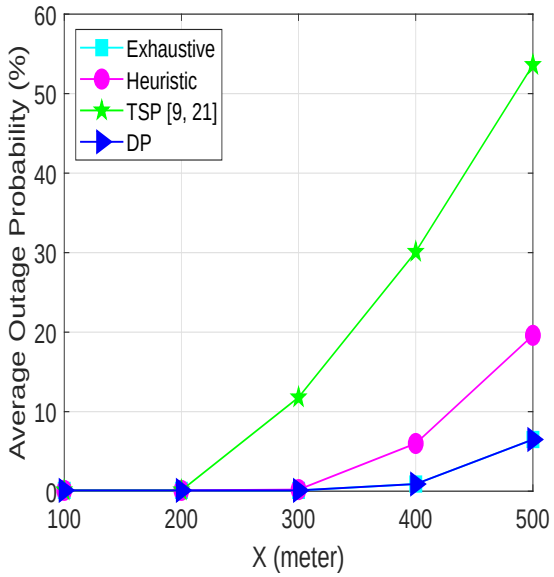

FIGURE 3.7: Average OP versus network size, e.g., $A = x^2$ (m^2).

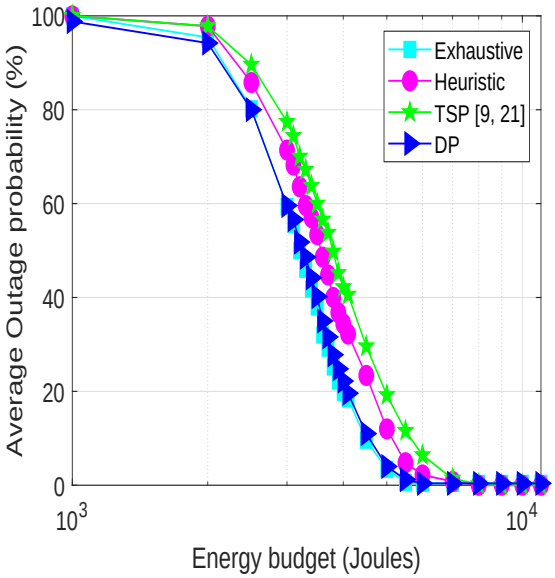

FIGURE 3.8: Average OP (%) versus energy budget.

It is found that at a lower value of $n_{\min}$, the outage performance is degraded. This is expected since allocating more speed is needed to satisfy the GUs' RT, but the $V_{\max}$ is limited. Furthermore, in Figs. 3.5 and 3.6, the average outage probability decreases when we decrease the number of GUs from 6 to 4.

Fig. 3.7 represents the OP as a function of network size (i.e., x (meters)) with $K = 7$, $V_{\max} = 45$ m/s, $n_{\min} = 15$ seconds, $n_{\max} = 65$ seconds, $Q_k = 10$ Mbits, $G = 15$ dB, $B = 3$ Mhz and $E_{\text{tot}} = 500$ KJoules. Whereas the UAV's coverage area is assumed to be a square and it can be calculated as $A = x^2$ (m^2), e.g., Fig. 3.1. It is observed that with the increasing of x, the average OP is significantly increasing for four schemes. This is expected since more traveling velocity $V_{\max}$ is needed to compensate the latency requirement which is in contradiction with the $V_{\max}$ limitation.

Next, we examine the energy consumption of the proposed optimization in Section 3.3.2 and compare with the TSP-based reference scheme in [13, 15]. For a fair comparison, we assume that $V_{\max}$ is sufficiently large so that all schemes have at least one path satisfying the RT constraint. Once a feasible set of paths is obtained based on the TSP solution, proposed Algorithms 1, 2 and 3, we apply the optimization $\mathcal{P}_2^{\text{EE}}$ to minimize the total UAV's energy consumption.

Fig. 3.8 illustrates the average OP versus energy budget (Joules), where the RT requirements n_k ranging between 3 and 15 seconds, $K = 4$, $\epsilon = 0.001$. It is the same with Figs.

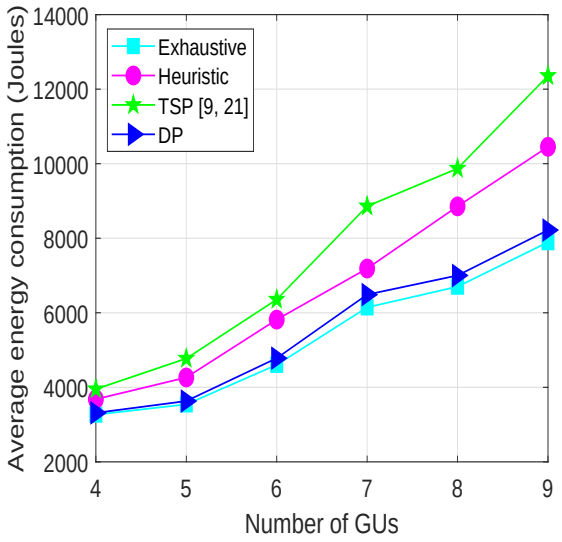

FIGURE 3.9: Average energy consumption vs. number of GUs.

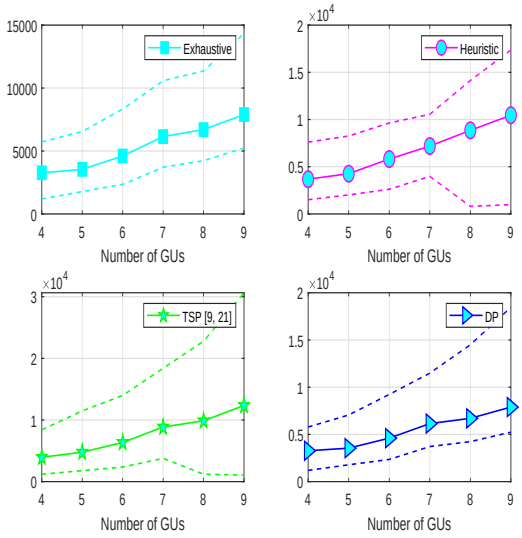

FIGURE 3.10: Average, minimum, and maximum values of energy consumption (Joules).

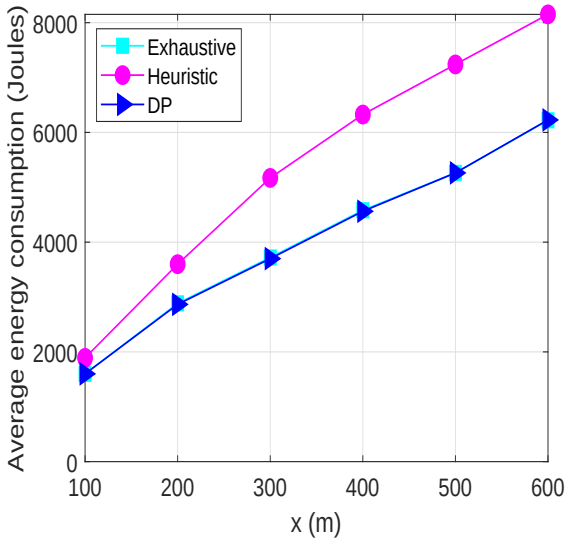

FIGURE 3.11: Average energy consumption vs. network size.

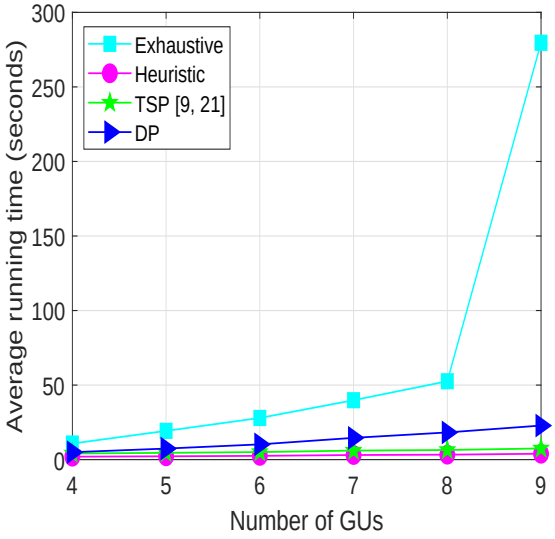

FIGURE 3.12: Average calculation time vs. number of GUs.

3.4 and 3.5, the outage probability value of DP converges to that of the exhaustive search which outperforms the heuristic and reference methods. Furthermore, when the value of energy budget is large enough, the OP of all algorithms converges to the saturation value. It is because the OP is dependent on the energy budget and the RT constraint, as well as the $\mathbb{P}\{R_k < \overline{R}_k\} = \epsilon$, i.e., constraints C1 and C3 in (3.12).

Fig. 3.9 plots the energy consumption (Joules) of all schemes as a function of the number of GUs, i.e., K, with $n_{\min} = 3$ seconds, $n_{\max} = 15$ seconds, $\Psi = K$, $Q_k = 10$ Mbits, $\epsilon = 0.001$, $G = 15$ dB. A similar observation is that our proposed designs significantly reduce the UAV's consumed energy compared with the reference. This is due to the fact that the reference (TSP-based) always selects the shortest path regardless of the GUs' RT requirements. Consequently, in order to satisfy all GUs' RT constraint, the UAV (in this case) has to fly with a higher velocity than in our proposed designs. Obviously, serving more GUs requires more energy consumption, as shown in these figures. Fig. 3.10 describes the details of the maximum and minimum energy consumption for each algorithm.

Fig. 3.11 evaluates the average energy consumption versus network size with $n_{\min} = 15$ seconds, $n_{\max} = 60$ seconds, $\Psi = K = 4$, $Q_k = 10$ Mbits. In Fig. 3.9, we assume that the velocity $V_{\max}$ is sufficiently large to make sure that the TSP scheme exists one feasible path which is infeasible in practical. Thus, in Fig. 3.11, we compare the average energy consumption of the exhaustive search, heuristic, and DP algorithms with $V_{\max} = 50$ m/s. We can observe that, for a larger network size, the energy consumption is increasing. Due to the fact that, the energy consumption depends not only on velocity but also on traveling distance (from eq. (3.11)). Specifically, the energy consumption value of DP is very close to that of the exhaustive algorithm. Moreover, the heuristic consumes more energy compared to that of exhaustive search and DP schemes and the gap between them increases proportionally with the network size.

Last, to illustrate the complexity of all algorithms, Fig. 3.12 shows the average running time (seconds) as a function of the number of GUs. Clearly, the exhaustive search (Algorithm 1) imposes the largest running time, which increases exponentially with the number of GUs, as it tries all possible paths. The heuristic search (Algorithm 2) and dynamic programing (Algorithm 3) consume much less time compared with Algorithm 1. From practical aspects, Algorithm 3 is preferred as it has a relatively small complexity while achieving good performance. Algorithm 2 consumes less time than Algorithm 3, but it has lower performance, i.e., the OP and energy consumption. Although having a short running time, the TSP-based reference has a poor performance, which is far worse than the proposed Algorithms, as shown in Figs. 3.5 to 3.10.

3.5 Summary

In this chapter, we make a first attempt to design the coarse trajectory for the energy minimization in UAV-enabled wireless communications with latency constraints. The proposed approach can be extended to a fine trajectory, e.g., waypoints based on VBS placement and convex optimization (WVC) [13] and fly-hover-communication (FHC) [15]. However, it leads to new challenges since [13] and [15] do not take the latency constraints into consideration. Thus, FHC and WVC can not be directly applied to the problem investigated in this chapter. Fortunately, the proposed algorithms in our work, i.e., exhaustive, heuristic, and DP in Section III-A, become initial feasible paths for the block coordinate descend (BCD) in combination with the successive convex approximation (SCA) method [14] that can be considered as a new method to obtain the fine trajectory, e.g., FHC and WVC. Moreover, a variable velocity can also be achieved by applying this new approach.

We have investigated the energy-efficient trajectory design for UAV-assisted communications networks which take into consideration latency requirements from the GUs. Concretely, we minimize the total energy consumption via jointly optimizing the UAV trajectory and velocity while satisfying the RT constraints and energy budget. The problem was non-convex, which was solved via two consecutive steps. Firstly, we proposed two algorithms for UAV trajectory design while satisfying the GUs' latency constraints based on the TSPTW. Secondly, for given feasible trajectories, we minimized the total energy consumption via a joint design of the UAV's velocities in all hops. Then, the best path was selected as the designed trajectory of UAV. It was shown via numerical results that our proposed designs outperform the TSP scheme in terms of both energy consumption and outage probability.

Chapter 4

Full-Duplex UAV Relay-assisted Emergency Communications in IoT Networks.

Unmanned aerial vehicle (UAV) communication has emerged as a prominent technology for emergency communications (e.g., natural disaster) in the Internet of Things (IoT) networks to enhance the ability of disaster prediction, damage assessment, and rescue operations promptly. A UAV can be deployed as a flying base station (BS) to collect data from time-constrained IoT devices and then transfer it to a ground gateway (GW). In general, the latency constraint at IoT devices and UAV's limited storage capacity highly hinder practical applications of UAV-assisted IoT networks. In this paper, full-duplex (FD) radio is adopted at the UAV to overcome these challenges. In addition, half-duplex (HD) scheme for UAV-based relaying is also considered to provide a comparative study between two modes (viz., FD and HD). Herein, a device is considered to be successfully served iff its data is collected by the UAV and conveyed to GW timely during flight time. In this context, we aim to maximize the number of served IoT devices by jointly optimizing bandwidth, power allocation, and the UAV trajectory while satisfying each device's requirement and the UAV's limited storage capacity. The formulated optimization problem is troublesome to solve due to its non-convexity and combinatorial nature. Towards appealing applications, we first relax binary variables into continuous ones and transform the original problem into a more computationally tractable form. By leveraging inner approximation framework, we derive newly approximated functions for non-convex parts and then develop a simple yet efficient iterative algorithm for its solutions. Next, we attempt to maximize the total throughput subject to the number of served IoT devices. Finally, numerical results show that the proposed algorithms significantly outperform benchmark approaches in terms of

the number of served IoT devices and system throughput.

The chapter is organized as follows. Introduction to the current state of the art is discussed in Section 4.1. The system model and problem formulation are given in Section 4.2. The proposed iterative algorithm for FD is presented in Section 4.3. Section 4.4 devotes for the HD scheme. Numerical results are illustrated in Section 4.5, and Section 4.6 concludes the chapter.

4.1 Introduction to FD UAV Relay-assisted Emergency Communications in IoT networks

In 1999, the British technology pioneer Kevin Ashton introduced the concept of the Internet-of-Things (IoT) to describe a system in which all devices with sensors can connect to each other [200]. IoT has the potential to significantly enhance the quality of human life such as smart home, health care, wearable devices, agriculture, smart city, autonomous vehicles, and smart grid [125,201]. The number of IoT connections of all types is estimated to reach almost 25 billion by 2025 [140]. However, the growing demand for communications is becoming a great challenge for IoT networks due to limited spectral resources at terrestrial base stations (BSs). Besides, BSs are deployed in fixed locations and antenna height to serve a fixed geographical area, and resources cannot be rapidly shifted elsewhere. Especially in emergency communications, whereas BSs are potentially isolated or damaged after a natural disaster, or when BSs are unable to serve all users as they are overloaded during peak hours. This raises a question of how to support the communication needs of a massive number of IoT devices with restricted resources without compromising the network performance [202]. Fortunately, due to the high maneuverability and flexible deployment, unmanned aerial vehicle (UAV) communications could become a promising technology to overcome the above shortcomings [203]. Due to energy constraints, IoT devices are commonly unable to propagate over a long distance. Thus, the UAV can fly closer to devices, harvest the IoT data, and then transmit it to the BS/control center, which is out of the transmission range of these devices.

Extensive studies have been carried out to investigate UAV-assisted IoT communication networks [204–208]. The work in [204] studied the joint optimal 3D deployment of UAVs, uplink (UL) power control, and device association in an IoT network. Specifically, the authors proposed a new framework for efficiently distributing UAVs to collect information in the UL from IoT users. In [205], the authors optimized the data gathering efficiency of a UAV-assisted IoT network, subject to the power budget, the energy capacity, and the total transmission time for IoT devices. Herein, a multi-antenna UAV was operated, which followed a circular trajectory and served IoT devices to create a virtual multi-input

multi-output (MIMO) channel. Reference [206] presented a robust central system orchestrator (SO) that was designed to provide value-added IoT services (VAIoTS). Whereas the SO keeps the entire details about UAVs including their current locations, flight missions, total energy budget, and their onboard IoT devices. To obtain an efficient UAV selection mechanism corresponding to each task requirement, the authors proposed three solutions, namely, energy-aware UAV, fair trade-off UAV, and delay-aware UAV selection. A novel UAV-aided IoT communication network to provide energy-efficient data gathering and accurate 3D device positioning of IoT devices was proposed in [207], whereas a UAV was deployed as an aerial anchor node and a flying data collector. Particularly, UAVs could serve not only as aerial BSs but also as powerful IoT components that are capable of communications, sensing, and data analysis while hovering in the air [208]. Note that none of above-mentioned works in [204–208] have investigated the influences of latency constraint on network performance.

Furthermore, despite noticeable achievements for data collection in UAV-assisted IoT networks [70, 74–76, 204–208], aforementioned works also did not take FD scheme into consideration. To efficiently exploit the radio spectrum, FD transmission was adopted in UAV communications [209–212]. By applying a circular trajectory and decode-and-forward (DF) relaying strategy, the work in [209] maximized instantaneous data rate by a joint design of beam-forming and power allocation, under individual and sum-power constraint for the source and relay users. In [210], the authors investigated the spectrum sharing planning problem for FD UAV relaying systems with underlaid device-to-device (D2D) communications, which aims to maximize the sum throughput. The work in [211] maximized the energy efficiency (EE) by jointly optimizing UAV trajectory, as the transmit and jamming powers of a source and a UAV, respectively. Besides, a new system model for UAV-enabled FD wireless-powered IoT networks was proposed in [212], in which three optimization problems, namely, total-time minimization, sum-throughput maximization, and total energy minimization problem, were investigated.

Unlike previous studies such as [70, 74–78] that only investigate timely data exchange on the UL or DL channel utilizing HD mode, this work proposes a novel system model in UAV relay-assisted IoT networks that further explores the impact of requested timeout (RT) constraints for both UL and DL transmissions. To the best of our knowledge, this is the first work to jointly optimizes total bandwidth, transmission power, trajectory design, storage capacity, and latency constraint in UAV relay-assisted IoT networks. To this end, we formulate two optimization problems and develop efficient iterative algorithms to obtain a sub-optimal solution. In summary, our contributions are as follows:

1. We propose a novel UAV relay-assisted IoT model that takes into account the latency requirement for UL and DL channels to improve the freshness of information.

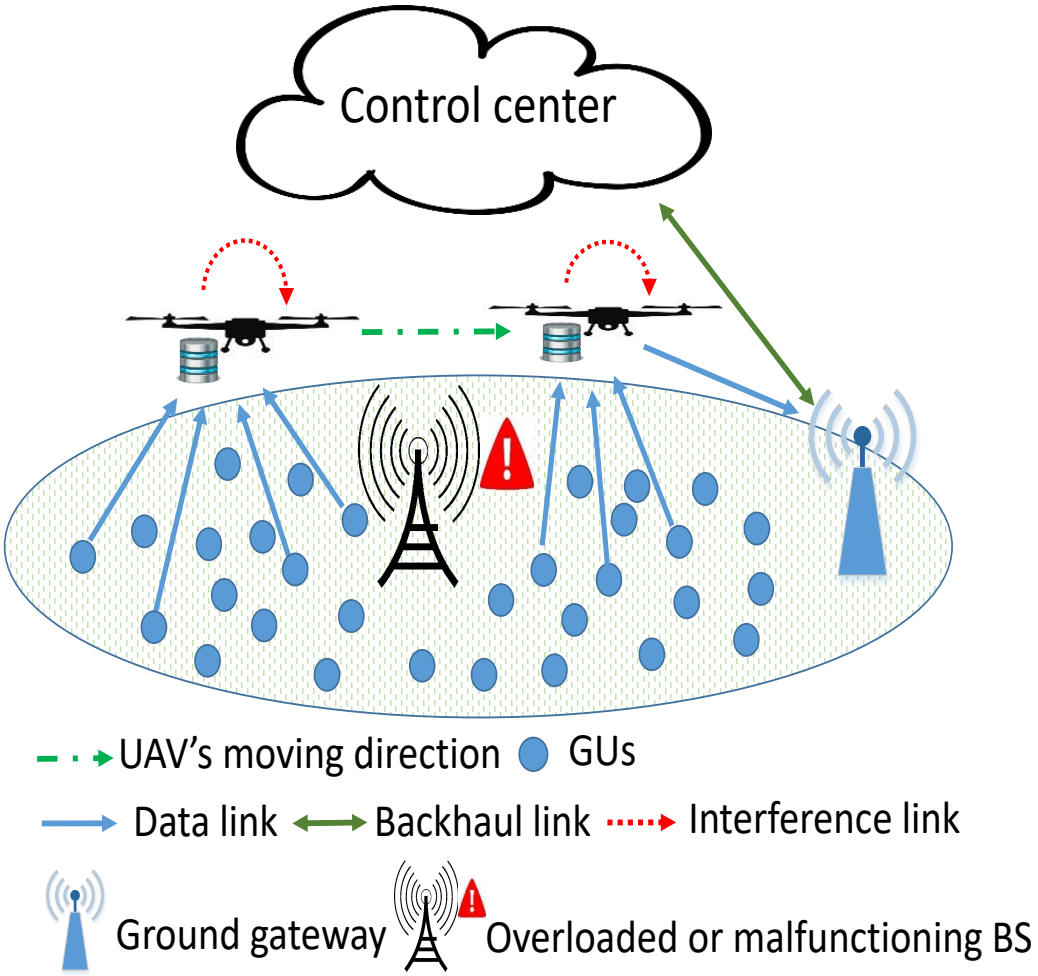

FIGURE 4.1: System model: the UAV is deployed as a flying BS to collect the data from IoT devices and then transmit to GW.

Therein, UAV-enabled FD relaying is exploited as an effective mean to enhance network performance, i.e., increasing the number of served IoT devices, throughput, and reducing latency. For instance, the reduced latency and high throughput owing to FD operation can take the virtual/augmented reality (VR/AR) experiences or emergency communications to the next level. Besides, it also helps to overcome UAV's limited storage capacity. Moreover, UAV-enabled HD relaying is also investigated to fully capitalize on UAV benefits for time-sensitive data collection in IoT networks.

2. We formulate a generalized optimization problem to maximize the total number of

served IoT devices under the UAV's maximum speed constraint, total traveling time constant, maximum transmit power of devices/UAV, limited cache size of UAV, and latency constraints for both UL and DL. The formulation belongs to the difficult class of mixed-integer non-convex optimization problem, which is generally NP-hard. We first relax binary variables into continuous ones and penalize the objective by introducing a penalty function. We then develop an iterative computational procedure for its solutions, which guarantees convergence to at least a local optimal. The key idea behind our approach is to derive newly approximated functions for non-convex parts by employing the inner approximation (IA) framework [213].

3. Inspired by the practical requirement in human safety measurements, the more data we have collected, the better our predictions are. This motivates us to investigate the optimization problem in order to maximize the total collected throughput subject to a given number of served IoT users.

4. The proposed schemes' effectiveness is revealed via numerical results, which show significant improvements in both number of served IoT devices and the total amount of collected throughput compared with the benchmarks. More specifically, the Benchmark FD and Benchmark HD schemes are respectively designed similar to the proposed FD-based and HD-based methods but with fixed resource allocation or fixed trajectory.

5. Compared to our conference [214], we have made the following major revisions. Firstly, the work in [214] only considers the throughput maximization problem with an assumption of perfect CSI from IoT devices to UAV. Moreover, the details of mathematical analysis are not provided in [214]. In this manuscript, we have updated the channel model considering the approximated rate functions for both uplink and downlink, as given in Lemma 1. Besides, we have provided the IA framework in Section III and detailed the proof of Proposition 1 in Appendix D. We have added an efficient method to generate an initial feasible point to start the IA-based algorithm in Section III-B. Lastly, we have reproduced all simulation results in Section V due to the change of channel model. In addition, we have also added Fig. 3 to illustrate the UAV's trajectories.

4.2 System Model

We consider a UAV-aided cooperative wireless IoT network, where a UAV is deployed to assist the existing terrestrial communication infrastructure in the case of adverse conditions or natural calamities, as shown in Fig. 4.1. In emergency communications, the ground base station (GBS) is either partially or completely damaged after a natural disaster or in the

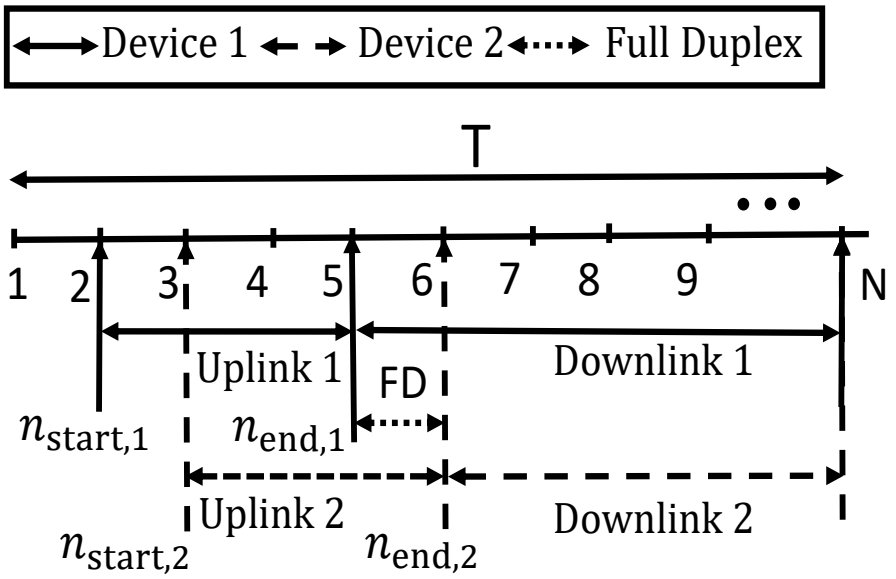

FIGURE 4.2: Illustration of the data transmission process of 2 IoT devices with N time intervals. The first IoT device with initial data transmission time at $n_{\text{start},1} = 2$, timeout at $n_{\text{end},1} = 5$. The second IoT device with initial data transmission time at $n_{\text{start},2} = 3$, timeout at $n_{\text{end},2} = 6$. The UAV operates in the FD mode from time slots 5 to 6 since two devices utilize the same sub-carrier.

case that the GBS is overloaded during the peak hours due to its incapability of handling all the devices at the same time (e.g., a sporting event) [215]. The latter case has been recognized as one of the key scenarios that need to be effectively solved by fifth-generation (5G) wireless communication [215,216]. Concretely, a UAV helps to relay data from a set of K IoT devices (or GUs), denoted by $\mathcal{K} \triangleq \{1, \ldots, K\}$, to a GW. Each IoT device is equipped with a single antenna and works in HD mode. Due to the SWAP (size, weight, and power) limitations, the UAV, acting as an on-demand relay, is equipped with one FD antenna, which can simultaneously be used for data transmission and reception. Specifically, the UAV can operate in FD or HD mode depending on the system designer. It hovers over the considered area to effectively gather data from IoT devices and then transmit it to the GW using UL and DL communication, respectively. Due to limited energy budget, we restrain the total serving time of UAV as T. We assume that each device is active at different time instances t, where $0 \leq t \leq T$. The location of device k is denoted as $\mathbf{w}_k \in \mathbb{R}^{2\times 1}, k \in \mathcal{K}$. We assume that the locations of IoT devices together with their data sizes, the initial data transmission time (i.e., $n_{\text{start},k}$ with $k \in \mathcal{K}$), and latency requirement (i.e., $n_{\text{end},k}$ with

$k \in \mathcal{K}$) are known to the UAV through the control center.[1] Denote $n_{\text{start},k}$ and $n_{\text{end},k}$ by the initial data transmission time and timeout constraint of the device k, respectively, for $k \in \mathcal{K}$. It is assumed that the UAV should collect data from device k within $n_{\text{end},k}$ units of time. For simplicity, we assume that the UAV flies at a constant altitude of H (meters), e.g., imposed by the regulatory authority for safety considerations. The location of UAV projected on the ground is denoted as $\mathbf{q}(t) \in \mathbb{R}^{2\times 1}$, with $0 \leq t \leq T$ [15].

4.2.1 UAV-to-Ground and Ground-to-UAV Channel Model

For ease of exposition, the time horizon T is discretized into N equally spaced time intervals, i.e., $T = N\delta_t$ with δ_t denotes the primary slot length. Moreover, let $\mathcal{N} = \{1, \ldots, N\}$ denote a set of all time slots. Note that the UAV location can be assumed to be approximately unchanged during each time slot compared to the distance from the UAV to IoT devices since δ_t is chosen sufficiently small. Then, the UAV trajectory $\mathbf{q}(t)$ during time horizon T can be represented as $(\mathbf{q}[n])_{n=1}^{N}$, where $\mathbf{q}[n]$ denotes the UAV's horizontal location at n-th time interval. Let $V_{\max}$ denote the maximum velocity of the UAV, then the UAV's speed constraint can be presented as

$$\|\mathbf{q}[n] - \mathbf{q}[n-1]\| \leq \delta_d = V_{\max}\delta_t, n = 2, ..., N. \tag{4.1}$$

For notation convenience, let us denote the k-th IoT device and UAV by k and U, respectively. Henceforth, $1k$ and $2k$ represent for the UL (i.e., $k \rightarrow$ U) and DL (i.e., U $\rightarrow$ GW), respectively. Then, the time-dependence distance from $k \rightarrow$ U or U $\rightarrow$ GW (i.e., $1k$ or $2k$), is given by

$$d_{ik}[n] = \sqrt{H^2 + \|\mathbf{q}[n] - \mathbf{w}\|^2}, i \in \{1, 2\},\ \forall n,\ k, \tag{4.2}$$

where $\mathbf{w} \in \{\mathbf{w}_k, \mathbf{w}_0\}$, with $\mathbf{w}_0$ denotes the location of GW.

In realistic scenarios, the devices are located in different environments, e.g., rural, urban, suburban, etc. Thus, a generalized channel model consisting of both line-of-sight (LOS) and non-line-of-sight (NLOS) channel elements is considered. In this work, we consider a practical channel model that takes into account both large-scale and small-scale fading channels [217]. Specifically, the channel coefficient at the n-th time slot, denoted by $h_{ik}[n]$, can be written as [70, 194]

$$h_{ik}[n] = \sqrt{\omega_{ik}[n]}\tilde{h}_{ik}[n], \tag{4.3}$$

where $\omega_{ik}[n]$ represents for the large-scale fading effects and $\tilde{h}_{ik}[n]$ accounts for Rician

[1]The control center can take care of the corresponding computations and informs the UAV through separate signaling, without affecting the performance of the considered framework.

small-scale fading coefficient. Specifically, $\omega_{ik}[n]$ can be modeled as

$$\omega_{ik}[n] = \omega_0 d_{ik}^{-\alpha}[n], \tag{4.4}$$

where ω_0 is the average channel power gain at the reference distance $d = 1$ meter, and $\alpha \geq 2$ is the path loss exponent for the Rician fading channel [70]. Then, the small scale fading $\tilde{h}_{ik}[n]$ with an expected value $\mathbb{E}\left[|\tilde{h}_{ik}[n]|^2\right] = 1$, is given by

$$\tilde{h}_{ik}[n] = \sqrt{\frac{G}{1+G}}\bar{h}_{ik}[n] + \sqrt{\frac{1}{1+G}}\hat{h}_{ik}[n], \tag{4.5}$$

where G is the Rician factor; $\bar{h}_{ik}[n]$ and $\hat{h}_{ik}[n] \sim \mathcal{CN}(0,1)$ denote the deterministic LoS and the NLoS component (Rayleigh fading) during time slot n, respectively.

Due to the UL and DL channels' coexistence using the same frequency at n-th time slot, the self-interference (SI) may occur at the UAV. Without loss of generality, once the UAV finishes data collection from device k, then the transmission from UAV to GW can be conducted.[2]

Let us denote by $x_{1k}[n]$ and $x_{2k}[n]$ the data symbols with unit power (i.e., $\mathbb{E}\left[|x_{1k}[n]|^2\right] = 1$ and $\mathbb{E}\left[|x_{2k}[n]|^2\right] = 1$) sent $k \to \mathrm{U}$ and $\mathrm{U} \to \mathrm{GW}$ at time slot n, respectively. We consider the transmission process for relaying the device k's data consisting of two phases: the UL from device k to UAV and the DL from UAV to GW. As a result, the received signals of device k at the UAV and GW are respectively given by

$$y_{1k}[n] = \sqrt{p_{1k}[n]}h_{1k}[n]x_{1k}[n] + \sqrt{\rho^{\mathrm{RSI}}}g_{\mathrm{U}}[n]\sum_{k^*\in\mathcal{K}\setminus k}\sqrt{p_{2k^*}[n]}x_{2k^*}[n] + n_0, \tag{4.6}$$

$$y_{2k}[n] = \sqrt{p_{2k}[n]}h_{2k}[n]x_{2k}[n] + n_0, \tag{4.7}$$

where RSI represents for residual self-interference term, $\sqrt{\rho^{\mathrm{RSI}}}g_{\mathrm{U}}[n]\sum_{k^*\in\mathcal{K}\setminus k}\sqrt{p_{2k^*}[n]}x_{2k^*}[n]$ is the RSI power after all interference cancellations [219–222], $\rho^{\mathrm{RSI}} \in [0,1)$ is the degree of RSI, $n_0 \sim \mathcal{CN}(0,\sigma^2)$ denotes the additive white Gaussian noise (AWGN); $p_{1k}[n]$ and $p_{2k}[n]$ are the transmit power of the device k and UAV on the UL and DL to transmit the device k's data at time slot n; $g_{\mathrm{U}}[n]$ denotes the fading loop channel at the UAV, which interferes UL reception due to concurrent downlink transmission [223, 224].

To deal with the issues involved in limited resources and the UAV's self-interference, we consider the resources allocation (i.e., bandwidth and transmit power) for the UL and

[2]In this work, we adopt a (decode-and-forward) DF relaying technique [142, 218]; thus, the UAV needs to complete receiving all the data from device k before relaying to GW to guarantee the data encoding properly. Moreover, a sufficiently large time period is assumed to carry out the data transfer as well as the decoding process at the UAV.

DL. Thus, the achievable rate (bits/s) of links from $k \to$ U or U $\to$ GW to transmit the data of device k at time slot n are respectively given as

$$r_{ik}[n] = a_{ik}[n]B\log_2\left(1+\Gamma_{\mathrm{ik}}\right), i \in \{1,2\}, \tag{4.8}$$

where $\Gamma_{\mathrm{1k}} \triangleq \frac{p_{1k}[n]|\tilde{h}_{1k}[n]|^2\omega_0}{\left(H^2+\|\mathbf{q}[n]-\mathbf{w}_k\|^2\right)^{\alpha/2}\left(\phi^{\mathrm{RSI}}\sum\limits_{k^*\in\mathcal{K}\setminus k}p_{2k^*}[n]+\sigma^2\right)}$, $\Gamma_{\mathrm{2k}} \triangleq \frac{p_{2k}[n]|\tilde{h}_{2k}[n]|^2\omega_0}{\left(H^2+\|\mathbf{q}[n]-\mathbf{w}_0\|^2\right)^{\alpha/2}\sigma^2}$, $\phi^{\mathrm{RSI}} \triangleq \rho^{\mathrm{RSI}}|g_{\mathrm{U}}[n]|^2$, σ^2 denotes the noise power of the AWGN; B denotes the total bandwidth in hertz (Hz) of the system; $a_{1k}[n]B$ and $a_{2k}[n]B$ are the total bandwidth allocated for the UL and DL to transmit data of k-th device during time slot n, respectively. Herein, $a_{1k}[n]$ and $a_{2k}[n]$ represent for the spectrum allocation for devices and the UAV, respectively. Note that instantaneous CSI elements (i.e., $|\tilde{h}_{1k}[n]|^2$ and $|\tilde{h}_{2k}[n]|^2$) are difficult to obtain in advance. Moreover, $|\tilde{h}_{1k}[n]|^2$ and $|\tilde{h}_{2k}[n]|^2$ are random variables, thus instantaneous rates (i.e., $r_{1k}[n]$ and $r_{2k}[n]$) are also random variables. Therefore, the expected values of received rates at the UAV/GW are expressed as [133, 151]

$$\mathbb{E}\Big[r_{ik}[n]\Big] = a_{ik}[n]B\mathbb{E}[\log_2\Big(1+\Gamma_{ik}\Big)], i \in \{1,2\}, k \in \mathcal{K}. \tag{4.9}$$

Due to the troublesome of deriving the probability density function, it raises a difficulty in obtaining the closed-form expression of $r_{ik}[n]$. Thus, we provide lower-bound functions of $\mathbb{E}\Big[r_{ik}[n]\Big]$ as follows:

Lemma 3. *The lower bounds of* $\mathbb{E}\Big[r_{1k}[n]\Big]$ *and* $\mathbb{E}\Big[r_{2k}[n]\Big]$ *are respectively given as*

$$\bar{r}_{1k}[n] = a_{1k}[n]B\log_2\left(1+\frac{e^{-E}p_{1k}[n]\omega_0}{(H^2+\|\mathbf{q}[n]-\mathbf{w}_k\|^2)^{\alpha/2}\Big(\phi^{\mathrm{RSI}}\sum\limits_{k^*\in\mathcal{K}\setminus k}p_{2k^*}[n]+\sigma^2\Big)}\right), \tag{4.10}$$

$$\bar{r}_{2k}[n] = a_{2k}[n]B\log_2\left(1+\frac{e^{-E}p_{2k}[n]\omega_0}{(H^2+\|\mathbf{q}[n]-\mathbf{w}_0\|^2)^{\alpha/2}\sigma^2}\right). \tag{4.11}$$

Proof. The corresponding proof is provided in Appendix A.1. □

In practice, for a large number of resources, $a_{1k}[n]$ and $a_{2k}[n]$ are approximately continuous between 0 and 1. Thus, the bandwidth allocation should satisfy:

$$\sum_{k\in\mathcal{K}} a_{ik}[n] \le 1, \forall n,\ i \in \{1,2\}, \tag{4.12}$$

$$0 \le a_{ik}[n] \le 1, \forall k, n. \tag{4.13}$$

Based on (4.10) and (4.11), the throughput (in bits) received on the UL or DL to

transmit device k's data during time slot n, can be written as

$$C_{ik}[n] = \delta_t R_{ik}[n], \text{ where } i \in \{1, 2\}, \tag{4.14}$$

where

$$R_{ik}[n] = \begin{cases} \bar{r}_{ik}[n], \text{if } n \in \mathcal{T}_{ik}, \\ 0, \qquad \text{otherwise}, \end{cases} \tag{4.15}$$

Herein, $\mathcal{T}_{1k} \triangleq \{n_{\text{start},k}, \ldots, n_{\text{end},k}\}$, $\mathcal{T}_{2k} \triangleq \{n_{\text{end},k} + 1, \ldots, N\}$; (4.14) means that the UAV only can collect the data from device k (or transmit data to the GW) during time period $\mathcal{T}_{1k}$ (or $\mathcal{T}_{2k}$). Otherwise, the data transmission rate is treated as zero. Specifically, the UAV only transmits device k's data to GW iff it finishes the data collection process for that device. Moreover, the total throughput over N time slots received on the UL and DL are denoted as $C_{1k} = \sum\limits_{n \in \mathcal{T}_{1k}} \delta_t R_{1k}[n]$ and $C_{2k} = \sum\limits_{n \in \mathcal{T}_{2k}} \delta_t R_{2k}[n]$, respectively.

To assist in the mathematical problem formulation, we introduce a new binary variable λ_k as

$$\lambda_k = \begin{cases} 1, \text{Device } k \text{ is successfully served by the UAV}, \\ 0, \qquad\qquad\qquad\qquad\qquad \text{otherwise}. \end{cases} \tag{4.16}$$

Definition 4. *The value of λ_k should be equal to one iff the device k's data is collected by the UAV while additionally guaranteeing its successful reception at the GW.*

Let S_k denotes the data size (in bits) needed to transmit from device k to GW. Then, we have the RT constraint for transmitting the device k's data on the UL and DL are expressed as, respectively

$$\lambda_k \frac{S_k}{R_{1k}} \leq (n_{\text{end},k} - n_{\text{start},k} + 1)\delta_t, \forall k, \tag{4.17}$$

$$\lambda_k \frac{S_k}{R_{2k}} \leq (N - n_{\text{end},k})\delta_t, \forall k, \tag{4.18}$$

where $R_{ik} = \sum\limits_{n \in \mathcal{T}_{ik}} R_{ik}[n]$, with $i \in \{1, 2\}$; (4.17) means that the device k must transmit information to the UAV before timeout constraint, i.e., $n_{\text{end},k}$; (4.18) implies that the data transmission process to transmit the device k's data from U $\rightarrow$ GW is performed during the serving time of the UAV.[3]

[3]We consider the system model in which the UAV does not transmit the data during taking off and landing [225]. Thus, the data transmission process only occurs when the UAV is flying in the sky.

4.2.2 Caching Model

The UAV has a cache with a storage capacity of C. Due to the limited cache size of the UAV, it can utilize FD mode to release the storage and improve the network throughput. Considering a storage limitation, the total number of files cached at the UAV should not exceed its available storage capacity, i.e.,

$$\sum_{k\in\mathcal{K}}\left(\sum_{l=1}^{n} C_{1k}[l]-\sum_{l=1}^{n-1} C_{2k}[l]\right)\leq C, \tag{4.19}$$

where $\sum\limits_{l=1}^{n} C_{1k}[l] \triangleq \lambda_k S_k - \sum\limits_{l=n+1}^{N} C_{1k}[l]$.

Note that, in order to spend a part of storage capacity for future use, i.e., a free cache size to store new data streams, the amount of data stored at the UAV is calculated as the size of files collected from all devices till n-th time slot minus files transmitted to GW till $(n-1)$-th time slot as in (4.19).

4.2.3 Problem Formulation

In this section, we aim to maximize the total number of served IoT devices by jointly optimizing the UAV trajectory $\mathbf{q}[n]$, the allocation of resources (i.e., bandwidth and transmit power assigned for UL and DL), and take into account the storage limitation, under the assumption that the locations, initial transmission time, and the timeout constraint of all IoT devices are known a priori.

Let us denote $\mathbf{q}=\{\mathbf{q}[n],\forall n\}$, $\mathbf{a}=\{a_{1k}[n],a_{2k}[n],k\in\mathcal{K},n\in\mathcal{N}\}$, $\mathbf{p}=\{p_{1k}[n],p_{2k}[n],k\in\mathcal{K},n\in\mathcal{N}\}$, $\boldsymbol{\lambda}=\{\lambda_k,k\in\mathcal{K}\}$. Based on the above developments, the problem for maximizing number of served IoT devices can be mathematically formulated as follows:

$$\mathcal{P}^{\mathrm{FD}}: \quad \max_{\mathbf{q},\mathbf{a},\mathbf{p},\boldsymbol{\lambda}} \quad \|\boldsymbol{\lambda}\|_1 \tag{4.20}$$

$$\texttt{s.t.} \quad \lambda_k \in \{0,1\}, \forall k, \tag{4.21}$$

$$\delta_t \min(R_{1k}, R_{2k}) \geq \lambda_k S_k, \forall k, \tag{4.22}$$

$$\lambda_k \frac{S_k}{R_{1k}} \leq (n_{\mathrm{end},k} - n_{\mathrm{start},k} + 1)\delta_t, \forall k, \tag{4.23}$$

$$\lambda_k \frac{S_k}{R_{2k}} \leq (N - n_{\mathrm{end},k})\delta_t, \forall k, \tag{4.24}$$

$$\sum_{k\in\mathcal{K}} \left(\lambda_k S_k - \sum_{l=n+1}^{N} \delta_t R_{1k}[l] - \sum_{l=1}^{n-1} \delta_t R_{2k}[l] \right) \leq C, \forall n, \tag{4.25}$$

$$\sum_{k\in\mathcal{K}} a_{ik}[n] \leq 1, \forall n, \tag{4.26}$$

$$0 \leq a_{ik}[n] \leq 1, \forall k, n, \tag{4.27}$$

$$\mathbf{q}[1] = \mathbf{q}_{\mathrm{I}}, \mathbf{q}[N] = \mathbf{q}_{\mathrm{F}}, \tag{4.28}$$

$$\|\mathbf{q}[n] - \mathbf{q}[n-1]\| \leq \delta_d, n = 2, \ldots, N, \tag{4.29}$$

$$0 \leq p_{1k}[n] \leq P_k^{\max}[n], \forall k, n, \tag{4.30}$$

$$0 \leq \sum_{k\in\mathcal{K}} p_{2k}[n] \leq P_{\mathrm{U}}^{\max}[n], \forall n, \tag{4.31}$$

where constraint (4.22) means that each IoT device need to upload an amount of data S_k. In constraint (4.28), $\mathbf{q}_{\mathrm{I}}$ and $\mathbf{q}_{\mathrm{F}} \in \mathbb{R}^{2\times 1}$ denote the beginning and ending locations of UAV projected onto horizontal plane, respectively; (4.29) signifies the maximum speed constraint of the UAV; constraints (4.30) and (4.31) imply maximum transmit power constraints.

The problem $\mathcal{P}^{\mathrm{FD}}$ is a mixed integer non-linear program (MINLP), which is NP-hard. Moreover, the binary constraint (4.21) and the non-convex constraints (4.22) to (4.25) introduces intractability. Therefore, it is cumbersome to find a direct solution of $\mathcal{P}^{\mathrm{FD}}$. However, a suitable solution (local or global optimal) may be obtained by employing adequate relaxations to $\mathcal{P}^{\mathrm{FD}}$. In this regard, we provide a transformation mechanism for $\mathcal{P}^{\mathrm{FD}}$, followed by its corresponding solution in the succeeding section.

4.3 Proposed Iterative Algorithm for solving $\mathcal{P}^{\mathrm{FD}}$

This section provides an iterative algorithm based on the IA method to solve the design problem. The principle of IA framework can be detailed as follows. Let us consider the

following non-convex problem

$$\min_{x\in\mathbb{R}^n} \quad f(x) \tag{4.32}$$

$$\texttt{s.t.} \qquad h_m(x) \leq 0, m = \{1,\ldots,M\}, \tag{4.33}$$

where $f(x)$ and $h_m(x)$ are non-convex and continuous differentiable functions over $\mathbb{R}^n$. he key idea of IA is to replace non-convex functions by its approximated convex ones. Let us denote $\bar{f}^{(j)}(x)$ and $\bar{h}_m^{(j)}(x), \forall m$ are new convex functions, satisfying the properties listed in [226], i.e.,

$$f(x) \leq \bar{f}^{(j)}(x) \text{ and } h_m(x) \leq \bar{h}_m^{(j)}(x), \tag{4.34}$$

$$f(x^{(j)}) = \bar{f}^{(j)}(x^{(j)}) \text{ and } h_m(x^{(j)}) = \bar{h}_m^{(j)}(x^{(j)}), \tag{4.35}$$

$$\left.\frac{\partial f(x)}{\partial x}\right|_{x=x^{(j)}} = \left.\frac{\partial \bar{f}^{(j)}(x)}{\partial x}\right|_{x=x^{(j)}} \text{and } \left.\frac{\partial h_m(x)}{\partial x}\right|_{x=x^{(j)}} = \left.\frac{\partial \bar{h}_m^{(j)}(x)}{\partial x}\right|_{x=x^{(j)}}, \tag{4.36}$$

where $x^{(j)} \in \mathcal{F} \triangleq \{x|\text{s.t. } (4.33)\}$ is feasible region for problem (4.32). In some special scenarios, the approximated functions $(\bar{f}^{(j)}(x), \bar{h}_m^{(j)}(x))$ can be easily obtained by adopting first-order Taylor approximation of $(f(x), h_m(x))$ at feasible point $x^{(j)}$. Consequently, we solve the approximate convex program at iteration j of an iterative algorithm, which is given by

$$\min_{x\in\mathbb{R}^n} \quad \bar{f}^{(j)}(x) \tag{4.37}$$

$$\texttt{s.t.} \qquad \bar{h}_m^{(j)}(x) \leq 0, m = \{1,\ldots,M\}, \tag{4.38}$$

A general iterative algorithm to solve (4.37) is presented as follows: *i*) Generate the initial feasible point $x^{(0)} \in \mathcal{F}$; *ii*) At iteration j, the optimal solution $x^\star$ is obtained by solving (4.37); *iii*) Update $x^{(j+1)} \triangleq x^\star$ and $j = j+1$; *iv*) Repeats steps $(ii)-(iii)$ until convergence. The detailed proof of convergence can be found in [213, 226].

4.3.1 Tractable Formulation for $\mathcal{P}^{\text{FD}}$

In this section, we aim to make problem $(\mathcal{P}^{\text{FD}})$ more tractable by relaxing the binary variables of (4.21) into continuous values, i.e., $0 \leq \lambda_k \leq 1$. To obtain near-exact binary solutions at optimum, we introduce the penalty function to penalize uncertainties of the binary nature. It is straightforward to see that $\lambda_k \in \{0,1\} \Leftrightarrow \Big(0 \leq \lambda_k \leq 1 \;\&\; \lambda_k - (\lambda_k)^2 \leq 0\Big)$. We see that the convex function $\mathbb{P}(\boldsymbol{\lambda}) \triangleq \sum_{k\in\mathcal{K}} \lambda_k(\lambda_k - 1)$ with $0 \leq \lambda_k \leq 1, \forall k$ is always non-positive and can be used to measure the degree of satisfaction of (4.21). Similar to [227, 228], instead of handling the non-convex constraint $\lambda_k - (\lambda_k)^2 \leq 0$, we maximize

the penalty function $\mathbb{P}(\boldsymbol{\lambda})$ to achieve its satisfaction by incorporating it in the objective function (see, e.g., [229, Chapter 16]). Hence, the parameterized relaxed problem with penalty parameter $\mu \in \mathbb{R}^+$ is expressed as

$$\mathcal{P}^{\mathrm{FD}}_{\mathrm{relaxed}}: \quad \max_{\mathbf{q},\mathbf{a},\mathbf{p},\boldsymbol{\lambda}} \quad \|\boldsymbol{\lambda}\|_1 + \mu\mathbb{P}(\boldsymbol{\lambda}) \tag{4.39}$$

$$\mathtt{s.t.} \quad 0 \leq \lambda_k \leq 1, \forall k, \tag{4.40}$$

$$(4.22) \text{ to } (4.31). \tag{4.41}$$

Remark 5. *Note that in the parameterized relaxed problem* $\mathcal{P}^{\mathrm{FD}}_{\mathrm{relaxed}}$ (4.39)*, the binary variables in the original problem* (4.20) *are relaxed to continuous ones between 0 and 1. Therefore, if* $\lambda_k, \forall k$ *are all binary at optimal, then the relaxation is tight and the obtained solution is also a feasible solution of problem* (4.20)*. Theoretically,* $\mathbb{P}(\boldsymbol{\lambda})$ *should be zero at convergence to guarantee the same objective value with* (4.20) *under the sufficiently large value of* μ*. Nevertheless, there exists a numerical tolerance in computation and it can be accepted if* $\mathbb{P}(\boldsymbol{\lambda}) < \epsilon$*, where* ϵ *is a very small chosen value corresponding to a large value of* μ *[227, 230, 231].*

However, a direct application of IA method to solve $\mathcal{P}^{\mathrm{FD}}_{\mathrm{relaxed}}$ is inapplicable due to non-concavity of the objective function and non-convexity of constraints in (4.22)-(4.25) as well as strong coupling among optimization variables. In what follows, we transform (4.39) into an equivalent non-convex problem where the IA method can be applied. In this context, we introduce slack variables $z_{1k}[n]$, $z_{2k}[n]$, and $t_{1k}[n]$ such that $\left(H^2 + \|\mathbf{q}[n] - \mathbf{w}_k\|^2\right) \leq (z_{1k}[n])^{2/\alpha}$, $\left(H^2 + \|\mathbf{q}[n] - \mathbf{w}_0\|^2\right) \leq (z_{2k}[n])^{2/\alpha}$, and $\phi^{\mathrm{RSI}} \sum\limits_{k^* \in \mathcal{K}\setminus k} p_{2k^*}[n] + \sigma^2 \leq t_{1k}[n]$, respectively, where $\alpha \geq 2$ for Rician fading channel [70, 232, 233], by which (4.10) and (4.11) can be rewritten as

$$\bar{r}_{1k}[n] \geq r^{\mathrm{lb}}_{1k}[n] \triangleq a_{1k}[n] B \log_2\left(1 + \frac{e^{-E} p_{1k}[n]\omega_0}{z_{1k}[n] t_{1k}[n]}\right), \tag{4.42}$$

$$\bar{r}_{2k}[n] \geq r^{\mathrm{lb}}_{2k}[n] \triangleq a_{2k}[n] B \log_2\left(1 + \frac{e^{-E} p_{2k}[n]\omega_0}{z_{2k}[n]\sigma^2}\right). \tag{4.43}$$

By substituting (4.42) and (4.43) into (4.14) and (4.15), we respectively obtain $C^{\mathrm{lb}}_{ik}[n]$, and $R^{\mathrm{lb}}_{ik}[n]$, where $i \in \{1, 2\}$. Moreover, we have $R^{\mathrm{lb}}_{ik} = \sum\limits_{n \in \mathcal{T}_{ik}} R^{\mathrm{lb}}_{ik}[n]$ and $C^{\mathrm{lb}}_{ik} = \sum\limits_{n \in \mathcal{T}_{ik}} \delta_t R^{\mathrm{lb}}_{ik}[n]$. Let us denote $\mathbf{z} = \{z_{1k}[n], z_{2k}[n], n \in \mathcal{N}, k \in \mathcal{K}\}$, $\mathbf{t} = \{t_{1k}[n], k \in \mathcal{K}, n \in \mathcal{N}\}$. Then, the

problem $\mathcal{P}^{\mathrm{FD}}_{\mathrm{relaxed}}$ can be reformulated as

$$\mathcal{P}^{\mathrm{FD}}_{\mathrm{relaxed},1}: \quad \max_{\mathbf{q},\mathbf{a},\mathbf{p},\boldsymbol{\lambda},\mathbf{z},\mathbf{t}} \quad \|\boldsymbol{\lambda}\|_1 + \mu\mathbb{P}(\boldsymbol{\lambda}) \tag{4.44}$$

$$\texttt{s.t.} \quad (4.40), (4.26)-(4.31), \tag{4.45}$$

$$H^2 + \|\mathbf{q}[n] - \mathbf{w}_k\|^2 \leq (z_{1k}[n])^{2/\alpha}, \forall k, n,$$

$$H^2 + \|\mathbf{q}[n] - \mathbf{w}_0\|^2 \leq (z_{2k}[n])^{2/\alpha}, \forall n, \tag{4.46}$$

$$\phi^{\mathrm{RSI}} \sum_{k^* \in \mathcal{K} \setminus k} p_{2k^*}[n] + \sigma^2 \leq t_{1k}[n], \forall k, n, \tag{4.47}$$

$$\lambda_k \frac{S_k}{R^{\mathrm{lb}}_{1k}} \leq (n_{\mathrm{end},k} - n_{\mathrm{start},k} + 1)\delta_t, \forall k, \tag{4.48}$$

$$\lambda_k \frac{S_k}{R^{\mathrm{lb}}_{2k}} \leq (N - n_{\mathrm{end},k})\delta_t, \forall k, \tag{4.49}$$

$$\delta_t \min(R^{\mathrm{lb}}_{1k}, R^{\mathrm{lb}}_{2k}) \geq \lambda_k S_k, \forall k, \tag{4.50}$$

$$\sum_{k \in \mathcal{K}} \delta_t R^{\mathrm{lb}}_{2k} \geq \sum_{k \in \mathcal{K}} \lambda_k S_k, \forall k \in \mathcal{K}, \tag{4.51}$$

$$\sum_{k \in \mathcal{K}} \left(\lambda_k S_k - \sum_{l=n+1}^{N} \delta_t R_{1k}[l] - \sum_{l=1}^{n-1} \delta_t R_{2k}[l] \right) \leq C, \forall k, n. \tag{4.52}$$

It is noteworthy that $\mathcal{P}^{\mathrm{FD}}_{\mathrm{relaxed},1}$ is a much simpler form in comparison to $\mathcal{P}^{\mathrm{FD}}$, but the possibility of a direct solution still seem unviable. This is due to the fact that joint computations of the optimization parameters (related to (4.48)-(4.52)) introduces non-convexity to the problem. However, it is still possible to solve the problem in an iterative manner, with alternating optimization of involved parameters. In the following, we discuss the above-mentioned approach in detail.

4.3.2 Proposed IA-based Algorithm

We are now in position to convexify (4.44) by applying the IA method [213] under which the non-convex parts are completely exposed.

Approximation of the objective function: The objective (4.44) is a convex function in $\boldsymbol{\lambda}$, which is useful to apply the IA method. In particular, the convex function $\mathbb{P}(\boldsymbol{\lambda})$ is iteratively replaced by the linear function $\hat{\mathbb{P}}^{(j)}(\boldsymbol{\lambda})$:

$$\begin{aligned} \widehat{\mathbb{P}}^{(j)}(\boldsymbol{\lambda}) &\triangleq \mathbb{P}(\boldsymbol{\lambda}^{(j)}) + \nabla\mathbb{P}(\boldsymbol{\lambda}^{(j)})\left(\boldsymbol{\lambda} - \boldsymbol{\lambda}^{(j)}\right) \\ &= \sum_{k \in \mathcal{K}} \left(\lambda_k(2\lambda_k^{(j)} - 1) - (\lambda_k^{(j)})^2 \right), \end{aligned} \tag{4.53}$$

where $\mathbb{P}(\boldsymbol{\lambda}^{(j)}) = \widehat{\mathbb{P}}^{(j)}(\boldsymbol{\lambda}^{(j)})$. As a result, the objective function in problem $\mathcal{P}^{\text{FD}}_{\text{relaxed}-1}$ can be replaced by $\|\boldsymbol{\lambda}\|_1 + \mu\widehat{\mathbb{P}}^{(j)}(\boldsymbol{\lambda})$.

Approximation of $r^{\text{lb}}_{1k}[n]$ and $r^{\text{lb}}_{2k}[n]$: Before proceeding further, we can express $r^{\text{lb}}_{ik}[n]$, $i \in \{1,2\}$ as

$$r^{\text{lb}}_{ik}[n] = a_{ik}[n]\Phi_{ik}[n], \tag{4.54}$$

where

$$\Phi_{1k}[n] \triangleq B\log_2\left(1 + \frac{e^{-E}p_{1k}[n]\omega_0}{z_{1k}[n]t_{1k}[n]}\right), \tag{4.55}$$

$$\Phi_{2k}[n] \triangleq B\log_2\left(1 + \frac{e^{-E}p_{2k}[n]\omega_0}{z_{2k}[n]\sigma^2}\right). \tag{4.56}$$

To approximate (4.55) and (4.56), we first introduce the following lemmas:

Lemma 6. *Consider a concave function $h(x,y) \triangleq \sqrt{xy},\ x>0,\ y>0$. Its convex upper bound at given points $x^{(j)}$ and $y^{(j)}$ can be given by [219, Appendix B], [226]:*

$$h(x,y) \le \frac{\sqrt{x^{(j)}}}{2\sqrt{y^{(j)}}}y + \frac{\sqrt{y^{(j)}}}{2\sqrt{x^{(j)}}}x. \tag{4.57}$$

Lemma 7. *Consider a function $h_1(x,y,z) \triangleq \ln\left(1+\frac{x}{yz}\right)$ and $h_2(x,z) \triangleq \ln\left(1+\frac{x}{z}\right), x>0,\ y>0,\ z>0$. The lower bound of $h_1(x,y,z)$ and $h_2(x,z)$ at given point $x^{(j)}$, $y^{(j)}$, and $z^{(j)}$ which are expressed as*

$$h_1(x,y,z) \ge \ln\left(1+\frac{x^{(j)}}{y^{(j)}z^{(j)}}\right) - \frac{x^{(j)}}{y^{(j)}z^{(j)}} + 2\frac{\sqrt{x^{(j)}}\sqrt{x}}{y^{(j)}z^{(j)}} - \frac{x^{(j)}\left(x + \frac{y^{(j)}}{2z^{(j)}}z^2 + \frac{z^{(j)}}{2y^{(j)}}y^2\right)}{y^{(j)}z^{(j)}\left(x^{(j)} + y^{(j)}z^{(j)}\right)}, \tag{4.58}$$

$$h_2(x,z) \ge \ln\left(1+\frac{x^{(j)}}{z^{(j)}}\right) - \frac{x^{(j)}}{z^{(j)}} + 2\frac{\sqrt{x^{(j)}}\sqrt{x}}{z^{(j)}} - \frac{x^{(j)}(x+z)}{z^{(j)}\left(x^{(j)} + z^{(j)}\right)}. \tag{4.59}$$

Proof. See Appendix A.2. □

Based on lemmas 4.57 and 7, $\Phi_{1k}[n]$ and $\Phi_{1k}[n]$ are lower bounded by

$$\Phi_{1k}[n] \ge \bar{\Phi}_{1k}[n] \triangleq B\Big(\Xi_1 + \Xi_2 - \Xi_3\Big), \tag{4.60}$$

$$\Phi_{2k}[n] \ge \bar{\Phi}_{2k}[n] \triangleq B\Big(\Xi_4 + \Xi_5 - \Xi_6\Big), \tag{4.61}$$

where $\Xi_1, \Xi_2, \Xi_3, \Xi_4, \Xi_5$, and Ξ_6 are defined in Appendix A.3.

By introducing slack variable $\Phi_{ik}^{\mathrm{lb}}[n]$, $i \in \{1,2\}$, we have

$$\bar{\Phi}_{ik}[n] \geq \Phi_{ik}^{\mathrm{lb}}[n]. \tag{4.62}$$

Consequently, $r_{ik}^{\mathrm{lb}}[n]$, $i \in \{1,2\}$ is converted to the following constraints:

$$r_{ik}^{\mathrm{lb}}[n] \geq \bar{r}_{ik}^{\mathrm{lb}}[n] = a_{ik}[n]\Phi_{ik}^{\mathrm{lb}}[n]. \tag{4.63}$$

Besides, since $a_{ik}[n]\Phi_{ik}^{\mathrm{lb}}[n]$ is non-convex functions. To deal with these constraints, we substitute $a_{ik}[n]\Phi_{ik}^{\mathrm{lb}}[n]$ by equivalent Difference of Convex (DC) function $0.25\Big[(a_{ik}[n] + \Phi_{ik}^{\mathrm{lb}}[n])^2 - (a_{ik}[n] - \Phi_{ik}^{\mathrm{lb}}[n])^2\Big]$. Then, we apply the first-order Taylor approximation to approximate the convex function $(a_{ik}[n] + \Phi_{ik}[n])^2$ at the $(j+1)$-th iteration, respectively. Hence, functions $\bar{r}_{ik}^{\mathrm{lb}}[n]$ in (4.63) is given by

$$\begin{aligned} a_{ik}[n] \quad & \Phi_{ik}^{\mathrm{lb}}[n] \\ \geq \quad & \frac{\left(a_{ik}^{(j)}[n] + \Phi_{ik}^{\mathrm{lb},(j)}[n]\right)^2}{4} + \frac{\left(a_{ik}^{(j)}[n] + \Phi_{ik}^{\mathrm{lb},(j)}[n]\right)}{2} \\ \times \quad & \left(a_{ik}[n] - a_{ik}^{(j)}[n] + \Phi_{ik}^{\mathrm{lb}}[n] - \Phi_{ik}^{\mathrm{lb},(j)}[n]\right) - \frac{\left(a_{ik}[n] - \Phi_{ik}^{\mathrm{lb}}[n]\right)^2}{4} \triangleq \tilde{r}_{ik}^{\mathrm{lb}}[n] \end{aligned} \tag{4.64}$$

To convexify (4.48)-(4.52), we introduce the slack variable $\hat{r}_{ik}^{\mathrm{lb}}[n]$, with $i \in \{1,2\}$, the constraints (4.64) is innerly approximated by the following convex constraint:

$$\tilde{r}_{ik}^{\mathrm{lb}}[n] \geq \hat{r}_{ik}^{\mathrm{lb}}[n], i \in \{1,2\}. \tag{4.65}$$

As a result, substituting $\hat{r}_{ik}^{\mathrm{lb}}[n]$ into (4.14), (4.15), we obtain $\widehat{C}_{ik}^{\mathrm{lb}}[n]$, $\widehat{R}_{ik}^{\mathrm{lb}}[n]$. Moreover, we have $\widehat{R}_{ik}^{\mathrm{lb}} = \sum\limits_{n \in \mathcal{T}_{ik}} \widehat{R}_{ik}^{\mathrm{lb}}[n]$, $\widehat{C}_{ik}^{\mathrm{lb}} = \sum\limits_{n \in \mathcal{T}_{ik}} \delta_t \widehat{R}_{ik}^{\mathrm{lb}}[n]$. Let us denote $\mathbf{\Phi} = \{\Phi_{1k}^{\mathrm{lb}}[n], \Phi_{2k}^{\mathrm{lb}}[n], \forall k, n\}$ and $\mathbf{r} = \{\hat{r}_{1k}^{\mathrm{lb}}[n], \hat{r}_{2k}^{\mathrm{lb}}[n], \forall k, n\}$. Bearing all the above developments in mind, we solve the

following approximate convex program at the $(j+1)$-th iteration:

$$\mathcal{P}_{\text{convex}}: \quad \max_{\mathbf{\Psi}} \quad \sum_{k\in\mathcal{K}} \lambda_k + \mu\widehat{\mathbb{P}}^{(j)}(\boldsymbol{\lambda}) \tag{4.66}$$

$$\texttt{s.t.} \quad (4.26)-(4.31), (4.40), (4.46), (4.65), \tag{4.67}$$

$$\lambda_k \frac{S_k}{\widehat{R}^{\text{lb}}_{1k}} \leq (n_{\text{end},k} - n_{\text{start},k} + 1)\delta_t, \forall k, \tag{4.68}$$

$$\lambda_k \frac{S_k}{\widehat{R}^{\text{lb}}_{2k}} \leq (N - n_{\text{end},k})\delta_t, \forall k, \tag{4.69}$$

$$\delta_t \min\Big(\widehat{R}^{\text{lb}}_{1k}, \widehat{R}^{\text{lb}}_{2k}\Big) \geq \lambda_k S_k, \forall k, \tag{4.70}$$

$$\sum_{k=1}^{K} \delta_t \widehat{R}^{\text{lb}}_{2k} \geq \sum_{k=1}^{K} \lambda_k S_k, \tag{4.71}$$

$$\sum_{k\in\mathcal{K}} \left(\lambda_k S_k - \sum_{l=n+1}^{N} \delta_t \widehat{R}^{\text{lb}}_{1k}[l] - \sum_{l=1}^{n-1} \delta_t \widehat{R}^{\text{lb}}_{2k}[l]\right) \leq C, \forall k, n. \tag{4.72}$$

where $\mathbf{\Psi} \triangleq \{\mathbf{q}, \mathbf{a}, \mathbf{p}, \boldsymbol{\lambda}, \mathbf{z}, \mathbf{t}, \mathbf{\Phi}, \mathbf{r}\}$ and $\mathbf{\Psi}^{(j)} \triangleq \{\mathbf{q}^{(j)}, \mathbf{a}^{(j)}, \mathbf{p}^{(j)}, \boldsymbol{\lambda}^{(j)}, \mathbf{z}^{(j)}, \mathbf{t}^{(j)}, \mathbf{\Phi}^{(j)}\}$ as the feasible point for (4.66) at iteration j. The convex program (4.66) can be solved by using standard convex optimization solvers [199]. To ensure the feasibility of (4.66) at the first iteration, an appropriate starting point $\mathbf{\Psi}^{(0)}$ is necessary. This selection should be made such that the feasibility of (4.70) is always guaranteed while additionally satisfying other constraints. Therefore, we successively solve the following simplified version of (4.66):

$$\mathcal{P}^{\text{FD}}_{\text{feasible}}: \quad \max_{\mathbf{\Psi}, \{\tau_k\}_{k=1}^{K}} \quad \min_{\forall k} \tau_k \tag{4.73}$$

$$\texttt{s.t.} \quad \delta_t \min\Big(\widehat{R}^{\text{lb}}_{1k}, \widehat{R}^{\text{lb}}_{2k}\Big) - \lambda_k S_k \geq \tau_k, \forall k, \tag{4.74}$$

$$(4.67)-(4.69), (4.71), (4.72), \tag{4.75}$$

where τ_k is the slack variable. The initial feasible point $\Psi^{(0)}$ is obtained until problem (4.73) is successfully solved and $\tau_k \geq 0, \forall k$. Then, the sub-optimal solution is obtained by successively solving (4.66) and updating the involved variables until satisfying the convergence condition (discussed below in detail). Finally, a pseudo-code for solving (4.20) is summarized in Algorithm 4.

Algorithm 4 Proposed IA Based Design to Solve (4.20)

1: **REQUIRE**
2: Set $j := 0$ and and solve (4.73) to generate an initial feasible point $\Psi^{(0)}$.
3: **REPEAT**
4: Solve (4.66) to obtain the optimal solution $\Psi^{\star} \triangleq (\mathbf{q}^{\star}, \mathbf{a}^{\star}, \mathbf{p}^{\star}, \boldsymbol{\lambda}^{\star}, \boldsymbol{z}^{\star}, \boldsymbol{t}^{\star}, \boldsymbol{\Phi}^{\star}, \boldsymbol{r}^{\star})$.
5: Update $\mathbf{q}^{(j+1)} := \mathbf{q}^{\star}, \mathbf{a}^{(j+1)} := \mathbf{a}^{\star}, \mathbf{p}^{(j+1)} := \mathbf{p}^{\star}, \boldsymbol{\lambda}^{(j+1)} := \lambda^{\star}, \boldsymbol{z}^{(j+1)} := \boldsymbol{z}^{\star}, \boldsymbol{t}^{(j+1)} := \boldsymbol{t}^{\star}$, $\boldsymbol{\Phi}^{(j+1)} := \boldsymbol{\Phi}^{\star}$.
6: Set $j := j + 1$.
7: **UNTIL**
8: Convergence

4.3.3 Convergence and Complexity Analysis:

Convergence Analysis

Algorithm 1 is mainly based on inner approximation, where its convergence is proved in [213, 226]. To be self-contained, we introduce the following proposition.

Proposition 8. *The proposed Algorithm 4 yields a sequence of improved solutions converging to at least a local optimum of the relaxed problem* $\mathcal{P}^{\mathrm{FD}}_{\mathrm{relaxed}}$.

Proof. See Appendix A.4. □

Complexity Analysis

We now provide the complexity analysis for each iteration in Algorithm 0. Since problem (4.66) is convex, several solvers employing the interior point method can be applied to solve efficiently [199]. More specifically, the convex problem (4.66) involves $N(7 + 8K) + 4K$ linear and quadratic constraints, and $5N(1 + 3K) + K$ scalar real variables. As a result, the per-iteration computational complexity required to solve (4.66) is $\mathcal{O}(N(7 + 8K) + 4K)^{0.5}(5N(1 + 3K) + K)^3$ [234, Chapter 6]. It results in the overall complexity of $\mathcal{O}\Big(N_i(N(7 + 8K) + 4K)^{0.5}(5N(1 + 3K) + K)^3\Big)$, where N_i is the number of iterations to reach a local optimal solution.

4.3.4 Throughput Maximization:

In an emergency case or during a natural disaster, data needs to be collected promptly to assess the current situation in a given area. The more collected information we have, the better our predictions are. This motivates us to present a new problem that maximizes the total amount of collected data with a given number of served IoT devices subjected to

Algorithm 5 Proposed IA-based Iterative Algorithm to Solve (4.79)

1: **REQUIRE**
2: Set $j := 0$ and generate an initial feasible point $\Psi^{(0)}$ for all constraints in (4.79).
3: **REPEAT**
4: Solve (4.79) to obtain the optimal solution $\boldsymbol{\Psi}^\star \triangleq (\mathbf{q}^\star, \mathbf{a}^\star, \mathbf{p}^\star, \boldsymbol{\lambda}^\star, \boldsymbol{z}^\star, \boldsymbol{t}^\star, \boldsymbol{\Phi}^\star, \boldsymbol{r}^\star)$.
5: Update $\mathbf{q}^{(j+1)} := \mathbf{q}^\star, \mathbf{a}^{(j+1)} := \mathbf{a}^\star, \mathbf{p}^{(j+1)} := \mathbf{p}^\star, \boldsymbol{\lambda}^{(j+1)} := \boldsymbol{\lambda}^\star, \boldsymbol{z}^{(j+1)} := \boldsymbol{z}^\star, \boldsymbol{t}^{(j+1)} := \boldsymbol{t}^\star, \boldsymbol{\Phi}^{(j+1)} := \boldsymbol{\Phi}^\star$.
6: Set $j := j + 1$.
7: **UNTIL**
8: Convergence.

certain quality-of-service (QoS) constraints

$$\mathcal{P}^{\mathrm{FD}}_{\mathrm{rate}}: \quad \max_{\mathbf{q},\mathbf{a},\mathbf{p},\boldsymbol{\lambda}} \sum_{k\in\mathcal{K}} \delta_t \min(R_{1k}, R_{2k}) \tag{4.76}$$

$$\texttt{s.t.} \quad \|\boldsymbol{\lambda}\|_1 \geq \lambda_{\mathrm{thresh}}, \tag{4.77}$$

$$(4.21) - (4.31), \tag{4.78}$$

where constraint (4.78) means that the total number of served IoT devices must be greater than or equal to a predefined threshold value, i.e., $\lambda_{\mathrm{thresh}}$.

Similar to $\mathcal{P}^{\mathrm{FD}}$, the problem $\mathcal{P}^{\mathrm{FD}}_{\mathrm{rate}}$ is also a MINLP, which is NP-hard. Fortunately, by applying the relaxation method as in Section 4.3, (4.76) is rewritten as

$$\mathcal{P}^{\mathrm{FD}}_{\mathrm{rate,convex}}: \quad \max_{\Psi} \sum_{k\in\mathcal{K}} \delta_t \min(\widehat{R}^{\mathrm{lb}}_{1k}, \widehat{R}^{\mathrm{lb}}_{2k}) + \mu \widehat{\mathbb{P}}^{(j)}(\boldsymbol{\lambda}) \tag{4.79}$$

$$\texttt{s.t.} \quad (4.67) - (4.72) \tag{4.80}$$

where $\widehat{R}^{\mathrm{lb}}_{ik}$ can be obtained as in Section 4.3.2.

Consequently, the solution of problem $\mathcal{P}^{\mathrm{FD}}_{\mathrm{rate,convex}}$ can be found by successively solving a simpler convex program, as summarized in Algorithm 5.

4.4 Half Duplex Mode Scheme

4.4.1 Maximizing the Number of Served IoT devices:

In order to stress the benefits of our proposed method using FD mode, we will describe the problem again by considering HD mode at the UAV in this section. Then, (4.6) and (4.7) can be rewritten as

$$y^{\mathrm{HD}}_{ik}[n] = \sqrt{p_{ik}[n]} h_{ik}[n] x_{ik}[n] + n_0, \; i \in \{1, 2\}. \tag{4.81}$$

In (4.81), the UAV only transmits data to the GW when it finishes collecting data from all GUs in HD mode. Consequently, the RSI is disappear compared to that of (4.6). Thus, the achievable rate (bits/s) of link from $k \to \text{U}$ or $\text{U} \to \text{GW}$ to transmit the data of device k at time slot n is given as

$$r_{ik}^{\text{HD}}[n] = a_{ik}[n]B\log_2\left(1 + \frac{p_{ik}[n]|\tilde{h}_{1k}[n]|^2\omega_0}{\left(H^2 + \|\mathbf{q}[n] - \mathbf{w}\|^2\right)^{\alpha/2}\sigma^2}\right), i \in \{1, 2\}, \tag{4.82}$$

where $\mathbf{w}$ equals to $\mathbf{w}_k$ and $\mathbf{w}_0$ corresponding to i equals to 1 and 2, respectively.

As the transformations to obtain (4.11), the approximated result of $r_{ik}^{\text{HD}}[n]$ can be expressed as

$$\bar{r}_{ik}^{\text{HD}}[n] = a_{ik}[n]B\log_2\left(1 + \frac{e^{-E}p_{ik}[n]\omega_0}{\left(H^2 + \|\mathbf{q}[n] - \mathbf{w}\|^2\right)^{\alpha/2}\sigma^2}\right). \tag{4.83}$$

Proof. It can be obtained similar to the proof of (4.7). □

By replacing (4.83) into the equations (4.14) and (4.15), we obtain $C_{1k}^{\text{HD}}[n]$, $C_{2k}^{\text{HD}}[n] = C_{2k}[n]$, $R_{1k}^{\text{HD}}[n]$, and $R_{2k}^{\text{HD}}[n] = R_{2k}[n]$, respectively. Then, we reformulate the problem of maximizing the total number of served IoT devices as follows

$$\mathcal{P}^{\text{HD}}: \quad \max_{\mathbf{q},\mathbf{a},\mathbf{p},\boldsymbol{\lambda}} \quad \|\boldsymbol{\lambda}\|_1 \tag{4.84}$$

$$\texttt{s.t.} \quad (4.21), (4.24), (4.26) - (4.31), \tag{4.85}$$

$$\delta_t \min(R_{1k}^{\text{HD}}, R_{2k}) \geq \lambda_k S_k, \forall k, \tag{4.86}$$

$$\lambda_k \frac{S_k}{R_{1k}} \leq (n_{\text{end},k} - n_{\text{start},k} + 1)\delta_t, \forall k, \tag{4.87}$$

$$\sum_{k\in\mathcal{K}}\left(\lambda_k S_k - \sum_{l=n+1}^{N}\delta_t R_{1k}[l] - \sum_{l=1}^{n-1}\delta_t R_{2k}[l]\right) \leq C, \forall n. \tag{4.88}$$

The problem $\mathcal{P}^{\text{HD}}$ is non-convex because the binary constraint (4.21) and other non-convex constraints (4.24), (4.86), (4.87), and (4.88). In order to seek a suitable solution, we first relax the binary constraint (4.21) as in (4.45). Then, by introducing $z_{1k}^{\text{HD}}[n]$ and $z_{2k}^{\text{HD}}[n]$ such that $\left(H^2 + \|\mathbf{q}[n] - \mathbf{w}_k\|^2\right) \leq (z_{1k}^{\text{HD}}[n])^{2/\alpha}$ and $\left(H^2 + \|\mathbf{q}[n] - \mathbf{w}_0\|^2\right) \leq (z_{2k}^{\text{HD}}[n])^{2/\alpha}$, respectively, with $\alpha \geq 2$ for Rician fading channel [70, 232, 233], by which the (4.83) can be

expressed as

$$\bar{r}_{ik}^{\mathrm{HD}}[n] = a_{ik}[n]B\log_2\left(1+\frac{e^{-E}p_{ik}[n]\omega_0}{z_{ik}^{\mathrm{HD}}[n]\sigma^2}\right), \text{ with } i \in \{1,2\}. \tag{4.89}$$

It is easy to see that the $\bar{r}_{ik}^{\mathrm{HD}}[n]$ is totally the same as $\bar{r}_{2k}^{\mathrm{lb}}[n]$ in (4.11). Thus, we can apply the IA method for $\bar{r}_{2k}^{\mathrm{lb}}[n]$ in Section 4.3 to $\bar{r}_{ik}^{\mathrm{HD}}[n]$. As a result, $r_{ik}^{\mathrm{HD}}[n]$ can be rewritten as

$$\bar{r}_{ik}^{\mathrm{HD}}[n] = a_{ik}[n]\Phi_{ik}^{\mathrm{HD}}[n]. \tag{4.90}$$

where

$$\Phi_{ik}^{\mathrm{HD}}[n] = B\log_2\left(1+\frac{e^{-E}p_{ik}[n]\omega_0}{z_{ik}^{\mathrm{HD}}[n]\sigma^2}\right). \tag{4.91}$$

Similar to (4.62), $\Phi_{ik}[n]$ is lower bounded by

$$\Phi_{ik}^{\mathrm{HD}}[n] \geq \bar{\Phi}_{ik}^{\mathrm{HD}}[n], \tag{4.92}$$

where $\bar{\Phi}_{1k}^{\mathrm{HD}}[n]$ and $\bar{\Phi}_{2k}^{\mathrm{HD}}[n]$ can be calculated as $\bar{\Phi}_{2k}[n]$, see Appendix A.2.

As in (4.63), it follows that

$$r_{ik}^{\mathrm{HD}}[n] \geq r_{ik}^{\mathrm{HD,lb}}[n] = a_{ik}[n]\Phi_{ik}^{\mathrm{HD,lb}}[n], \tag{4.93}$$

where $\Phi_{ik}^{\mathrm{HD,lb}}[n]$ is a new slack variable which is lower bound of $\bar{\Phi}_{ik}^{\mathrm{HD}}[n]$. Then, we apply the first order Taylor approximation for $a_{ik}[n]\Phi_{ik}^{\mathrm{HD,lb}}[n]$, it yields to

$$r_{ik}^{\mathrm{HD,lb}}[n] \geq \bar{r}_{ik}^{\mathrm{HD,lb}}[n], \tag{4.94}$$

where $\bar{r}_{ik}^{\mathrm{HD,lb}}[n]$ and $\bar{r}_{ik}^{\mathrm{HD,lb}}[n]$ can be represented as in RHS of (4.64).

In turn, by introducing a slack variable $\widehat{r}_{ik}^{\mathrm{HD,lb}}[n]$, the constraint (4.94) is innerly approximated by the following convex constraints:

$$\bar{r}_{ik}^{\mathrm{HD,lb}}[n] \geq \widehat{r}_{ik}^{\mathrm{HD,lb}}[n]. \tag{4.95}$$

In Algorithm 6, we propose an iterative algorithm to solve the problem (4.84). At the j-th iteration, it solves the following convex program:

Algorithm 6 Proposed IA-based Iterative Algorithm to Solve (4.96)

1: **REQUIRE** Set $j := 0$ and generate an initial feasible point $\Psi^{(0)}$ for all constraints in (4.96).
2: **REPEAT**
3: Solve (4.96) to obtain the optimal solution $\boldsymbol{\Psi}^\star \triangleq (\mathbf{q}^\star, \mathbf{a}^\star, \mathbf{p}^\star, \boldsymbol{\lambda}^\star, \boldsymbol{z}^\star, \boldsymbol{\Phi}^\star, \boldsymbol{r}^\star)$.
4: Update $\mathbf{q}^{(j+1)} := \mathbf{q}^\star, \mathbf{a}^{(j+1)} := \mathbf{a}^\star, \mathbf{p}^{(j+1)} := \mathbf{p}^\star, \boldsymbol{\lambda}^{(j+1)} := \boldsymbol{\lambda}^\star, \boldsymbol{z}^{(j+1)} := \boldsymbol{z}^\star$.
5: **UNTIL**
6: Convergence

$$\mathcal{P}^{\mathrm{HD}}_{\mathrm{convex}}: \quad \max_{\Psi} \quad \sum_{k\in\mathcal{K}} \lambda_k + \mu\widehat{\mathbb{P}}^{(j)}(\boldsymbol{\lambda}) \tag{4.96}$$

$$\texttt{s.t.} \quad (4.26)-(4.31), (4.40), (4.95), \tag{4.97}$$

$$\delta_t \min(\widehat{R}^{\mathrm{HD,lb}}_{1k}, \widehat{R}^{\mathrm{HD,lb}}_{2k}) \geq \lambda_k S_k, \forall k, \tag{4.98}$$

$$\lambda_k \frac{S_k}{\widehat{R}^{\mathrm{HD,lb}}_{1k}} \leq (n_{\mathrm{end},k} - n_{\mathrm{start},k} + 1)\delta_t, \forall k, \tag{4.99}$$

$$\sum_{k\in\mathcal{K}} \left(\lambda_k S_k - \sum_{l=n+1}^{N} \delta_t \widehat{R}^{\mathrm{HD,lb}}_{1k}[l] - \sum_{l=1}^{n-1} \delta_t \widehat{R}^{\mathrm{HD,lb}}_{2k}[l]\right) \leq C, \forall n, \tag{4.100}$$

$$\lambda_k \frac{S_k}{\widehat{R}^{\mathrm{HD,lb}}_{2k}} \leq (N - n_{\mathrm{end},k})\delta_t, \forall k, \tag{4.101}$$

$$\left(H^2 + \|\mathbf{q}[n] - \mathbf{w}_k\|^2\right) \leq (z^{\mathrm{HD}}_{1k}[n])^{2/\alpha},$$

$$\left(H^2 + \|\mathbf{q}[n] - \mathbf{w}_0\|^2\right) \leq (z^{\mathrm{HD}}_{2k}[n])^{2/\alpha}. \tag{4.102}$$

Similar to (4.66), we adopt penalty function in objective to guarantee the convergence of λ_k value to either 0 or 1, $\forall k \in \mathcal{K}$. The initial feasible point to solve (4.96) can be obtained similar to (4.73).

Complexity Analysis

The convex problem (4.96) involves $N(7+8K)+4K$ linear and quadratic constraints, and $3N(1+4K)+K$ scalar real variables. As a result, the per-iteration complexity required to solve (4.96) is $(N(7+8K)+4K)^{0.5}(3N(1+4K)+K)^3$. It results in the overall complexity is $\mathcal{O}\Big(N_i(N(7+8K)+4K)^{0.5}(3N(1+4K)+K)^3\Big)$, with N_i is the number of iterations to reach a local solution.

Algorithm 7 Proposed IA-based Iterative Algorithm to Solve (4.105)

1: **REQUIRE**
2: Set $j := 0$ and generate an initial feasible point $\Psi^{(0)}$ for all constraints in (4.105).
3: **REPEAT**
4: Solve (**??**) to obtain the optimal solution $\boldsymbol{\Psi}^\star \triangleq (\mathbf{q}^\star, \mathbf{a}^\star, \mathbf{p}^\star, \boldsymbol{\lambda}^\star, \boldsymbol{z}^\star, \boldsymbol{\Phi}^\star, \boldsymbol{r}^\star, \boldsymbol{t}^\star)$.
5: Update $\mathbf{q}^{(j+1)} := \mathbf{q}^\star, \mathbf{a}^{(j+1)} := \mathbf{a}^\star, \mathbf{p}^{(j+1)} := \mathbf{p}^\star, \boldsymbol{\lambda}^{(j+1)} := \boldsymbol{\lambda}^\star, \boldsymbol{z}^{(j+1)} := \boldsymbol{z}^\star, \boldsymbol{t}^{(j+1)} := \boldsymbol{t}^\star, \boldsymbol{\Phi}^{(j+1)} := \boldsymbol{\Phi}^\star$.
6: Set $j := j + 1$.
7: **UNTIL**
8: Convergence

4.4.2 Throughput Maximization:

In this section, we reuse all the slack variables as introduced in Sections 4.3.4 and 4.4.1. First, the throughput maximization problem for HD mode can be presented as:

$$\mathcal{P}^{\mathrm{HD}}_{\mathrm{rate}}: \quad \max_{\mathbf{q},\mathbf{a},\mathbf{p},\boldsymbol{\lambda}} \sum_{k\in\mathcal{K}} \delta_t \min(R^{\mathrm{HD}}_{1k}, R^{\mathrm{HD}}_{2k}) \tag{4.103}$$

$$\mathtt{s.t.} \quad (4.77), (4.85) - (4.88). \tag{4.104}$$

By following the same steps presented in Section 4.3.4, we obtain the following convex optimization problem:

$$\mathcal{P}^{\mathrm{HD}}_{\mathrm{rate-convex}}: \quad \max_{\boldsymbol{\Psi}} \sum_{k\in\mathcal{K}} \delta_t \min(\widehat{R}^{\mathrm{HD,lb}}_{1k}, \widehat{R}^{\mathrm{HD,lb}}_{2k}) + \mu\widehat{\mathbb{P}}^{(j)}(\boldsymbol{\lambda}) \tag{4.105}$$

$$\mathtt{s.t.} \quad (4.77), (4.97) - (4.102), \tag{4.106}$$

where $\widehat{R}^{\mathrm{HD,lb}}_{ik}$ can be obtained as in Section IV-A. Due to the convexity of problem $\mathcal{P}^{\mathrm{HD}}_{\mathrm{rate}}$, the solution of problem $\mathcal{P}^{\mathrm{HD}}_{\mathrm{rate}}$ can be iteratively obtained as in Algorithm 7.

4.5 Numerical Results

In this section, we present numerical results to evaluate the proposed joint bandwidth allocation and transmit power for the devices/UAV as well as the UAV trajectory design in UAV-assisted IoT networks. We consider a system with K IoT devices that are randomly distributed in a horizontal plane, i.e, area $= x^2$ (m^2), with $x = 500$ m. We assume that the GW, the initial location, and end location of the UAV are located at (0, 500 m), $\mathbf{q}_{\mathrm{I}}$ = [500 m, 200 m], and $\mathbf{q}_{\mathrm{F}}$ = [300 m, 0], respectively. The UAV flight altitude is invariant at $H = 100$ m [15]. The total bandwidth is $B = 20$ MHz. Thus, the total AWGN power is $\sigma^2 = -174 + 10\log_{10}(B) = -100.9897$ dBm. The transmit power budget of the UAV and IoT devices is respectively set as $P^{\max}_{\mathrm{U}} = 18$ dBm and $P^{\max}_k = 10$ dBm.

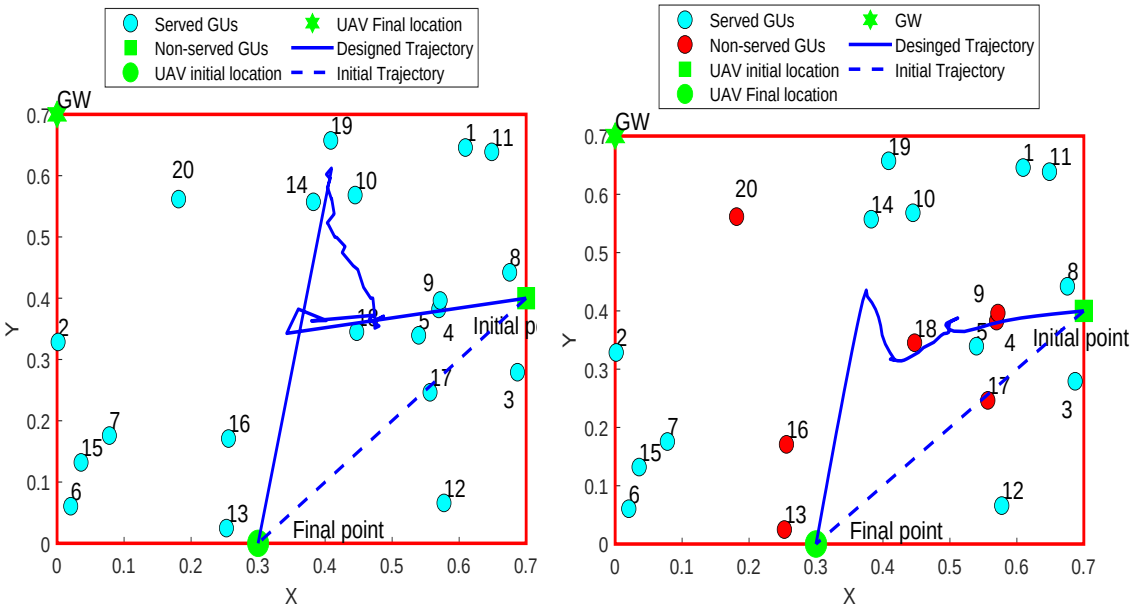

(a) FD mode.

(b) HD mode.

FIGURE 4.3: Geometry distribution of GUs and the UAV trajectory

Other parameters are set as follows: maximum speed $V_{\max} = 50$ m/s, path loss exponent $\alpha = 2.4$, ω_0 = -30 dB, $S_k \in [10, 70]$ Mbits, one time slot duration $\delta_t = 0.5$ s, the maximum collection time deadline for each device k $n_{\text{end},k}$ is uniformly distributed between $n_{\text{end},k}^{\min}$ and $n_{\text{end},k}^{\max}$. The RSI suppression ρ^{RSI} is set to -80 dB [114, 235]. To show the superiority of our designs, we compare the proposed methods with benchmark schemes. Herein, the benchmark FD 2 (BFD2) and benchmark HD 2 (BHD2) are respectively implemented similar to Algorithms 0 and 0 with fixed resource allocation, i.e., $a_{1k}[n] = a_{1k}[n] = \frac{1}{K}$, $p_{1k}[n] = P_k^{\max}[n]$, $p_{2k}[n] = \frac{P_U^{\max}}{K}$. The benchmark FD 1 (BFD1) and benchmark HD 1 (BHD1) are implemented with a fixed trajectory, i.e., linear from initial to final locations.

4.5.1 Maximizing the Number of Served IoT devices:

Fig. 4.3 plots the UAV's designed trajectory corresponding to FD and HD mode, with $N = 70$ times slots, $\eta_{\text{start},k} \in [2, 15]$, $\eta_{\text{end},k} \in [25, 50]$, area = 700 m $\times$ 700 m, $C = 1000$, and S_k values are ranging from 10 to 55 Mbits, $P_{\text{U}}^{\max} = 19$ dBm and $P_k^{\max} = 10$ dBm. In additions, the GW, initial location, and end location of the UAV are respectively set as $(0, 700$ m$)$, $\mathbf{q}_{\text{I}} = (700$ m$, 400$ m$)$, $\mathbf{q}_{\text{I}} = (300$ m$, 0)$. First, we observe that the proposed FD

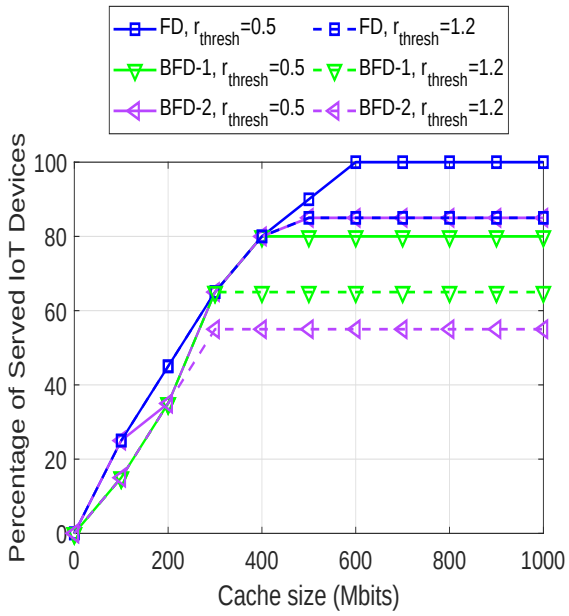

FIGURE 4.4: Percentage of served devices vs. cache size in FD mode with different value of r_{thresh}.

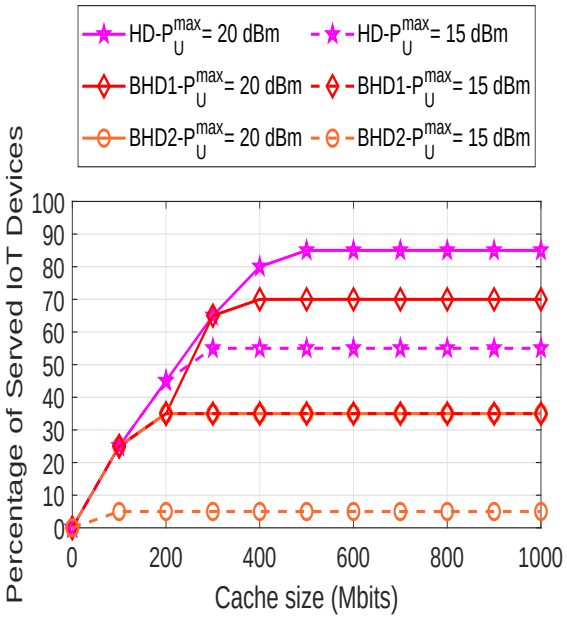

FIGURE 4.5: Percentage of served devices vs. cache size in HD mode with different value of $P_k^{\max}[n]$.

method significantly improves the number of served IoT devices than the HD method, i.e., 20 and 13 served GUs in FD and HD mode, respectively. Besides, the UAV can fly closer to GW and GUs in FD than in HD mode. It is because the UAV transfers device k's data to GW right after it finishes gathering data of that IoT device in FD-based scheme. While in HD mode, the UAV only operates in the downlink transmission when it completes the data acquisition for all users on the uplink to prevent RSI at the UAV. Consequently, the UAV in the FD scheme has more time to fly closer to GW and GUs. Thus, it obtains a higher probability of satisfying the GUs' RT. The UAV in the HD mode can collect information and fulfill the latency constraint for each IoT device, but it has less time to move forward GUs/GW to collect/offload the generated data. Thus, the performance in the HD-based method is degraded.

In Fig. 4.4, we investigate the performance of FD-based schemes with different QoS requirements. Specifically, the QoS is defined as the minimum rate threshold at the UAV/GW to successfully decode the signal, i.e., $r_{1k,\text{thresh}}[n]$ and $r_{2k,\text{thresh}}[n]$. For simplicity, we assume that $r_{1k,\text{thresh}}[n] = r_{2k,\text{thresh}}[n] = r_{\text{thresh}}$. It can be seen that the more the minimum rate threshold is required, the fewer users the system can serve. This is because the UAV tends to come closer or spend more time around an IoT device to gain a higher rate requirement.

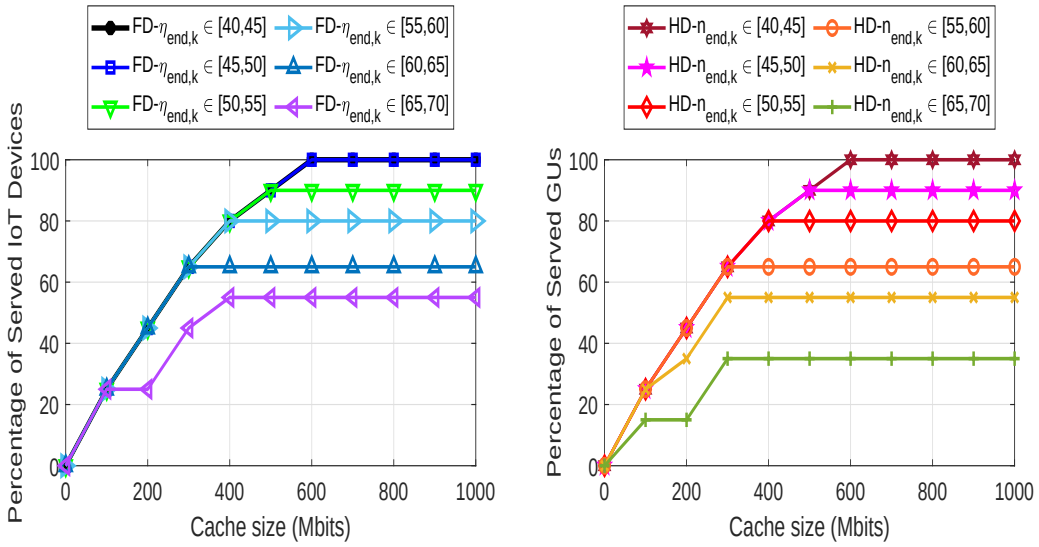

(a) Full-duplex mode (b) Half-duplex mode

FIGURE 4.6: Percentage of served devices vs. cache size with different range of $n_{\text{end,k}}$.

As a result, the UAV has less chance of serving more devices due to limited flight time and latency constraints per IoT user. Another observation is that for larger cache sizes, the number of served users increases. It is due to the fact that the UAV has more capacity to store incoming data. Thus, the UAV can serve more users before offloading information to GW. Similar to Fig. 4.3, our proposed FD algorithm achieves a much better percentage of served IoT devices compared to BFD1 and BFD2 schemes, respectively. Particularly, the performance of the BFD2 outperforms BFD1 with a small QoS requirement, i.e., $r_{\text{thresh}} = 0.5$. However, the BFD2's performance is inferior to that of BFD1 method with a large QoS value, i.e., $r_{\text{thresh}} = 1.2$. This is due to the fixed resource allocation per each time slot n in these algorithms. This additionally leads to fluctuations in data transmission rate values with low variance during time slot n, i.e., $r_{1k}[n]$ and $r_{2k}[n]$. Thus, when the r_{thresh} value is still lower than the average rate of the BFD2, the performance is not significantly affected. Nevertheless, if r_{thresh} is large enough, the performance of BFD2 will drastically be influenced.

Fig. 4.5 depicts the percentage of served IoT devices versus cache size with different value of $P_k^{\max}[n]$. The parameters are set up similarly as shown in Fig. 4.4, e.g., $r_{\text{thresh}} = 0.5$. First, we observe that HD-based schemes' performance is interior to that of FD counterparts. In particular, at $P_{\text{U}}^{\max} = 20$ dBm and $C = 800$, the HD method only serves up to 85 % number of users, while the FD scheme can serve all IoT devices with $P_{\text{U}}^{\max} = 18$

dBm and $C = 800$, as shown in Fig. 4.4. This also confirms the advantages of the FD system. Second, it can be easily seen that the HD scheme outperforms benchmark ones, i.e., BHD1 and BHD2. Specifically, at $P_{\mathrm{U}}^{\max} = 20$ dBm and $C = 500$, the HD algorithm can serve 85% of GUs, and the BHD1 achieves less than 15% OP. In comparison, the BHD2 scheme imposes a 35% percentage of served IoT devices. In Figs. 4.4 and 4.5, the proposed FD and HD algorithms provide significantly better performance than those benchmarks, which shows the superiority of these designed schemes compared to other ones.

Fig. 4.6 shows the impact of different value of $\eta_{\mathrm{end,k}}$ on our system, with $N = 80$, $K = 20$, area = 500 m × 500 m, $P_{\mathrm{U}}^{\max} = 18$ dBm, $P_k^{\max} = 15$ dBm, $\eta_{\mathrm{start},k} \in [2, 20]$, and S_k value is ranging from 10 to 55 Mbits. It is observed that the percentage of served users increases corresponding to $\eta_{\mathrm{end},k} \in [65, 70]$, $[60, 65]$, $[55, 60]$, $[50, 55]$, $[45, 50]$, $[40, 45]$, respectively. It can be explained by constraint (4.22), which describes the condition of the user being successfully served. Since the total throughput collected is proportional to the time duration allocated to the UL/DL. When the given time for UL from an IoT device to a UAV is large enough, the number of served IoT users depends significantly on the time allocation for DL from UAV to GW. Furthermore, the time period for DL is calculated as $N - \eta_{\mathrm{end},k}^{\min}$ and $N - \eta_{\mathrm{end},k}^{\max}$ for the FD and HD schemes, respectively. We see that the period of time allocated for DL in the FD algorithm is higher than that in the HD algorithm, such that the performance of the FD scheme outperforms the HD one. Specifically, the total number of served IoT users obtained from the HD scheme equals that of the FD method when the value of $N - \eta_{\mathrm{end},k}^{\max}$ is large enough. For instance, in Figs. 4.6(a) and 4.6(b), both proposed methods can serve the maximum number of IoT devices when $\eta_{\mathrm{end},k} \in [40, 45]$ and $C \geq 600$. In this scenario, the UAV should work in HD mode for simplicity of operation in realistic implementation.

In Fig. 4.7, we investigate the effect of data size on system performance, where $K = 20$, $B = 5$ Mhz, $\eta_{\mathrm{start},k} \in [2, 20]$, $n_{\mathrm{end},k}^{\min} = 30$ time slots, and $n_{\mathrm{end},k}^{\max} = 55$ time slots, with $N = 70$ time slots. As inferred from the results, the FD algorithm significantly improves the percentage of the served IoT devices compared to the HD algorithm for all values of cache size. Specifically, at $S_k \in [10, 30]$ Mbits and $C = 400$ Mbits, the FD scheme can serve 85% of IoT users on the network while HD imposes 40% of IoT users served. Furthermore, performance is degraded by increasing packet size S_k due to limited available resources for IoT devices or the UAV, i.e., $P_{\mathrm{U}}^{\max}$, $P_k^{\max}$, $V_{\max}$, and B. Besides, when the S_k value is small, corresponding to low data rate IoT devices, i.e., $S_k \in [1, 10]$ Mbits, the number of IoT users successfully served by proposed methods converge to a saturation value. Therefore, the UAV can operate in HD mode instead of FD one.

Fig. 4.8 illustrates the percentage of served IoT devices versus network size (maximum number of IoT devices located in the network area) with different data sizes, where $B = 10$ MHz, $N = 70$, $P_{\mathrm{U}}^{\max} = 18$ dBm, $P_k^{\max} = 15$ dBm, $n_{\mathrm{start,k}} \in [2, 15]$ seconds, $n_{\mathrm{end,k}}^{\min} = 25$ time slots, $n_{\mathrm{end,k}}^{\max} = 55$ time slots, and $C = 1000$ Mbits. Similar to Figs. 4.3-4.7, the percentage of IoT devices served by the FD method is better than the HD one. In addition, the

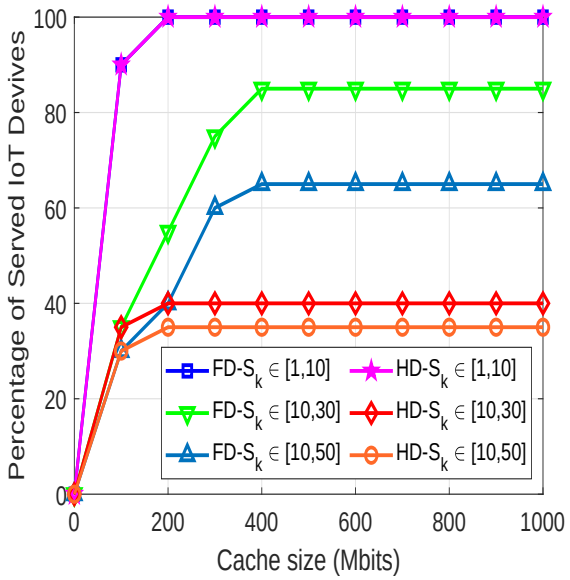

FIGURE 4.7: Percentage of served devices vs. cache sizes with different data size S_k.

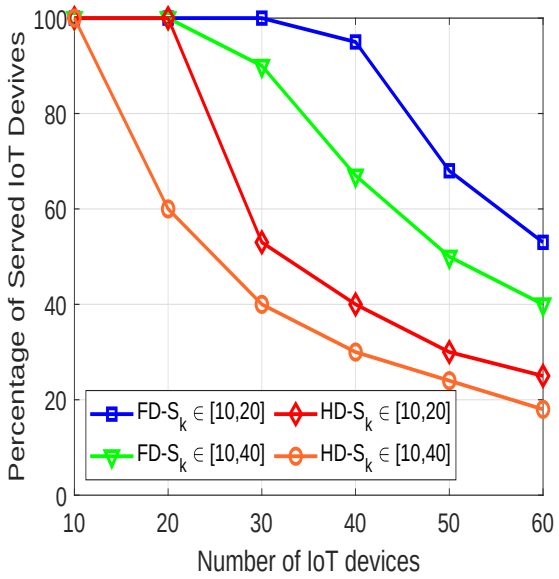

FIGURE 4.8: Percentage of served devices vs. number of IoT devices.

percentage of served users is reduced by increasing the number of IoT users in the same network area. It is due to limited resources (i.e., bandwidth and transmit power allocated for UL and DL) and $V_{\max}$ when more IoT devices are considered. Besides, the percentage of served users will enlarge by decreasing the packet sizes S_k. This is expected because the UAV needs to spend more time and resources to compensate for higher S_k increase.

Fig. 4.9 presents the results corresponding to the percentage of served GUs versus $P_{\mathrm{U}}^{\max}$ with different $n_{\mathrm{end},k}$ values. As shown, the number of served users is enhanced by increasing the power budget, i.e., $P_{\mathrm{U}}^{\max}$. Furthermore, FD scheme provides better results than HD scheme when $P_{\mathrm{U}}^{\max}$ is relatively small, e.g., $P_{\mathrm{U}}^{\max} < 22$ dBm with $n_{\mathrm{end},k} \in [40, 50]$ seconds. Nevertheless, the HD method can obtain the same number of served users as the FD method when the $P_{\mathrm{U}}^{\max}$ value is large, e.g., $P_{\mathrm{U}}^{\max} \geq 22$ dBm with $n_{\mathrm{end},k} \in [40, 50]$ seconds. This is because the FD mode suffers from RSI, which significantly increases the noise power in the UAV compared to the HD mode. In addition, RSI is linearly proportional to $P_{\mathrm{U}}^{\max}$ as in (4.8). Therefore, when $P_{\mathrm{U}}^{\max}$ is large, the UAV should operate in HD mode since the FD mode requires more energy, which may exceed the system energy budget. It is due to the fact that in FD mode, the UAV starts to transmit data to GW earlier than in HD mode, which is highlighted in Fig. 4.5. This results in higher energy consumption in the UAV when it manoeuvers in FD mode.

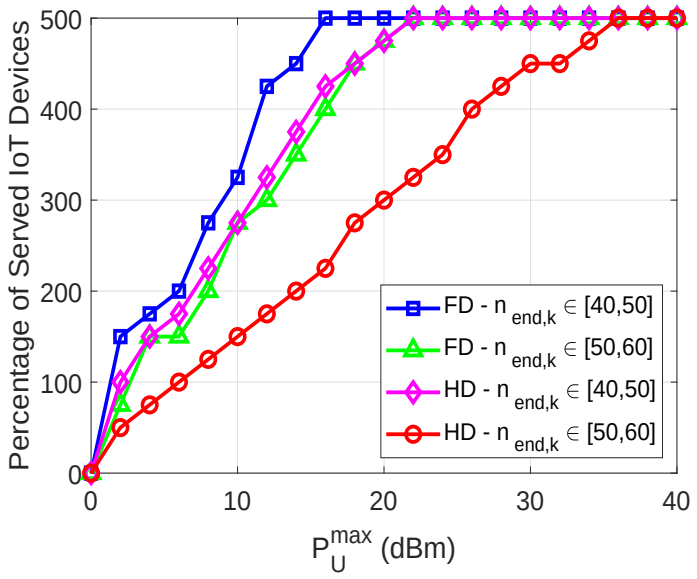

FIGURE 4.9: Percentage of served devices vs. $P_{\mathrm{U}}^{\max}$ with different data size.

4.5.2 Throughput Maximization:

In the following, we present the corresponding results for the total throughput maximization problem described in Sections 4.3.4 and 4.4.2. In Fig. 4.10, the total achieved throughput is given as a function of network sizes, i.e., area is ranging from 500 m $\times$ 500 m to 900 m $\times$ 900 m, with $K = 20$, S_k is ranging from 20 to 70 Mbits, $B = 10$ Mbits, $N = 70$ time slots, $n_{\mathrm{start},k} \in [2, 20]$ seconds, and $n_{\mathrm{end},k} \in [30, 45]$ seconds. Specifically, the achieved throughput is defined as the total throughput that the UAV transfers from GUs to GW. Herein, we only take into account the throughput of successfully served GUs. We found that the proposed algorithms (i.e, FD and HD) significantly improve throughput performance compared to references (i.e., BFD1, BFD2, BHD1, BHD2) for all values of network sizes, i.e., x (meters). Specifically, at $x = 700$ m, FD algorithm can obtain 788 Mbits and BFD1 algorithm achieves less than 131 Mbits. Whereas BFD2, HD, BHD1, and BHD2 impose 230, 537, 372, and 140 Mbits, respectively. In particular, an interesting result is that HD is even better than BFD2, which underlines the superiority of the proposed algorithms over the references. That is due to the benefits of optimizing resource allocation.

In Fig. 4.11, we investigate the effect of system bandwidth on maximum throughput, with $K = 20$, area = 700 m $\times$ 700 m, S_k ranging from 10 to 70 Mbits, $P_{\mathrm{U}}^{\max} = 18$ dBm and $P_k^{\max} = 10$ dBm, $N = 70$ time slots, $n_{\mathrm{start},k} \in [2, 20]$ seconds, and $n_{\mathrm{start},k} \in [45, 55]$ seconds. Maximum throughput is defined as the total throughput that the UAV can convey to the

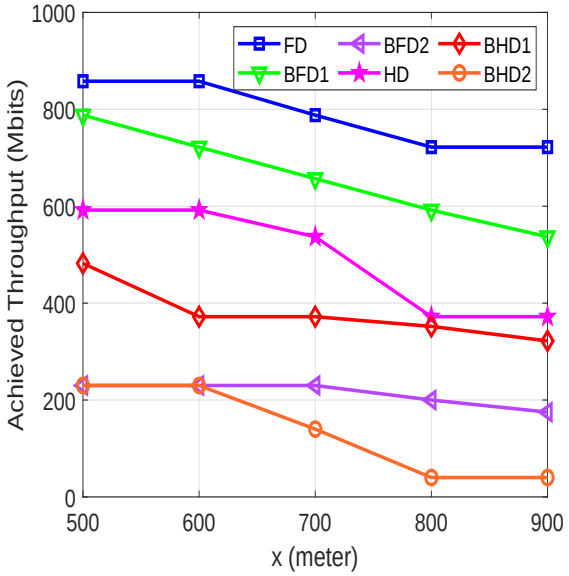

FIGURE 4.10: Total achievable throughput vs. different network sizes.

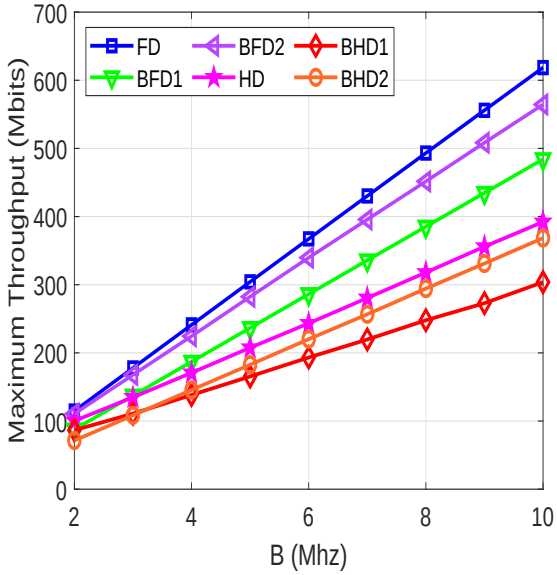

FIGURE 4.11: Maximum system throughput vs. different bandwidth.

GW regardless of whether or not each GU is successfully served. It has been observed that all schemes achieve better performance with an increase in total bandwidth. This is because the higher the bandwidth allocation, the greater the transmission can be achieved. Fig. 4.11 shows that FD schemes' performance is significantly better than the HD ones, since the UAV has more time to transfer collected data to GW in FD-based methods compared to HD-based ones. Therefore, they can be considered suitable for practical high throughput applications.

4.6 Summary

In this chapter, we investigated the resource allocation and trajectory design for UAV-assisted FD IoT networks with the emergency communication system, taking into account latency requirements of IoT devices and the limited storage capacity of the UAV. In this context, we formulated a novel problem to maximize the total number of served IoT devices via a joint optimization of the UAV trajectory, allocated bandwidth, as well as the transmission power of IoT devices and UAV while satisfying the requested timeout constraints and storage capacity. Due to non-convexity of the formulated problem, we first transformed the original problem into a tractable form, which is then solved using an iterative algorithm with a polynomial computational complexity per iteration. Besides, pertaining

to the realistic requirements for improving the estimation accuracy in a natural disaster or emergency scenario, we proposed an additional optimization problem in order to maximize the total collected data while satisfying the threshold of a minimum number of served IoT devices. We illustrated via numerical results that the proposed designs outperform the benchmark schemes in terms of both the total number of served IoT devices and the amount of collected data. Notably, in the scenarios such as when IoT devices' RT is not stringent, in the case of small data size, or required $P_{\mathrm{U}}^{\max}$ is large, the UAV should operate in the HD mode for a simple implementation.

Chapter 5

Backscatter- and Cache-assisted UAV Communications

Unmanned aerial vehicle (UAV) has been widely adopted in wireless systems due to its flexibility, mobility, and agility. Nevertheless, a limited onboard battery greatly hinders UAV to prolong the serving time from communication tasks that need a high power consumption in active RF communications. Fortunately, caching and backscatter communication (BackCom) are appealing technology for energy-efficient communication systems. This motivates us to investigate a wireless communication network with backscatter- and cache-assisted UAV technology. We assume a UAV with a cache memory is deployed as a flying backscatter device (BD), term the UAV-enabled BD (UB), to relay the source's signals to the destination. Besides, the UAV can harvest energy from the source's RF signals and then utilizes it for backscattering information to the destination. In this context, we aim to maximize the total throughput by jointly optimizing the dynamic time splitting (DTS) ratio and the UB's trajectory with caching capability at the UB. The formulation is troublesome to directly solve since they are mixed-integer non-convex problems. To find solutions, we decompose the original problem into two sub-problems, whereas we first optimize the DTS ratio for a given UB's trajectory and the UB's trajectory is finally optimized for a given DTS ratio. By using the KKT conditions, closed-form expressions for the optimal values of the DTS ratio are obtained, which greatly reduce the computation time. Moreover, the solution of the second sub-problem can be acquired by adopting the successive convex approximation (SCA) technique. Consequently, efficient alternating algorithms are proposed for both EH models by leveraging the block coordinate descent (BCD) method. Finally, the intensive numerical results demonstrate that our proposed schemes achieve significant throughput gain in comparison to the benchmark schemes.

The rest of the chapter is organized as follows. Introduction to the current state of

the art is discussed in Section 5.1. The system model and problem formulation are given in Section 5.2. The proposed iterative algorithm for solving linear EH model-based UAV-enabled BackCom is presented in Section 5.3. Numerical results are illustrated in Section 5.4, and Section 5.5 summarize the chapter.

5.1 Introduction to Backscatter- and Cache-assisted UAV Communications

Unmanned aerial vehicles (UAVs) have attracted significant attention from both academia and industry due to their flexible deployment, low cost, and high maneuverability [3, 203]. Indeed, UAVs have enabled various applications such as military, agriculture, transportation, search and rescue missions, surveillance and monitoring, telecommunications [3,15,78, 121, 203, 203, 236, 237]. Particularly, if properly designed and deployed, UAVs can provide efficient solutions for wireless communication networks. Specifically, UAVs can be utilized as aerial/flying base stations (BSs) to support terrestrial BSs that are located in fixed locations and cannot be shifted elsewhere. Especially, in a natural disaster where terrestrial BSs are damaged or isolated, portable BSs do exist but they have to be moved using ground vehicles which is problematic when infrastructures for publication transportation systems may be destroyed. Consequently, UAVs can be swiftly deployed to disseminate vital information to people or help them to communicate with authorities as soon as possible [78,121]. For industrial applications, Google Project Wing and Amazon Prime Air have built and tested drones deliveries that could be used after a disaster (i.e., flood, earthquake) or in extreme weather conditions [9]. They expect to develop an advanced delivery system where drones help to bring medications or foods to people in the areas that conventional vehicles cannot reach. Besides, Facebook Halts Aquila and Google Loon projects aim at beaming internet access to people around the world who cannot connect to the Internet by using drones/balloons [10]. Furthermore, AT&T and Qualcomm are planning to adopt UAVs for facilitating large-scale wireless communications in 5G networks [12].

Recently, UAVs have been proposed as relays to improve the connectivity of networks [18, 121, 212, 238–240]. Especially, in case direct communications links are missing due to shadowing or un-communication devices by the BSs during peak hours. In these cases, UAVs are deployed as relays to help convey information from the source to the destination. In [238], the authors studied UAVs-assisted self-organized device-to-device (D2D) networks. Specifically, they aimed to maximize the total throughput via jointly optimizing the channel allocation, relay deployment, and relay assignment. Li et al. [239] investigated the joint positioning and power control to maximize the sum rate of UAV relay networks, wherein the UAV utilized two-way communications between the BS and a set of users. The works in [18] and [240] investigated the secure transmission in UAV relay networks. Sharma et al. in [18] proposed a novel secure 3D UAV relaying for hybrid

satellite-terrestrial networks (HSTNs) in the presence of a flying eavesdropper and then they investigate secrecy outage probability and the probability of non-zero secrecy capacity. Sun et al. [240] studied secure transmissions of millimeter-wave simultaneous wireless information and power transfer (SWIPT) UAV relay networks with multiple eavesdroppers. In contrast to [18, 238–240] that only considered half-duplex (HD), [121] and [212] investigated the rotary-wing UAV-enabled FD Internet-of-Things (IoT) networks.

Notably, the UAVs in the above works emit active RF signals to the destination requiring high energy consumption which reduces the lifetime of UAVs with a limited onboard battery. In this regard, backscatter communication (BackCom) is a promising solution since a typical backscatter circuit's power consumption is usually in the order of μW [124, 126], which is significantly lower than that of active RF transmission, i.e., in Watts. Consequently, BackCom has recently emerged as a key concern for UAV communication networks [134–138]. In [138], the authors proposed two novel schemes termed the transmit-backscatter protocol and transmit-backscatter relay protocol corresponding to the presence or absence of a direct link between backscatter user and receiver in UAV-aided BackCom networks. Yang et al. [134] considered a UAV-aided BackCom network comprising of backscatter devices (BDs) and carrier emitters (CEs) that are randomly distributed on the ground. They aimed at maximum energy efficiency (EE) by jointly optimizing the BDs' scheduling, the UAV's trajectory, and the CEs' transmit power. Farajzadeh et al. [135] proposed a novel UAV data collection in NOMA BackCom networks, where the UAV acted both as a power source and a data collector. The objective was to jointly design several backscatter devices, UAV's altitude, and backscatter coefficient to maximize the total successfully decoded bits while minimizing the UAV's flight time. The same authors in [136] studied the first work that considered UAV as an enabler to improve over-the-air computation (AirComp)'s performance. Hu et al. [137] proposed the first work that investigated secure transmissions in UAV-aided BackCom networks. Despite prominent achievements in UAV-assisted BackCom networks in [134–138], aforementioned works do not take caching into consideration.

Recent works have shown that some popular files are repeatedly demanded by users, which accounts for a massive portion of data traffic [241, 242]. By storing a part of popular content in the cache of edge nodes, wireless caching is a promising method to reduce traffic load, especially during peak hours [243]. Some recent works such as in [167–171] have been recently devoted to cache-assisted UAV communications. Xu et al. [167] proposed a novel scheme to overcome the endurance issue at the UAV by utilizing proactive caching. Specifically, they aimed at minimizing the weighted sum of the file caching cost and the retrieval cost by jointly optimizing the UAV communication scheduling, UAV trajectory, and file caching policy. Cheng et al. [168] proposed a novel scheme to assure the secure transmission for UAV relay networks with caching capability. The learning-based approaches in cache-enabled UAV communications were investigated in [169–171]. Chen et al. [169] proposed the first work to analyze the utilization of caching in UAV communications based on

conceptor-based echo state networks (ESNs). Different from existing works that focused on finite-time horizon offline trajectory design, Chai et al. [170] proposed an online trajectory and resource allocation optimization for cache-enabled UAV wireless communications. Wu et al. [171] adopted a convolutional neural network (CNN)-based deep supervised learning scheme for pushing up the decision-making speed in the highly dynamic vehicular networks.

From the above discussions and the fact that wireless power, caching and BackCom are energy-efficient communication technologies for UAV communication networks, this paper investigates a caching UAV-enabled BackCom network with SWIPT, in which a UAV can store a part of popular contents in its cache. Besides, the UAV is equipped with a energy harvester circuit that can harvest the RF signal from the source and then use this energy for BackCom and active transmission to the destination. In contrast to the above works in [134–138] that only consider UAV as a transmitter/receiver, this work considers UAV as an aerial BD which harvests energy from the source's RF signal and then utilizes this energy for backscattering signal to the destination. *To our best knowledge, this is the first work that jointly considers the combination of SWIPT, caching and backscatter in UAV networks.* In summary, our contributions are as follows:

1. We propose a novel backscatter- and cache-assisted wireless powered UAV communication network. Specifically, caching and backscatter can reduce the power consumption while source S provides power to the UAV, thus overcoming the sustainability issue in the UAV. In particular, this is the first work that jointly considers UAV, SWIPT, caching, and BackCom, which imposes great challenges in system modeling and problem-solving.

2. Because the UB flies from initial to final locations, it cannot hover over the source all the time. Thus, the dynamic time splitting (DTS) ratio and the UB trajectory should be carefully designed to maximize the total system throughput while still satisfying the energy constraint. If τ_n is large, thus more time is allocated for data transmission but less time is used for energy harvesting and vice versa. Consequently, there exists a trade-off for the DTS ratio in each time slot which directly impacts the amount of harvested energy and data rate.

3. Motivated by the above considerations, we formulate an optimization problem to maximize the total collected throughput at the destination, subject to constraints on the limited flying time, UB's maximum speed, UB's trajectory, and DTS ratio in each time slot. The formulation is non-convex problem and challenges to be solved.

4. We decompose the problem into two sub-problems, wherein we first optimize the DTS ratio for a given UB's trajectory, followed by the trajectory optimization for a given DTS ratio. Particularly, the closed-form expressions for the DTS ratio is

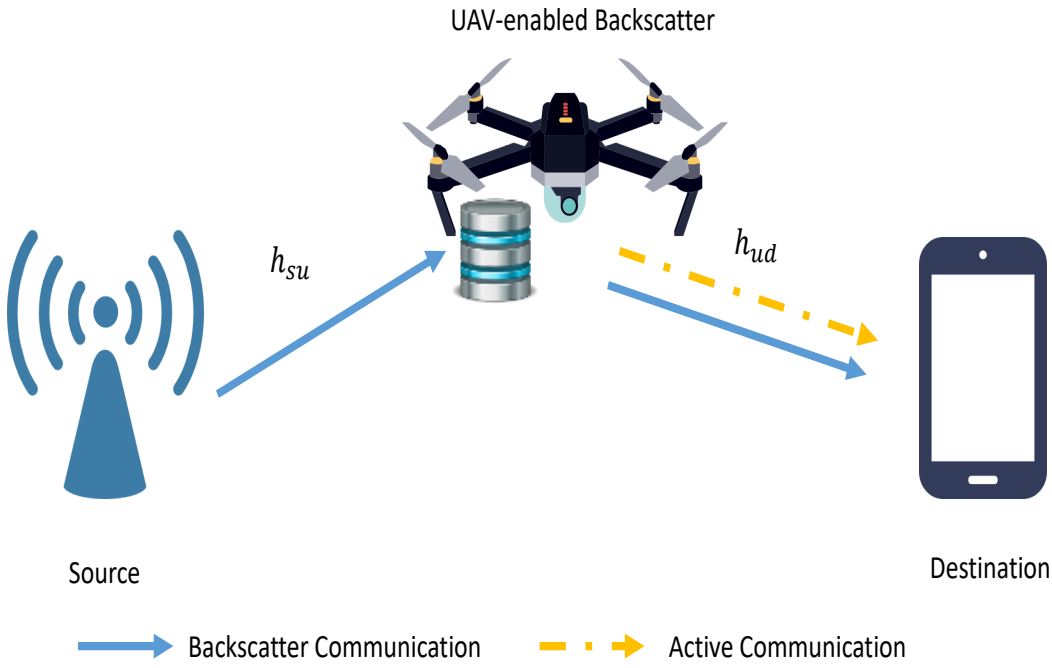

FIGURE 5.1: System model: The cache-aided UAV can perform BackCom and active transmission to convey the data from a source to a destination, wherein the UB is quipped with a energy harvester which harvests energy from the transmit RF signal.

derived which dramatically reduces the computation time. The trajectory optimization sub-problem can be solved by leveraging the successive convex approximation (SCA) technique. Based on the solutions of these sub-problems, we propose two-layer alternating algorithms to solve formulated problems adopting the block coordinate descent (BCD) method.

5. The effectiveness of the proposed schemes is demonstrated via numerical results, which show significant enhancements concerning the total collected throughput at the destination in comparison to the benchmark schemes. Specifically, the benchmark schemes are designed similar to that of our proposed algorithm but without caching capability or with a fixed DTS ratio or with a fixed trajectory.

5.2 System Model and Problem Formulation

We consider a cache-assisted UAV-enabled BackCom network, where a UAV is equipped with a backscatter circuit, namely UAV-enabled backscatter device (UB), to assist the

source to transmit data to the destination as shown in Fig. 5.1. Herein, we assume that the direct transmission link from the source to the destination is impossible due to a heavy obstacle or severe fading. In this work, we focus on communication links between the source to the UB and from the UB to the destination with an assumption that all other users are successfully served by the source through terrestrial communication. Notably, non-terrestrial communication is recognized as a key component to provide cost-effective and high-capacity connectivity in future 5G and beyond/6G wireless networks [244]. The flight altitude of UAV is assumed to be fixed at H meter. We assume the total flying time of UB is T. To make the problem tractable, the time period T is equally divided into N time slots of $\delta_t = T/N$. Consequently, the location of the UAV at time slot n is $\mathbf{q}_n$, with $n \in \mathcal{N} = \{0, \ldots, N\}$. Moreover, the locations of the source and the destination are assumed to be fixed at $\mathbf{w}_s$ and $\mathbf{w}_d$, respectively.

5.2.1 Ground-to-Air Channel Model

By denoting V_{max} as a maximum speed of the UB, the UB's constraints can be represented as

$$\|\mathbf{q}_{n+1} - \mathbf{q}_n\| \leq \delta_d = V_{\max}\delta_t, n = 0, \ldots, N-1. \tag{5.1}$$

$$\mathbf{q}_0 = \mathbf{q}_{\mathrm{I}}, \mathbf{q}_N = \mathbf{q}_{\mathrm{F}}, \tag{5.2}$$

where $\mathbf{q}_{\mathrm{I}}$ and $\mathbf{q}_{\mathrm{F}}$ is the initial and final location of the UB.

For analytical convenience, let us denote the source, destination, and UB by s, d, and u, respectively. Consequently, the distance from $s \to u$ or $u \to d$ at time slot n is given as

$$d_{iu}^n = \sqrt{H^2 + \|\mathbf{q}_n - \mathbf{w}_i\|^2}, i \in \{s, d\}, \ \forall n, \tag{5.3}$$

where $\mathbf{w}_s$ and $\mathbf{w}_d$ are fixed locations of the source and destination.

This chapter considers a realistic channel model consisting of both line-of-sight (LOS) and non-line-of-sight (NLOS) channel. This is because the UB can operate in different environments, e.g., urban, sub-urban, or rural area. Particularly, we take large-scale fading and small-scale fading into consideration [78, 217]. Concretely, the channel coefficient h_{iu}^n at time slot n is given as

$$h_{iu}^n = \sqrt{\psi_{iu}^n}\tilde{h}_{iu}^n, \tag{5.4}$$

where ψ_{iu}^n and $\tilde{h}_{iu}^n$ denotes the large-scale fading and small-scale fading during time slot n,

respectively. Specifically, $\psi_{iu}[n]$ can be written as

$$\psi_{iu}^n = \omega_0 (d_{iu}^n)^{-\alpha}, \tag{5.5}$$

where ω_0 represents the reference channel gain at $d_{iu} = 1$ meter, and α denotes the path loss exponent. The small-scale fading $\tilde{h}_{iu}^n$ with $\mathbb{E}\left[|\tilde{h}_{iu}^n|^2\right] = 1$, can be modeled as

$$\tilde{h}_{iu}^n = \sqrt{\frac{K}{1+K}}\bar{h}_{iu}^n + \sqrt{\frac{1}{1+K}}\hat{h}_{iu}^n, \tag{5.6}$$

where $\bar{h}_{iu}^n$ accounts for deterministic LoS, $\hat{h}_{iu}^n$ denotes the NLoS component, and K is the Rician factor.

5.2.2 Caching Model

We consider a general caching model at the UB, whereas the UB needs to retrieve the information from its cache to serve the destination. Specifically, the UB is able to store $0 \leq \sigma \leq 1$ parts of each file in its cache[1]. Henceforth, σ is considered as the caching coefficient in this chapter. When the destination requests a file, a part σ of this file is already stored in the UB's storage. Therefore, the source only needs to send the remainder of the required file to the UB before its transmission to the destination via backscatter. Moreover, the caching scheme adopted in this chapter can be considered as a lower bound method in comparison with the case when UB knew the content popularity.

5.2.3 Energy Harvesting and Energy Consumption Constraints

Due to the limited energy storage at the UB, EH becomes a promising solution in prolonging the lifetime of the UB. We design a dynamic time-splitting mechanism wherein the UB communication can be divided into two dynamic phases within a time slot. Specifically, a fraction τ_n and $(1-\tau_n)$ of duration δ_t are used for backscattering signal and EH at the UB, respectively. In the second phase of $(1-\tau_n)\delta_t$, the harvested energy expression at the UB at time slot n is given by [245].

$$E_h^n = E_{\mathrm{L}}^n \triangleq \mu(1-\tau_n)\delta_t P_{\mathrm{WPT}} \mathbb{E}[|h_{su}^n|^2], \tag{5.7}$$

where P_{WPT} is the transmit power at the source during $(1-\tau_n)\delta_t$ of n-th time slot, E_{L}^n is the harvested energy, μ denotes the energy harvesting efficiency corresponding to the LEH model and τ_n represents the DTS ratio at time slot n. More specifically, $\tau_n = 1$ means that

[1]This caching method is also known as probabilistic caching.

all the signal is backscattered to the receiver during time slot n and $\tau_n = 0$ indicates that all the signal is used for EH.

The energy consumption of UAV consists of three parts: energy consumption due to propulsion, backscatter, and active communications. Specifically, the propulsion energy consumption of UAV during time slot n can be represented as [15, 78]

$$E_{\text{fly}}^n(\mathbf{q}) = P_0\left(\delta_t + \kappa_1\Delta_n^2\right) + P_1\sqrt{\sqrt{\delta_t^4 + \kappa_2^2\Delta_n^4} - \kappa_2\Delta_n^2} + \frac{\kappa_3\Delta_n^3}{\delta_t^2}, \tag{5.8}$$

where $\Delta_n \triangleq \|\mathbf{q}_{n+1} - \mathbf{q}_n\|$, $P_0 \triangleq \frac{\delta}{8}\rho s A\Omega^3 R^3$, $P_1 = (1+I)\frac{W^{3/2}}{\sqrt{2\rho A}}$, $\kappa_1 = \frac{3}{\Omega^2 R^2}$, $\kappa_2 = \frac{1}{2v_0^2}$, and $\kappa_3 = 0.5 d_0 \rho s A$, with $I = 0.1$ is the incremental correction factor to induced power and other parameters can be explained as in Table I of [15].

The energy consumption due to BackCom during time slot n is represented as $\tau_n\delta_t P_b$, where P_b is the circuit power of the UB during backscatter period [245]. Moreover, P_u denote the transmit power of UAV. We then have the following energy constraint

$$\sum_{i=1}^{n}\left(E_{\text{fly}}^n(\mathbf{q}) + \tau_n\delta_t\Big(P_b + P_u\Big)\right) \leq \sum_{i=1}^{n} E_h^n, \tag{5.9}$$

where the constraint (5.9) guarantees that the total UAV's energy consumption should be less than or equal to the summation of harvested energy of the UB until time slot $n \in \mathcal{N}$.

By substituting (5.7) into (5.9), we have

$$\sum_{i=1}^{n}\left(E_{\text{fly}}^n(\mathbf{q}) + \tau_n\delta_t\Big(P_b + P_u\Big)\right) \leq \sum_{i=1}^{n}\frac{\mu(1-\tau_n)\delta_t\omega_0 P_{\text{WPT}}}{\left(H^2 + \|\mathbf{q}_n - \mathbf{w}_s\|^2\right)^{\alpha/2}}, \tag{5.10}$$

where $\mathbb{E}[h_{su}^n] = \frac{\omega_0}{\left(H^2+\|\mathbf{q}_n-\mathbf{w}_s\|^2\right)^{\alpha/2}}$.

5.2.4 UAV-enabled backscatter (UB)

In this work, we consider a UB as a flying backscatter device to reflect the signal from source to destination. To avoid the co-channel interference on the uplink (UL) and downlink (DL), time-division duplexing (TDD) is utilized in this system [133]. Specifically, we consider DTS method to divide each time slot into two parts. In this context, $(1-\tau_n)\delta_t$ and $\tau_n\delta_t$ are the fraction of time for EH on the UL from $s \to u$ and the DL from $u \to d$, respectively,

where $0 \leq \tau_n \leq 1$ denotes the DTS ratio at the time slot n.

Let us denote the symbol transmitted from the source during time slot n by x_s^n with unit power $\mathbb{E}[|x_s^n|^2] = 1$. Then, the received signal at the UB during time slot n is given by

$$y_u^n = \sqrt{P_s} h_{su}^n x_s^n + n_u, \tag{5.11}$$

where P_s is the transmit power of source S used for information transmission, and $n_u \sim \mathcal{CN}(0, \sigma_u^2)$ denotes the additive white Gaussian noise (AWGN) at the UB. Let us denote x_u^n as the backscatter information signal at time slot n, the transmitted signal of the UB is then given as [246]

$$x_u^n = \sqrt{\eta_u^n P_s} h_{su}^n x_s^n, \tag{5.12}$$

where η_u^n represents the backscatter coefficient during time slot n. Since η_u^n can not reach 1 in practice due to material and circuit losses [246]. Hence, we set a threshold for $\eta_u^n \leq \eta_{\max}$, with $0 < \eta_{\max} < 1$. Moreover, the additional noise and signal processing delay are ignored in (5.12) which are widely utilized in [245–247]. Consequently, the received signal at destination during time slot n is given as

$$y_d^n = h_{ud}^n x_u^n + \sqrt{P_u} h_{ud}^n x_s^n + n_d, \tag{5.13}$$

where the first and second element represent the received signal at the destination due to active data transmission and backscattering; $n_d \sim \mathcal{CN}(0, \sigma_d^2)$ denote the additive white Gaussian noise (AWGN) at the destination. Note that the backscatter noise power, i.e, $\sqrt{\eta_u^n} n_u$, is much smaller than baseband noise power [248], thus it is eliminated from (5.13). By substituting (5.12) into (5.13), we have

$$y_d^n = \underbrace{h_{ud}^n x_u^n}_{\text{Information from S}} + \underbrace{\lceil \sigma \rceil \sqrt{P_u} h_{ud}^n x_{\text{cache}}^n}_{\text{Cached information}} + n_d, \tag{5.14}$$

where x_{cache}^n denotes a fraction of requested information that was cached at the UAV. $\sqrt{P_s} h_{ud}^n x_s^n$ and $\sqrt{P_u} h_{ud}^n x_s^n$ are the backscattering and active RF signal to transmit received signal from source S during time slot n. Moreover, $\lceil \sigma \rceil \sqrt{P_u} h_{ud}^n x_{\text{cache}}^n$ means that if the UAV has cached a σ fraction of the requested file in its storage, thus it can transmit the cached signal to the destination. Further, n_d is the noise power at the destination which is an independent and identically distributed (i.i.d.) complex Gaussian random variable with zero mean and variance σ_d^2. Thus, the SNR at the destination are represented as

$$\gamma_d^n = \frac{\eta_u^n P_s |h_{su}^n|^2 |h_{ud}^n|^2 + P_u \lceil \sigma \rceil |h_{ud}^n|^2}{\sigma_d^2}, \tag{5.15}$$

Then, the achievable rate (in bps) at the UB and the destination during time slot n can be respectively calculated as

$$R_u^n = B\log_2\Big(1+\gamma_u^n\Big), \tag{5.16}$$

$$R_d^n = B\log_2\Big(1+\gamma_d^n\Big), \tag{5.17}$$

where B denotes the sytem bandwidth in hertz (Hz); $\gamma_u^n = P_s|h_{su}^n|^2/\sigma_u^2$, B is the total bandwidth. Especially, the instantaneous channel state information (CSI) (i.e., h_{su}^n and h_{ud}^n) are random variables, thus the instantaneous rate is also a random variable. Thus, the approximated received rate of the UB and the destination are adopted, which can be expressed as [133]

$$\bar{R}_u^n = B\mathbb{E}[\log_2\Big(1+\gamma_u^n\Big)], \tag{5.18}$$

$$\bar{R}_d^n = B\mathbb{E}[\log_2\Big(1+\gamma_d^n\Big)]). \tag{5.19}$$

As explicit, it is difficult to obtain the closed-form expression of $\bar{R}_u^n$ and $\bar{R}_d^n$, and hence the approximation functions for $\bar{R}_u^n$ and $\bar{R}_d^n$ are expressed as in the following lemma:

Lemma 9. *The approximation expressions of $\bar{R}_u^n$ and $\bar{R}_d^n$ are respectively given as*

$$\bar{R}_u^n \triangleq B\log_2\left(1+\frac{e^{-E}\omega_0 P_s}{\Big(H^2+\|\mathbf{q}_n-\mathbf{w}_s\|^2\Big)^{\alpha/2}\sigma_u^2}\right), \tag{5.20}$$

$$\bar{R}_d^n \triangleq B\log_2\left(1+\frac{\Theta\Big(\eta_u^n\omega_0 P_s + P_u\lceil\sigma\rceil\Big(d_{su}^n\Big)^{\alpha}\Big)}{\varrho}\right), \tag{5.21}$$

where $\Theta \triangleq \frac{e^{-E}\omega_0}{\sigma_d^2}$, $\bar{P}_u \triangleq P_u\lceil\sigma\rceil$, $\varrho \triangleq \Big(H^2+\|\mathbf{q}_n-\mathbf{w}_s\|^2\Big)^{\alpha/2}\Big(H^2+\|\mathbf{q}_n-\mathbf{w}_d\|^2\Big)^{\alpha/2}$.

Proof. See Appendix B.1. □

5.2.5 Problem Formulation

This section aims at maximizing the total data transmission from $u \to d$ by jointly optimizing the DTS ratio and UB trajectory with consideration of a linear EH model. Let us define $\mathbf{q} \triangleq \{\mathbf{q}_n, n \in \mathcal{N}\}$, $\boldsymbol{\tau} \triangleq \{\tau_n, n \in \mathcal{N}\}$. Then, the problem is mathematically formulated as

follows

$$\mathcal{P}_1: \quad \max_{\mathbf{q},\boldsymbol{\tau}} \; B\sum_{n\in\mathcal{N}}\tau_n\delta_t\log_2\left(1+\frac{\Theta\Big(\eta_u^n\omega_0 P_s+\bar{P}_u\Big(d_{su}^n\Big)^{\alpha}\Big)}{\varrho}\right) \tag{5.22}$$

s.t.

$$B\sum_{n\in\mathcal{N}}\tau_n\delta_t\log_2\left(1+\frac{e^{-E}\omega_0 P_s}{\Big(H^2+\|\mathbf{q}_n-\mathbf{w}_s\|^2\Big)^{\alpha/2}\sigma_u^2}\right)+\sigma S$$
$$\geq B\sum_{n\in\mathcal{N}}\tau_n\delta_t\log_2\left(1+\frac{\Theta\Big(\eta_u^n\omega_0 P_s+\bar{P}_u\Big(d_{su}^n\Big)^{\alpha}\Big)}{\varrho}\right), \tag{5.23}$$

$$B\sum_{n\in\mathcal{N}}\tau_n\delta_t\log_2\left(1+\frac{\Theta\Big(\eta_u^n\omega_0 P_s+\bar{P}_u\Big(d_{su}^n\Big)^{\alpha}\Big)}{\varrho}\right)\geq S, \tag{5.24}$$

$$\sum_{i=1}^{n}\Big(E_{\text{fly}}^n(\mathbf{q})+\tau_n\delta_t\Big(P_b+P_u\Big)\Big)\leq\sum_{i=1}^{n}\frac{\mu(1-\tau_n)\delta_t\omega_0 P_{\text{WPT}}}{\Big(H^2+\|\mathbf{q}_n-\mathbf{w}_s\|^2\Big)^{\alpha/2}}, \tag{5.25}$$

$$\|\mathbf{q}_{n+1}-\mathbf{q}_n\|\leq\delta_d=V_{\max}\delta_t, n=0,\ldots,N-1, \tag{5.26}$$

$$\mathbf{q}_0=\mathbf{q}_{\text{I}},\mathbf{q}_N=\mathbf{q}_{\text{F}}, \tag{5.27}$$

$$0\leq\tau_n\leq 1, n\in\mathcal{N}, \tag{5.28}$$

where S is the demanded data (in bits) by the destination; constraint (5.23) guarantees a non-empty caching at the UB; constraint (5.24) means that the total transmitted data on the DL from $u\rightarrow d$ should be larger than or equal to the demanded data of the destination; constraint (5.28) implies that the DTS ratio value must be less than or equal to 1.

The problem $\mathcal{P}_1$ is a non-convex problem, which is NP-hard. Specifically, the objective function, constraints (5.23), (5.24), (5.25) are non-convex. Thus, it is troublesome to find the direct solution of $\mathcal{P}_1$. In the succeeding section, we introduce an efficient method to solve it.

5.3 Proposed Alternating Algorithm for Solving $\mathcal{P}_1$

To tackle the non-convexity of the problem $\mathcal{P}_1$, we first decompose $\mathcal{P}_1$ into two sub-problems, wherein we first target the optimization of DTS ratio for a given trajectory, and we perform the trajectory optimization for a given DTS ratio. By employing the

block coordinate descent (BCD) method [249], we propose an efficient iterative algorithm wherein we alternately optimize three subproblems until the algorithm converges to a given threshold, $\epsilon > 0$.

5.3.1 Dynamic Time Splitting Ratio Optimization:

For any given UB trajectory $\mathbf{q}$, the DTS ratio $\boldsymbol{\tau}$ can be obtained by solving the following optimization problem:

$$\mathcal{P}_1^{\boldsymbol{\tau}}: \quad \max_{\boldsymbol{\tau}} \quad \sum_{n\in\mathcal{N}} \tau_n \delta_t \bar{R}_d^n \tag{5.29}$$

$$\texttt{s.t.} \quad \sum_{n\in\mathcal{N}} \tau_n \delta_t \bar{R}_u^n + \sigma S \geq \sum_{n\in\mathcal{N}} \tau_n \delta_t \bar{R}_d^n,$$

$$\sum_{n\in\mathcal{N}} \tau_n \delta_t \bar{R}_d^n \geq S, \tag{5.30}$$

$$\sum_{i=1}^{n} \Big(E_{\text{fly}}^n(\mathbf{q}) + \tau_n \delta_t \Big(P_b + P_u \Big) \Big) \leq \sum_{i=1}^{n} \frac{\mu(1-\tau_n)\delta_t \omega_0 P_{\text{WPT}}}{\Big(H^2 + \|\mathbf{q}_n - \mathbf{w}_s\|^2 \Big)^{\alpha/2}}, \tag{5.31}$$

$$0 \leq \tau_n \leq 1, n \in \mathcal{N}. \tag{5.32}$$

It is clear that $\mathcal{P}_1^{\boldsymbol{\tau}}$ is a linear optimization problem, and hence is convex. Moreover, it is easy to verify that the Slater's condition holds for $\mathcal{P}_1^{\boldsymbol{\tau}}$ and thus the KKT conditions are sufficient for optimality [199, Section 5.5]. Then, the Lagrangian function corresponding to problem $\mathcal{P}_1^{\boldsymbol{\tau}}$ is expressed as

$$\mathcal{L}(\boldsymbol{\tau}, \lambda_1, \lambda_2, \lambda_3, \lambda_4) \triangleq F(\tau) + \lambda_1 G(\boldsymbol{\tau}) + \lambda_2 H(\boldsymbol{\tau}) + \lambda_3 I(\boldsymbol{\tau}) + \lambda_4 J(\boldsymbol{\tau}), \tag{5.33}$$

with

$$F(\boldsymbol{\tau}) \triangleq \sum_{n\in\mathcal{N}} \tau_n \delta_t \bar{R}_d^n \tag{5.34}$$

$$G(\boldsymbol{\tau}) \triangleq \Big(\sum_{n\in\mathcal{N}} \tau_n \delta_t \bar{R}_u^n + \sigma S - \sum_{n\in\mathcal{N}} \tau_n \delta_t \bar{R}_d^n \Big) \geq 0 \tag{5.35}$$

$$H(\boldsymbol{\tau}) \triangleq \sum_{n\in\mathcal{N}} \tau_n \delta_t \bar{R}_d^n - S \geq 0, \tag{5.36}$$

$$I(\boldsymbol{\tau}) \triangleq \sum_{i=1}^{n} \chi_1 (1-\tau_n) - \sum_{i=1}^{n} \Big(E_{\text{fly}}^n(\mathbf{q}) + \tau_n \delta_t \Big(P_b + P_u \Big) \Big) \geq 0, \tag{5.37}$$

$$J(\boldsymbol{\tau}) \triangleq 1 - \tau_n \geq 0. \tag{5.38}$$

where λ_1, λ_2, λ_3, λ_4 is the Lagrangian dual variables; $\chi_1 \triangleq \frac{\mu \delta_t \omega_0 P_{\text{WPT}}}{\Big(H^2 + \|\mathbf{q}_n - \mathbf{w}_s\|^2 \Big)^{\alpha/2}}$.

The stationarity condition is given as

$$\begin{aligned} &\frac{\partial \mathcal{L}(\boldsymbol{\tau}, \lambda_1, \lambda_2, \lambda_3, \lambda_4)}{\partial \boldsymbol{\tau}} \\ &= \sum_{n\in\mathcal{N}} \delta_t \bar{R}_d^n + \lambda_1 \Big(\sum_{n\in\mathcal{N}} \delta_t \bar{R}_u^n - \sum_{n\in\mathcal{N}} \delta_t \bar{R}_d^n \Big) \\ &+ \lambda_2 \sum_{n\in\mathcal{N}} \delta_t \bar{R}_d^n - \lambda_3 \Big(\sum_{n\in\mathcal{N}} \chi_1 + \sum_{n\in\mathcal{N}} \delta_t \Big(P_b + P_u \Big) \Big) - \lambda_4 = 0. \end{aligned} \tag{5.39}$$

The conditions for primal feasibility are given as (5.35), (5.36), (5.37), and (5.38). Then, the complementary slackness conditions can be expressed as follows

$$\lambda_1 G(\boldsymbol{\tau}) = 0, \tag{5.40}$$

$$\lambda_2 H(\boldsymbol{\tau}) = 0, \tag{5.41}$$

$$\lambda_3 I(\boldsymbol{\tau}) = 0, \tag{5.42}$$

$$\lambda_4 J(\boldsymbol{\tau}) = 0. \tag{5.43}$$

Furthermore, the dual feasibility conditions should hold $\lambda_1, \lambda_2, \lambda_3, \lambda_4 \geq 0$. The solution is then postulated in the following theorem.

Theorem 10. *The optimal value $\{\tau_n^\star\}$ to problem $\mathcal{P}_1^{\boldsymbol{\tau}}$ can be expressed as*

$$\tau_n^\star = \begin{cases} \left[\dfrac{\sigma S}{N\delta_t(\bar{R}_d^n - \bar{R}_u^n)}\right]_0^1, \ \text{iff}\, \bar{R}_d^n > \bar{R}_u^n, \forall n \in \mathcal{N} \\ \left[\dfrac{\chi_1 - E_{\text{fly}}^n(\mathbf{q})}{\chi_1 + \delta_t\Big(P_b + P_u\Big)}\right]_0^1. \end{cases} \tag{5.44}$$

From Eq. (5.44)*, we report two possible solutions of $\{\tau_n^\star\}$. In order to reach to an optimal outcome, we select the best solution that maximizes the objective function in $\mathcal{P}_1^{\tau}$. Particularly, the optimal value of $\{\tau_n^\star\}$ from* (5.44) *must be guaranteed to be inside the feasible set, i.e.,* $0 \leq \tau_n \leq 1$.

Proof. See Appendix B.2. □

5.3.2 Trajectory Optimization:

For given values of $\boldsymbol{\tau}$, the UAV trajectory $\mathbf{q}$ can be achieved by solving the following problem

$$\mathcal{P}_1^{\mathbf{q}}: \qquad \max_{\mathbf{q}} \ \ B\sum_{n\in\mathcal{N}} \tau_n \delta_t \log_2\left(1 + \frac{\Theta\Big(\eta_u^n \omega_0 P_s + \bar{P}_u\Big(d_{su}^n\Big)^\alpha\Big)}{\varrho}\right) \tag{5.45}$$

$$\texttt{s.t.}$$

$$B\sum_{n\in\mathcal{N}} \tau_n \delta_t \log_2\left(1 + \frac{e^{-E}\omega_0 P_s^n}{\Big(H^2 + \|\mathbf{q}_n - \mathbf{w}_s\|^2\Big)^{\alpha/2}\sigma_u^2}\right) + \sigma S$$

$$\geq B\sum_{n\in\mathcal{N}} \tau_n \delta_t \log_2\left(1 + \frac{\Theta\Big(\eta_u^n \omega_0 P_s + \bar{P}_u\Big(d_{su}^n\Big)^\alpha\Big)}{\varrho}\right), \tag{5.46}$$

$$B\sum_{n\in\mathcal{N}} \tau_n \delta_t \log_2\left(1 + \frac{\Theta\Big(\eta_u^n \omega_0 P_s + \bar{P}_u\Big(d_{su}^n\Big)^\alpha\Big)}{\varrho}\right) \geq S, \tag{5.47}$$

$$\sum_{i=1}^{n}\Big(E_{\text{fly}}^{n}(\mathbf{q})+\tau_n\delta_t\Big(P_b+P_u\Big)\Big)$$
$$\leq\sum_{i=1}^{n}\frac{\mu(1-\tau_n)\delta_t\omega_0P_s}{\Big(H^2+\|\mathbf{q}_n-\mathbf{w}_s\|^2\Big)^{\alpha/2}}, \tag{5.48}$$
$$(5.26),(5.27), \tag{5.49}$$

The problem $\mathcal{P}_1^{\mathbf{q}}$ is still non-convex, which is difficult to efficiently solve by utilizing standard optimization methods. To make $\mathcal{P}_1^{\mathbf{q}}$ more tractable, we firstly introduce slack variables z_1^n and z_2^n such that $\Big(H^2+\|\mathbf{q}_n-\mathbf{w}_s\|^2\Big)\leq(z_1^n)^{2/\alpha}$ and $\Big(H^2+\|\mathbf{q}_n-\mathbf{w}_d\|^2\Big)\leq(z_2^n)^{2/\alpha}$, respectively. Let us denote $\mathbf{z}\triangleq\{z_1^n,z_2^n,n\in\mathcal{N}\}$, by which the problem $\mathcal{P}_1^{\mathbf{q}}$ is rewritten as

$$\mathcal{P}_{1.1}^{\mathbf{q}}: \quad \max_{\mathbf{q},\mathbf{z}} \quad B\sum_{n\in\mathcal{N}}\tau_n\delta_t\log_2\left(1+\frac{\Theta\Big(\eta_u^n\omega_0P_s+\bar{P}_uz_1^n\Big)}{z_1^nz_2^n}\right) \tag{5.50}$$
$$\texttt{s.t.} \quad \Big(H^2+\|\mathbf{q}_n-\mathbf{w}_s\|^2\Big)\leq(z_1^n)^{2/\alpha}, \tag{5.51}$$
$$\Big(H^2+\|\mathbf{q}_n-\mathbf{w}_d\|^2\Big)\leq(z_2^n)^{2/\alpha}, \tag{5.52}$$
$$B\sum_{n\in\mathcal{N}}\tau_n\delta_t\log_2\left(1+\frac{e^{-E}\omega_0P_s^n}{z_1^n\sigma_u^2}\right)+\sigma S$$
$$\geq B\sum_{n\in\mathcal{N}}\tau_n\delta_t\log_2\left(1+\frac{\Theta\Big(\eta_u^n\omega_0P_s+\bar{P}_uz_1^n\Big)}{z_1^nz_2^n}\right), \tag{5.53}$$
$$B\sum_{n\in\mathcal{N}}\tau_n\delta_t\log_2\left(1+\frac{\Theta\Big(\eta_u^n\omega_0P_s+\bar{P}_uz_1^n\Big)}{z_1^nz_2^n}\right)\geq S, \tag{5.54}$$
$$\sum_{i=1}^{n}\Big(E_{\text{fly}}^{n}(\mathbf{q})+\tau_n\delta_t\Big(P_b+P_u\Big)\Big)\leq\sum_{i=1}^{n}\frac{\mu(1-\tau_n)\delta_t\omega_0P_s}{z_1^n}, \tag{5.55}$$
$$(5.26),(5.27), \tag{5.56}$$

Note that the problem $\mathcal{P}_{1.1}^{\mathbf{q}}$ is simpler than $\mathcal{P}_1^{\mathbf{q}}$, but it is still difficult to be directly

solved. This is because the objective function is convex and the non-convexity of constraints (5.53), (5.54), and (5.55). In the following, we transform $\mathcal{P}_{1.1}^{\mathfrak{q}}$ into a convex form by introducing the following lemmas:

Lemma 11. *For any given $z_1^{n,j}$ and $z_2^{n,j}$ at j-th iteration, $\log_2\left(1+\frac{e^{-E}\omega_0 P_s^n}{z_1^n\sigma_u^2}\right)$ and $\log_2\left(1+\frac{\Theta\left(\eta_u^n\omega_0 P_s+\bar{P}_u z_1^n\right)}{z_1^n z_2^n}\right)$ are respectively lower bounded by*

$$\log_2\left(1+\frac{e^{-E}\omega_0 P_s}{z_1^n\sigma_u^2}\right)\geq \log_2\left(1+\frac{e^{-E}\omega_0 P_s}{z_1^{n,j}\sigma_u^2}\right)-\frac{e^{-E}\omega_0 P_s(z_1^n-z_1^{n,j})}{z_1^{n,j}(z_1^{n,j}\sigma_u^2+e^{-E}\omega_0 P_s)\ln 2}\triangleq\Theta_1, \tag{5.57}$$

$$\begin{aligned}\log_2\left(1+\frac{\Theta\left(\eta_u^n\omega_0 P_s+\bar{P}_u z_1^n\right)}{z_1^n z_2^n}\right)&\geq \log_2\left(1+\frac{\Theta\left(\eta_u^n\omega_0 P_s+\bar{P}_u z_1^{n,j}\right)}{z_1^{n,j}z_2^{n,j}}\right)\\&-\frac{\Theta\eta_u^n\omega_0 P_s(z_1^n-z_1^{n,j})}{z_1^{n,j}\left(\Theta\eta_u^n\omega_0 P_s+z_1^{n,j}(\Theta\bar{P}_u+z_2^{n,j})\right)\ln 2}\\&-\frac{\Theta\left(\eta_u^n\omega_0 P_s+\bar{P}_u z_1^{n,j}\right)(z_2^n-z_2^{n,j})}{z_2^{n,j}\left(\Theta\eta_u^n\omega_0 P_s+z_1^{n,j}(\Theta\bar{P}_u+z_2^{n,j})\right)\ln 2}\triangleq\Theta_2.\end{aligned} \tag{5.58}$$

Proof. It is observed that $\log_2\left(1+1/x\right)$ and $\log_2\left(1+(A_2+A_3x)/xy\right)$ are convex functions, with $x>0$ and $y>0$, see Appendix B.3. Then, we adopt the first-order Taylor approximation to respectively approximate above convex functions at any given feasible points x^j, y^j as

$$\log_2\left(1+\frac{A_1}{x}\right)\geq\log_2\left(1+\frac{A_1}{x^j}\right)-\frac{A_1}{x^j(x^j+A_1)\ln 2}(x-x^j), \tag{5.59}$$

$$\begin{aligned}\log_2\left(1+\frac{A_2+A_3x}{xy}\right)&\geq\log_2\left(1+\frac{A_2+A_3x^j}{x^jy^j}\right)-\frac{A_2(x-x^j)}{x^j\left(A_2+x^j(A_3+y^j)\right)\ln 2}\\&-\frac{\left(A_2+A_3x^j\right)(y-y^j)}{y^j\left(A_2+x^j(A_3+y^j)\right)\ln 2}.\end{aligned} \tag{5.60}$$

By applying $A_1\triangleq e^{-E}\omega P_s$, $x\triangleq z_1^n$, $y\triangleq z_2^n$, $A_2\triangleq\Theta\eta_u^n\omega_0 P_s$, and $A_3\triangleq\Theta P_u$ then the Lemma 11 is proved. □

Lemma 12. *For any given $z_1^{n,j}$ at the j-th iteration, the lower bound of $1/z_1^n$ can be*

expressed as

$$\frac{1}{z_1^n} \geq \frac{1}{z_1^{n,j}} - \frac{1}{(z_1^{n,j})^2}(z_1^n - z_1^{n,j}) \triangleq \tilde{z}_1^n. \tag{5.61}$$

Then, we obtain the following optimization problem:

$$\mathcal{P}_{1.2}^{\mathbf{q}}: \quad \max_{\mathbf{q},\mathbf{z}} \quad B\sum_{n\in\mathcal{N}} \tau_n \delta_t \Theta_2 \tag{5.62}$$

$$\texttt{s.t.} \quad (5.26), (5.27), (5.51), (5.52), \tag{5.63}$$

$$B\sum_{n\in\mathcal{N}} \tau_n \delta_t \Theta_1 + \sigma S \geq B\sum_{n\in\mathcal{N}} \tau_n \delta_t \Theta_2, \tag{5.64}$$

$$B\sum_{n\in\mathcal{N}} \tau_n \delta_t \Theta_2 \geq S, \tag{5.65}$$

$$\sum_{i=1}^{n}\Big(E_{\text{fly}}^n(\mathbf{q}) + \tau_n\delta_t\Big(P_b + P_u\Big)\Big) \leq \sum_{i=1}^{n}\mu(1-\tau_n)\delta_t\omega_0 P_s \tilde{z}_1^n. \tag{5.66}$$

The problem $\mathcal{P}_{1.2}^{\mathbf{q}}$ is still non-convex due to the second term of $E_{\text{fly}}^n(\mathbf{q})$ (5.8). To tackle this issue, we introduce slack variable y_n, such that

$$\sqrt{\delta_t^4 + \kappa_2^2\Delta_n^4} - \kappa_2\Delta_n^2 \leq y_n^2, \forall n \in \mathcal{N}. \tag{5.67}$$

After some manipulations, it yields

$$\frac{\delta_n^4}{y_n^2} \leq y_n^2 + 2\kappa_2\Delta_n^2. \tag{5.68}$$

Consequently, the second term of $E_{\text{fly}}^n(\mathbf{q})$ can be substituted by $P_1 y_n$ and $E_{\text{fly}}^n(\mathbf{q})$ is replaced by its upper bound

$$E_{\text{fly}}^n(\mathbf{q}) \leq P_0\left(\delta_t + \kappa_1\Delta_n^2\right) + P_1 y_n + \frac{\kappa_3\Delta_n^3}{\delta_t^2} \triangleq \bar{E}_{\text{fly}}^n(\mathbf{q}), \tag{5.69}$$

With the above manipulations, $\mathcal{P}_{1.3}^{\mathbf{q}}$ can be re-written as

$$\mathcal{P}_{1.3}^{\mathbf{q}}: \quad \max_{\mathbf{q},\mathbf{z}} \quad B\sum_{n\in\mathcal{N}}\tau_n\delta_t\Theta_2 \tag{5.70}$$

$$\texttt{s.t.} \quad (5.26),(5.27),(5.51),(5.52),(5.64),(5.65), \tag{5.71}$$

$$\sum_{i=1}^{n}\Big(\bar{E}_{\text{fly}}^{n}(\mathbf{q})+\tau_n\delta_t\Big(P_b+P_u\Big)\Big) \leq \sum_{i=1}^{n}\mu(1-\tau_n)\delta_t\omega_0 P_s\tilde{z}_1^n \tag{5.72}$$

$$\frac{\delta_n^4}{y_n^2}\leq y_n^2+2\kappa_2\left\|\mathbf{q}_{n+1}-\mathbf{q}_n\right\|^2,\forall n \tag{5.73}$$

The problem $\mathcal{P}_{1.3}^{\mathbf{q}}$ is still non-convex due to non-convex constraint (5.73). Thus, we apply first-order Taylor to convexify (5.73) as follows

$$\frac{\delta_n^4}{y_n^2}\leq (y_n^j)^2+2y_n^j\Big(y_n-y_n^j\Big)-2\kappa_2\left\|\mathbf{q}_{n+1}^j-\mathbf{q}_n^j\right\|^2 + 4\kappa_2\Big(\mathbf{q}_{n+1}^j-\mathbf{q}_n^j\Big)^T\Big(\mathbf{q}_{n+1}-\mathbf{q}_n\Big),\forall n. \tag{5.74}$$

Bearing all the above discussions in mind, we solve the following approximate convex problem at the j-th iteration:

$$\mathcal{P}_{1.4}^{\mathbf{q}}: \quad \max_{\mathbf{q},\mathbf{z}} \quad B\sum_{n\in\mathcal{N}}\tau_n\delta_t\Theta_2 \tag{5.75}$$

$$\texttt{s.t.}$$

$$(5.26),(5.27),(5.51),(5.52),(5.65),(5.72), \tag{5.76}$$

$$\frac{\delta_n^4}{y_n^2}\leq (y_n^j)^2+2y_n^j\Big(y_n-y_n^j\Big)-2\kappa_2\left\|\mathbf{q}_{n+1}^j-\mathbf{q}_n^j\right\|^2 +4\kappa_2\Big(\mathbf{q}_{n+1}^j-\mathbf{q}_n^j\Big)^T\Big(\mathbf{q}_{n+1}-\mathbf{q}_n\Big),\forall n. \tag{5.77}$$

Since the objective function and all constraints pf $\mathcal{P}_{1.4}^{\mathbf{q}}$ are convex, thus it can be directly solved by applying standard optimization methods [199]. To this end, we propose an iterative algorithm based on the solutions of three sub-problems. The alternating algorithm is summarized as in Algorithm 8.

To ensure the feasibility of Algorithm 8, an appropriate initial point is required. In our setup, we set $\eta_u^{n,j}=\eta_{\max}$, $\tau_{n,j}=0.5$. Notably, the convergence of Algorithm 8 depends on the initial trajectory. The initial UAV trajectory should be selected such that the feasibility of (5.72) is fulfilled while also guaranteeing other constraints. Thus, we can obtain $\mathbf{q}^j$ by

Algorithm 8 Proposed Iterative Algorithm to Solve $\mathcal{P}_1$

1: **REQUIRE**
2: Set $j := 0$ and initialize $\mathbf{q}^j$, $\boldsymbol{\tau}^j$.
3: **REPEAT**
4: Solve $\mathcal{P}_1^{\boldsymbol{\tau}}$ for given $\{\mathbf{q}^j\}$ and denote the optimal solution as $\boldsymbol{\tau}^\star$.
5: Solve$\mathcal{P}_1^{\mathbf{q}}$ for given $\{\boldsymbol{\tau}^{j+1}\}$ and denote the optimal solution as $\mathbf{q}^\star$.
6: Update the local point $\boldsymbol{\tau}^{j+1} = \boldsymbol{\tau}^\star$ and $\mathbf{q}^{j+1} = \mathbf{q}^\star$.
7: Set $j := j + 1$.
8: **UNTIL**
9: Convergence

solving the simplified version of $\mathcal{P}_{1.4}^{\mathbf{q}}$ as follows

$$\mathcal{P}_{\text{feasible}}^{\mathbf{q}}: \quad \max_{\mathbf{q},\{\zeta_n\}_{n=1}^N} \ \min_{n\in\mathcal{N}} \zeta_n \tag{5.78}$$

s.t.

$$(5.26), (5.27), (5.51), (5.52), (5.64), (5.65), (5.77), \tag{5.79}$$

$$\sum_{i=1}^{n} \mu(1-\tau_n)\delta_t\omega_0 P_s \tilde{z}_1^n - \sum_{i=1}^{n}\left(\bar{E}_{\text{fly}}^n(\mathbf{q}) + \tau_n\delta_t\Big(P_b + P_u\Big)\right) \geq \zeta_n, \forall n. \tag{5.80}$$

where ζ_n is the slack variable. The initial UAV trajectory is obtained until problem $\mathcal{P}_{\text{feasible}}^{\mathbf{q}}$ is successfully solved and $\zeta \geq 0,\ \forall n$.

5.3.3 Convergence and Complexity Analysis

Convergence Analysis

Proposition 13. *The proposed Algorithm 8 provides a solution that converges to at least a locally optimal solution.*

Proof. Let us define $\Pi(\boldsymbol{\tau}^j, \mathbf{q}^j)$ and $\Pi_{\text{lb}}^{\mathbf{q}}(\boldsymbol{\tau}^j, \mathbf{q}^j)$ as the objective values of $\mathcal{P}_1$ and $\mathcal{P}_{1.4}^{\mathbf{q}}$ at the j-th iteration. In the $(j+1)$-th iteration, at line 2 of Algorithm 8, we have

$$\Pi(\boldsymbol{\tau}^j, \mathbf{q}^j) \overset{i}{\leq} \Pi(\boldsymbol{\tau}^{j+1}, \mathbf{q}^j). \tag{5.81}$$

The inequality (i) holds since $\boldsymbol{\tau}^{j+1}$ is an optimal solution of $\mathcal{P}_1^{\boldsymbol{\tau}}$. Then, at line 3 of Algorithm 8, we have

$$\begin{aligned}\Pi(\boldsymbol{\tau}^{j+1}, \mathbf{q}^j) &\overset{i2}{=} \Pi_{\text{lb}}^{\mathbf{q}}(\boldsymbol{\tau}^{j+1}, \mathbf{q}^j) \\ &\overset{i3}{\leq} \Pi_{\text{lb}}^{\mathbf{q}}(\boldsymbol{\tau}^{j+1}, \mathbf{q}^{j+1}) \overset{i4}{\leq} \Pi(\boldsymbol{\tau}^{j+1}, \mathbf{q}^{j+1}).\end{aligned} \tag{5.82}$$

TABLE 5.1: Simulation Parameters

Parameters	Values
UAV's altitude, H	10 meters [138]
Maximum speed, $V_{\max}$	20 m/s [138]
Noise power, σ^2	-90 dB [138]
Path loss exponent, α	2.3 [121]
Backscatter circuit power consumption P_b	$10^{-6}W$ [251]
Channel power gain at reference distance, ω_0	-30 dB [138]
Time slot duration, δ_t	0.5 second
Error tolerance threshold, ϵ	10^{-4}
Energy harvesting coefficient, μ	0.84 [252]
Maximum backscatter coefficient, $\eta_{\max}$	0.5 [246]
Transmit power of source used for information transmission, P_s	16 dBm
Transmit power of source used for charging the UAV, P_{WPT}	[27,40] dB [85]
Demanded data of the destination, S	50 Mbits
Error tolerance, ϵ	10^{-4}

The equality $(i2)$ holds since the first-order Taylor approximation as in (5.57), (5.58), (5.61), and (5.74) are tight at given point $\mathbf{q}^j$, and the inequality $(i3)$ holds since $\mathbf{q}^{j+1}$ is an optimal solution of $\mathcal{P}_{1.4}^{\mathbf{q}}$. Furthermore, the inequality $(i4)$ holds since the optimal value of $\mathcal{P}_{1.4}^{\mathbf{q}}$ is a lower bound of $\mathcal{P}_1^{\mathbf{q}}$ at given $\mathbf{q}^{j+1}$. From (5.82) and (5.81), we have $\Pi(\boldsymbol{\tau}^j, \mathbf{q}^j) \leq \Pi(\boldsymbol{\tau}^{j+1}, \mathbf{q}^{j+1})$ which proves that the objective value of $\mathcal{P}_1$ is non-decreasing over the iterations. Moreover, the objective value of $\mathcal{P}_1$ is restricted by an upper bound value due to the limited total traveling time T, transmit power P_s, UB transmit power P_u, and maximum value of $\eta_{\max}$. Thus, the convergence of Algorithm 8 is assured. □

Complexity Analysis

We provide the worst-case complexity analysis for Algorithm 8. Since the problem $\mathcal{P}_1^{\boldsymbol{\tau}}$ can be solved by using the proposed closed-form expressions, thus the complexity is mainly relied on addressing $\mathcal{P}_1^{\mathbf{q}}$. Moreover, the problem $\mathcal{P}_1^{\mathbf{q}}$ includes logarithmic form, thus its complexity is $\mathcal{O}\Big(L_1(3N)^{3.5}\Big)$, where $3N$ is the number of scalar variables and L_1 is the number of iterations to update UB trajectory [250]. Then, the overall complexity of Algorithm 8 is $\mathcal{O}\Big(L_2L_1(3N)^{3.5}\Big)$ where L_2 is the number of iterations until convergence.

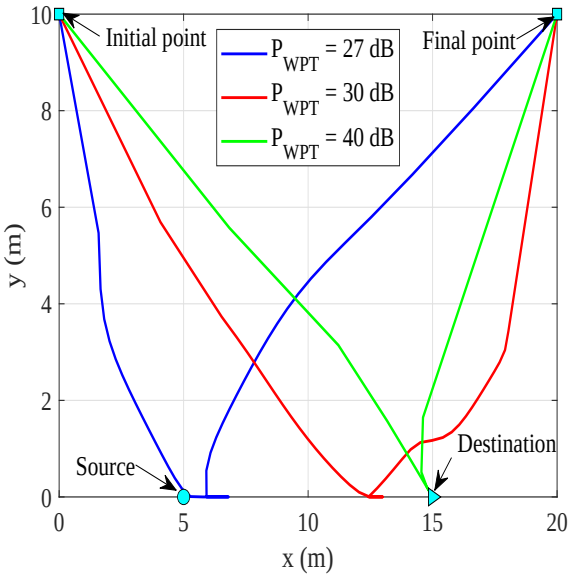

FIGURE 5.2: UB trajectory obtained by our proposed scheme with different values of P_{WPT}.

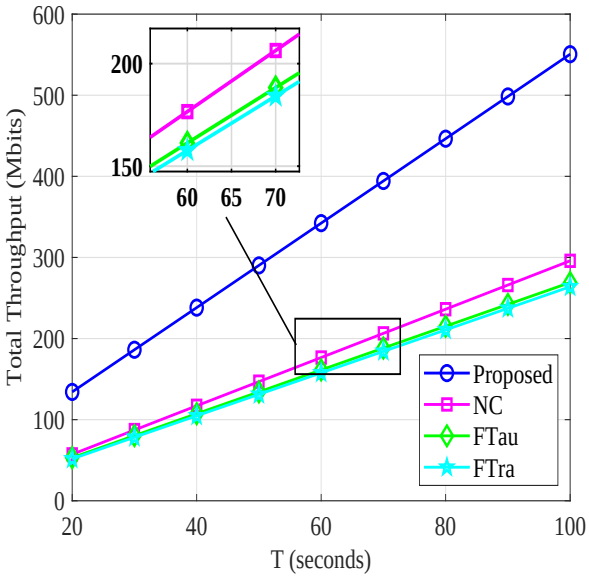

FIGURE 5.3: Total throughput versus traveling time T.

5.4 Simulation Results

In this section, the numerical results are given to validate the performance of our proposed scheme. We assume that the horizontal locations of the source and destination are set as $\mathbf{w}_s = [5m, 0]^T$ and $\mathbf{w}_d = [15m, 0]^T$, respectively. The UB's initial and final locations are respectively set $\mathbf{q}_{\text{I}} = [0, 10m]^T$ and $\mathbf{q}_{\text{F}} = [20m, 10m]^T$. The UB altitude is fixed at $H = 10$ meters with maximum transmit power $P_u \in [5, 10]$ mW and maximum velocity $V_{\max} = 20$ m/s [138]. Moreover, the transmit power of source S used for WPT and information transmission are set as $P_{\text{WPT}} \in [27, 40]$ dB [85] and $P_s = 16$ dBm, respectively. the power channel gain at reference distance $d = 1m$ is -30 dB [138] and the noise power at the source and destination is -90 dB [**?**]. The circuit power consumption of typical backscatter trasmitter is less than 1 μW [251], thus we set $P_b = 10^{-6}$ W. The maximum backscatter coefficient equals to 0.5 [246]. Each time slot duration equals to 0.5 second and energy harvesting coefficient is 0.84 [252]. The system bandwidth is $B = 1$ Mhz. The error tolerance threshold of alternating algorithms is set to $\epsilon = 10^{-4}$. To highlight the designed algorithms, we compare our proposed methods with benchmark schemes. Specifically, benchmark schemes are described as follows:

- No caching (NC): Similar to Algorithm 8 but without caching capability.

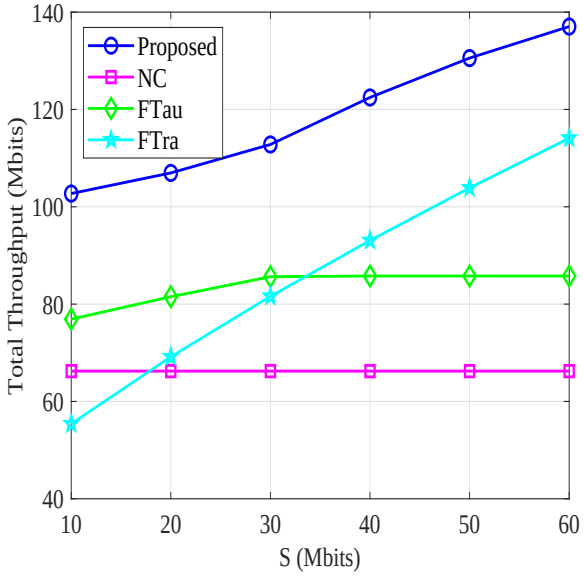

FIGURE 5.4: Total throughput versus demanded data of the destination S.

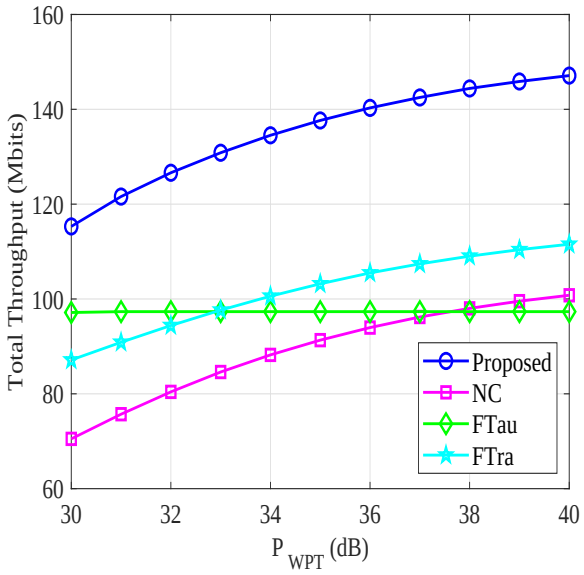

FIGURE 5.5: Total throughput versus P_{WPT}.

- Fixed DTS ratio (FTau): Similar to Algorithm 8 but with fixed DTS ratio, $\tau_n = 0.5$.
- Fixed trajectory (LFTra): Similar to Algorithm 8 but with fixed trajectory, wherein the UB flies from initial position to the middle point between source and destination then it returns to the final position.

Fig. 5.2 illustrates the UB trajectories obtained for the proposed algorithm at different charging power values of the source, i.e., P_{WPT} equals to 27 dB, 30 dB, and 40 dB. Moreover, δ_t and P_s = are set as 0.5 second and 16 dBm, respectively. It can be seen from Fig. 5.2 that the P_{WPT} significantly affects the UB's trajectory. Specifically, the UB tends to fly from the initial point to the source node and then return back to the final location when P_{WPT} is equal to 27 dB. Besides, the UB can move towards the destination with the increase of P_{WPT} values. For instance, when the charging power of the source is increased from 27 dB to 40 dB, UB will move in the direction closer to the destination location to improve the total throughput. This is because when the P_{WPT} is small, the UB should fly closer to source S to improve the harvested energy, which can satisfy constraint (5.25). Especially, the harvested energy is maximized as the UB can hover over the source location, as explained in the right-hand sight (RHS) of (5.25). Furthermore, when the P_{WPT} value is high enough, the constraint (5.25) can be guaranteed. Thus, the UB can fly closer to the destination to maximize achievable throughput.

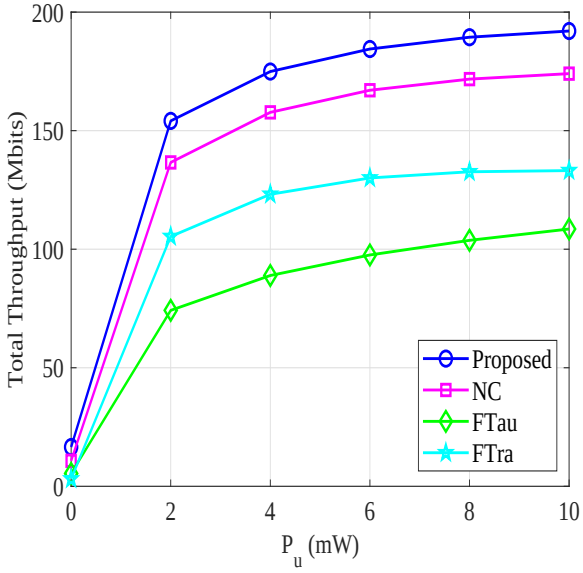

FIGURE 5.6: Total throughput versus transmit power of the UAV P_u.

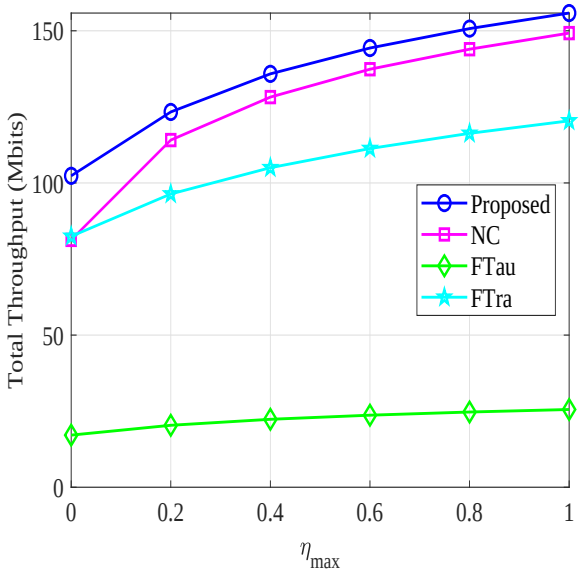

FIGURE 5.7: Total throughput versus $\eta_{\max}$.

In Fig. 5.3, we investigate the influence of total traveling time to the performance with $\delta_t = 0.5$ second, $P_s = 40$ mW, $P_u = 5$ mW, $S = 50$ Mbits, $P_{\text{WPT}} = 33$ dB. We observe that all the algorithms are linearly increasing with a higher number of traveling time T (in seconds). This is expected since the total collected throughput at the destination is proportional to the reflection time as in (5.22). As inferred from the results, the proposed algorithms significantly improve the total throughput (bps) as compared with the benchmarks. Specifically, at $T = 100$ seconds, the proposed algorithm can support a throughput up to 550.59 Mbps while the NC, FTau, FTra schemes respectively impose 295.85, 269.07, and 263.88. This demonstrates the superiority of our proposed method that jointly optimizes dynamic time splitting ratio and trajectory with caching at the UB compared to benchmark schemes with no caching capability, fixed DTS ratio, or fixed trajectory.

In Fig. 5.4, we study the influences of the demanded data S (in bits) to the total throughput, with $T = 30$ seconds, $P_s = 5$ mW, $V_{\max} = 20$ m/s, $H = 8$ m. We see that the performance of NC method is unaltered by increasing the demanded data S. This can be explained that since NC does not cache a part of requested file for data transmission to destination, we then have $\sigma S = 0$. Therefore, increasing the value of S has no effect on the NC scheme. Furthermore, our proposed algorithm performs much better than benchmark ones. Specifically, at $S = 60$ Mbits, the jointly optimization method can serve 137.03 Mbits while the NC, FTau, and FTra achieve less than 51.66 %, 37.39 %, and 16.71 %,

respectively. One more interesting point that can be observed from Fig. 5.4 is that the FTau scheme can achieve a better performance than FTra when the demanded data is small, i.e., $S < 30$ Mbits. Nevertheless, FTau's performance has deteriorated compared to FTra when $S > 30$ Mbits. Particularly, the performance of FTra is converged to a saturation value by growing S. This is because the total throughput is restricted by other resources, i.e., transmit power P_s, traveling time T, reflection time τ_n.

Fig. 5.5 illustrated the influences of the charging power of the source S on the achievable throughput of all schemes, with $P_u = 5$ mW, $P_s = 10$ mW, $\sigma = 0.7$, $T = 30$ seconds. First, we can see that the performance of the proposed, NC, and FTra is significantly enhanced with the increase of the P_{WPT} values while the NC performance looks unchanged. In fact, the total throughput of the NC scheme is slightly increased from 97.15 to 97.33 Mbits when P_{WPT} is from 30 to 31 dB. This is because the more the transmit power is assigned, the higher the harvested energy is achieved. Therefore, the UB can have more reflection time, i.e., higher value of τ_n, which satisfies the energy constraints as in Eqs. (5.10). Consequently, the system throughput is improved. However, because the NC scheme has a fixed τ value, the allocated time for data transmission is then unchanged, which restricts the NC's performance. Fig. 5.5 still shows the superiority of our proposed scheme over benchmark ones. More specifically, the Proposed, NC, FTAU, and FTra impose 115.3, 70.5, 97.15, and 87.14 Mbits when P_{WPT} equals 30 dB, respectively.

In Fig. 5.6, the total throughput is presented as a function of the transmit power of the UB P_u, where $T = 30$ seconds, $V_{\max} = 20$ m/s, $H = 5$ m, $S = 60$ Mbits. It is observed that the UB transmit power has dramatic impact on the total throughput obtained at the destination. Specifically, the obtained throughput of proposed scheme increases from 174.94 to 184.44 Mbits corresponding to P_u value equals to 4 and 6 mW, respectively. This is due to the fact that the total collected throughput depends on the transmit power P_u as shown in Eq. (5.22). Specially, we also compare our schemes in the use case of both passive with active transmission and when we only use passive mode (i.e., $P_u = 0$). Obviously, all schemes' performance when used in the active and passive transmission is far superior to that when using only passive mode. Specifically, the total throughput of our proposed, NC, Ftau, and Ftra is 16.56, 10.76, 5.4, and 3.1 when $P_u = 0$, respectively, while it can respectively obtain 154.12, 136.6, 74.21, and 105.36 when $P_u = 2$ mW. Nevertheless, increasing P_u does not always significantly improve network performance. For example, the performance of the Proposed scheme only slightly increases from 189.41 to 192.03 when P_u from 8 to 10 mW. This is because the throughput depends not only on transmit power of UB, but also on other factors such as bandwidth, flying time, source transmit power.

Fig. 5.7 presents an evaluation of the total throughput versus the maximum value of backscatter coefficient $\eta_{\max}$, with $T = 100$ seconds, $V_{\max} = 20$ m/s, $H = 8$ m, $P_u = 5$ mW, $S = 50$ Mbits, and $T = 20$ seconds. It is observed that the achievable throughput of all schemes is dramatically improved with the increase of the backscattering coefficient $\eta_{\max}$. Specifically, at $\eta_{\max} = 0.2$ (or 0.4), the total throughput of the proposed scheme is 123.33

Mbits (or 135.85 Mbits), respectively, while the NC obtains less than 7.49 % (or 5.62 %). Whereas the FTau and FTra respectively impose less than 83.49 % (or 83.56 %) and 21.85 % (or 22.7 %) compared to the proposed method. Particularly, we also depict the total throughput of all schemes in the case of no backscattering communications, i.e., $\eta_{\max} = 0$. Specifically, our proposed method is still better than other benchmarks in this scenario. Moreover, the performance of NC is worse than FTra, and the FTau is still the worst one. This demonstrates the superiority of our proposed joint optimization compared to other methods in practice with different parameters.

5.5 Summary

In this paper, a new self-energized EH model has been proposed to power the UAV communications. In this context, we have investigated the cache-assisted wireless powered UAV-enabled backscatter communciations. Specifically, we maximized the total throughput via jointly optimizing DTS ratio and trajectory. The formulated problem was non-convex which is troublesome to solve. Thus, we proposed efficient alternating algorithm based on BCD method and SCA technique to solve it. Particularly, the optimal DTS ratio for a given UB trajectory was derived in closed-form expression which significantly reduced the complexity of proposed solutions. We illustrated via simulation results that the proposed methods outperformed reference schemes in term of total throughput. Particularly, the simulation results showed the superiority of our design over scenarios with active or passive transmission only.

Chapter 6

Satellite- and Cache-assisted UAV Communications

Although fifth-generation (5G) mobile communication systems are being deployed worldwide, significant challenges due to the explosive growth of mobile data traffic still remain. This motivates the development of next-generation networks, i.e., beyond 5G or six-generation (6G), to provide ubiquitous connectivity and high-capacity. The combination of satellite, drone, and terrestrial network technologies shows great potential for next-generation systems to provide universal wireless access. In this chapter, we consider LEO satellite- and cache-assisted UAV communications for content delivery networks. Specifically, caching is provided by the UAV to reduce backhaul congestion, and the LEO satellite assists the UAV's backhaul link. In this context, we aim to maximize the minimum achievable throughput per ground user (GU) by jointly optimizing cache placement, the UAV's transmit power, bandwidth allocation, and trajectory with a limited cache capacity and operation time. The formulated problem is challenging to solve directly due to its non-convexity and combinatorial nature. To find a solution, the original problem is decomposed into three sub-problems: (1) cache placement optimization with fixed UAV resources (i.e., bandwidth and transmit power) and trajectory, followed by (2) the UAV bandwidth and transmit power optimization with fixed cache placement vector and trajectory, and finally, (3) we optimize the UAV trajectory with fixed cache placement and UAV resources. Based on the solutions of sub-problems, an efficient alternating algorithm is proposed utilizing the block coordinate descent (BCD) and successive convex approximation (SCA) methods. Simulation results show that the max-min throughput and total achievable throughput enhancement can be achieved by applying our proposed algorithm instead of other benchmark schemes.

The rest of the chapter is organized as follows. Introduction to the current state of the

art is discussed in Section 6.1. The system model and problem formulation are given in Section 6.2. The proposed iterative algorithm for solving satellite- and cache-aided UAV communications is presented in Section 6.3. Numerical results are depicted in Section 6.4, and Section 6.5 concludes the paper.

6.1 Introduction to Satellite- and Cache-assisted UAV Communications

Although fifth-generation (5G) wireless systems are being deployed around the world [88], the explosive growth of mobile data traffic still poses significant challenges for future networks, i.e., beyond 5G or 6G. It is predicted that individual user data rates will exceed 100 Gbps by 2030, and overall mobile data traffic will reach 5016 exabytes per month [89]. To overcome these challenges, the research community is working towards a sixth-generation (6G) system [90, 91]. Notably, the integration of satellite, aerial, and terrestrial networks is promoted as a key factor in providing high-capacity and ubiquitous connectivity for 6G [19, 90, 92].

Satellite communication (Satcom) has received considerable attention from both industry and academia due to its ability to provide wide-area coverage, e.g., telemedicine, military, satellite-assisted maritime communication, rescue missions, and disaster management system (DMS) [93–95]. Essentially, satellites are installed in geostationary earth orbit (GEO), medium earth orbit (MEO), and/or low earth orbit (LEO), which can complement and support terrestrial communication networks. Compared to its GEO and MEO counterparts, LEO Satcom operates at much lower altitudes, i.e., from 160 km to 2000 km [96], and it provides lower path losses and transmission latency. Therefore, many projects such as SpaceX, SPUTNIX, OneWeb, and Kepler plan to launch thousands of LEO satellites for providing globally seamless and high throughput communications cooperating with terrestrial communications [97]. Because of these benefits, many works have studied the hybrid LEO satellite-terrestrial communication networks [98–100]. You et al. [98] studied massive MIMO transmission for LEO satellite communications using full frequency reuse (FFR) and statistical channel state information (sCSI). In [99], the authors proposed a novel grant-free random access (GFRA) scheme to reduce the access delay in LEO satellite-enabled Internet of things (IoT) networks. In [100], they designed a Stackelberg game-based pricing mechanism for terrestrial and satellite operators by jointly optimizing the Ka-band spectrum allocation, C-band user association, and data service pricing.

In contrast to Satcom, the UAV can fly at much lower altitudes, and thus it can serve as a flying BS to serve GUs due to its flexibility, ease of deployment, and maneuverability. Herein, the satellite can provide a stable backhaul link to the UAV when terrestrial infrastructures are unavailable or have been destroyed after a disaster [90, 93]. Recently,

many works investigated the combination of satellite and UAVs in the integrated satellite-UAV-terrestrial network (ISUTN) [93, 105–107]. While [93, 105, 106] only considered dominated LoS channel in UAV communications, [107] proposed a general analytic framework for energy-efficient beamforming scheme of a satellite-aerial-terrestrial network (SATN). Specifically, satellite-UAV links follow Shadowed-Rician fading while the UAV-user links undergo Rician fading model. Nevertheless, these works [93,105–107], did not take caching into consideration.

Recent studies have shown that some popular contents are requested repeatedly by users, causing the majority of data traffic [242, 253]. Notably, UAVs only serve GUs by connecting to the content server via a wireless backhaul. However, with the explosive growth of the data traffic, the backhaul link can be overloaded due to limited capacity, reducing the user experience. Caching of popular content at the network edge has emerged as a solution to effectively eliminate bottlenecks to backhaul links, especially during peak traffic time. Furthermore, caching techniques can prolong the UAV's lifetime since the UAV can pre-store popular files in its cache to prevent repeated requests from GUs on backhaul links. Therefore, many works have extensively studied the benefits of caching in UAV communications [151, 167, 168, 170, 254, 255]. Ji et al. [254] maximized minimum throughput among GUs by jointly optimizing cache placement, UAV trajectory, and transmission power. Chai et al. [170] proposed an online cache-enabled UAV wireless design through jointly optimizing UAV trajectory, transmission power, and caching scheduling. In [167], the authors utilized proactive caching at GUs to overcome the UAV endurance issue via jointly optimizing the caching policy, UAV trajectory, and communication scheduling. Specifically, all the files are cached cooperatively at specified GUs. If a file is requested, it can be served locally if that GU contains the requested file; otherwise, it can be retrieved from neighboring users through device-to-device (D2D) communications. In [151], the authors adopted caching and backscatter communication (BackCom) to improve UAV lifetime. Specifically, they aimed to maximize total throughput via jointly optimizing the backscatter coefficient, dynamic time splitting ratio, and the UAV trajectory with linear and non-linear energy harvesting models. In [168], Cheng et al. proposed a new scheme to ensure the security of UAV wireless networks through jointly optimizing the UAV trajectory and time schedule. For GUs with caching capabilities, the UAV could broadcast files to them and prevent eavesdropping. For GUs without caching, the authors maximized the minimum average secrecy rate to guarantee GUs' security. In [255], Zhao et al. investigated caching- and UAV-assisted secure transmission for scalable videos in hyper-dense networks via interference alignment. In this work, both UAVs and small-cell base stations (SBSs) were equipped with caches to store popular videos at off-peak hours. To ensure secure transmission, the idle SBSs were exploited to generate jamming signal to disrupt eavesdropping.

Unlike previous works that only investigated the integration between satellite and UAV [105–107] or UAV and caching [151, 167, 168, 170, 254, 255], there are very few works

on satellite- and cache-assisted UAV communication networks in the literature [102, 256]. Shushi et al. [102] studied the energy-aware coded caching design cache-enabled satellite-UAV vehicle integrated network (CSUVIN). Notably, the authors in [102] aimed to minimize the total energy consumption of GEO satellite and UAV but did not solve the problem of maximizing the minimum throughput of GUs. In [256], the authors investigated a satellite-UAV mobile edge caching system in IoT networks, where the IoT users acted as relays to transfer information from satellite to UAV due to the assuming that there was no direct satellite-to-UAV transmission but stable links existed between the satellite and sensor users. Further, they considered limited storage capacity for the IoT users but not as a caching model for content-based networks. In the literature, reference [254] is the most relevant to our work. Nevertheless, [254] considered one-tier data transmission between UAVs to GUs. *In our work, we investigate a two-tier data transmission system model including satellite-to-UAV and UAV-to-user data transmissions.* This is motivated by the fact that the UAV only can pre-store a portion of popular content during off-peak hours and then forward this information to GUs. Due to the limited storage cache size, the UAV cannot store all the files in its cache. In the case that a GU demands content but is not stored in UAV's cache, the UAV will ask the LEO satellite to send the required file on the backhauling link. Moreover, reference [254] assumed that the transmitter only serves up to one requester at a time slot, which is an inefficient method. In this work, we assume that *the UAV can serve multiple GUs simultaneously to improve network performance, i.e., max-min throughput.* Motivated by these observations, our work proposes a novel system model in satellite- and cache-assisted UAV wireless networks that further explores the impact of data transmission latency for backhaul link from satellite-to-UAV due to large distance and limited resource allocation, which makes the problem design even more challenging to solve and has not been investigated before. *To the best of our knowledge, this is the first work that maximizes the GUs' minimum throughput via jointly optimizing UAV's bandwidth, UAV's transmit power, trajectory design, and cache placement in LEO satellite- and cache-assisted UAV wireless networks.* In summary, our contributions are as follows:

1. We propose a novel satellite- and cache-assisted UAV communication system. Specifically, caching techniques can reduce the burden on the backhaul link during peak times and prolong the UAV's lifetime. In addition, the LEO satellite helps to deliver requested content that is not cached by the UAV.

2. We formulate an optimization problem to maximize the minimum throughput at GUs, subject to the UAV's limited operation time, the UAV's maximum speed, the UAV's trajectory, limited cache capacity of the UAV, bandwidth allocation for the access link from the UAV to GUs, transmit power allocation at the UAV to transmit data of GU k. The formulation belongs to a mixed-integer nonlinear programming (MINLP) problem, which is challenging to solve. Especially, the binary nature of

caching decision-making variables makes it more troublesome.

3. We solve the problem by decomposing it into three sub-problems: (1) cache placement optimization with given UAV resources (i.e., bandwidth and transmit power) and trajectory, followed by (2) the UAV bandwidth and transmit power optimization with given cache placement vector and trajectory, and finally, (3) we optimize the UAV trajectory with given cache placement vector and UAV resources. Based on the sub-problems' obtained solutions, we propose an iterative algorithm to solve the non-convex optimization problem by adopting the block coordinate descent (BCD) method and successive convex approximation (SCA) techniques.

4. The proposed algorithm's effectiveness is shown via simulation results. In particular, our approach yields an improvement up to 26.64%, 79.79%, and 87.96% in max-min throughput compared to the benchmark scheme one (BS1), benchmark scheme two (BS2), and benchmark scheme three (BS3), respectively. More specifically, BS1, BS2, and BS3 are designed similarly to the proposed algorithm but with fixed trajectory, no caching capability, and fixed resource allocation, respectively.

6.2 System Model and Problem Formulation

We consider the downlink of a wireless communication system consisting of a LEO satellite constellation [106], a UAV acts as a flying base station (BS), and a set of K ground users (GUs) denoted by $\mathcal{K} = \{1, \ldots, k, \ldots, K\}$. All GUs are assumed to be within the coverage area of the considered LEO satellite, but it cannot take advantages of the benefits from broadband service since they are not equipped with expensive high-gain antennas [93]. Therefore, the UAV acts as an aerial BS to serve GUs on the access links (ALs), wherein it requests the demanded contents from satellite on the backhaul link (BL). Notably, the satellite backhaul for content delivery is selected because it can broadcast content to multiple UAVs. Further, we assume that the cells of multiple UAVs do not interfere either because they are geographically distant or they use different frequencies; thus, we focus on studying a single UAV. To reduce the problem of congestion in the backhaul link, the UAV is equipped with a cache [121,254,257] and it can pre-store a part of popular contents from a ground base station (GBS) during off-peak hours and then forward this information to the GUs. We assume that the flight time of the UAV is T due to the limited battery capacity. For ease of analysis, T is divided into N equal time slot with duration δ_t, denoted by $\mathcal{N} \triangleq \{1, \ldots, n \ldots, N\}$. Since δ_t is chosen sufficiently small, the distance between the UAV and GU k is assumed to be unchanged during each time slot n [78]. Moreover, we utilize the Cartesian coordinate system, whereas the location of GU k is $\mathbf{w}_k \in \mathbb{R}^{2\times 1}, k \in \mathcal{K}$. For ease of analysis, the UAV's altitude is assumed to be fixed at H_u meters during the flight, e.g., this is imposed by the regulator for safety requirements. The horizontal location of

TABLE 6.1: List of Notation

Notations	Descriptions
$\mathcal{K}$	The set of K ground users, $k \in \mathcal{K}$
$\mathcal{N}$	The set of N time slots, $n \in \mathcal{N}$
$\mathcal{F}$	The set of F contents in the network, $f \in \mathcal{F}$
T	Total flying time of the UAV
δ_t	Duration of one time slot n, with $n \in \mathcal{N}$
δ_d	Maximum distance that the UAV can travel during time slot n, with $n \in \mathcal{N}$
$\mathbf{w}_k \in \mathbb{R}^{2\times 1}, k \in \mathcal{K}$	Cartersian coordinates of the GU k
$\mathbf{q}_n \in \mathbb{R}^{2\times 1}, k \in \mathcal{K}$	The horizontal location of the UAV during time slot n, with $n \in \mathcal{N}$
H_u	The flying altitude of the UAV
d_{1k}	Distance between satellite and the UAV
d_{2k}^n	Distance between the UAV and GU k during time slot n
h_{1k}^n	Channel coefficient between satellite and the UAV to transmit the demanded data for GU k
h_{2k}^n	Channel coefficient between the UAV and GU k
η_f	Binary variable $\eta_f \in \{0, 1\}$ indicates the UAV caches content f or not
b_{2k}^n	$0 \leq b_{2k}^n \leq 1$ denotes the allocation bandwidth for the UAV to transmit GU k's requested content during time slot n
p_{2k}^n	The UAV transmit power to convey GU k's requested content during time slot n
β_0	Channel gain at the reference distance, i.e., $d_0 = 1$ meter
S	Maximum number of contents that the UAV can cache

the UAV during time slot n is denoted by $\mathbf{q}_n = [x_n, y_n]$. Key notations used in this work are listed in Table 6.1.

6.2.1 Caching Model

The satellite is assumed to access to a set of F contents, denoted by $\mathcal{F} \triangleq \{1, \ldots, f, \ldots, F\}$. All contents are assumed to have the same size of Q bits. For different size contents, they can be split into several chunks with equal size [93, 258]. Therefore, this assumption is applicable in realistic scenarios. In this chapter, we consider Zipf distribution which is the most popular content popularity model [253]. Then, the demanded probability for any

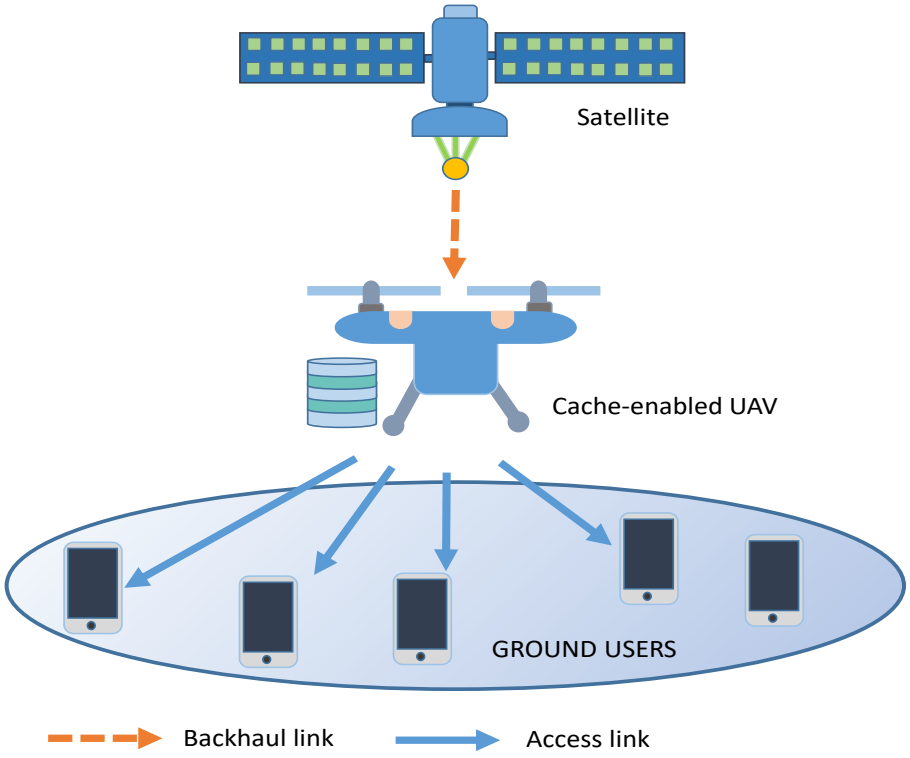

FIGURE 6.1: System model: The cache-aided UAV acts as a flying base station to transfer data to ground users, wherein the satellite can provide backhaul link to the UAV.

content f being requested by GU k is given by

$$P_f = \frac{f^{-\varrho}}{\sum_{i=1}^{F} i^{-\varrho}}, \tag{6.1}$$

where ϱ is the Zipf skewness factor with $0 < \varrho < 1$ and $\sum_{f \in \mathcal{F}} P_f = 1$.

We assume that the UAV can proactively cache a part of popular contents in its storage during off-peak hours. Specifically, this chapter utilizes the placement-then-delivery method. Notably, cache placement is also a part of the optimization problem, which is performed offline before the UAV takes off. Due to the limited storage cache size, the UAV cannot store all files in its cache. In case a GU requests content but is not cached by the UAV, the UAV will ask the satellite to send the required file on the BL. Let us define

$\boldsymbol{\eta} \triangleq \{\eta_f, \forall f \in \mathcal{F}\}$ as the cache placement vector of the UAV, where $\eta_f \in \{0, 1\}$. Specifically, $\eta_f = 1$ means that the UAV caches content f, thus the GU k can directly obtain file f from the UAV. Otherwise, $\eta_f^n = 0$ indicates that the UAV does not cache file f, it thus makes a request from the satellite to serve any GU k. Without loss of generality, once the UAV has received the requested content of the device k, then it will begin transmitting the requested content to that user.[1]

To overcome the problem of wireless BL congestion during peak hours, the UAV is equipped with SQ bits storage capacity, where S is the maximum number of contents that can be stored at the UAV. Due to the limited cache size, the UAV cannot store all contents, thus we have $S < F$. Moreover, each GU demands content independently. Considering the limited cache storage, the caching constraint can be given by

$$\sum_{f \in \mathcal{F}} \eta_f \leq S. \tag{6.2}$$

6.2.2 Channel Model

Let $V_{\max}$ be the maximum UAV speed, leading to the following constraints:

$$\|\mathbf{q}_n - \mathbf{q}_{n-1}\| \leq \delta_d = V_{\max}\delta_t, n = 1, \ldots, N, \tag{6.3}$$

$$\mathbf{q}_0 = \mathbf{q}_{\mathrm{I}}, \mathbf{q}_N = \mathbf{q}_{\mathrm{F}}, \tag{6.4}$$

where δ_d denotes the maximum distance that UAV can travel during any time slot n; $\mathbf{q}_{\mathrm{I}}$ and $\mathbf{q}_{\mathrm{F}}$ are the start point and end point of the UAV.

For analytical convenience, let us denote the satellite, UAV, and GU k by s, u, and k, respectively. Henceforth, $1k$ and $2k$ are respectively denote the BL (i.e., $s \to u$) and AL (i.e., $u \to k$) to transmit the GU k's demanded data. Therefore, the distance from $u \to k$ is expressed as

$$d_{2k}^n = \sqrt{H_u^2 + \|\mathbf{q}_n - \mathbf{w}_k\|^2}. \tag{6.5}$$

We assume that the UAV's altitude is high enough; thus, the channel between satellite and UAV is dominated by LoS link with a limited number of scattered path [104, 107]. Propagation measurement in [259] mentions that the majority of the total signals transmitted from a satellite to a receiver is predominant by the LoS link. In this regard, the channel coefficient between $s \to u$ at time slot n to transmit GU k's data is expressed as

[1] In this chapter, we use a (decode-and-forward) DF relaying technique [142]; therefore, the UAV needs to complete getting the requested data from the satellite before relaying to GU k to ensure the properly encoded data.

$h_{1k}^n \triangleq \beta_0 (d_{1k}^n)^{-\alpha}$, where β_0 is the channel gain at a reference distance, i.e., $d_0 = 1$ meter, α is the path loss exponent, d_{1k}^n denote the distance between the UAV and satellite at time slot n. Thanks to recent developing techniques, the Doppler shift at the satellite and UAV are assumed to be estimated and compensated accurately [260, 261]. We assume that the satellite starts from an initial point and moves along the x-axis with velocity v_s [106]. Specifically, orbital velocity v_s can be calculated as [262]

$$v_s = \sqrt{\frac{GM}{(R_e + H_s)}}, \tag{6.6}$$

where $G = 6.67259\ 10^{-11}\ \mathrm{m^3 kg^{-1} s^{-2}}$ is the Universal Constant of Gravitation, $M = 5.9736\ 10^{24}$ kg is the mass of the Earth, $R_e = 6371$ km is the radius of the Earth, H_s is altitude of the satellite above the Earth's surface.

In practice, GUs operate in a variety of environments, e.g., suburban, urban, rural. Therefore, a generalized transmission model comprising of line-of-sight (LOS) and non-line-of-sight (NLOS) components is considered [78, 121, 217]. In this context, a practical channel model is considered as follows

$$h_{2k}^n = \sqrt{\beta_{2k}^n} \tilde{h}_{2k}^n, \tag{6.7}$$

where β_{2k}^n represents the large-scale fading due to distance and $\tilde{h}_{2k}^n$ denotes the small-scale fading channel model. Specifically, β_{2k}^n is modeled as

$$\beta_{2k}^n \triangleq \beta_0 (d_{2k}^n)^{-\alpha} = \frac{\beta_0}{(H_u^2 + \|\mathbf{q}_n - \mathbf{w}_k\|^2)^{\alpha/2}}, \tag{6.8}$$

where $d_{2k}^n \triangleq \frac{1}{(H^2 + \|\mathbf{q}_n - \mathbf{w}_k\|^2)^{1/2}}$ is the distance between the UAV and GU k at time slot n.

Refer to [78, 121, 217], the small-scale fading $\tilde{h}_{uk}^n$ with $\mathbb{E}[|\tilde{h}_{2k}^n|^2] = 1$, can be expressed as

$$\tilde{h}_{2k}^n = \sqrt{\frac{K}{1+K}} \bar{h}_{2k}^n + \sqrt{\frac{1}{1+K}} \hat{h}_{2k}^n, \tag{6.9}$$

where the Rician factor K is defined as the ratio between the direct path's power and scattered paths' power. Besides, $\bar{h}_{2k}^n$ and $\hat{h}_{2k}^n$ denote the LoS and the NLoS (Rayleigh fading) channel components .

Without loss of generality, when the UAV receives all requested data from the satellite, then the transmission from $u \to k$ can be conducted.[2] Let x_{1k}^n and x_{2k}^n denote the symbols

[2]In this chapter, we utilize a decode-and-forwarding (DF) relaying technique, thus, the UAV needs to complete getting the requested data from the satellite before relaying to GU k to ensure the properly

with unit power ($\mathbb{E}\left[|x_{1k}^n|^2\right] = 1$ and $\mathbb{E}\left[|x_{2k}^n|^2\right] = 1$) sent $s \to u$ and $u \to k$ during time slot n, respectively. Consequently, the received signals at the UAV or GU k can be expressed as

$$y_{ik}^n = \sqrt{p_{ik}^n} h_{ik}^n x_{ik}^n + n_0, \text{ with } i \in \{1, 2\}, \tag{6.10}$$

where p_{1k}^n and p_{2k}^n respectively denote the transmit power of the LEO satellite and the UAV on the backhaul link (BL) and access link (AL) to transmit the GU k's data during n-th time slot; $n_0 \sim \mathcal{CN}(0, \sigma^2)$ is the additive white Gaussian noise (AWGN) at the UAV or GU k. Notably, the interference caused by the link between $s \to u$ on the link $u \to k$ is neglected since they use different frequencies.

Next, the achievable rate (in bps) from $s \to u$ and $u \to k$ to transmit the GU k's data during n-th time slot are respectively calculated as

$$r_{1k}^n = B_{1k} \log_2 \left(1 + \Gamma_{1\mathrm{k}}^n\right), \tag{6.11}$$

$$r_{2k}^n = b_{2k}^n B_{2k} \log_2 \left(1 + \Gamma_{2\mathrm{k}}^n\right), \tag{6.12}$$

where $\Gamma_{1\mathrm{k}}^n \triangleq \frac{p_{1k}^n |h_{1k}^n|^2}{\sigma^2}$, $\Gamma_{2\mathrm{k}}^n \triangleq \frac{p_{2k}^n |\tilde{h}_{2k}^n|^2 \beta_0}{\left(H_u^2 + \|\mathbf{q}_n - \mathbf{w}_k\|^2\right)^{\alpha/2} \sigma^2}$, B_{2k} denotes the total bandwidth from the UAV to GUs (in Hz); B_{1k} and $b_{2k}^n B_{2k}$ respectively denote the allocated bandwidth for the BL and AL to transmit GU k's data during time slot n. For a large amount of resources in practice, b_{2k}^n is approximately continuous between 0 and 1. Particularly, since the channel coefficient h_{2k}^n is a random variable, thus the achievable rate r_{2k}^n is also a random variable. Consequently, we pay attention to get the approximated rate, are given as

$$\bar{r}_{2k}^n = b_{2k}^n B_{2k} \mathbb{E}\Big[\log_2 \left(1 + \Gamma_{2k}^n\right)\Big]. \tag{6.13}$$

Because the closed-form expression of $\mathbb{E}[r_{2k}^n]$ is difficult to obtain, and thus a lower bound for $\mathbb{E}[r_{2k}^n]$ is adopted, which yields the following lemma:

Lemma 14. *The approximation result of $\bar{r}_{2k}^n$ is given as*

$$\bar{r}_{2k}^n = b_{2k}^n B_{2k} \log_2 \left(1 + \frac{e^{-E} p_{2k}^n \beta_0}{\left(H_u^2 + \|\mathbf{q}_n - \mathbf{w}_k\|^2\right)^{\alpha/2} \sigma^2}\right). \tag{6.14}$$

Proof. We define a function $f(z) = \mathbb{E}_Z[\log_2(1 + e^{\ln z})]$, with $z > 0$, then we have

$$f(z) \geq \log_2 \left(1 + e^{\mathbb{E}_Z[\ln z]}\right) \triangleq \hat{f}(z). \tag{6.15}$$

encoded data.

where the inequality (6.15) holds based on Jensen's inequality for a convex function $\log_2(1+e^{\ln z})$ w.r.t. z.

Let us denote $z \triangleq \frac{p_{2k}^n |\tilde{h}_{2k}^n|^2 \beta_0}{\left(H^2+\|\mathbf{q}_n-\mathbf{w}_n\|^2\right)^{\alpha/2}\sigma^2}$. Because z is an exponentially distributed random variable, its parameter is $\lambda_Z = (\mathbb{E}[Z])^{-1} = \frac{\zeta_{1k}}{p_{2k}^n \beta_0}$, with $\zeta_{1k} \triangleq \left(H^2 + \|\mathbf{q}_n - \mathbf{w}_n\|^2\right)^{\alpha/2}\sigma^2$. By applying [263, Eq. 4.331.1], $\mathbb{E}_Z[\ln z]$ can be calculated as

$$\begin{aligned}\mathbb{E}_Z[\ln z] &= \int_0^{+\infty} \lambda_Z e^{-z\lambda_Z} \ln z dz = -\Big(\ln(\lambda_Z) + E\Big), \\ &= \ln \frac{p_{2k}^n \beta_0}{\zeta_{1k}} - E, \end{aligned} \tag{6.16}$$

where E is the Euler-Mascheroni constant, i.e., $E = 0.5772156649$ as in [263, Eq. 8.367.1].

By substituting (6.16) into (6.15) and combining with (6.13), we obtain (6.14). Thus, the Lemma 14 is proof. □

From (6.14), the bandwidth allocation on the AL is applied to efficiently utilize the resource. Besides, the spectrum allocation should satisfy:

$$\sum_{k\in\mathcal{K}} b_{2k}^n \leq 1, \forall n, \tag{6.17}$$

$$0 \leq b_{2k}^n \leq 1, \forall k, n. \tag{6.18}$$

From (6.14), the achievable throughput of user k (in bits) during flight time T can be given as

$$\Upsilon_{2k} = \delta_t P_{k,f} \left[\eta_f \sum_{n_{1k}}^{N} \bar{r}_{2k}^n + (1-n_f) \sum_{n_{2k}+1}^{N} \bar{r}_{2k}^n \right], \tag{6.19}$$

where the first component represents the case when the UAV pre-stores the file f in its cache, i.e., $n_f = 1$, and thus it can transmit directly to GU k; While the second component means that the UAV does not cache the file f, i.e., $n_f = 0$, it thus starts transmitting data to GU k when it finishes receiving the requested file from the satellite; n_{1k} denotes the first time slot during the flight time T; n_{2k} signifies the time slot in which the UAV completely received GU k's requested file from the satellite.

6.2.3 Problem Formulation

In this section, we aim to maximize the minimum achievable throughput among GUs through jointly optimizing the cache placement, resources allocation (i.e., bandwidth and transmit power of the UAV to convey the GU k's data at time slot n), and the UAV

trajectory, with the assumption that the GUs' locations, the UAV altitude, and the satellite height are known a priori.

Let $\mathbf{q} \triangleq \{\mathbf{q}_n, \forall n\}$, $\mathbf{b} \triangleq \{b_{2k}^n, n \in \mathcal{N}, k \in \mathcal{K}\}$, $\mathbf{p} \triangleq \{p_{2k}^n, n \in \mathcal{N}, k \in \mathcal{K}\}$, $\boldsymbol{\eta} \triangleq \{\eta_f, \forall f \in \mathcal{F}\}$. Based on the above discussions, the optimization problem is formulated as follows

$$\mathcal{P}_1^{\text{Sat}}: \quad \max_{\mathbf{q},\mathbf{b},\mathbf{p},\boldsymbol{\eta}} \min_{\forall k \in \mathcal{K}} \Upsilon_{2k} \tag{6.20}$$

$$\texttt{s.t.} \quad \delta_t \sum_{n=n_{1k}}^{n_{2k}} B_{1k} \log_2 \left(1 + \frac{p_{1k}^n \beta_0}{(d_{1k}^n)^\alpha \sigma^2}\right) \geq (1 - \eta_f) Q,$$

$$\forall n, k, \tag{6.21}$$

$$\eta_f \in \{0, 1\}, \forall f \in \mathcal{F}, \tag{6.22}$$

$$\sum_{f \in \mathcal{F}} \eta_f \leq S, \forall f, \tag{6.23}$$

$$\sum_{k \in \mathcal{K}} b_{2k}^n \leq 1, \forall n, k, \tag{6.24}$$

$$0 \leq b_{2k}^n \leq 1, \forall n, \tag{6.25}$$

$$\|\mathbf{q}_n - \mathbf{q}_{n-1}\| \leq \delta_d, n = 1, \ldots, N, \tag{6.26}$$

$$\mathbf{q}_0 = \mathbf{q}_I, \mathbf{q}_N = \mathbf{q}_F, \tag{6.27}$$

$$0 \leq \sum_{k \in \mathcal{K}} p_{2k}^n \leq P_u^{\max}, \forall n, \tag{6.28}$$

where constraint (6.21) guarantees that the non-cached file f is transmitted from satellite to the UAV; n_{1k} and n_{2k} denote the start and end data transmission time from satellite to the UAV to convey GU k's requested file, respectively; without loss of generality, n_{1k} is set to zero; (6.22) be the binary variable for the UAV to cache file f or not; (6.23) means that the total number of contents cached at the UAV should be less than or equal to the storage capacity; (6.24) and (6.25) signify the bandwidth allocation constraints; (6.26) shows the maximum velocity constraint of the UAV; constraint (6.27) explains for the start and end points of the UAV; constraint (6.28) implies that the transmit power of the UAV is restrained by its maximum power budget.

It is troublesome to obtain the direct solution of $\mathcal{P}_1^{\text{Sat}}$ since this is a mixed-integer non-linear program (MINLP), which is NP-hard. Specifically, the objective function is a max-min and non-convex function. Besides, the binary nature of constraint (6.22) and the non-convexity of (6.26), which introduces intractability. In the next section, an efficient method is proposed to solve it.

6.3 Proposed Iterative Algorithm for Solving $\mathcal{P}_1^{\text{Sat}}$

6.3.1 Tractable formulation for $\mathcal{P}_1^{\text{Sat}}$

It can be seen that the n_{2k} value in problem $\mathcal{P}_1^{\text{Sat}}$ is not determined, thus we cannot solve $\mathcal{P}_1$ if n_{2k} is a variable. Consequently, we intend to find a specified value for n_{2k}. In the case that file f is stored at the UAV, we have $t_{1k} = 0$. Otherwise, from (6.11), the total transmission time to transmit GU k's data from $s \to u$ can be specified as

$$t_{1k} \triangleq \frac{(1-\eta_f)Q}{\bar{r}_{1k}}. \tag{6.29}$$

where $\bar{r}_{1k} \triangleq \frac{\sum\limits_{\forall n \in \mathcal{N}} r_{1k}^n}{N}$ is the average data transmission rate from $s \to u$ during flying time T.

Based on (6.29), we have

$$n_{2k} \triangleq n_{1k} + \left\lceil \frac{t_{1k}}{\delta_t} \right\rceil, \tag{6.30}$$

where without loss of generality, we assume that $n_{2k} \leq N$.

Let us introduce an auxiliary variable $\chi(\mathbf{q}, \mathbf{b}, \mathbf{p}, \boldsymbol{\eta}) \triangleq \min\limits_{\forall k \in \mathcal{K}} \delta_t \sum\limits_{n \in \mathcal{N}} \bar{r}_{2k}^n$ to transform the max-min problem $\mathcal{P}_1$ into maximization problem, we then have

$$\mathcal{P}_{1.1}: \quad \max_{\mathbf{q},\mathbf{b},\mathbf{p},\boldsymbol{\eta},\chi} \quad \chi(\mathbf{q}, \mathbf{b}, \mathbf{p}, \boldsymbol{\eta}) \tag{6.31}$$

$$\texttt{s.t.} \quad \Upsilon_{2k} \geq \chi, \forall k, \tag{6.32}$$

$$(6.21) - (6.28), \tag{6.33}$$

To overcome the non-convexity of the problem $\mathcal{P}_1$, we first decompose $\mathcal{P}_1$ into three sub-problems, wherein we first optimize the cache placement for a given trajectory and resource allocation, followed by the optimization of resource allocation (i.e., bandwidth and transmit power allocation) for a given trajectory and cache placement, and finally, we perform the UAV trajectory optimization for a given cache placement and resource allocation. Based on the block coordinate descent (BCD) method [125, 249] and SCA technique [264], an efficient iterative algorithm is proposed, whereas three sub-problems are alternately optimized until convergence.

6.3.2 Subproblem 1: Cache Placement Optimization

For any given $\mathbf{b}^j$, $\mathbf{p}^j$, and $\mathbf{q}^j$, the cache placement $\boldsymbol{\eta}$ can be obtain by solving the following optimization problem:

$$\mathcal{P}_1^{\boldsymbol{\eta}}: \quad \max_{\boldsymbol{\eta},\chi} \quad \chi(\mathbf{q}^j, \mathbf{b}^j, \mathbf{p}^j, \boldsymbol{\eta}) \tag{6.34}$$

$$\texttt{s.t.} \quad \delta_t \sum_{n=n_{1k}}^{n_{2k}} \bar{r}_{1k} \geq (1-\eta_f)Q, \forall n, k, \tag{6.35}$$

$$\Upsilon_{2k} \geq \chi, \forall k, \tag{6.36}$$

$$\eta_f \in \{0,1\}, \forall f \in \mathcal{F}, \tag{6.37}$$

$$\sum_{f\in\mathcal{F}} \eta_f \leq S, \forall f. \tag{6.38}$$

It can be seen that the problem $\mathcal{P}_1^{\boldsymbol{\eta}}$ is non-convex due to the binary nature of constraint (6.37). To overcome this issue, we first relax the binary cache placement variable into continuous ones. As a result, $\mathcal{P}_1^{\boldsymbol{\eta}}$ can be re-written as

$$\mathcal{P}_{1.1}^{\boldsymbol{\eta}}: \quad \max_{\boldsymbol{\eta},\chi} \quad \chi(\mathbf{q}^j, \mathbf{b}^j, \mathbf{p}^j, \boldsymbol{\eta}) \tag{6.39}$$

$$\texttt{s.t.} \quad 0 \leq \eta_f \leq 1, \forall f, \tag{6.40}$$

$$(6.35), (6.36), (6.38). \tag{6.41}$$

It is observed that the problem $\mathcal{P}_{1.1}^{\boldsymbol{\eta}}$ is convex since the objective function and constraints are convex, i.e., linear. Consequently, the problem $\mathcal{P}_{1.1}^{\boldsymbol{\eta}}$ can be solved by using standard methods [199]. Nevertheless, since the cache placement variable is relaxed into continuous values between 0 and 1, and thus it does not ensure that the η_f can converge to 0 or 1. Thus, we introduce a penalty function $\mathbb{P}(\eta_f) \triangleq \eta_f \ln(\eta_f) + (1-\eta_f)\ln(1-\eta_f)$, which is convex for $\lambda_k \geq 0$ [121, 265]. Hence, the sub-problem $\mathcal{P}_{1.1}^{\boldsymbol{\eta}}$ is reformulated as,

$$\mathcal{P}_{1.2}^{\boldsymbol{\eta}}: \quad \max_{\boldsymbol{\eta},\chi} \quad \Big(\chi(\mathbf{q}^j, \mathbf{b}^j, \mathbf{p}^j, \boldsymbol{\eta}) + \kappa\mathbb{P}(\eta_f)\Big) \tag{6.42}$$

$$\texttt{s.t.} \quad (6.40), (6.41). \tag{6.43}$$

where $\kappa > 0$ is a penalty factor. Especially, the objective in $\mathcal{P}_{1.2}^{\boldsymbol{\eta}}$ is a difference of concave function, i.e., $f(\eta_f, \chi) \triangleq \Big(\chi(\mathbf{q}^j, \mathbf{b}^j, \mathbf{p}^j, \boldsymbol{\eta}) - (-\kappa\mathbb{P}(\eta_f))\Big)$ with convex constraints. As a result, the problem $\mathcal{P}_{1.2}^{\boldsymbol{\eta}}$ becomes a DC Programming Problem (DCP). To transform $\mathcal{P}_{1.2}^{\boldsymbol{\eta}}$ become a convex problem, we substitute $\mathbb{P}(\eta_f)$ in the objective by its first-order Taylor

expansion at $(j+1)$-th iteration:

$$\widehat{\mathbb{P}}(\eta_f) \triangleq \kappa\Big(\mathbb{P}(\eta_f^{(j)}) + \triangledown\mathbb{P}(\eta_f^{(j)})\big(\eta_f - \eta_f^{(j)}\big)\Big), \tag{6.44}$$

where

$$\triangledown\mathbb{P}(\eta_f^{(j)}) = 2\eta_f^{(j)} - 1. \tag{6.45}$$

Thus, we have

$$\widehat{\mathbb{P}}(\eta_f) \triangleq \kappa\Big(\eta_f(2\eta_f^{(j)} - 1) - (\eta_f^{(j)})^2\Big). \tag{6.46}$$

According to the above discussions, sub-problem $\mathcal{P}_{1.2}^{\boldsymbol{\eta}}$ is approximately converted to the following linear programming (which is obtained by substituting convex component and ignoring the constant parts in the objective):

$$\mathcal{P}_{1.3}^{\boldsymbol{\eta}}: \qquad \max_{\boldsymbol{\eta},\chi} \quad \Big(\chi(\mathbf{q}^j, \mathbf{b}^j, \mathbf{p}^j, \boldsymbol{\eta}) + \widehat{\mathbb{P}}(\eta_f)\Big) \tag{6.47}$$

$$\texttt{s.t.} \qquad (6.40), (6.41). \tag{6.48}$$

Remark 15. *For cache placement optimization in Algorithm 0, we only solve the relaxed problem* (6.47) *instead of the original problem* (6.34)*, where the binary cache placement variable* $\boldsymbol{\eta}$ *in the original problem* (6.34) *is relaxed to continuous values between 0 and 1. Notably, if the cache placement variable* $\boldsymbol{\eta}$ *obtained by Algorithm 1 can converge to binary values, then the relaxation is tight and the solution in* (6.47) *is also a feasible solution of the problem* (6.34)*. Especially, with an appropriate, sufficiently large, and positive value of the penalty parameter* κ*, the relaxed problem* (6.47) *is equivalent to the original problem* (6.34)*, as clearly mentioned in [266, Theorem 2.1] or in the introduction of [267].*

Remark 16. *The solutions of sub-problem* $\mathcal{P}_{1.3}^{\boldsymbol{\eta}}$ *can be obtained by applying standard optimization solver, i.e., CVX [199]. Besides, we observe that constraint* (6.40) *is equivalent to* (6.37) *when we achieve the optimal solutions of* $\mathcal{P}_{1.3}^{\boldsymbol{\eta}}$*. By applying the lower bound result in* (6.44)*, it can be seen that the feasible solutions for* $\mathcal{P}_{1.3}^{\boldsymbol{\eta}}$ *are also satisfy* $\mathcal{P}_{1}^{\boldsymbol{\eta}}$*, which means that we can obtain at least a locally optimal solution.*

6.3.3 Subproblem 2: UAV Bandwidth and Transmit Power Optimization

For any given cache placement $\boldsymbol{\eta}^j$ and UAV trajectory $\mathbf{q}^j$, $\mathbf{b}$ and $\mathbf{p}$ can be obtained by solving the following optimization problem:

$$\mathcal{P}_1^{\mathbf{b},\mathbf{p}}: \quad \max_{\mathbf{b},\mathbf{p},\chi} \ \chi(\mathbf{q}^j, \mathbf{b}, \mathbf{p}, \boldsymbol{\eta}^j) \tag{6.49}$$

$$\texttt{s.t.} \quad \zeta_{\mathbf{b},\mathbf{p}}^n \geq \chi, \forall n, k, \tag{6.50}$$

$$\delta_t \sum_{n=n_{1k}}^{n_{2k}} \bar{r}_{1k} \geq (1-\eta_f)Q, \forall n, k, \tag{6.51}$$

$$\sum_{f\in\mathcal{F}} \eta_f \leq S, \forall f, \tag{6.52}$$

$$\sum_{k\in\mathcal{K}} b_{2k}^n \leq 1, \forall n, k, \tag{6.53}$$

$$0 \leq b_{2k}^n \leq 1, \forall n, k, \tag{6.54}$$

$$0 \leq \sum_{k\in\mathcal{K}} p_{2k}^n \leq P_u^{\max}, \forall n, \tag{6.55}$$

where

$$\zeta_{\mathbf{b},\mathbf{p}}^n \triangleq \delta_t P_{k,f} b_{2k}^n B_{2k} \left[n_f \sum_{n_{1k}}^{N} \Phi_{\mathbf{p}}^n + (1-n_f) \sum_{n_{2k}+1}^{N} \Phi_{\mathbf{p}}^n \right], \tag{6.56}$$

$$\Phi_{\mathbf{p}}^n \triangleq \log_2 \left(1 + \frac{e^{-E} p_{2k}^n \beta_0}{\left(H_u^2 + \|\mathbf{q}_n - \mathbf{w}_k\|^2 \right)^{\alpha/2} \sigma^2} \right). \tag{6.57}$$

Due to the non-convexity of constraints (6.50), sub-problem $\mathcal{P}_1^{\mathbf{b},\mathbf{p}}$ is also non-convex. To make $\mathcal{P}_1^{\mathbf{b},\mathbf{p}}$ more tractable, we first introduce slack variable $\bar{\Phi}_{\mathbf{p}}^n$ such that

$$\Phi_{\mathbf{p}}^n \triangleq \log_2 \left(1 + \frac{e^{-E} p_{2k}^n \beta_0}{\left(H_u^2 + \|\mathbf{q}_n - \mathbf{w}_k\|^2 \right)^{\alpha/2} \sigma^2} \right) \geq \bar{\Phi}_{\mathbf{p}}^n. \tag{6.58}$$

Consequently, $\zeta_{\mathbf{b},\mathbf{p}}^n$ is converted to the following constraint

$$\zeta_{\mathbf{b},\mathbf{p}}^n \geq \delta_t P_{k,f} B_{2k} \times \left[n_f \sum_{n_{1k}}^{N} b_{2k}^n \bar{\Phi}_{\mathbf{p}}^n + (1-n_f) \sum_{n_{2k}+1}^{N} b_{2k}^n \bar{\Phi}_{\mathbf{p}}^n \right] \triangleq \bar{\zeta}_{\mathbf{b},\mathbf{p}}^n. \tag{6.59}$$

Lemma 17. *For any given $b_{2k}^{n,j}$ and $\bar{\Phi}_{\mathbf{p}}^{n,j}$ at $(j+1)$-th iteration, the lower bound of $\bar{\zeta}_{\mathbf{b},\mathbf{p}}^{n}$ is expressed as*

$$\begin{aligned}\bar{\zeta}_{\mathbf{b},\mathbf{p}}^{n} &\geq \delta_t P_{k,f} B_{2k} \\ &\times \left[n_f \sum_{n_{1k}}^{N} \Theta_{\mathbf{b},\mathbf{p}}^{n} + (1-n_f) \sum_{n_{2k}+1}^{N} \Theta_{\mathbf{b},\mathbf{p}}^{n} \right] \triangleq \widehat{\zeta}_{\mathbf{b},\mathbf{p}}^{n}, \end{aligned} \tag{6.60}$$

where

$$\begin{aligned}\Theta_{\mathbf{b},\mathbf{p}}^{n} \triangleq \frac{\left(b_{2k}^{n,j} + \bar{\Phi}_{\mathbf{p}}^{n,j}\right)^2}{4} + \frac{\left(b_{2k}^{n,j} + \bar{\Phi}_{\mathbf{p}}^{n,j}\right)}{2} \times \Big(b_{2k}^{n} - b_{2k}^{n,j} \\ + \bar{\Phi}_{\mathbf{p}}^{n} - \bar{\Phi}_{\mathbf{p}}^{n,j}\Big) - \frac{\left(b_{2k}^{n} - \bar{\Phi}_{\mathbf{p}}^{n}\right)^2}{4}. \end{aligned} \tag{6.61}$$

Proof. It is observed that $b_{2k}^{n}\widehat{\Phi}_{2k}^{n}$ is a non-convex function. To make it tractable, we replace $b_{2k}^{n}\bar{\Phi}_{2k}^{n}$ by an equivalent different of convex function $0.25\Big[\Big(b_{2k}^{n} + \bar{\Phi}_{2k}^{n}\Big)^2 - \Big(b_{2k}^{n} - \bar{\Phi}_{2k}^{n}\Big)^2\Big]$. Then, we adopt first-order Taylor expansion to approximate function $0.25\Big(b_{2k}^{n} + \bar{\Phi}_{2k}^{n}\Big)^2$ as follow

$$\begin{aligned}0.25\Big(b_{2k}^{n} + \bar{\Phi}_{2k}^{n}\Big)^2 \geq \frac{\left(b_{2k}^{n,j} + \bar{\Phi}_{2k}^{n,j}\right)^2}{4} + \frac{\left(b_{2k}^{n,j} + \bar{\Phi}_{2k}^{n,j}\right)}{2} \times \\ \Big(b_{2k}^{n} - b_{2k}^{n,j} + \widehat{\Phi}_{2k}^{n} - \bar{\Phi}_{2k}^{n,j}\Big). \end{aligned} \tag{6.62}$$

Consequently, by substituting the lower bound of $0.25\Big(b_{2k}^{n}+\bar{\Phi}_{2k}^{n}\Big)^2$ as in (6.62) into $0.25\Big[\Big(b_{2k}^{n}+ \bar{\Phi}_{2k}^{n}\Big)^2 - \Big(b_{2k}^{n} - \bar{\Phi}_{2k}^{n}\Big)^2\Big]$, the lower bound of $b_{2k}^{n}\bar{\Phi}_{2k}^{n}$ can be obtained as (6.60), which finishes the proof. □

Bearing all the above developments in mind, the problem $\mathcal{P}_1^{\mathbf{b},\mathbf{p}}$ is re-formulated as

$$\mathcal{P}_{1.1}^{\mathbf{b},\mathbf{p}}: \quad \max_{\mathbf{b},\mathbf{p},\chi} \ \chi(\mathbf{q}^j, \mathbf{b}, \mathbf{p}, \boldsymbol{\eta}^j) \tag{6.63}$$

$$\texttt{s.t.} \quad \widehat{\zeta}_{\mathbf{b},\mathbf{p}}^n \geq \chi, \forall n, k, \tag{6.64}$$

$$\log_2\left(1 + \frac{e^{-E} p_{2k}^n \beta_0}{\left(H_u^2 + \|\mathbf{q}_n - \mathbf{w}_k\|^2\right)^{\alpha/2} \sigma^2}\right) \geq \bar{\Phi}_{\mathbf{p}}^n, \quad \forall n, k, \tag{6.65}$$

$$(6.51) - (6.55). \tag{6.66}$$

Remark 18. *It is noted that the problem $\mathcal{P}_{1.1}^{\mathbf{b},\mathbf{p}}$ is a convex problem because the objective function and all constraints are convex. Therefore, it can be numerically solved via standard optimization solvers such as CVX [199]. By applying the lower bound as in Lemma 17, the set of feasible solutions for $\mathcal{P}_{1.1}^{\mathbf{b},\mathbf{p}}$ is also a subset feasible solutions for $\mathcal{P}_1^{\mathbf{b},\mathbf{p}}$. Thus, it guarantees that at least a locally optimal solution can be achieved.*

6.3.4 Subproblem 3: UAV Trajectory Optimization

For any given bandwidth allocation $\mathbf{b}^j$, UAV transmit power $\mathbf{p}^j$, and cache placement $\boldsymbol{\eta}^j$, the UAV trajectory $\mathbf{q}$ can be obtained by solving following optimization problem

$$\mathcal{P}_1^{\mathbf{q}}: \quad \max_{\mathbf{q},\chi} \ \chi(\mathbf{q}, \mathbf{b}^j, \mathbf{p}^j, \boldsymbol{\eta}^j) \tag{6.67}$$

$$\texttt{s.t.} \quad \zeta_{\mathbf{q}}^n \geq \chi, \forall n, k, \tag{6.68}$$

$$\delta_t \sum_{n=n_{1k}}^{n_{2k}} \bar{r}_{1k} \geq (1 - \eta_f) Q, \forall n, k, \tag{6.69}$$

$$\sum_{f \in \mathcal{F}} \eta_f \leq S, \forall f, \tag{6.70}$$

$$\|\mathbf{q}_n - \mathbf{q}_{n-1}\| \leq \delta_d = V_{max} \delta_t, n = 1, \ldots, N, \tag{6.71}$$

$$\mathbf{q}_0 = \mathbf{q}_I, \mathbf{q}_N = \mathbf{q}_F, \tag{6.72}$$

where

$$\zeta_{\mathbf{q}}^{n} \triangleq \delta_t P_{k,f} b_{2k}^{n} B_{2k} \left[n_f \sum_{n_{1k}}^{N} \Phi_{\mathbf{q}}^{n} + (1 - n_f) \sum_{n_{2k}+1}^{N} \Phi_{\mathbf{q}}^{n} \right], \tag{6.73}$$

$$\Phi_{\mathbf{q}}^{n} \triangleq \log_2 \left(1 + \frac{\psi}{\left(H_u^2 + \|\mathbf{q}_n - \mathbf{w}_k\|^2 \right)^{\alpha/2}} \right), \tag{6.74}$$

$$\psi \triangleq \frac{e^{-E} p_{2k}^{n} \beta_0}{\sigma^2}. \tag{6.75}$$

The problem $\mathcal{P}_1^{\mathbf{q}}$ is a non-convex optimization problem due to the non-convexity of constraints (6.68) and the combinatorial of designing UAV trajectory. To convexify (6.68), we introduce slack variable such that $\left(H_u^2 + \|\mathbf{q}_n - \mathbf{w}_k\|^2 \right) \leq (\nu_{2k}^{n})^{2/\alpha}$. Let us denote $\boldsymbol{\nu} \triangleq \{\nu_{2k}^{n}, \forall n, k\}$, then the sub-problem $\mathcal{P}_1^{\mathbf{q}}$ can be re-written as

$$\mathcal{P}_{1.1}^{\mathbf{q}}: \quad \max_{\mathbf{q},\boldsymbol{\nu},\chi} \ \chi(\mathbf{q}, \mathbf{b}^j, \mathbf{p}^j, \boldsymbol{\eta}^j) \tag{6.76}$$

$$\texttt{s.t.} \quad \left(H_u^2 + \|\mathbf{q}_n - \mathbf{w}_k\|^2 \right) \leq (\nu_{2k}^{n})^{2/\alpha}, \forall n, k, \tag{6.77}$$

$$\bar{\zeta}_{\mathbf{q}}^{n} \geq \chi, \forall n, k, \tag{6.78}$$

$$(6.69) - (6.72), \tag{6.79}$$

where

$$\bar{\zeta}_{\mathbf{q}}^{n} \triangleq \delta_t P_{k,f} b_{2k}^{n} B_{2k} \left[n_f \sum_{n_{1k}}^{N} \bar{\Phi}_{\mathbf{q}}^{n} + (1 - n_f) \sum_{n_{2k}+1}^{N} \bar{\Phi}_{\mathbf{q}}^{n} \right], \tag{6.80}$$

$$\bar{\Phi}_{\mathbf{q}}^{n} \triangleq \log_2 \left(1 + \frac{\psi}{\nu_{2k}^{n}} \right). \tag{6.81}$$

It is noted that the problem $\mathcal{P}_{1.1}^{\mathbf{q}}$ is still non-convex. To solve this problem, we transform $\mathcal{P}_{1.1}^{\mathbf{q}}$ into a convex form by giving following lemmas:

Lemma 19. *For any given $\nu_{2k}^{n,j}$ at $(j+1)$-th iteration, $\bar{\Phi}_{\mathbf{q}}^{n} \triangleq \log_2 \left(1 + \frac{\psi}{\nu_{2k}^{n}} \right)$ is lower bounded by*

$$\bar{\Phi}_{\mathbf{q}}^{n} \geq \log_2 \left(1 + \frac{\psi}{\nu_{2k}^{n,j}} \right) - \frac{\psi(\nu_{2k}^{n} - \nu_{2k}^{n,j})}{\nu_{2k}^{n,j}(\nu_{2k}^{n,j} + \psi) \ln 2} \triangleq \hat{\Phi}_{\mathbf{q}}^{n}. \tag{6.82}$$

Algorithm 9 Proposed Iterative Algorithm to Solve $\mathcal{P}_1^{\text{Sat}}$

1: **REQUIRE**
2: Set $j := 0$ and initialize $\mathbf{b}^j$, $\mathbf{p}^j$, and $\mathbf{q}^j$.
3: **REPEAT**
4: Solve $\mathcal{P}_1^{\boldsymbol{\eta}}$ for given $\{\mathbf{b}^j, \mathbf{p}^j, \mathbf{q}^j\}$ and denote the optimal solution as $\boldsymbol{\eta}^{j+1}$.
5: Solve $\mathcal{P}_1^{\mathbf{b},\mathbf{p}}$ for given $\{\boldsymbol{\eta}^{j+1}, \mathbf{q}^j\}$ and denote the optimal solution as $\mathbf{b}^{j+1}$ and $\mathbf{p}^{j+1}$.
6: Solve $\mathcal{P}_1^{\mathbf{q}}$ for given $\{\boldsymbol{\eta}^{j+1}, \mathbf{b}^{j+1}, \mathbf{p}^{j+1}\}$ and denote the optimal solution as $\mathbf{q}^{j+1}$.
7: Set $j := j + 1$.
8: **UNTIL**
9: Convergence

Proof. Due to the convexity of the function $f(x) = \log_2(1 + 1/x)$ with $x > 0$. By applying the first-order Taylor expansion to achieve the lower bound of $f(x)$ at given feasible point x^j as

$$\log_2\left(1 + \frac{\Omega_1}{x}\right) \geq \log_2\left(1 + \frac{\Omega_1}{x^j}\right) - \frac{\Omega_1(x - x^j)}{x^j(x^j + \Omega_1)\ln 2}. \tag{6.83}$$

By adopting $\Omega_1 = \psi$ and $x = \nu_{2k}^n$, the Lemma 19 is then proved. □

Consequently, we have

$$\bar{\zeta}_{\mathbf{q}}^n \geq \delta_t P_{k,f} B_{2k} \left[n_f \sum_{n_{1k}}^{N} \hat{\Phi}_{\mathbf{q}}^n + (1 - n_f) \sum_{n_{2k}+1}^{N} \hat{\Phi}_{\mathbf{q}}^n \right] \triangleq \hat{\zeta}_{\mathbf{q}}^n. \tag{6.84}$$

Bearing all the above discussions in mind, the problem $\mathcal{P}_{1.1}^{\mathbf{q}}$ is re-formulated as

$$\mathcal{P}_{1.2}^{\mathbf{q}}: \quad \max_{\mathbf{q},\boldsymbol{\nu},\chi} \ \chi(\mathbf{q}, \mathbf{b}^j, \mathbf{p}^j, \boldsymbol{\eta}^j) \tag{6.85}$$

$$\texttt{s.t.} \quad (6.70) - (6.72), (6.77), \tag{6.86}$$

$$\widetilde{\zeta}_{\mathbf{q}}^n \geq \chi, \forall n, k, \tag{6.87}$$

Because the objective function and all constraints of $\mathcal{P}_{1.2}^{\mathbf{q}}$ are convex, thus problem $\mathcal{P}_{1.2}^{\mathbf{q}}$ can be directly solved by using standard methods [199]. Consequently, we propose an alternating algorithm based on three sub-problem solutions described in Algorithm 10.

6.3.5 Convergence and Complexity Analysis

Convergence Analysis

Proposition 20. *From the proposed iterative Algorithm 10, we can obtain at least a locally optimal solution.*

Proof. Let us define $\Xi(\boldsymbol{\eta}^j, \mathbf{b}^j, \mathbf{p}^j, \mathbf{q}^j)$, $\Xi_{\text{lb}}^{\mathbf{b},\mathbf{p}}(\boldsymbol{\eta}^j, \mathbf{b}^j, \mathbf{p}^j, \mathbf{q}^j)$, and $\Xi_{\text{lb}}^{\mathbf{q}}(\boldsymbol{\eta}^j, \mathbf{b}^j, \mathbf{p}^j, \mathbf{q}^j)$ as the objective values of $\mathcal{P}_1$, $\mathcal{P}_{1.1}^{\mathbf{b},\mathbf{p}}$, and $\mathcal{P}_{1.2}^{\mathbf{q}}$ at the j-th iteration. In the $(j+1)$-th iteration, in step 2 of Algorithm 10, we have

$$\Xi(\boldsymbol{\eta}^j, \mathbf{b}^j, \mathbf{p}^j, \mathbf{q}^j) \overset{i}{\leq} \Xi(\boldsymbol{\eta}^{j+1}, \mathbf{b}^j, \mathbf{p}^j, \mathbf{q}^j). \tag{6.88}$$

The inequality (i) holds because $\boldsymbol{\eta}^{j+1}$ is a optimal solution of $\mathcal{P}_1^{\boldsymbol{\eta}}$. After that, in step 3 of Algorithm 10, we have

$$\begin{aligned}\Xi(\boldsymbol{\eta}^{j+1}, \mathbf{b}^j, \mathbf{p}^j, \mathbf{q}^j) &\overset{i2}{=} \Xi^{\mathbf{b},\mathbf{p}}(\boldsymbol{\eta}^{j+1}, \mathbf{b}^j, \mathbf{p}^j, \mathbf{q}^j) \\ &\overset{i3}{\leq} \Xi^{\mathbf{b},\mathbf{p}}(\boldsymbol{\eta}^{j+1}, \mathbf{b}^{j+1}, \mathbf{p}^{j+1}, \mathbf{q}^j) \\ &\overset{i4}{\leq} \Xi(\boldsymbol{\eta}^{j+1}, \mathbf{b}^{j+1}, \mathbf{p}^{j+1}, \mathbf{q}^j).\end{aligned} \tag{6.89}$$

The inequality $(i2)$ holds because first-order Taylor approximation at points $\mathbf{b}^j$ and $\mathbf{p}^j$ is tight as in constraint (6.58), (6.59), and (6.60) [264]. Moreover, the inequality $(i3)$ holds since $\mathbf{b}^{j+1}$ and $\mathbf{p}^{j+1}$ are optimal solutions of $\mathcal{P}_{1.1}^{\mathbf{b},\mathbf{p}}$. Then, the inequality $(i4)$ holds because the objective value of $\mathcal{P}_{1.1}^{\mathbf{b},\mathbf{p}}$ is a lower bound to that of $\mathcal{P}_1^{\mathbf{b},\mathbf{p}}$ at given points $\mathbf{b}^{j+1}$ and $\mathbf{p}^{j+1}$. Further, in step 4, we have

$$\begin{aligned}\Xi(\boldsymbol{\eta}^{j+1}, \mathbf{b}^{j+1}, \mathbf{p}^{j+1}, \mathbf{q}^j) &\overset{i5}{=} \Xi_{\text{lb}}^{\mathbf{q}}(\boldsymbol{\eta}^{j+1}, \mathbf{b}^{j+1}, \mathbf{p}^{j+1}, \mathbf{q}^j) \\ &\overset{i6}{\leq} \Xi_{\text{lb}}^{\mathbf{q}}(\boldsymbol{\eta}^{j+1}, \mathbf{b}^{j+1}, \mathbf{p}^{j+1}, \mathbf{q}^{j+1}) \\ &\overset{i7}{\leq} \Xi(\boldsymbol{\eta}^{j+1}, \mathbf{b}^{j+1}, \mathbf{p}^{j+1}, \mathbf{q}^{j+1}).\end{aligned} \tag{6.90}$$

The equality $(i5)$ holds because the first-order Taylor expansion at given point $\mathbf{q}^j$ as in (6.82), (6.84), and (**??**) are tight, and the inequality $(i6)$ holds since $\mathbf{q}^{j+1}$ is a optimal solution of $\mathcal{P}_{1.2}^{\mathbf{q}}$. Furthermore, the inequality $(i7)$ holds since the optimal value of $\mathcal{P}_{1.2}^{\mathbf{q}}$ is a lower bound of $\mathcal{P}_1^{\mathbf{q}}$ at given $\mathbf{q}^{j+1}$.

From (6.88) to (6.90), we conclude that $\Xi(\boldsymbol{\eta}^j, \mathbf{b}^j, \mathbf{p}^j, \mathbf{q}^j) \leq \Xi(\boldsymbol{\eta}^{j+1}, \mathbf{b}^{j+1}, \mathbf{p}^{j+1}, \mathbf{q}^{j+1})$, which shows that the objective value of $\mathcal{P}_1$ is non-decreasing as the number of iteration increases. Further, the objective value of $\mathcal{P}_1$ is limited by an upper bound value due to the maximum transmit power $P_u^{\max}$, restricted traveling time T, and maximum bandwidth allocation for each GU. Therefore, this guarantees for the convergence of Algorithm 10. □

Complexity Analysis

We analyze the worst-case complexity of Algorithm 10. Because $\mathcal{P}_{1.3}^{\boldsymbol{\eta}}$ is a linear programming and it can be solved by using interior method with computational complexity is $\mathcal{O}\Big[L_1\Big((F+1+NK)^{0.5}(N+3)^3\Big)\Big]$, where L_1, $(N+3)$, and $(F+1+NK)$ denote the number of iterations required to update the cache placement, the number of variables, the number of constraints, respectively [234]. Further, the problem $\mathcal{P}_1^{\mathbf{b},\mathbf{p}}$ includes $(7NK+2K+3N+1)$ linear or quadratic constraints and $(5NK+1)$ variables, thus its complexity is $\mathcal{O}\Big[L_2\Big((7NK+2K+3N+1)^{0.5}(5NK+1)^3\Big)\Big]$, where L_2 is the number of iterations to update bandwidth and power allocation. Next, the problem $\mathcal{P}_1^{\mathbf{q}}$ includes $(3NK+2K+3N+2)$ linear or quadratic constraints and $(3NK+2N+1)$ variables, thus its complexity is $\mathcal{O}\Big[L_3\Big((3NK+2K+3N+2)^{0.5}(3NK+2N+1)^3\Big)\Big]$, where L_3 is the number of iterations to update the UAV trajectory. Then, the overall complexity of Algorithm 0 is $\mathcal{O}\Big[L_4\Big(L_1\Big((F+1+NK)^{0.5}(N+3)^3\Big)+L_2\Big((7NK+2K+3N+1)^{0.5}(5NK+1)^3\Big)+L_3\Big((3NK+2K+3N+2)^{0.5}(3NK+2N+1)^3\Big)\Big)\Big]$ where L_4 is the number of iterations until convergence.

6.4 Simulation Results

In this section, numerical results are given to validate the proposed method, which jointly optimizes cache placement, resource allocation (i.e., bandwidth and transmit power), and the UAV trajectory design in satellite- and cache-aided UAV communication networks. We consider a system with one LEO satellite, one cache-enabled UAV, and K GUs which is distributed in a horizontal plane, i.e., Area $= x^2$ (km^2), with $x = 1$ km or 2 km. We assume that the UAV's initial and final locations are respectively located at $\mathbf{q}_{\mathrm{I}} = [1; 0.7]$ km and $\mathbf{q}_{\mathrm{F}} = [0.3; 0]$ km. The flight altitudes of the LEO satellite and the UAV are fixed at 2000 km and 1 km, respectively [268]. The maximum bandwidth for the AL from $u \to k$ is $B_{2k} = 20$ Mhz. Therefore, the AWGN power is $\sigma^2 = -174 + 10\log_{10} B \simeq -101$ dBm. The maximum transmit powers of the satellite and the UAV are respectively set as $p_{1k}^n = 49.03$ dBm and $P_u^{\max}$ is ranging from 5 to 40 dBm [93, 254]. Without other stated, other parameters are set as: path-loss exponent $\alpha = 2$, the maximum UAV velocity $V_{\max} = 50$ m/s, one time slot duration $\delta_t = 0.5$ second, channel gain at the reference distance $\beta_0 =$ -40 dB, total number of file $F = 30$ files, one file size $Q = 40$ Mbits, UAV's cache size $S = 10$ files, Zipf skewness factor $\varrho = 0.8$ [258]. The error tolerance of iterative algorithm is set to $\epsilon = 10^{-4}$. The LEO satellite's orbital velocity is set to 6.9005 km/s based on (6.6). The initial point of the LEO satellite is $[-345; 0]$ km. The penalty parameter κ is initialized to 0.1 and incremented as $\kappa = 1.1\kappa$ until $\kappa \leq 10$. To show the superiority of our design, we compare the proposed scheme with the following benchmark schemes:

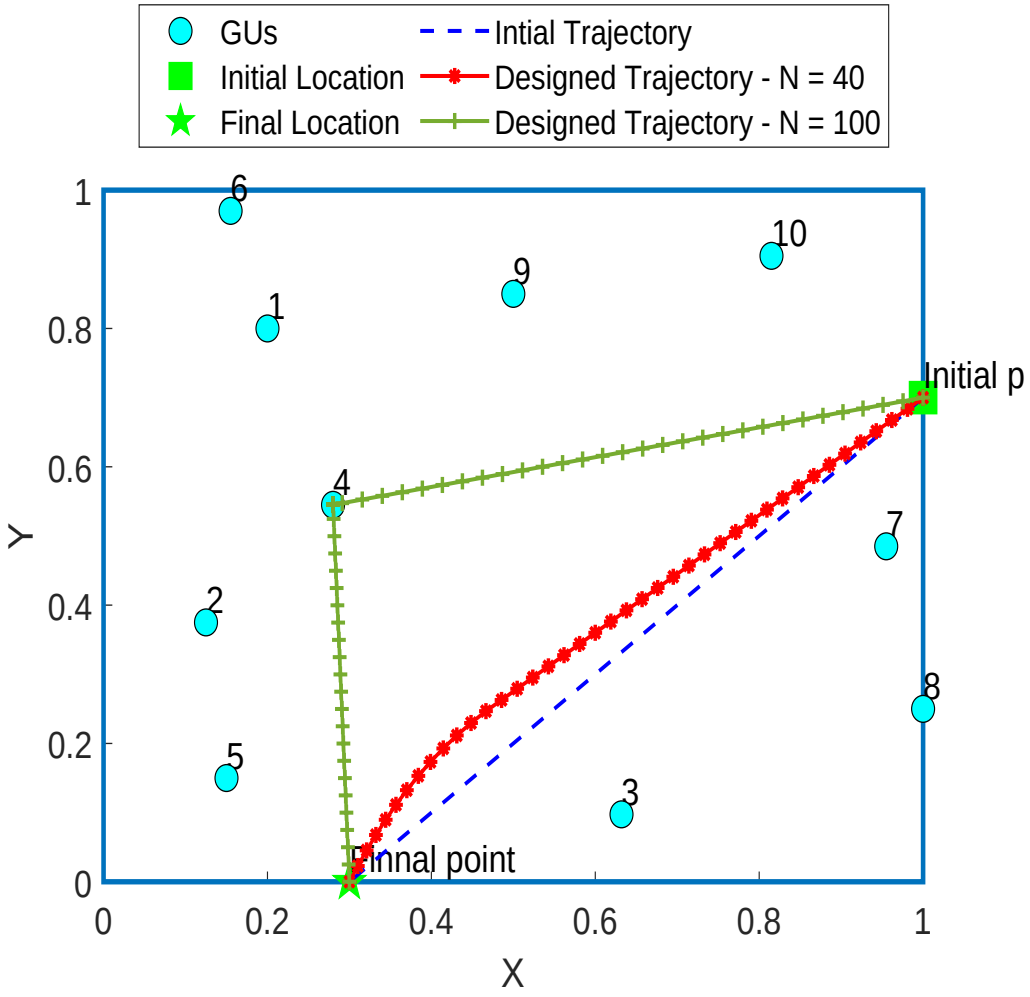

FIGURE 6.2: Geometry distribution of GUs and the UAV trajectories.

- Benchmark scheme 1 (BS1): UAV bandwidth and transmit power optimization with caching capability and fixed trajectory, i.e., a linear trajectory from initial to final locations [254].
- Benchmark scheme 2 (BS2): UAV bandwidth, transmit power, and trajectory optimization without caching capability [258].
- Benchmark scheme 3 (BS3): UAV trajectory optimization with caching capability

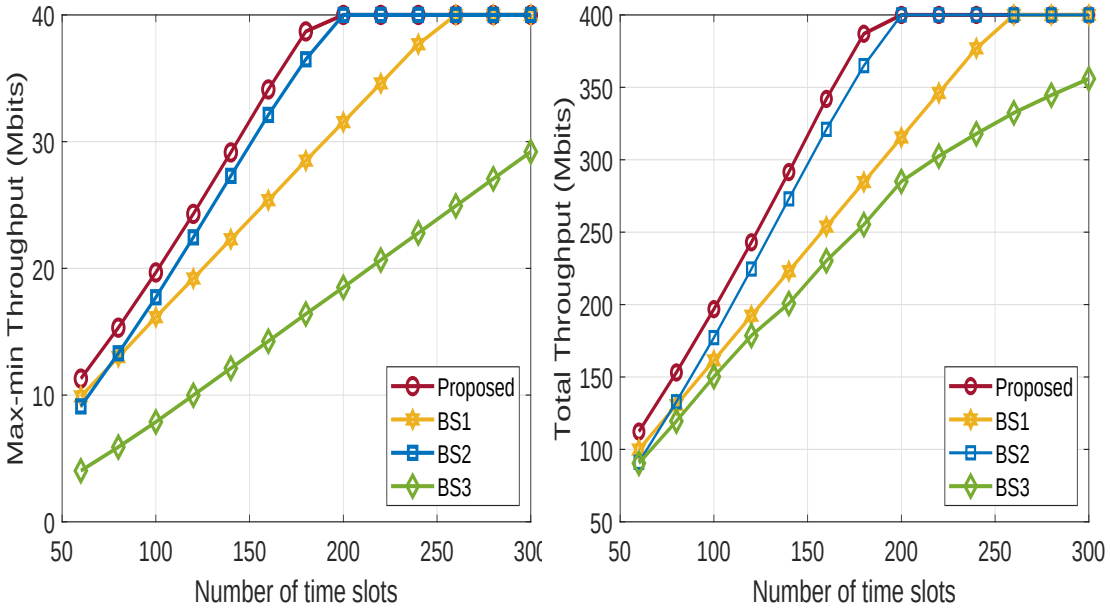

(a) Max-min throughput (b) Total throughput

FIGURE 6.3: Max-min throughput and total throughput vs. number of time slots.

and fixed resource allocation, i.e., $b_{2k}^n \triangleq \frac{1}{K}$, $p_{2k}^n \triangleq \frac{P_u^{\max}}{K}$ [254].

Fig. 6.2 plots the geometric distribution of GUs and the UAV trajectories for different traveling times, i.e., N equals 40 and 100 time slots, with $B_{1k} = 50$ Mbits. First, we observe that the UAV flies from the initial point to the furthest point where it can transmit information to GUs then back to the final point. In contrast to the [254] reference, in which the authors assume that the transmitter only serves up to one requester at a time slot, which is impractical and inefficient. In this work, we assume that the UAV can serve multiple GUs simultaneously to improve network performance, i.e., max-min throughput. It leads to the fact that the UAV tends to fly to a point that keeps a relative distance to all GUs instead of flying to each GU's location as in [254, Figure 7]. Further, it can be explained that if the UAV tries to fly closer to some GUs, thus it only helps to improve the throughput for these GUs while other users' performance is degraded. Thus, it does not guarantee the fairness between all GUs, which is the main purpose of this work. Furthermore, we also find that by increasing the total flight time T, the UAV trajectory range becomes larger as it has more time to get closer to each GU, which improves the max-min throughput.

Fig. 6.3 describes max-min throughput and total throughput as functions of total

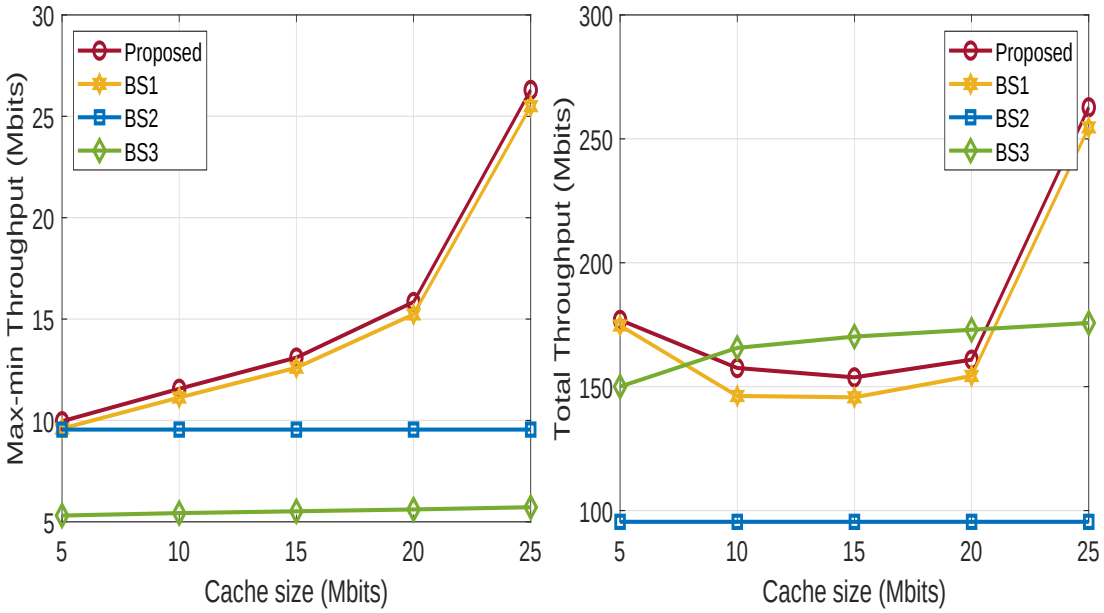

(a) Max-min throughput (b) Total throughput

FIGURE 6.4: Max-min throughput and total throughput vs. cache size (Mbits).

flight time or the number of time slots N, where $B_{1k} = 50$ Mbits, $P_u^{\max} = 15$ dBm, $Q = 40$ Mbits. First, we observe that all schemes' performance increases significantly with larger values of the number of time slots. That is because the higher the traveling time, the more data transmission rate per GU can be obtained. Therefore, the minimum throughput value is improved. It can be seen that the proposed method always achieves the best performance as compared with other schemes. Moreover, as the travel time is large enough, the performance of BS1 and BS2 methods can achieve the same performance as the proposed method. For example, the minimum throughput of BS1 and BS2 can reach 40 Mbits when the number of time slots is greater than 260 and 200, respectively; while BS3 always has the lowest value. In Fig. 6.3.5, the total throughput is illustrated as a function of traveling time. We can see that Fig. 6.3.5 has similar properties as Fig. 6.3.5. It shows the total throughput that the UAV successfully transfers to all GUs. Similar to Fig. 6.3.5, when the number of time slot is lower than 80, the BS1 is better than the BS2 scheme. Further, the proposed scheme is still the best one. Specifically, the throughput performance of the proposed algorithm can serve up to 387 Mbits and the BS1 can achieve less than 26.46 %, i.e., 284.6 Mbits, when $N = 180$. In comparison, the BS2 and BS3 scheme imposes a 365 and 255.24 Mbits of total throughput, respectively.

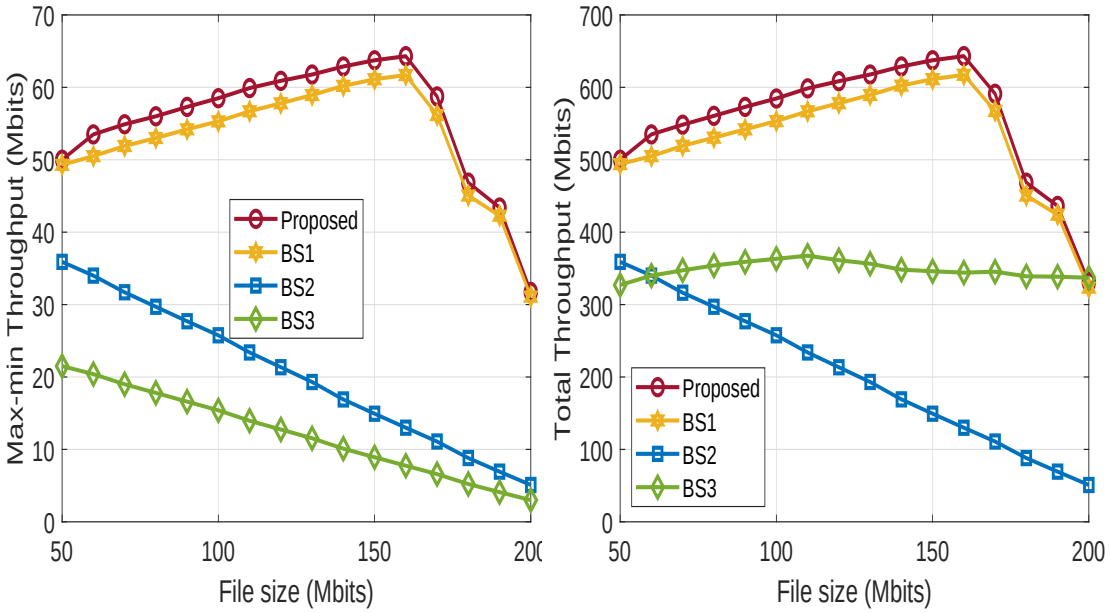

(a) Max-min throughput (b) Total throughput

FIGURE 6.5: Max-min throughput and total throughput vs. demanded data size (Mbits).

In Fig. 6.4, we study the influences of cache size, i.e., the number of files that can be stored at the UAV, on the network performance, where $Q = 60$ Mbits, $N = 80$, $B_{1k} = 20$ Mbits, $x = 2$ km. From the results, it can be seen that the proposed algorithm significantly enhances the minimum and total throughput compared to the benchmarks for all cache sizes. It is expected since the UAV has stored part of the requested files in their memory. Thus, it does not need to demand from the satellite, which incurs more delay. As a result, the UAV has more time to communicate with GUs, and a higher data rate can be obtained. For instance, the minimum throughput of the proposed and BS1 schemes get 15.84 and 15.2 Mbits respectively at cache size equals 20 Mbits. Moreover, the BS2 and BS3 impose 9.55 and 5.61 Mbits, respectively. One more noticeable point in Fig. 6.4 is the performance of the BS2 scheme independent of the cache size values. This is because the BS2 method is implemented without considering caching capability at the UAV. Notably, when the cache size is ranging from 10 to 20, the BS3 method can achieve better total throughput compared to other schemes.

In Fig. 6.5, we plot the max-min throughput as a function of the file size (in Mbits), where $N = 120$, $x = 2$ km. From the results, it is shown that the proposed scheme greatly improves the performance compared to the references for all file sizes. Specifically, at

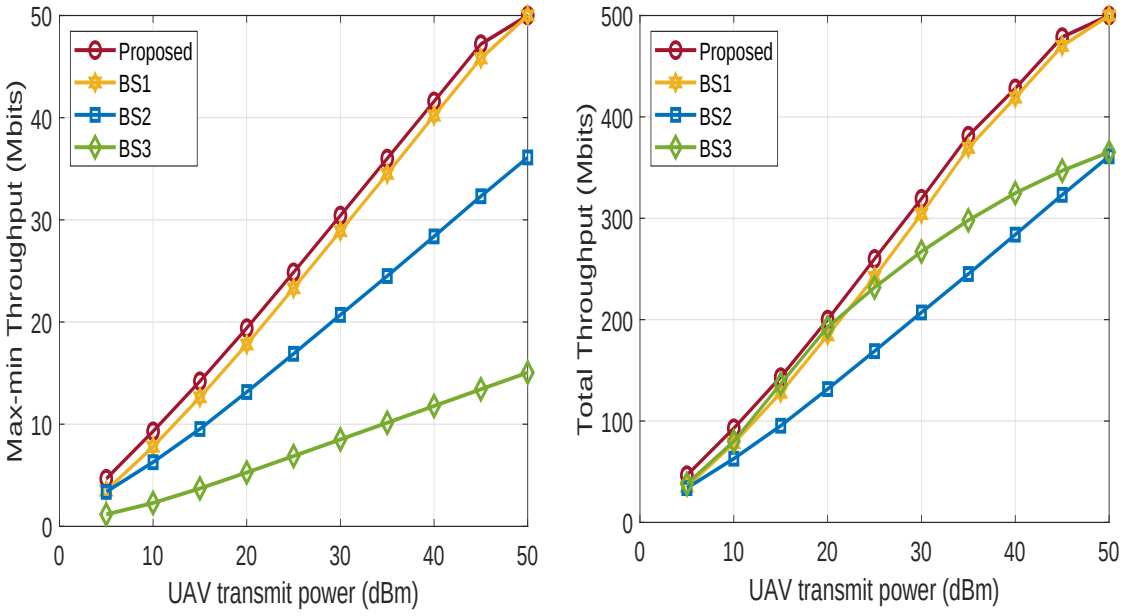

(a) Max-min throughput (b) Total throughput

FIGURE 6.6: Max-min throughput and total throughput vs. UAV transmit power (dBm).

demanded data equals 160 Mbits, the max-min throughput value of proposed method is 64.4 Mbits, and the BS1 achieve less than 4.5%, i.e., 61.5 Mbits. Whereas the BS2 and BS3 impose 13 and 7.75, respectively. Notably, we also find that the performance of the proposed method and BS1 optains the maximum value at the optimal file size, then it will decreases. While the performance of BS2 and BS3 decreases dramatically. This shows the superiority of the resource and cache placement optimization in the proposed scheme and BS1 compared to BS2 and BS3. Nevertheless, for a given resource (i.e., bandwidth, transmit power, UAV speed, and total flight time), when the file size is too large (i.e., file size is larger than 160 Mbits), the performance of the proposed scheme and BS1 decreases significantly. This is due to the fact that the larger the file size, the more latency is required to transmit the requested data from the satellite to the UAV on the backhaul link. Therefore, the UAV has less time to transmit data to GUs.

Fig. 6.6 presents the results corresponding to the max-min throughput versus UAV transmit power $P_u^{\max}$, where $N = 100$, $Q = 50$ Mbits, $S = 10$. As illustrated, system performance is enhanced by increasing the power budget, i.e., $P_u^{\max}$. That is due to the fact that the higher the transmit power, the higher the data transmission rate can be obtained, as shown in Eqs. (6.11) and (6.12). Furthermore, the proposed scheme provides a better

result in comparison with the benchmark ones when the transmit power is small, i.e., $P_u^{\max} \leq 50$ dBm. Nevertheless, the BS1 method can obtain the same max-min throughput as the proposed method when $P_u^{\max}$ value is large, e.g., $P_u^{\max} \geq 50$ dBm. In this scenario, the UAV should operate in the BS1 scheme due to its simplicity and fast employment. However, inherent restrictions of UAV is the limitation on size, weight, and power capability (SWAP). Thus, the proposed scheme is the best one that can adapt to all scenarios in practice.

6.5 Summary

This paper studied LEO satellite- and cache-assisted UAV communications. Especially, we proposed a novel system model that jointly considers UAV, caching, and satellite communications in content delivery networks. In this context, we maximized the minimum achievable throughput among GUs via joint optimization of the cache placement, resource allocation, and UAV trajectory. Because the formulated problem was in the form of MINLP, it is difficult to solve directly. Thus, we transformed the original problem into a solvable form using an alternative algorithm based on BCD method and SCA techniques. Extensive simulation results showed that our proposed algorithm improves up to 26.64%, 79.79%, and 87.96% in the max-min throughput compared to BS1, BS2, and BS3, respectively. Notably, in the cases such as the UAV transmit power or the total traveling time size is large enough, the UAV should operate in fixed trajectory mode for a simple implementation.

Chapter 7

Conclusions and Future Works

A summary and the main conclusions of our work in this dissertation are provided in Section 7.1. Finally, Section 7.2 provides protential directions for future works.

7.1 Main Conclusion

In recent years, developments in the field of UAV communications motivates researchers to propose a number of interesting ideas. In this dissertation, we focused on the trajectory design and resource allocation of the UAV system. The main structure of our thesis can be summarized as follows:

- In the first chapter, we provided an overview of the recent advantages and applications of UAV-enabled communication systems. Then, we present the limitations and technical challenges without being investigated in the aforementioned works.
- In chapter 2, we have studied the trajectory design for energy minimization in UAV-enabled wireless systems with latency constraints. To this end, first, we designed three algorithms, namely, exhaustive search, heuristic algorithm, and dynamic algorithm to find a set of feasible paths satisfying the latency constraint at each GU. Then, based on the given feasible paths, we minimized the total energy consumption and the best path is selected as the lower energy consumption one. The results obtained from this work can provide an initial feasible path for UAV-enabled DL data transmission problems with latency requirements.
- In chapter 3, we have studied FD- and UAV-assisted emergency communications to collect data from IoT devices and transfer them to the ground gateway. In particular, to guarantee the latency constraints of each IoT data, we have proposed a novel

system model to jointly optimize the maximum transmit power of devices/UAV, the allocated bandwidth for DL and UL, and the UAV trajectory. The results have shown that by intelligently designing the UAV trajectory, the proposed algorithms gain significance compared to the benchmarks. Particularly, the outcome of this work can provide the first framework for designers to model a latency-sensitive data collection in the IoT ecosystem .

- In chapter 4, we have studied the throughput performance of a UAV acting as a relay to transfer information from source to destination. We have considered two type of communications including passive (or backscatter) and active communications. We have provided an efficient algorithm to maximize the achievable throughput at the destination. The results obtained from this work can provide a new approach for researchers in designing an energy efficiency of a low-power UAV in a practice scenario.

- In chapter 5, we have investigated the LEO satellite and UAV communication in DL transmission. In particular, we considered a practice delay transmission from satellite to UAV due to large distance, and the UAV trajectory is optimized to maximize the minimum throughput that transmits to GUs during a limited flight time. To our best knowledge, this is the first comprehensive study that jointly considers UAV, caching, and SatCom in content delivery networks. Thus, it provides a novel system model and a new approach that has not been investigated before.

7.2 Future Works

Although there is a considerable amount of research on UAV communications, during my Ph.D., I have discovered many other interesting problems that should be investigated to further understanding the UAV networks. In the following, we list some open problems:

7.2.1 Possible Extensions

- **Further analysis of the UAV trajectory design based on TSPTW**: The TSPTW-based trajectory design for UAV communications have investigated in Chapter 2 could be further extended into many fascinating directions. First, chapter 2 only provides a coarse trajectory design to satisfy the latency constraints of the downlink from UAV to GUs. One interesting problem is finding a fine trajectory based on the results obtained in Chapter 2, which can further improve the network performance, i.e., reduce the energy consumption at the UAV. Besides, another problem is to jointly select the paths and optimize the velocity, which requires advanced optimization techniques but might further improve the UAV's performance. Further,

the problem of considering dynamic network topology is also an appealing direction. In this case, an adaptive solution that optimizes the UAV trajectory on the fly is required. Furthermore, this research result motivates the trajectory design for multi-UAV scenario, in which multiple UAVs jointly serve the ground users. Pursuing the optimal solution in this case requires advanced optimization techniques and may need collaboration among the UAVs.

- **More Insights on the UAV relay-assisted emergency Communications framework**: In Chapter 3 of this dissertation, a study of FD- and UAV-assisted latency-sensitive on both DL and UL was provided. In the process,a simple model, whereas the UAV and GUs were equipped with single antenna, was used for analysis. The outcome of this work will motivate future works in UAV-aided wireless systems. One possible problem is to extend this work to a multi-antenna UAV system, which imposes higher complexity but might further improve the network performance. Another promising problem is to consider low complexity yet efficient machine learning approaches to provide a reliable prediction of the LoS probability for any pair of UAV and GU locations, hence leading to enhance performance assurance.

- **Consideration a more generalized UAV relay network**: The framework provided in Chapter 4 considers an investigation assuming the backscatter and caching in UAV communication where a UAV plays as a relay to transfer information to the destination. The outcome of this work will motivate future research directions: i. The study of a multi-antenna UAV system, which increases complexity but might further improve the system performance; ii. Another promising direction is to consider intelligent reflecting surface (IRS); iii. The study of a more general system model with multiple UAVs and multiple ground users; iv. The existence of a direct link between source and destination is a more general model; v. Research on physical layer security in the presence of an eavesdropper and a friendly jammer; vi. The UAV can apply the NOMA technique to serve two users at the same time.

- **Satellite-UAV-Terrestrial communications**: The outcome of chapter 5 will motivate future works in satellite and UAV wireless systems: i. One possible problem is to extend this work to a multi-UAV system, which imposes higher complexity but might further improve the network performance; ii. Another promising direction is to consider mobile edge computing in which the satellite plays as a cloud center (CC), the UAV is a relay to transfer offloading information from GUs to CC. Specifically, we can formulated a dynamic task offloading and scheduling problem by jointly optimizing the computing offloading task, task scheduling, resource allocation, and UAV trajectory.

7.2.2 New Problems

- **UAV-assisted Symbiotic Communications**: There are several studies on UAV communication in IoT networks. Nevertheless, due to the unprecedented increase of mobile and IoT devices, current network architectures are becoming overwhelmed with growing data traffic demands due to the limited resources, i.e., spectrum and energy. Recently, symbiotic is emerged as a promising solution for IoT networks to overcome the above issues. Generally, symbiotic radio is the combination of cognitive radio networks (CRN) and backscatter communications (BackCom). Therefore, it inherits benefits from both techniques, which are spectrum efficiency and lower power consumption. Moreover, the benefits of UAVs for IoT communications have been intensively investigated in the literature due to the high mobility, swift, and low-cost deployment. Consequently, the combination of UAV and symbiotic can become a hot topic in the next few years.

- **UAV with Mobile Edge Computing**: Due to the explosive surge of resource intensive applications such as interactive gaming, face recognition, augmented reality (AR), and virtual reality (VR), that impose stringent demands on high computation capability, and low-latency processing. Nevertheless, the limited storage, energy, and computation resources of mobile users make them unsuitable for processing resource-hungry applications. Mobile Edge Computing (MEC) was recently proposed to overcome the above issues due to its compute-intensive capability and close proximity to end-users. Besides, UAVs can be employed to improve the quality of service (QoS) and the channel conditions since they can provide LoS links to GUs. Therefore, the utilization of UAVs as flying computing servers as well as relays can provide low latency-aware mobile services.

- **Artificial Intelligence for UAV-Enabled Wireless Networks**: UAVs are considered as one of the promising technologies for the next-generation wireless communication networks due to their mobility and ability to establish LoS links with GUs. However, the still exists many problems that need to be solved in UAV communications. Especially, the problem of how to design the UAV system in online or real-time scenarios is still needed to be studied. For example, during a natural disaster, terrestrial infrastructure can be destroyed or compromised, affecting the ability of people to communicate with the outside world. In this context, an intelligent UAV equipped with machine learning (e.g., deep reinforcement learning) can be proposed to determine the optimal location of the UAV to maximize the final reward adaptively in real-time, e.g., the important information disseminated to people in the isolated area as soon as possible with unknown environments after a disaster. Another example is that an AI-based UAV can prioritize one more important task in real-world situations while performing another, e.g. when flying for broadcast information, it receives SOS

information from a person on the ground. One more example is the UAV swarm in a battlefield environment, herein the UAVs should be designed to have the ability to self-control and make the right decisions in the highly dynamic environment to finish the mission as best as possible. Recently, federated learning has been received significant attention from wireless communication community. Due to the privacy concerns of mobile users and limited communication resources and computing capability of UAVs, it is impractical to send raw data from GUs to UAV servers for model training. There is a need to develop a federated learning framework for UAVs networks, which can efficiently provide asynchronous distributed computing by allowing local training of the model.

- **Blockchain-Envisioned UAV Communication**: Secure communication in UAV networks has been intensively investigated by both academic and industry experts, but there are still many unsolved challenges. Specifically, traditional UAV communication is not enough to deal with the high maneuverability and dynamic features of UAV in ultra-high speed and low latency requirements in 5G and beyond networks. Therefore, there is a need for a secure and efficient network for UAV communications. Blockchain technology can be considered as a good security solution in UAV-enabled 6G communication since it provides scalability, adaptability, transparency, and immutability to the UAV networks. Furthermore, the blockchain-based UAV in 6G networks helps in various areas, such as disaster management, product delivery, surveillance operations, supply chain management, etc., to provide efficient, secure, and effective communication.

Appendix A

Appendices for Chapter 4

A.1 Proof for Lemma 3 in Chapter 4

Proof for (4.10) *and* (4.11): We consider a function $f(z) = \mathbb{E}_Z[\log_2(1 + e^{\ln z})]$, $z > 0$. By adopting Jensen's inequality for convex function $\log_2(1 + e^{\ln z})$, it yields

$$f(z) \geq \log_2\Big(1 + e^{\mathbb{E}_Z[\ln z]}\Big). \tag{A.1}$$

Let us denote $Z \triangleq \Gamma_{1\mathrm{k}} = \frac{p_{1k}[n]|\tilde{h}_{1k}[n]|^2\omega_0}{\Big(H^2+\Big\|\mathbf{q}[n]-\mathbf{w}_k\Big\|^2\Big)^{\alpha/2}\Big(\phi^{\mathrm{RSI}}\sum\limits_{k^*\in\mathcal{K}\setminus k} p_{2k^*}[n]+\sigma^2\Big)}$. Thus, this is an exponentially distributed random variable with parameter $\lambda_Z \triangleq (\mathbb{E}[Z])^{-1} = \frac{\zeta_{1k}}{p_{1k}[n]\omega_0}$ with $\zeta_{1k} \triangleq \Big(H^2 + \Big\|\mathbf{q}[n] - \mathbf{w}_k\Big\|^2\Big)^{\alpha/2}\Big(\phi^{\mathrm{RSI}}\sum\limits_{k^*\in\mathcal{K}\setminus k} p_{2k^*}[n] + \sigma^2\Big)$. By applying [263, Eq. 4.331.1], $\mathbb{E}_Z[\ln z]$ can be calculated as

$$\begin{aligned}\mathbb{E}_Z[\ln z] &= \int_0^{+\infty} \lambda_Z e^{-z\lambda_Z} \ln z dz = -\Big(\ln(\lambda_Z) + E\Big),\\ &= \ln\frac{p_{1k}[n]\omega_0}{\zeta_{1k}} - E,\end{aligned} \tag{A.2}$$

where E is the Euler-Mascheroni constant, i.e., $E = 0.5772156649$ as in [263, Eq. 8.367.1].

By substituting (A.2) into (A.1), we obtain (4.10). Similar to (4.10), we also easily achieve (4.11) by adopting $Z \triangleq \Gamma_{2\mathrm{k}}$.

A.2 Proof for Lemma 7 in Chapter 4

As in [221, Eq. (20)], we have

$$h_1(x,y,z) \geq \ln\left(1+\frac{x^{(j)}}{y^{(j)}z^{(j)}}\right) - \frac{x^{(j)}}{y^{(j)}z^{(j)}} + 2\frac{\sqrt{x^{(j)}}\sqrt{x}}{y^{(j)}z^{(j)}} - \frac{x^{(j)}\left(x+yz\right)}{y^{(j)}z^{(j)}\left(x^{(j)}+y^{(j)}z^{(j)}\right)}, \quad \text{(A.3)}$$

$$h_2(x,z) \geq \ln\left(1+\frac{x^{(j)}}{z^{(j)}}\right) - \frac{x^{(j)}}{z^{(j)}} + 2\frac{\sqrt{x^{(j)}}\sqrt{x}}{z^{(j)}} - \frac{x^{(j)}\left(x+z\right)}{z^{(j)}\left(x^{(j)}+z^{(j)}\right)}. \quad \text{(A.4)}$$

By applying (4.57), the upper bound of yz in (A.3) is given by

$$yz \leq \frac{y^{(j)}}{2z^{(j)}}z^2 + \frac{z^{(j)}}{2y^{(j)}}y^2, \quad \text{(A.5)}$$

with $x \geq 0$, $y \geq 0$, $z \geq 0$, $x^{(j)} \geq 0$, $y^{(j)} \geq 0$, $z^{(j)} \geq 0$.

Then, replacing (A.5) into (A.3), we obtain (4.58) and (4.59). The Lemma 2 is hence proved.

A.3 Proof for Equations (4.60) and (4.61) in Chapter 4

From (A.5), the upper bound of $z_k[n]t_{1k}[n]$ in $r_{1k}^{\text{lb}}[n]$ is:

$$z_k[n]t_{1k}[n] \leq \left(z_{1k}[n]t_{1k}[n]\right)^{\text{ub}} \triangleq \frac{z_{1k}^{(j)}[n]\left(t_{1k}[n]\right)^2}{2t_{1k}^{(j)}[n]} + \frac{t_{1k}^{(j)}[n]\left(z_{1k}[n]\right)^2}{2z_{1k}^{(j)}[n]}. \quad \text{(A.6)}$$

By making use of (4.58), (4.59), and (A.6), the lower bound of $\Phi_{1k}[n]$ and $\Phi_{2k}[n]$ are, respectively

$$\Phi_{1k}[n] \geq \bar{\Phi}_{1k}[n] \triangleq B\Big(\Xi_1 + \Xi_2 - \Xi_3\Big), \quad \text{(A.7)}$$

$$\Phi_{2k}[n] \geq \bar{\Phi}_{2k}[n] \triangleq B\Big(\Xi_4 + \Xi_5 - \Xi_6\Big), \quad \text{(A.8)}$$

where

$$\begin{aligned}
\Xi_1 &\triangleq \log_2\left(1+\frac{e^{-E}p_{1k}^{(j)}[n]\omega_0}{z_{1k}^{(j)}[n]t_{1k}^{(j)}[n]}\right)-\frac{e^{-E}p_{1k}^{(j)}[n]\omega_0}{z_{1k}^{(j)}[n]t_{1k}^{(j)}[n]\ln 2},\\
\Xi_2 &\triangleq e^{-E}\omega_0\frac{2\sqrt{p_{1k}^{(j)}[n]}\sqrt{p_{1k}[n]}}{z_{1k}^{(j)}[n]t_{1k}^{(j)}[n]\ln 2},\\
\Xi_3 &\triangleq \frac{e^{-E}p_{1k}^{(j)}[n]\omega_0}{\left(e^{-E}p_{1k}^{(j)}[n]\omega_0+z_{1k}^{(j)}[n]t_{1k}^{(j)}[n]\right)z_{1k}^{(j)}[n]t_{1k}^{(j)}[n]\ln 2}\\
\times &\left(e^{-E}p_{1k}[n]\omega_0+\frac{z_{1k}^{(j)}[n]\left(t_{1k}[n]\right)^2}{2t_{1k}^{(j)}[n]}+\frac{t_{1k}^{(j)}[n]\left(z_{1k}[n]\right)^2}{2z_{1k}^{(j)}[n]}\right),\\
\Xi_4 &\triangleq \log_2\left(1+\frac{e^{-E}p_{2k}^{(j)}[n]\omega_0}{z_{2k}^{(j)}[n]\sigma^2}\right)-\frac{e^{-E}p_{2k}^{(j)}[n]\omega_0}{z_{2k}^{(j)}[n]\sigma^2\ln 2},\\
\Xi_5 &\triangleq \frac{e^{-E}\omega_0}{z_{2k}^{(j)}[n]\sigma^2\ln 2}2\sqrt{p_{2k}^{(j)}[n]}\sqrt{p_{2k}[n]},\\
\Xi_6 &\triangleq \frac{e^{-E}p_{2k}^{(j)}[n]\omega_0}{e^{-E}p_{2k}^{(j)}[n]\omega_0+z_{2k}^{(j)}[n]\sigma^2}\times\frac{\left(e^{-E}p_{2k}[n]\omega_0+z_{2k}[n]\sigma^2\right)}{z_{2k}^{(j)}[n]\sigma^2\ln 2}.
\end{aligned}$$

A.4 Proof for Proposition 8 in Chapter 4

To be self-contained, we briefly provide the convergence analysis as follows. First, we recall that the approximate functions presented in Section 4.3 satisfy properties of the IA algorithm [213,226]. Let $\mathbb{F}(\mathbf{\Psi})$ and $\widetilde{\mathbb{F}}(\mathbf{\Psi})$ denote the objective function of (4.20) and (4.66), respectively. Following the IA principle, the approximated function's feasible region is a subset of the feasible region of original problem. Thus, it is true that

$$\mathbb{F}(\mathbf{\Psi})\geq\widetilde{\mathbb{F}}(\mathbf{\Psi}),\ \forall\mathbf{\Psi}, \tag{A.9}$$

$$\mathbb{F}(\mathbf{\Psi}^{(j)})=\widetilde{\mathbb{F}}(\mathbf{\Psi}^{(j)}),\ \forall\mathbf{\Psi}. \tag{A.10}$$

Thus, it follows that

$$\mathbb{F}(\mathbf{\Psi}^{(j+1)})\geq\widetilde{\mathbb{F}}(\mathbf{\Psi}^{(j+1)})\geq\widetilde{\mathbb{F}}(\mathbf{\Psi}^{(j)})=\mathbb{F}(\mathbf{\Psi}^{(j)}), \tag{A.11}$$

where the first inequality is due to (A.9). The second inequality is attributed to the fact that $\mathbf{\Psi}^{(j+1)}$ is a better solution for (4.20) than $\mathbf{\Psi}^{(j)}$ [226, Property iv of Lemma 2.2].

Moreover, since the sequence $\{\mathbb{F}(\mathbf{\Psi}^{(j)})\}$ is bounded due to the power constraints (4.30) and (4.31), the bandwidth constraints (4.25) and (4.26), and the limited flying time, the sequence $\{\mathbf{\Psi}^{(j)}\}$ will converge, as shown in [226, Corollary 2.3]. Thus, each accumulation point $\mathbf{\Psi}^{\star}$ of the sequence $\{\mathbf{\Psi}^{(j)}\}$ is a KKT point as in [213, Theorem 1]. Consequently, we can obtain at least a locally optimal solution according to [213, Corollary 1], which completes the proof.

Appendix B

Appendices for Chapter 5

B.1 Proof for Lemma 9 in Chapter 5

Proof for (5.20): Firstly, we consider a function $f(x) = \mathbb{E}_X[\log_2(1 + e^{\ln x})]$, $x > 0$. Based on Jensen's inequality for convex function $\log_2(1 + e^{\ln x})$, we have

$$f(x) \geq \log_2\left(1 + e^{\mathbb{E}_X[\ln x]}\right). \tag{B.1}$$

Let us denote $x \triangleq P_s|h_{su}^n|^2/\sigma_u^2$ and apply [263, Eq. 4.331.1], we then have

$$\begin{aligned}\mathbb{E}_X[\ln x] &= \int_0^{+\infty} \lambda_{su} e^{-\lambda_{su}x} \ln x dx = -(\ln \lambda_{su} + E) \\ &= \ln\left(P_s\omega_0(d_{su}^n)^{-\alpha}/\sigma_u^2\right) - E,\end{aligned} \tag{B.2}$$

where E is the Euler-Mascheroni constant, i.e., $E = 0.5772156649$ as in [263, Eq. 8.367.1]; $\mathbb{E}[x] = P_s\omega_0(d_{su}^n)^{-\alpha}/\sigma_u^2$, and $\lambda_{su} = \left(\mathbb{E}[x]\right)^{-1} = \left(P_s\omega_0(d_{su}^n)^{-\alpha}/\sigma_u^2\right)^{-1}$.

By substituting (B.2) into (B.1), we obtain the equation expression (5.20).

Proof for (5.21): Secondly, we consider a function $f(x, y) = \mathbb{E}_{X,Y}[\log_2(1 + xy)]$, $x > 0$, $y > 0$, whereas x and y are two independent random variables. Based on Jensen's inequality for concave function $\log_2(1 + xy)$ with respect to (w.r.t.) y, we have

$$f(x, y) \leq \mathbb{E}_X\left[\log_2\left(1 + x\mathbb{E}_Y[y]\right)\right] \triangleq \hat{f}(x, y). \tag{B.3}$$

Then, by applying Jensen's inequality for convex function $\log_2(1 + e^{\ln x})$ with respect

to (w.r.t.) x, we have

$$\begin{aligned}\hat{f}(x,y) &= \mathbb{E}_X\Big[\log_2\Big(1+e^{\ln x}\mathbb{E}_Y[y]\Big)\Big] \\ &\geq \log_2\Big(1+e^{\mathbb{E}_X[\ln x]}\mathbb{E}_Y[y]\Big) \triangleq \tilde{f}(x,y). \end{aligned} \tag{B.4}$$

From (**??**) and (B.4), we see that $\tilde{f}(x,y)$ can serve as an approximation function of $f(x,y)$ but it is not a lower bound or an upper bound of $f(x,y)$.

Let us denote $x \triangleq |h_{ud}^n|^2$, $y \triangleq \frac{\eta_u^n P_s |h_{su}^n|^2 + \bar{P}_u}{\sigma_d^2}$, and apply [263, Eq. 4.331.1], we then have

$$\begin{aligned}\mathbb{E}_X[\ln x] &= \int_0^{+\infty} \lambda_{su} e^{-\lambda_{su} x} \ln x dx = -(\ln \lambda_{su} + E) \\ &= \ln \frac{\omega_0}{\Big(H^2 + \|\mathbf{q}_n - \mathbf{w}_d\|^2\Big)^{\alpha/2}} - E, \end{aligned} \tag{B.5}$$

$$\mathbb{E}_Y[y] = \mathbb{E}\Big[\psi_{ud}|\tilde{h}_{ud}^n|^2\Big] = \frac{\eta_u^n P_s \omega_0 (d_{su}^n)^{-\alpha} + \bar{P}_u}{\sigma_d^2}, \tag{B.6}$$

where $\mathbb{E}[x] = \frac{\omega_0}{\Big(H^2+\|\mathbf{q}_n-\mathbf{w}_d\|^2\Big)^{\alpha/2}}$, and $\lambda_{su} = \Big(\mathbb{E}[x]\Big)^{-1} = \left(\frac{\omega_0}{\Big(H^2+\|\mathbf{q}_n-\mathbf{w}_d\|^2\Big)^{\alpha/2}}\right)^{-1}$. Substituting (B.5) and (B.6) into (B.4), we obtain (5.21). Thus, the Lemma 9 is proof.

B.2 Proof for Theorem 10 in Chapter 5

It is easy to verify that if $\lambda_4 \neq 0$, thus $J(\boldsymbol{\tau}) = 0$ implying that $\tau_n = 1$ which is not a feasible solution. Thus, we conclude that $\lambda_4 = 0$.

In order to obtain the feasible solution, we evaluate all the cases as follows:

Case I: $\lambda_1 = 0 \implies G(\boldsymbol{\tau}) \neq 0$, $\lambda_2 = 0 \implies H(\boldsymbol{\tau}) \neq 0$, $\lambda_3 = 0 \implies I(\boldsymbol{\tau}) \neq 0$.

From (5.39), we have $\sum\limits_{n\in\mathcal{N}} \delta_t \bar{R}_d^n = 0$ which is unreasonable. Thus, this case can not occur.

Case II: $\lambda_1 = 0 \implies G(\boldsymbol{\tau}) \neq 0$, $\lambda_2 \neq 0 \implies H(\boldsymbol{\tau}) = 0$, $\lambda_3 = 0 \implies I(\boldsymbol{\tau}) \neq 0$.

From (5.39), we find that $\lambda_2 = -1$ which is unreasonable. Thus, this case can not occur.

Case III: $\lambda_1 \neq 0 \implies G(\boldsymbol{\tau}) = 0$, $\lambda_2 = 0 \implies H(\boldsymbol{\tau}) \neq 0$, $\lambda_3 = 0 \implies I(\boldsymbol{\tau}) \neq 0$.

From (5.39), we have $\lambda_1 = \frac{\sum\limits_{n\in\mathcal{N}} \delta_t \bar{R}_d^n}{\sum\limits_{n\in\mathcal{N}} \delta_t \bar{R}_d^n - \sum\limits_{n\in\mathcal{N}} \delta_t \bar{R}_u^n}$. If $\bar{R}_u^n = \bar{R}_d^n$, then we obtain $\lambda_1 = +\infty$. If $\bar{R}_u^n > \bar{R}_d^n$, then we obtain $\lambda_1 < 0$. All of these scenarios is unreasonable. If $\bar{R}_u^n < \bar{R}_d^n$,

then we obtain $\lambda_1 > 1$. Furthermore, from $G(\boldsymbol{\tau}) = 0$, we have

$$\tau_n^\star \triangleq \frac{\sigma S}{N\delta_t(\bar{R}_d^n - \bar{R}_u^n)}. \tag{B.7}$$

Based on (5.43), the optimal solution $\{\tau_n^\star\}$ can be obtained iff $\bar{R}_u^n < \bar{R}_d^n, \forall n \in \mathcal{N}$.

Case IV: $\lambda_1 = 0 \implies G(\boldsymbol{\tau}) \neq 0,\ \lambda_2 \neq 0 \implies H(\boldsymbol{\tau}) = 0,\ \lambda_3 \neq 0 \implies I(\boldsymbol{\tau}) = 0.$

From $H(\boldsymbol{\tau}) = 0$, we have $\tau_n = \frac{S}{N\delta_t \bar{R}_d^n}$. From $I(\boldsymbol{\tau}) = 0$, we obtain $\tau_n = \frac{\chi_1 - E_{\text{fly}}^n(\mathbf{q})}{\chi_1 + \delta_t\Big(P_b + P_u\Big)}$. It can be seen that there exists two different optimal values of τ which is contradictory. Hence, this case does not occur.

Case V: $\lambda_1 \neq 0 \implies G(\boldsymbol{\tau}) = 0,\ \lambda_2 = 0 \implies H(\boldsymbol{\tau}) \neq 0,\ \lambda_3 \neq 0 \implies I(\boldsymbol{\tau}) = 0.$

Case VI: $\lambda_1 \neq 0 \implies G(\boldsymbol{\tau}) = 0,\ \lambda_2 \neq 0 \implies H(\boldsymbol{\tau}) = 0,\ \lambda_3 = 0 \implies I(\boldsymbol{\tau}) \neq 0.$

Similar to case IV, we also obtain two different values of τ in case V and VI which is conflict. Thus, these cases are not occur.

Case VII: $\lambda_1 \neq 0 \implies G(\boldsymbol{\tau}) = 0,\ \lambda_2 \neq 0 \implies H(\boldsymbol{\tau}) = 0,\ \lambda_3 \neq 0 \implies I(\boldsymbol{\tau}) = 0.$

In this special scenario, we obtain up to three different values of τ which is unreasonable. Thus, this case is not occur.

Case VIII: $\lambda_1 = 0 \implies G(\boldsymbol{\tau}) \neq 0,\ \lambda_2 = 0 \implies H(\boldsymbol{\tau}) \neq 0,\ \lambda_3 \neq 0 \implies I(\boldsymbol{\tau}) = 0.$

From (5.39), we have

$$\begin{aligned} &\sum_{n\in\mathcal{N}} \delta_t \bar{R}_d^n - \lambda_3\Big(\chi_1 + \sum_{n\in\mathcal{N}} \delta_t\Big(P_b + P_u\Big)\Big) = 0 \\ &\iff \lambda_3 = \frac{\sum\limits_{n\in\mathcal{N}} \delta_t \bar{R}_d^n}{\chi_1 + \sum\limits_{n\in\mathcal{N}} \delta_t\Big(P_b + P_u\Big)}. \end{aligned} \tag{B.8}$$

Moreover, from $I(\boldsymbol{\tau}) = 0$, we have

$$\tau_n^\star = \frac{\chi_1 - E_{\text{fly}}^n(\mathbf{q})}{\chi_1 + \delta_t\Big(P_b + P_u\Big)}. \tag{B.9}$$

From (B.7), (B.9), and constraint (5.32), we can obtain (5.44) which completes the proof of Theorem 10.

B.3 Appendix C

First, we proof the convexity of function $f(x) = \log_2\Big(1 + 1/x\Big)$. By taking the second derivative of $f(x)$, we have

$$f''(x) = \frac{(1+2x)}{x^2(1+x)^2 \ln 2}. \tag{B.10}$$

It is easy to see that $f''(x) > 0$ with $x > 0$, thus function $f(x)$ is convex.

Second, we proof the convexity of function $f(x) = \log_2\Big(1 + (A_2 + A_3x)/xy\Big)$. The Hessian matrix of $f(x)$ can be calculated as

$$\boldsymbol{H}_f = \begin{bmatrix} \frac{A_2\Big(A_2+2x(A_3+y)\Big)}{x^2\Big(A_2+x(A_3+y)\Big)^2 \ln 2} & \frac{A_2}{\Big(A_2+x(A_3+y)\Big)^2 \ln 2} \\ \frac{A_2}{\Big(A_2+x\Big(A_3+y)\Big)^2 \ln 2} & \frac{(A_2+A_3x)(A_2+x(A_3+2y))}{y^2\Big(A_2+x(A_3+y)\Big)^2 \ln 2} \end{bmatrix} \tag{B.11}$$

Based on (B.11), it can be seen that trace of matrix $\boldsymbol{H}_f$ is a positive value, with $A_2, A_3, x, y > 0$.

Then, the determinant value of matrix $\boldsymbol{H}_f$ is calculated as

$$\mathrm{Det}\Big(\boldsymbol{H}_f\Big) = \frac{A_2\Big({A_2}^2 + 3A_2x\,(A_3+y) + 2A_3x^2\,(A_3+2y)\Big)}{x^2y^2(A_2+x\,(A_3+y))^3(\ln 2)^2}. \tag{B.12}$$

From (B.12), determinant of matrix $\boldsymbol{H}_f$ is positive with $A_2, A_3, x, y > 0$. Consequently, we can conclude that function $f(x)$ is convex since the Hessian matrix $\boldsymbol{H}_f$ is positive semi-definite [269].

Bibliography

[1] R. Shakeri, M. A. Al-Garadi, A. Badawy, A. Mohamed, T. Khattab, A. K. Al-Ali, K. A. Harras, and M. Guizani, "Design Challenges of Multi-UAV Systems in Cyber-Physical Applications: A Comprehensive Survey and Future Directions," *IEEE Commun. Surv. Tutor.*, vol. 21, no. 4, pp. 3340–3385, 2019.

[2] Z. Ullah, F. Al-Turjman, and L. Mostarda, "Cognition in UAV-Aided 5G and Beyond Communications: A Survey," *IEEE Trans. Cogn. Commun. Netw.*, vol. 6, no. 3, pp. 872–891, 2020.

[3] M. Mozaffari, W. Saad, M. Bennis, Y. Nam, and M. Debbah, "A tutorial on UAVs for wireless networks: Applications, challenges, and open problems," *IEEE Commun. Surveys Tuts.*, vol. 21, no. 3, pp. 2334–2360, 2019.

[4] M. E. Mkiramweni, C. Yang, J. Li, and W. Zhang, "A Survey of Game Theory in Unmanned Aerial Vehicles Communications," *IEEE Commun. Surveys Tuts.*, vol. 21, no. 4, pp. 3386–3416, 2019.

[5] A. Fotouhi, H. Qiang, M. Ding, M. Hassan, L. G. Giordano, A. Garcia-Rodriguez, and J. Yuan, "Survey on UAV Cellular Communications: Practical Aspects, Standardization Advancements, Regulation, and Security Challenges," *IEEE Commun. Surveys Tuts.*, vol. 21, no. 4, pp. 3417–3442, 2019.

[6] L. Xie, X. Cao, J. Xu, and R. Zhang, "Uav-enabled wireless power transfer: A tutorial overview," *IEEE Trans. Green Commun. Netw.*, pp. 1–1, 2021.

[7] H. Price, "Federal Aviation Administration (FAA) Forecast Fiscal Years 2017-2038," *Accessed: Feb*, vol. 25, p. 2019, 2018.

[8] "UAV Market Research Report, Analysis and Forecast to 2025," *www.marketsandmarkets.com/Market-Reports/unmanned-aerial-vehicles-uav-market*, June 2021.

[9] J. Stewart, "Google tests drone deliveries in project wing trials. bbc," 2014.

[10] L. Kelion, "Facebook's laser drones vs google's net-beaming balloons," *BBC News, http://www. bbc.com/news/technology-34780127*, 2015.

[11] A. Palmer, "Amazon wins FAA approval for Prime Air drone delivery fleet," *CNBC, published Aug*, vol. 31, 2020.

[12] "Paving the path to 5G: Optimizing commercial lte networks for drone communication," *https://www.qualcomm.com/news/onq/2016/09/06/paving-path-5goptimizing-commercial-lte-networks-drone-communication*, Oct. 2018.

[13] Y. Zeng, X. Xu, and R. Zhang, "Trajectory Design for Completion Time Minimization in UAV-Enabled Multicasting," *IEEE Trans. Wireless Commun.*, vol. 17, no. 4, pp. 2233–2246, 2018.

[14] C. Zhan and H. Lai, "Energy Minimization in Internet-of-Things System Based on Rotary-Wing UAV," *IEEE Wireless Commun. Lett.*, vol. 8, no. 5, pp. 1341–1344, 2019.

[15] Y. Zeng, J. Xu, and R. Zhang, "Energy Minimization for Wireless Communication With Rotary-Wing UAV," *IEEE Trans. Wireless Commun.*, vol. 18, no. 4, pp. 2329–2345, 2019.

[16] Y. Sun, D. Xu, D. W. K. Ng, L. Dai, and R. Schober, "Optimal 3D-Trajectory Design and Resource Allocation for Solar-Powered UAV Communication Systems," *IEEE Trans. Commun.*, vol. 67, no. 6, pp. 4281–4298, 2019.

[17] Y. Guo, S. Yin, and J. Hao, "Resource Allocation and 3-D Trajectory Design in Wireless Networks Assisted by Rechargeable UAV," *IEEE Wireless Commun. Lett.*, vol. 8, no. 3, pp. 781–784, 2019.

[18] P. K. Sharma and D. I. Kim, "Secure 3D mobile UAV relaying for hybrid satellite-terrestrial networks," *IEEE Trans. Wireless Commun.*, vol. 19, no. 4, pp. 2770–2784, 2020.

[19] M. Mozaffari, A. Taleb Zadeh Kasgari, W. Saad, M. Bennis, and M. Debbah, "Beyond 5G With UAVs: Foundations of a 3D Wireless Cellular Network," *IEEE Trans. Wireless Commun.*, vol. 18, no. 1, pp. 357–372, 2019.

[20] P. Kitjacharoenchai, M. Ventresca, M. Moshref-Javadi, S. Lee, J. M. Tanchoco, and P. A. Brunese, "Multiple traveling salesman problem with drones: Mathematical model and heuristic approach," *Computers & Industrial Engineering*, vol. 129, pp. 14–30, 2019.

[21] Y. Kergosien, C. Lenté, and J.-C. Billaut, "Home health care problem: An extended multiple traveling salesman problem," in *Proceedings of the 4th multidisciplinary international scheduling conference: theory and applications (MISTA 2009)*, 2009, pp. 85–92.

[22] V. A. Shim, K. C. Tan, and C. Y. Cheong, "A hybrid estimation of distribution algorithm with decomposition for solving the multiobjective multiple traveling salesman problem," *IEEE Trans. Syst. Man Cybern. Part C (Applications and Reviews)*, vol. 42, no. 5, pp. 682–691, 2012.

[23] P. Toth and D. Vigo, *The vehicle routing problem*. SIAM, 2002.

[24] B. M. Baker and M. Ayechew, "A genetic algorithm for the vehicle routing problem," *Computers & Operations Research*, vol. 30, no. 5, pp. 787–800, 2003.

[25] G. Laporte, "What you should know about the vehicle routing problem," *Naval Research Logistics (NRL)*, vol. 54, no. 8, pp. 811–819, 2007.

[26] J. Zirong, Z. Liang, and Z. Zhilong, "3d trajectory planning of uav based on dpga algorithm," *IEEE Access*, pp. 1–1, 2021.

[27] V. Roberge, M. Tarbouchi, and G. Labonte, "Comparison of parallel genetic algorithm and particle swarm optimization for real-time uav path planning," *IEEE Trans. Industr. Inform.*, vol. 9, no. 1, pp. 132–141, 2013.

[28] B. Abhishek, S. Ranjit, T. Shankar, G. Eappen, P. Sivasankar, and A. Rajesh, "Hybrid pso-hsa and pso-ga algorithm for 3d path planning in autonomous uavs," *SN Applied Sciences*, vol. 2, no. 11, pp. 1–16, 2020.

[29] C. Zhang, Z. Zhen, D. Wang, and M. Li, "UAV path planning method based on ant colony optimization," in *2010 Chinese Control and Decision Conference*. IEEE, 2010, pp. 3790–3792.

[30] S. Konatowski and P. Pawłowski, "Ant colony optimization algorithm for UAV path planning," in *2018 14th International Conference on Advanced Trends in Radioelecrtronics, Telecommunications and Computer Engineering (TCSET)*. IEEE, 2018, pp. 177–182.

[31] Q. Song, Q. Zhao, S. Wang, Q. Liu, and X. Chen, "Dynamic path planning for unmanned vehicles based on fuzzy logic and improved ant colony optimization," *IEEE Access*, vol. 8, pp. 62 107–62 115, 2020.

[32] H. Shiri, J. Park, and M. Bennis, "Massive Autonomous UAV Path Planning: A Neural Network Based Mean-Field Game Theoretic Approach," in *2019 IEEE Global Communications Conference (GLOBECOM)*, 2019, pp. 1–6.

[33] ——, "Remote UAV Online Path Planning via Neural Network-Based Opportunistic Control," *IEEE Wireless Commun. Lett.*, vol. 9, no. 6, pp. 861–865, 2020.

[34] Q. Liu, L. Shi, L. Sun, J. Li, M. Ding, and F. Shu, "Path Planning for UAV-Mounted Mobile Edge Computing With Deep Reinforcement Learning," *IEEE Transactions on Vehicular Technology*, vol. 69, no. 5, pp. 5723–5728, 2020.

[35] M. Samir, C. Assi, S. Sharafeddine, D. Ebrahimi, and A. Ghrayeb, "Age of Information Aware Trajectory Planning of UAVs in Intelligent Transportation Systems: A Deep Learning Approach," *IEEE Transactions on Vehicular Technology*, vol. 69, no. 11, pp. 12 382–12 395, 2020.

[36] L. Wang, K. Wang, C. Pan, W. Xu, N. Aslam, and L. Hanzo, "Multi-Agent Deep Reinforcement Learning-Based Trajectory Planning for Multi-UAV Assisted Mobile Edge Computing," *IEEE Trans. Cogn. Commun. Netw.*, vol. 7, no. 1, pp. 73–84, 2021.

[37] V. Roberge, M. Tarbouchi, and G. Labonté, "Fast Genetic Algorithm Path Planner for Fixed-Wing Military UAV Using GPU," *IEEE Trans. Aerosp. Electron. Syst.*, vol. 54, no. 5, pp. 2105–2117, 2018.

[38] C. Huang and J. Fei, "UAV path planning based on particle swarm optimization with global best path competition," *Int. J. Pattern Recognit. Artif. Intell.*, vol. 32, no. 06, p. 1859008, 2018.

[39] X. Liu, Y. Liu, N. Zhang, W. Wu, and A. Liu, "Optimizing trajectory of unmanned aerial vehicles for efficient data acquisition: A matrix completion approach," *IEEE Internet Things J.*, vol. 6, no. 2, pp. 1829–1840, 2019.

[40] L. Shugang, "The fuzzy based compact genetic algorithm for online TSP," in *2009 WRI Global Congress on Intelligent Systems*, vol. 2. IEEE, 2009, pp. 84–88.

[41] F. Yan, Y.-S. Liu, and J.-Z. Xiao, "Path planning in complex 3D environments using a probabilistic roadmap method," *International Journal of Automation and computing*, vol. 10, no. 6, pp. 525–533, 2013.

[42] Y.-S. Cho, D.-U. Kim, and D.-S. Kim, "Topology representation for the Voronoi diagram of 3D spheres," *International Journal of CAD/CAM*, vol. 5, no. 1, pp. 59–68, 2005.

[43] S. M. LaValle, *Planning algorithms*. Cambridge university press, 2006.

[44] S. Karaman and E. Frazzoli, "Sampling-based algorithms for optimal motion planning," *The international journal of robotics research*, vol. 30, no. 7, pp. 846–894, 2011.

[45] R. Geraerts, "Planning short paths with clearance using explicit corridors," in *2010 IEEE International Conference on Robotics and Automation*. IEEE, 2010, pp. 1997–2004.

[46] R. DuToit, M. Holt, M. Lyle, and S. Biaz, "UAV Collision Avoidance Using RRT* and LOS Maximization Technical Report# CSSE12-03."

[47] J. Valente, J. Del Cerro, A. Barrientos, and D. Sanz, "Aerial coverage optimization in precision agriculture management: A musical harmony inspired approach," *Computers and electronics in agriculture*, vol. 99, pp. 153–159, 2013.

[48] Z. W. Geem, J. H. Kim, and G. V. Loganathan, "A new heuristic optimization algorithm: harmony search," *simulation*, vol. 76, no. 2, pp. 60–68, 2001.

[49] B. Miller, K. Stepanyan, A. Miller, and M. Andreev, "3D path planning in a threat environment," in *Proc. 2011 50th IEEE Conference on Decision and Control and European Control Conference*. IEEE, 2011, pp. 6864–6869.

[50] F. Borrelli, D. Subramanian, A. U. Raghunathan, and L. T. Biegler, "MILP and NLP techniques for centralized trajectory planning of multiple unmanned air vehicles," in *Proc. 2006 American Control Conference*. IEEE, 2006, p. 6.

[51] I. A. Musliman, A. A. Rahman, V. Coors *et al.*, "Implementing 3D network analysis in 3D-GIS," *International archives of ISPRS*, vol. 37, no. part B, 2008.

[52] S. Koenig and M. Likhachev, "Improved fast replanning for robot navigation in unknown terrain," in *Proceedings 2002 IEEE international conference on robotics and automation (Cat. No. 02CH37292)*, vol. 1. IEEE, 2002, pp. 968–975.

[53] F. Schøler, A. la Cour-Harbo, and M. Bisgaard, "Generating approximative minimum length paths in 3D for UAVs," in *2012 IEEE Intelligent Vehicles Symposium*. IEEE, 2012, pp. 229–233.

[54] E. Masehian and M. Amin-Naseri, "A voronoi diagram-visibility graph-potential field compound algorithm for robot path planning," *Journal of Robotic Systems*, vol. 21, no. 6, pp. 275–300, 2004.

[55] F. Schøler, "3d path planning for autonomous aerial vehicles in constrained spaces," 2012.

[56] I. Hassanzadeh, K. Madani, and M. A. Badamchizadeh, "Mobile robot path planning based on shuffled frog leaping optimization algorithm," in *2010 IEEE International Conference on Automation Science and Engineering*. IEEE, 2010, pp. 680–685.

[57] Y. V. Pehlivanoglu, O. Baysal, and A. Hacioglu, "Path planning for autonomous UAV via vibrational genetic algorithm," *Aircraft Engineering and Aerospace Technology*, 2007.

[58] C.-T. Cheng, K. Fallahi, H. Leung, and K. T. Chi, "Cooperative path planner for UAVs using ACO algorithm with Gaussian distribution functions," in *2009 IEEE International Symposium on Circuits and Systems*. IEEE, 2009, pp. 173–176.

[59] L. Yang, J. Qi, J. Xiao, and X. Yong, "A literature review of UAV 3D path planning," in *Proceeding of the 11th World Congress on Intelligent Control and Automation*. IEEE, 2014, pp. 2376–2381.

[60] B. Schwarz, "Mapping the world in 3D," *Nature Photonics*, vol. 4, no. 7, pp. 429–430, 2010.

[61] L. Cheng, J. Gong, M. Li, and Y. Liu, "3D building model reconstruction from multi-view aerial imagery and lidar data," *Photogrammetric Engineering & Remote Sensing*, vol. 77, no. 2, pp. 125–139, 2011.

[62] R. Qin, "Analysis of critical parameters of satellite stereo image for 3D reconstruction and mapping," *arXiv preprint arXiv:1905.07476*, 2019.

[63] ——, "Rpc stereo processor (rsp)-a software package for digital surface model and orthophoto generation from satellite stereo imagery," *ISPRS Annals of the Photogrammetry, Remote Sensing and Spatial Information Sciences*, vol. 3, p. 77, 2016.

[64] C. Huang, F. Gao, J. Pan, Z. Yang, W. Qiu, P. Chen, X. Yang, S. Shen, and K.-T. Cheng, "Act: An autonomous drone cinematography system for action scenes," in *2018 IEEE International Conference on Robotics and Automation (ICRA)*. IEEE, 2018, pp. 7039–7046.

[65] T. Nägeli, L. Meier, A. Domahidi, J. Alonso-Mora, and O. Hilliges, "Real-time planning for automated multi-view drone cinematography," *ACM Transactions on Graphics (TOG)*, vol. 36, no. 4, pp. 1–10, 2017.

[66] B. Yang, T. L. Hawthorne, H. Searson, and E. Duffy, "High-Resolution UAV Mapping for Investigating Eelgrass Beds Along the West Coast of North America," in *Proc. IGARSS 2020 - 2020 IEEE International Geoscience and Remote Sensing Symposium*, 2020, pp. 6317–6320.

[67] C. A. Rokhmana and R. Andaru, "Utilizing UAV-based mapping in post disaster volcano eruption," in *Proc. 2016 6th International Annual Engineering Seminar (InAES)*, 2016, pp. 202–205.

[68] R. TaoZhang, "UAV 3D mapping with RGB-D camera," in *Pro. 2017 Chinese Automation Congress (CAC)*, 2017, pp. 2727–2731.

[69] P. S. et al., "Latency critical IoT applications in 5G: Perspective on the design of radio interface and network architecture," *IEEE Commun. Mag.*, vol. 55, no. 2, pp. 70–78, 2017.

[70] M. Samir, S. Sharafeddine, C. Assi, M. Nguyen, and A. Ghrayeb, "UAV trajectory planning for data collection from time-constrained IoT devices," *IEEE Trans. Wireless Commun.*, vol. 19, no. 1, pp. 34–46, Jan. 2020.

[71] A. Merwaday and I. Guvenc, "Uav assisted heterogeneous networks for public safety communications," in *Proc. 2015 IEEE Wireless Communications and Networking Conference Workshops (WCNCW)*, 2015, pp. 329–334.

[72] P. Vamvakas, E. E. Tsiropoulou, and S. Papavassiliou, "On the Prospect of UAV-assisted Communications Paradigm in Public Safety Networks," in *IEEE INFOCOM 2019 - IEEE Conference on Computer Communications Workshops (INFOCOM WKSHPS)*, 2019, pp. 762–767.

[73] M. Z. Anwar, Z. Kaleem, and A. Jamalipour, "Machine Learning Inspired Sound-Based Amateur Drone Detection for Public Safety Applications," *IEEE Trans. Veh. Technol.*, vol. 68, no. 3, pp. 2526–2534, 2019.

[74] J. Liu, X. Wang, B. Bai, and H. Dai, "Age-optimal trajectory planning for UAV-assisted data collection," in *IEEE Conf. Computer Commun. Works. (INFOCOM WKSHPS)*, 2018, pp. 553–558.

[75] M. Abd-Elmagid and H. Dhillon, "Average peak age-of-information minimization in UAV-assisted IoT networks," *IEEE Trans. Veh. Technol.*, vol. 68, no. 2, pp. 2003–2008, 2018.

[76] W. Li, L. Wang, and A. Fei, "Minimizing packet expiration loss with path planning in UAV-assisted data sensing," *IEEE Wireless Commun. Lett.*, vol. 8, no. 6, pp. 1520–1523, 2019.

[77] T. Dinh-Hieu, T. X. Vu, S. Chatzinotas, and B. Ottersten, "Energy-efficient Trajectory Design for UAV-enabled Wireless Communications with Latency Constraints," in *Proc. 2019 53rd Asilomar Conf.*, 2019, pp. 347–352.

[78] D. H. Tran, T. X. Vu, S. Chatzinotas, S. ShahbazPanahi, and B. Ottersten, "Coarse Trajectory Design for Energy Minimization in UAV-Enabled," *IEEE Trans. Veh. Technol.*, vol. 69, no. 9, pp. 9483–9496, 2020.

[79] Y. Zeng and R. Zhang, "Energy-Efficient UAV Communication With Trajectory Optimization," *IEEE Trans. Wireless Commun.*, vol. 16, no. 6, pp. 3747–3760, 2017.

[80] Y. Cai, Z. Wei, R. Li, D. W. K. Ng, and J. Yuan, "Joint Trajectory and Resource Allocation Design for Energy-Efficient Secure UAV Communication Systems," *IEEE Trans. Commun.*, vol. 68, no. 7, pp. 4536–4553, 2020.

[81] T. D. Hieu, B.-S. Kim *et al.*, "Stability-aware geographic routing in energy harvesting wireless sensor networks," *Sensors*, vol. 16, no. 5, p. 696, 2016.

[82] I. Krikidis, S. Timotheou, S. Nikolaou, G. Zheng, D. W. K. Ng, and R. Schober, "Simultaneous wireless information and power transfer in modern communication systems," *IEEE Commun. Mag.*, vol. 52, no. 11, pp. 104–110, 2014.

[83] "This drone could fly forever with wireless power," 2016, [Online] https://www.popularmechanics.com/flight/drones/a23023/wirelesspower- drone/.

[84] "Wirelessly powered drone," 2016, [Online] http://getcorp. com/wirelessly-powered-drone/.

[85] S. Yin, L. Li, and F. R. Yu, "Resource Allocation and Basestation Placement in Downlink Cellular Networks Assisted by Multiple Wireless Powered UAVs," *IEEE Trans. Veh. Technol.*, vol. 69, no. 2, pp. 2171–2184, 2020.

[86] D. N. K. Jayakody, T. D. P. Perera, A. Ghrayeb, and M. O. Hasna, "Self-energized UAV-assisted scheme for cooperative wireless relay networks," *IEEE Trans. Veh. Technol.*, vol. 69, no. 1, pp. 578–592, 2019.

[87] H. Yan, Y. Chen, and S.-H. Yang, "UAV-Enabled Wireless Power Transfer With Base Station Charging and UAV Power Consumption," *IEEE Trans. Veh. Technol.*, vol. 69, no. 11, pp. 12 883–12 896, 2020.

[88] J. O'Halloran, "Huge uptick in global 5G deployment across 2020," *www.computerweekly.com/news/252493760/Huge-uptick-in-global-5G-deployment-across-2020*, 2020.

[89] F. Tariq, M. R. A. Khandaker, K. K. Wong, M. A. Imran, M. Bennis, and M. Debbah, "A Speculative Study on 6G," *IEEE Wireless Commun.*, vol. 27, no. 4, pp. 118–125, 2020.

[90] W. Saad, M. Bennis, and M. Chen, "A vision of 6G wireless systems: Applications, trends, technologies, and open research problems," *IEEE Netw.*, vol. 34, no. 3, pp. 134–142, 2019.

[91] L. Zhen, A. K. Bashir, K. Yu, Y. D. Al-Otaibi, C. H. Foh, and P. Xiao, "Energy-Efficient Random Access for LEO Satellite-Assisted 6G Internet of Remote Things," *IEEE Internet of Things J.*, pp. 1–1, 2020.

[92] M. Giordani and M. Zorzi, "Non-terrestrial networks in the 6G era: Challenges and opportunities," *IEEE Netw.*, 2020.

[93] X. Li, W. Feng, Y. Chen, C. Wang, and N. Ge, "Maritime coverage enhancement using UAVs coordinated with hybrid satellite-terrestrial networks," *IEEE Trans. Commun.*, vol. 68, no. 4, pp. 2355–2369, 2020.

[94] S. K. Sharma, J. Querol, N. Maturo, S. Chatzinotas, and B. Ottersten, "System Modelling and Design Aspects of Next Generation High Throughput Satellites," *IEEE Commun. Lett.*, pp. 1–1, 2020.

[95] L. Lei, E. Lagunas, Y. Yuan, M. G. Kibria, S. Chatzinotas, and B. Ottersten, "Beam Illumination Pattern Design in Satellite Networks: Learning and Optimization for Efficient Beam Hopping," *IEEE Access*, vol. 8, pp. 136 655–136 667, 2020.

[96] ESA, "Low Earth orbit," *www.esa.int/ESA_Multimedia/ Images/2020/03/Low_Earth_orbit*, 2020.

[97] B. Di, L. Song, Y. Li, and H. V. Poor, "Ultra-Dense LEO: Integration of Satellite Access Networks into 5G and Beyond," *IEEE Wirel. Commun.*, vol. 26, no. 2, pp. 62–69, 2019.

[98] L. You, K. X. Li, J. Wang, X. Gao, X. G. Xia, and B. Ottersten, "Massive MIMO Transmission for LEO Satellite Communications," *IEEE J. Sel. Areas Commun.*, vol. 38, no. 8, pp. 1851–1865, 2020.

[99] Z. Zhang, Y. Li, C. Huang, Q. Guo, L. Liu, C. Yuen, and Y. L. Guan, "User Activity Detection and Channel Estimation for Grant-Free Random Access in LEO Satellite-Enabled Internet of Things," *IEEE Internet Things J.*, vol. 7, no. 9, pp. 8811–8825, 2020.

[100] R. Deng, B. Di, S. Chen, S. Sun, and L. Song, "Ultra-Dense LEO Satellite Offloading for Terrestrial Networks: How Much to Pay the Satellite Operator?" *IEEE Trans. Wireless Commun.*, vol. 19, no. 10, pp. 6240–6254, 2020.

[101] J. Yu, X. Liu, Y. Gao, and X. Shen, "3D Channel Tracking for UAV-Satellite Communications in Space-Air-Ground Integrated Networks," *IEEE J. Sel. Areas Commun.*, vol. 38, no. 12, pp. 2810–2823, 2020.

[102] S. Gu, X. Sun, Z. Yang, T. Huang, W. Xiang, and K. Yu, "Energy-Aware Coded Caching Strategy Design with Resource Optimization for Satellite-UAV-Vehicle Integrated Networks," *IEEE Internet Things J.*, pp. 1–1, 2021.

[103] P. K. Sharma, D. Gupta, and D. I. Kim, "Outage Performance of 3D Mobile UAV Caching for Hybrid Satellite-Terrestrial Networks," *IEEE Trans. Veh. Technol.*, pp. 1–1, 2021.

[104] J. Zhao, F. Gao, Q. Wu, S. Jin, Y. Wu, and W. Jia, "Beam Tracking for UAV Mounted SatCom on-the-Move With Massive Antenna Array," *IEEE J. Sel. Areas .Commun.*, vol. 36, no. 2, pp. 363–375, 2018.

[105] Z. Jia, M. Sheng, J. Li, D. Niyato, and Z. Han, "LEO Satellite-Assisted UAV: Joint Trajectory and Data Collection for Internet of Remote Things in 6G Aerial Access Networks," *IEEE Internet Things J.*, pp. 1–1, 2020.

[106] Y. Hu, M. Chen, and W. Saad, "Joint Access and Backhaul Resource Management in Satellite-Drone Networks: A Competitive Market Approach," *IEEE Trans. Wireless Commun.*, vol. 19, no. 6, pp. 3908–3923, 2020.

[107] Q. Huang, M. Lin, J. Wang, T. A. Tsiftsis, and J. Wang, "Energy Efficient Beamforming Schemes for Satellite-Aerial-Terrestrial Networks," *IEEE Trans. Commun.*, vol. 68, no. 6, pp. 3863–3875, 2020.

[108] P. Cerwall, P. Jonsson, and S. Carson, "Ericsson Mobility Report (June 2017)," *White Paper*, 2017.

[109] ——, "https://www.ericsson.com/en/mobility-report/dataforecasts/mobile-traffic-forecast," *Ericsson Report*, 2021.

[110] S.-M. Kim, J. Kim, H. Cha, M. S. Sim, J. Choi, S.-W. Ko, C.-B. Chae, and S.-L. Kim, "Opportunism in spectrum sharing for beyond 5G with sub-6 GHz: A concept and its application to duplexing," *IEEE Access*, vol. 8, pp. 148 877–148 891, 2020.

[111] S. K. Sharma, T. E. Bogale, L. B. Le, S. Chatzinotas, X. Wang, and B. Ottersten, "Dynamic spectrum sharing in 5G wireless networks with full-duplex technology:

Recent advances and research challenges," *IEEE Commun. Surv. Tutor.*, vol. 20, no. 1, pp. 674–707, 2017.

[112] A. A. McKenzie, "An interesting use of ultra-high frequency radio in a meteorological study," *Bull. Am. Meteorol Soc.*, vol. 16, no. 12, pp. 317–318, 1935.

[113] L. Espenschied, "The origin and development of radiotelephony," *Proc. Inst. Radio Eng.*, vol. 25, no. 9, pp. 1101–1123, 1937.

[114] D. Bharadia, E. McMilin, and S. Katti, "Full duplex radios," in *Proc. ACM SIGCOMM 2013 conf. SIGCOMM*, 2013, pp. 375–386.

[115] Y.-S. Choi and H. Shirani-Mehr, "Simultaneous transmission and reception: Algorithm, design and system level performance," *IEEE Trans. Wireless Commun.*, vol. 12, no. 12, pp. 5992–6010, 2013.

[116] H. Wang, J. Wang, G. Ding, J. Chen, Y. Li, and Z. Han, "Spectrum Sharing Planning for Full-Duplex UAV Relaying Systems With Underlaid D2D Communications," *IEEE J. Sel. Areas Commun.*, vol. 36, no. 9, pp. 1986–1999, 2018.

[117] A. Hajihoseini Gazestani, S. A. Ghorashi, Z. Yang, and M. Shikh-Bahaei, "Resource Allocation in Full-Duplex UAV Enabled Multi Small Cell Networks," *IEEE Trans. Mob. Comput.*, pp. 1–1, 2020.

[118] W. Shi, Y. Sun, M. Liu, H. Xu, G. Gui, T. Ohtsuki, B. Adebisi, H. Gacanin, and F. Adachi, "Joint UL/DL Resource Allocation for UAV-Aided Full-Duplex NOMA Communications," *IEEE Trans. Commun.*, pp. 1–1, 2021.

[119] L. Zhu, J. Zhang, Z. Xiao, X. Cao, X.-G. Xia, and R. Schober, "Millimeter-Wave Full-Duplex UAV Relay: Joint Positioning, Beamforming, and Power Control," *IEEE J. Sel. Areas Commun.*, vol. 38, no. 9, pp. 2057–2073, 2020.

[120] H.-T. Ye, X. Kang, J. Joung, and Y.-C. Liang, "Optimization for Full-Duplex Rotary-Wing UAV-Enabled Wireless-Powered IoT Networks," *IEEE Trans. Wireless Commun.*, vol. 19, no. 7, pp. 5057–5072, 2020.

[121] D.-H. Tran, V.-D. Nguyen, S. Chatzinotas, T. X. Vu, and B. Ottersten, "UAV Relay-Assisted Emergency Communications in IoT Networks: Resource Allocation and Trajectory Optimization," *IEEE Trans. Wireless Commun.*, pp. 1–1, 2021.

[122] T. Shafique, H. Tabassum, and E. Hossain, "Optimization of Wireless Relaying With Flexible UAV-Borne Reflecting Surfaces," *IEEE Trans. Commun.*, vol. 69, no. 1, pp. 309–325, 2021.

[123] H. Stockman, "Communication by means of reflected power," *Proc. of the IRE*, vol. 36, no. 10, pp. 1196–1204, 1948.

[124] X. Lu, D. Niyato, H. Jiang, D. I. Kim, Y. Xiao, and Z. Han, "Ambient backscatter assisted wireless powered communications," *IEEE Wireless Commun.*, vol. 25, no. 2, pp. 170–177, 2018.

[125] P. X. Nguyen, D. H. Tran, O. Onireti, P. T. Tin, S. Q. Nguyen, S. Chatzinotas, and H. V. Poor, "Backscatter-Assisted Data Offloading in OFDMA-based Wireless Powered Mobile Edge Computing for IoT Networks," *IEEE Internet Things J.*, pp. 1–1, 2021.

[126] N. Van Huynh, D. T. Hoang, X. Lu, D. Niyato, P. Wang, and D. I. Kim, "Ambient Backscatter Communications: A Contemporary Survey," *IEEE Commun. Surveys Tuts.*, vol. 20, no. 4, pp. 2889–2922, 2018.

[127] J. D. Griffin and G. D. Durgin, "Complete link budgets for backscatter-radio and RFID systems," *IEEE Antennas Propag. Mag.*, vol. 51, no. 2, pp. 11–25, 2009.

[128] A. Bletsas, S. Siachalou, and J. N. Sahalos, "Anti-collision backscatter sensor networks," *IEEE Trans. Wireless Commun.*, vol. 8, no. 10, pp. 5018–5029, 2009.

[129] Z. Ding and H. V. Poor, "On the Application of BAC-NOMA to 6G umMTC," *IEEE Commun. Lett.*, 2021.

[130] S. J. Nawaz, S. K. Sharma, B. Mansoor, M. N. Patwary, and N. M. Khan, "Non-coherent and backscatter communications: Enabling ultra-massive connectivity in 6G wireless networks," *IEEE Access*, 2021.

[131] R. Han, L. Bai, Y. Wen, J. Liu, J. Choi, and W. Zhang, "UAV-Aided Backscatter Communications: Performance Analysis and Trajectory Optimization," *IEEE J. Sel. Areas Commun.*, vol. 39, no. 10, pp. 3129–3143, 2021.

[132] ——, "UAV-Aided Backscatter Communications: Performance Analysis and Trajectory Optimization," *IEEE J. Sel. Areas Commun.*, 2021.

[133] M. Hua, L. Yang, C. Li, Q. Wu, and A. L. Swindlehurst, "Throughput Maximization for UAV-Aided Backscatter Communication Networks," *IEEE Trans. Commun.*, vol. 68, no. 2, pp. 1254–1270, 2020.

[134] G. Yang, R. Dai, and Y.-C. Liang, "Energy-efficient UAV backscatter communication with joint trajectory design and resource optimization," *arXiv preprint arXiv:1911.05553*, 2019.

[135] A. Farajzadeh, O. Ercetin, and H. Yanikomeroglu, "UAV data collection over NOMA backscatter networks: UAV altitude and trajectory optimization," in *Proc. 2019 IEEE Intern. Conf. Commun. (ICC)*. IEEE, 2019, pp. 1–7.

[136] A. Farajzadeh, O. Ercetin, and H. Yanikomeroglu, "Mobility-Assisted Over-the-Air Computation for Backscatter Sensor Networks," *IEEE Wireless Commun. Lett.*, vol. 9, no. 5, pp. 675–678, 2020.

[137] J. Hu, X. Cai, and K. Yang, "Joint trajectory and scheduling design for UAV aided secure backscatter communications," *IEEE Wireless Commun. Lett.*, pp. 1–1, 2020.

[138] M. Hua, L. Yang, C. Li, Q. Wu, and A. L. Swindlehurst, "Throughput maximization for UAV-aided backscatter communication networks," *IEEE Trans. Commun.*, vol. 68, no. 2, pp. 1254–1270, 2019.

[139] D. Ma, G. Lan, M. Hassan, W. Hu, and S. K. Das, "Sensing, computing, and communications for energy harvesting IoTs: A survey," *IEEE Commun. Surveys Tuts.*, vol. 22, no. 2, pp. 1222–1250, 2019.

[140] Ericsson, "Ericsson mobility report: November 2019," 2019.

[141] T. X. Tran and D. Pompili, "Joint task offloading and resource allocation for multi-server mobile-edge computing networks," *IEEE Trans. Veh. Technol.*, vol. 68, no. 1, pp. 856–868, 2018.

[142] T. D. Hieu, T. T. Duy, S. G. Choi *et al.*, "Performance evaluation of relay selection schemes in beacon-assisted dual-hop cognitive radio wireless sensor networks under impact of hardware noises," *Sensors*, vol. 18, no. 6, p. 1843, 2018.

[143] T. D. Hieu, T. T. Duy, and B.-S. Kim, "Performance enhancement for multihop harvest-to-transmit WSNs with path-selection methods in presence of eavesdroppers and hardware noises," *IEEE Sensors J.*, vol. 18, no. 12, pp. 5173–5186, 2018.

[144] W. Lu, P. Si, G. Huang, H. Han, L. Qian, N. Zhao, and Y. Gong, "SWIPT Cooperative Spectrum Sharing for 6G-Enabled Cognitive IoT Network," *IEEE Internet Things J*, vol. 8, no. 20, pp. 15 070–15 080, 2021.

[145] X. Zhang, J. Wang, and H. V. Poor, "Statistical Delay and Error-Rate Bounded QoS Provisioning for SWIPT Over CF M-MIMO 6G Mobile Wireless Networks Using FBC," *IEEE J. Sel. Top. Signal Process.*, vol. 15, no. 5, pp. 1272–1287, 2021.

[146] L. R. Varshney, "Transporting information and energy simultaneously," in *Proc. IEEE Int. Symp. Inf. Theory, Toronto, ON, Canada*, 2008, pp. 1612–1616.

[147] P. Grover and A. Sahai, "Shannon meets Tesla: Wireless information and power transfer," in *Proc. IEEE Int. Symp. Inf. Theory*, 2010, pp. 2363–2367.

[148] R. Zhang and C. K. Ho, "MIMO Broadcasting for Simultaneous Wireless Information and Power Transfer," *IEEE Trans. Wireless Commun.*, vol. 12, no. 5, pp. 1989–2001, 2013.

[149] A. A. Nasir, X. Zhou, S. Durrani, and R. A. Kennedy, "Wireless-Powered Relays in Cooperative Communications: Time-Switching Relaying Protocols and Throughput Analysis," *IEEE Trans. Commun.*, vol. 63, no. 5, pp. 1607–1622, 2015.

[150] H. Ding, X. Wang, D. B. da Costa, Y. Chen, and F. Gong, "Adaptive Time-Switching Based Energy Harvesting Relaying Protocols," *IEEE Trans. Commun.*, vol. 65, no. 7, pp. 2821–2837, 2017.

[151] H. Tran-Dinh, S. Gautam, S. Chatzinotas, and B. Ottersten, "Throughput Maximization for Wireless Communication systems with Backscatter- and Cache-assisted UAV Technology," *in Arxiv*, preprint arXiv:2011.07955.

[152] J. Wang, G. Wang, B. Li, H. Yang, Y. Hu, and A. Schmeink, "Massive MIMO Two-Way Relaying Systems with SWIPT in IoT Networks," *IEEE Internet Things J.*, pp. 1–1, 2020.

[153] T. N. Nguyen, M. Tran, T.-L. Nguyen, D.-H. Ha, and M. Voznak, "Performance Analysis of a User Selection Protocol in Cooperative Networks with Power Splitting Protocol-Based Energy Harvesting over Nakagami-m/Rayleigh Channels," *Electronics*, vol. 8, no. 4, p. 448, 2019.

[154] Y. Zou, J. Zhu, and X. Jiang, "Joint Power Splitting and Relay Selection in Energy-Harvesting Communications for IoT Networks," *IEEE Internet Things J.*, vol. 7, no. 1, pp. 584–597, 2020.

[155] A. Alsharoa, H. Ghazzai, A. E. Kamal, and A. Kadri, "Optimization of a power splitting protocol for two-way multiple energy harvesting relay system," *IEEE Trans. Green Commun. Netw.*, vol. 1, no. 4, pp. 444–457, 2017.

[156] D. H. Ha, T. N. Nguyen, M. H. Q. Tran, X. Li, P. T. Tran, and M. Voznak, "Security and Reliability Analysis of a Two-Way Half-Duplex Wireless Relaying Network Using Partial Relay Selection and Hybrid TPSR Energy Harvesting at Relay Nodes," *IEEE Access*, vol. 8, pp. 187 165–187 181, 2020.

[157] T. N. Nguyen, P. T. Tran, and M. Voznak, "Wireless Energy Harvesting Meets Receiver diversity: A Successful Approach for Two-Way Half-Duplex Relay Networks over Block Rayleigh Fading Channel," *Computer Networks*, vol. 172, p. 107176, 2020.

[158] X. Liu and X. Zhang, "Rate and Energy Efficiency Improvements for 5G-Based IoT With Simultaneous Transfer," *IEEE Internet of Things J.*, vol. 6, no. 4, pp. 5971–5980, 2019.

[159] E. Boshkovska, D. W. K. Ng, N. Zlatanov, and R. Schober, "Practical Non-Linear Energy Harvesting Model and Resource Allocation for SWIPT Systems," *IEEE Commun. Lett.*, vol. 19, no. 12, pp. 2082–2085, 2015.

[160] X. Sun, W. Yang, Y. Cai, Z. Xiang, and X. Tang, "Secure Transmissions in Millimeter Wave SWIPT UAV-Based Relay Networks," *IEEE Wireless Commun. Lett.*, vol. 8, no. 3, pp. 785–788, 2019.

[161] W. Feng, J. Tang, Y. Yu, J. Song, N. Zhao, G. Chen, K.-K. Wong, and J. Chambers, "Uav-enabled swipt in iot networks for emergency communications," *IEEE Wireless Commun.*, vol. 27, no. 5, pp. 140–147, 2020.

[162] W. Wang, J. Tang, N. Zhao, X. Liu, X. Y. Zhang, Y. Chen, and Y. Qian, "Joint Precoding Optimization for Secure SWIPT in UAV-Aided NOMA Networks," *IEEE Trans. Commun*, vol. 68, no. 8, pp. 5028–5040, 2020.

[163] J. Wang, B. Li, G. Wang, Y. Hu, and A. Schmeink, "Robust Design for UAV-Enabled Multiuser Relaying System With SWIPT," *IEEE Trans. Green Commun. Netw.*, vol. 5, no. 3, pp. 1293–1305, 2021.

[164] C. V. N. Index, "Global mobile data traffic forecast update," *Cisco White Paper, year=2016-2021.*

[165] L. Zhao, H. Li, N. Lin, M. Lin, C. Fan, and J. Shi, "Intelligent Content Caching Strategy in Autonomous Driving Toward 6G," *IEEE Trans. Intell. Transp. Syst.*, pp. 1–11, 2021.

[166] C. L. Stergiou, K. E. Psannis, and B. B. Gupta, "IoT-Based Big Data Secure Management in the Fog Over a 6G Wireless Network," *IEEE Internet Things J.*, vol. 8, no. 7, pp. 5164–5171, 2021.

[167] X. Xu, Y. Zeng, Y. L. Guan, and R. Zhang, "Overcoming endurance issue: UAV-enabled communications with proactive caching," *IEEE J. Sel. Areas Commun.*, vol. 36, no. 6, pp. 1231–1244, 2018.

[168] F. Cheng, G. Gui, N. Zhao, Y. Chen, J. Tang, and H. Sari, "UAV-relaying-assisted secure transmission with caching," *IEEE Trans. Commun.*, vol. 67, no. 5, pp. 3140–3153, 2019.

[169] M. Chen, M. Mozaffari, W. Saad, C. Yin, M. Debbah, and C. S. Hong, "Caching in the Sky: Proactive Deployment of Cache-Enabled Unmanned Aerial Vehicles for Optimized Quality-of-Experience," *IEEE J. Sel. Areas Commun.*, vol. 35, no. 5, pp. 1046–1061, 2017.

[170] S. Chai and V. K. N. Lau, "Online trajectory and radio resource optimization of cache-enabled UAV wireless networks with content and energy recharging," *IEEE Trans. Signal Process.*, vol. 68, pp. 1286–1299, 2020.

[171] H. Wu, F. Lyu, C. Zhou, J. Chen, L. Wang, and X. Shen, "Optimal UAV caching and trajectory in aerial-assisted vehicular networks: A learning-based approach," *IEEE J. Sel. Areas Commun.*, pp. 1–1, 2020.

[172] D. Lopez-Perez, I. Guvenc, G. de la Roche, M. Kountouris, T. Q. S. Quek, and J. Zhang, "Enhanced intercell interference coordination challenges in heterogeneous networks," *IEEE Wireless Commun.*, vol. 18, no. 3, pp. 22–30, 2011.

[173] T. X. Vu, H. D. Nguyen, T. Q. S. Quek, and S. Sun, "Adaptive Cloud Radio Access Networks: Compression and Optimization," *IEEE Trans. Signal Process.*, vol. 65, no. 1, pp. 228–241, 2017.

[174] T. X. Vu, T. V. Nguyen, and T. Q. S. Quek, "Power Optimization With BLER Constraint for Wireless Fronthauls in C-RAN," *IEEE Commun. Lett.*, vol. 20, no. 3, pp. 602–605, 2016.

[175] M. Mozaffari, W. Saad, M. Bennis, and M. Debbah, "Wireless communication using unmanned aerial vehicles (UAVs): Optimal transport theory for hover time optimization," *IEEE Trans. Wireless Commun.*, vol. 16, no. 12, pp. 8052–8066, 2017.

[176] M. Erdelj, E. Natalizio, K. R. Chowdhury, and I. F. Akyildiz, "Help from the Sky: Leveraging UAVs for Disaster Management," *IEEE Pervasive Comput.*, vol. 16, no. 1, pp. 24–32, 2017.

[177] K. Li, R. C. Voicu, S. S. Kanhere, W. Ni, and E. Tovar, "Energy Efficient Legitimate Wireless Surveillance of UAV Communications," *IEEE Trans. Veh. Technol.*, vol. 68, no. 3, pp. 2283–2293, 2019.

[178] M. Bacco, A. Berton, A. Gotta, and L. Caviglione, "IEEE 802.15.4 Air-Ground UAV Communications in Smart Farming Scenarios," *IEEE Commun. Lett.*, vol. 22, no. 9, pp. 1910–1913, 2018.

[179] D. Yang, Q. Wu, Y. Zeng, and R. Zhang, "Energy Tradeoff in Ground-to-UAV Communication via Trajectory Design," *IEEE Trans. Veh. Technol.*, vol. 67, no. 7, pp. 6721–6726, 2018.

[180] P. X. Nguyen, H. V. Nguyen, V. Nguyen, and O. Shin, "UAV-Enabled Jamming Noise for Achieving Secure Communications in Cognitive Radio Networks," in *Proc. 2019 16th IEEE CCNC*, 2019, pp. 1–6.

[181] Y. Cai, F. Cui, Q. Shi, M. Zhao, and G. Y. Li, "Dual-UAV-Enabled Secure Communications: Joint Trajectory Design and User Scheduling," *IEEE J. Sel. Areas Commun*, vol. 36, no. 9, pp. 1972–1985, 2018.

[182] M. Hua, Y. Wang, Q. Wu, H. Dai, Y. Huang, and L. Yang, "Energy-Efficient Cooperative Secure Transmission in Multi-UAV-Enabled Wireless Networks," *IEEE Trans. Veh. Technol.*, vol. 68, no. 8, pp. 7761–7775, 2019.

[183] L. Xiang, L. Lei, S. Chatzinotas, B. Ottersten, and R. Schober, "Towards Power-Efficient Aerial Communications via Dynamic Multi-UAV Cooperation," in *Proc. 2020 IEEE WCNC*, 2020, pp. 1–7.

[184] H. Kang, J. Joung, J. Ahn, and J. Kang, "Secrecy-Aware Altitude Optimization for Quasi-Static UAV Base Station Without Eavesdropper Location Information," *IEEE Commun. Lett.*, vol. 23, no. 5, pp. 851–854, 2019.

[185] B. Jiang, J. Yang, H. Xu, H. Song, and G. Zheng, "Multimedia Data Throughput Maximization in Internet-of-Things System Based on Optimization of Cache-Enabled UAV," *IEEE Internet Things J.*, vol. 6, no. 2, pp. 3525–3532, 2019.

[186] Y. A. Sambo, P. V. Klaine, J. P. B. Nadas, and M. A. Imran, "Energy Minimization UAV Trajectory Design for Delay-Tolerant Emergency Communication," in *Proc. 2019 IEEE ICC Works.*, 2019, pp. 1–6.

[187] Q. Song, S. Jin, and F. Zheng, "Completion Time and Energy Consumption Minimization for UAV-Enabled Multicasting," *IEEE Wireless Commun. Lett.*, vol. 8, no. 3, pp. 821–824, 2019.

[188] C. Zhan, Y. Zeng, and R. Zhang, "Energy-Efficient Data Collection in UAV Enabled Wireless Sensor Network," *IEEE Wireless Commun. Lett.*, vol. 7, no. 3, pp. 328–331, 2018.

[189] J. Gong, T. Chang, C. Shen, and X. Chen, "Flight Time Minimization of UAV for Data Collection Over Wireless Sensor Networks," *IEEE J. Sel. Areas Commun*, vol. 36, no. 9, pp. 1942–1954, 2018.

[190] Z. Hu, Z. Zheng, L. Song, T. Wang, and X. Li, "UAV Offloading: Spectrum Trading Contract Design for UAV-Assisted Cellular Networks," *IEEE Trans. Wireless Commun.*, vol. 17, no. 9, pp. 6093–6107, 2018.

[191] T. X. Vu, S. Chatzinotas, B. Ottersten, and T. Q. Duong, "Energy Minimization for Cache-Assisted Content Delivery Networks With Wireless Backhaul," *IEEE Wireless Commun. Lett.*, vol. 7, no. 3, pp. 332–335, 2018.

[192] Y. Dumas, J. Desrosiers, E. Gelinas, and M. M. Solomon, "An optimal algorithm for the traveling salesman problem with time windows," *Oper. Res.*, vol. 43, no. 2, pp. 367–371, 1995.

[193] M. M. Azari, F. Rosas, K. Chen, and S. Pollin, "Ultra Reliable UAV Communication Using Altitude and Cooperation Diversity," *IEEE Trans. Commun.*, vol. 66, no. 1, pp. 330–344, 2018.

[194] S. Gong, S. Wang, C. Xing, S. Ma, and T. Q. S. Quek, "Robust Superimposed Training Optimization for UAV Assisted Communication Systems," *IEEE Trans. Wireless Commun.*, vol. 19, no. 3, pp. 1704–1721, 2020.

[195] B. Bollobás, *Graph theory: an introductory course*. Springer Science & Business Media, 2012, vol. 63.

[196] N. Biggs, "The traveling salesman problem a guided tour of combinatorial optimization," 1986.

[197] A. Jeffrey and D. Zwillinger, *Table of integrals, series, and products*. Elsevier, 2007.

[198] M. Held and R. M. Karp, "A dynamic programming approach to sequencing problems," *J. Soc. Ind. Appl. Math.*, vol. 10, no. 1, pp. 196–210, 1962.

[199] S. Boyd, S. P. Boyd, and L. Vandenberghe, *Convex optimization*. Cambridge university press, 2004.

[200] K. Ashton, "That 'internet of things' thing," *RFID journal*, vol. 22, no. 7, pp. 97–114, 2009.

[201] Q. Pham, F. Fang, N. Ha, M. Le, Z. Ding, L. Le, and W. Hwang, "A survey of multi-access edge computing in 5G and beyond: Fundamentals, technology integration, and state-of-the-art," *IEEE Access*, 2019.

[202] S. Yan, M. Peng, and X. Cao, "A game theory approach for joint access selection and resource allocation in UAV assisted IoT communication networks," *IEEE Internet Things J.*, vol. 6, no. 2, pp. 1663–1674, 2018.

[203] Y. Zeng, Q. Wu, and R. Zhang, "Accessing from the sky: A tutorial on UAV communications for 5G and beyond," *P. IEEE*, vol. 107, no. 12, pp. 2327–2375, 2019.

[204] M. Mozaffari, W. Saad, M. Bennis, and M. Debbah, "Unmanned aerial vehicle with underlaid device-to-device communications: Performance and tradeoffs," *IEEE Trans. Wireless Commun.*, vol. 15, no. 6, pp. 3949–3963, Jun. 2016.

[205] W. F. J. Wang, Y. Chen, X. Wang, N. Ge, and J. Lu, "Uav-aided MIMO communications for 5G Internet of Things," *IEEE Internet Things J.*, vol. 6, no. 2, pp. 1731–1740, 2018.

[206] N. Motlagh, M. Bagaa, and T. Taleb, "Energy and delay aware task assignment mechanism for UAV-based IoT platform," *IEEE Internet Things J.*, vol. 6, no. 4, pp. 6523–6536, 2019.

[207] J. W. et al., "Energy-efficient data collection and device positioning in UAV-assisted IoT," *IEEE Internet Things J.*, vol. 7, no. 2, pp. 1122–1139, 2019.

[208] Z. Yuan, J. Jin, L. Sun, K. Chin, and G. Muntean, "Ultra-reliable IoT communications with UAVs: A swarm use case," *IEEE Commun. Mag.*, vol. 56, no. 12, pp. 90–96, 2018.

[209] Q. Song, F. Zheng, Y. Zeng, and J. Zhang, "Joint beamforming and power allocation for UAV-enabled full-duplex relay," *IEEE Trans. Veh. Technol.*, vol. 68, no. 2, pp. 1657–1671, 2018.

[210] H. Wang, J. Wang, G. Ding, J. Chen, Y. Li, and Z. Han, "Spectrum sharing planning for full-duplex UAV relaying systems with underlaid D2D communications," *IEEE J. Sel. Areas Commun.*, vol. 36, no. 9, pp. 1986–1999, 2018.

[211] B. Duo, Q. Wu, X. Yuan, and R. Zhang, "Energy Efficiency Maximization for Full-Duplex UAV Secrecy Communication," *IEEE Trans. Veh. Technol.*, vol. 69, no. 4, pp. 4590–4595, 2020.

[212] H. Ye, X. Kang, J. Joung, and Y. Liang, "Optimization for Full-Duplex Rotary-Wing UAV-Enabled Wireless-Powered IoT Networks," *IEEE Trans. Wireless Commun.*, 2020.

[213] B. Marks, "A general inner approximation algorithm for nonconvex mathematical programs," *Oper. Res.*, vol. 26, no. 4, pp. 681–683, 1978.

[214] D. H. Tran, V. D. Nguyen, S. Gautam, S. Chatzinotas, T. X. Vu, and B. Ottersten, "Resource allocation for uav relay-assisted iot communication networks," in *2020 IEEE Globecom Workshops (GC Wkshps*, 2020, pp. 1–7.

[215] Y. Zeng, R. Zhang, and T. J. Lim, "Wireless communications with unmanned aerial vehicles: Opportunities and challenges," *IEEE Trans. Commun.*, vol. 54, no. 5, pp. 36–42, May 2016.

[216] A. Osseiran, F. Boccardi, V. Braun, K. Kusume, P. Marsch, M. Maternia, O. Queseth, M. Schellmann, H. Schotten, H.Taoka *et al.*, "Scenarios for 5G mobile and wireless communications: the vision of the METIS project," *IEEE Commun. Mag.*, vol. 52, no. 5, pp. 26–35, 2014.

[217] Y. Yuan, L. Lei, T. X. Vu, S. Chatzinotas, S. Sun, and B. Ottersten, "Energy minimization in UAV-aided networks: actor-critic learning for constrained scheduling optimization," *in Arxiv*, preprint arXiv:2006.13610.

[218] H. Dinh Tran, D. Trung Tran, and S. G. Choi, "Secrecy performance of a generalized partial relay selection protocol in underlay cognitive networks," *Inter. J. Commun. Sys.*, vol. 31, no. 17, p. e3806, 2018.

[219] V. D. Nguyen, H. V. Nguyen, O. A. Dobre, and O. S. Shin, "A new design paradigm for secure full-duplex multiuser systems," *IEEE J. Select. Areas Commun.*, vol. 36, no. 7, pp. 1480–1498, July 2018.

[220] A. Sabharwal, P. Schniter, D. Guo, D. W. Bliss, S. Rangarajan, and R. Wichman, "In-band full-duplex wireless: Challenges and opportunities," *IEEE J. Select. Areas Commun.*, vol. 32, no. 9, pp. 1637–1652, Feb. 2014.

[221] V. D. Nguyen, T. Q. Duong, H. D. Tuan, O. S. Shin, and H. V. Poor., "Spectral and energy efficiencies in full-duplex wireless information and power transfer," *IEEE Trans. Commun*, vol. 65, no. 5, pp. 2220–2233, May 2017.

[222] H. V. Nguyen, V. D. Nguyen, O. A. Dobre, Y. Wu, and O. S. Shin, "Joint antenna array mode selection and user assignment for full-duplex MU-MISO systems," *IEEE Trans. Wireless Commun.*, vol. 18, no. 6, pp. 2946–2963, June 2019.

[223] M. Duarte, C. Dick, and A. Sabharwal, "Experiment-driven characterization of full-duplex wireless systems," *IEEE Trans. Wireless Commun.*, vol. 11, no. 12, pp. 4296–4307, Dec. 2012.

[224] N. Dan, T. Le-Nam, P. Pekka, and L. Matti, "On the spectral efficiency of full-duplex small cell wireless systems," *IEEE Trans. Wireless Commun.*, vol. 13, no. 9, pp. 4896–4910, 2014.

[225] U. Challita, W. Saad, and C. Bettstetter, "Interference management for cellular-connected UAVs: A deep reinforcement learning approach," *IEEE Trans. Wireless Commun.*, vol. 18, no. 4, pp. 2125–2140, April 2019.

[226] A. Beck, A. Ben-Tal, and L. Tetruashvili, "A sequential parametric convex approximation method with applications to nonconvex truss topology design problems," *J. Global Optim.*, vol. 47, no. 1, pp. 29–51, May 2010.

[227] E. Che, H. D. Tuan, and H. H. Nguyen, "Joint Optimization of Cooperative Beamforming and Relay Assignment in Multi-User Wireless Relay Networks," *IEEE Trans. Wireless Commun.*, vol. 13, no. 10, pp. 5481–5495, 2014.

[228] Y. Shi, H. D. Tuan, T. Q. Duong, H. V. Poor, and A. V. Savkin, "PMU Placement Optimization for Efficient State Estimation in Smart Grid," *IEEE J. Sel. Areas Commun.*, vol. 38, no. 1, pp. 71–83, 2020.

[229] J.-F. Bonnans, J. C. Gilbert, C. Lemaréchal, and C. A. Sagastizábal, *Numerical optimization: theoretical and practical aspects*. Springer Science & Business Media, 2006.

[230] T. T. Vu, D. T. Ngo, M. N. Dao, S. Durrani, D. H. N. Nguyen, and R. H. Middleton, "Energy Efficiency Maximization for Downlink Cloud Radio Access Networks With Data Sharing and Data Compression," *IEEE Trans. Wireless Commun.*, vol. 17, no. 8, pp. 4955–4970, 2018.

[231] T. T. Vu, D. T. Ngo, M. N. Dao, S. Durrani, and R. H. Middleton, "Spectral and Energy Efficiency Maximization for Content-Centric C-RANs With Edge Caching," *IEEE Trans. Commun.*, vol. 66, no. 12, pp. 6628–6642, 2018.

[232] T. S. Rappaport, *Wireless communications: principles and practice*. prentice hall PTR New Jersey, 1996, vol. 2.

[233] V. S. Abhayawardhana, I. J. Wassell, D. Crosby, M. P. Sellars, and M. G. Brown, "Comparison of empirical propagation path loss models for fixed wireless access systems," in *Proc. IEEE 61st Veh. Technol. Conf.*, vol. 1, 2005, pp. 73–77.

[234] A. Ben-Tal and A. Nemirovski, *Lectures on modern convex optimization: analysis, algorithms, and engineering applications*. SIAM, 2001.

[235] T. Zhang, C. Su, A. Najafi, and J. C. Rudell, "Wideband dual-injection path self-interference cancellation architecture for full-duplex transceivers," *IEEE J. Solid-State Circuits*, vol. 53, no. 6, pp. 1563–1576, 2018.

[236] M. Mozaffari, W. Saad, M. Bennis, and M. Debbah, "Mobile unmanned aerial vehicles (UAVs) for energy-efficient Internet of Things communications," *IEEE Trans. Wireless Commun.*, vol. 16, no. 11, pp. 7574 –7589, Dec. 2017.

[237] M. Hua, L. Yang, C. Pan, and A. Nallanathan, "Throughput maximization for full-duplex UAV aided small cell wireless systems," *IEEE Wireless Commun. Lett.*, 2019.

[238] X. Zhong, Y. Guo, N. Li, and Y. Chen, "Joint optimization of relay deployment, channel allocation, and relay assignment for UAVs-Aided D2D networks," *IEEE/ACM Trans. on Netw.*, vol. 28, no. 2, pp. 804–817, 2020.

[239] L. Li, T. Chang, and S. Cai, "UAV positioning and power control for two-way wireless relaying," *IEEE Trans. Wireless Commun.*, vol. 19, no. 2, pp. 1008–1024, 2020.

[240] X. Sun, W. Yang, Y. Cai, Z. Xiang, and X. Tang, "Secure transmissions in millimeter wave SWIPT UAV-based relay networks," *IEEE Wireless Commun. Lett.*, vol. 8, no. 3, pp. 785–788, 2019.

[241] J. Erman, A. Gerber, M. Hajiaghayi, D. Pei, S. Sen, and O. Spatscheck, "To cache or not to cache: The 3G case," *IEEE Internet Comput.*, vol. 15, no. 2, pp. 27–34, 2011.

[242] S. Mehrizi, S. Chatterjee, S. Chatzinotas, and B. Ottersten, "Online spatiotemporal popularity learning via variational bayes for cooperative caching," *IEEE Trans. Commun.*, pp. 1–1, 2020.

[243] S. Bommaraveni, T. X. Vu, S. Chatzinotas, and B. Ottersten, "Active content popularity learning and caching optimization with hit ratio guarantees," *IEEE Access*, vol. 8, pp. 151 350–151 359, 2020.

[244] M. Giordani and M. Zorzi, "Non-terrestrial communication in the 6G era: Challenges and opportunities," *arXiv preprint arXiv:1912.10226*, 2019.

[245] B. Lyu, C. You, Z. Yang, and G. Gui, "The optimal control policy for RF-powered backscatter communication networks," *IEEE Trans. Veh. Technol.*, vol. 67, no. 3, pp. 2804–2808, 2017.

[246] S. Xiao, H. Guo, and Y.-C. Liang, "Resource allocation for full-duplex-enabled cognitive backscatter networks," *IEEE Trans. Wireless Commun.*, vol. 18, no. 6, pp. 3222–3235, 2019.

[247] X. Kang, Y.-C. Liang, and J. Yang, "Riding on the primary: A new spectrum sharing paradigm for wireless-powered IoT devices," *IEEE Trans. Wireless Commun.*, vol. 17, no. 9, pp. 6335–6347, 2018.

[248] S. Gong, X. Huang, J. Xu, W. Liu, P. Wang, and D. Niyato, "Backscatter Relay Communications Powered by Wireless Energy Beamforming," *IEEE Trans. Commun.*, vol. 66, no. 7, pp. 3187–3200, 2018.

[249] M. Hong, M. Razaviyayn, Z.-Q. Luo, and J.-S. Pang, "A unified algorithmic framework for block-structured optimization involving big data: With applications in machine learning and signal processing," *IEEE Signal Process. Mag.*, vol. 33, no. 1, pp. 57–77, 2015.

[250] G. Zhang, Q. Wu, M. Cui, and R. Zhang, "Securing UAV communications via joint trajectory and power control," *IEEE Trans. Wireless Commun.*, vol. 18, no. 2, pp. 1376–1389, 2019.

[251] X. Lu, D. Niyato, H. Jiang, D. I. Kim, Y. Xiao, and Z. Han, "Ambient backscatter assisted wireless powered communications," *IEEE Wireless Commun.*, vol. 25, no. 2, pp. 170–177, 2018.

[252] N. Singh, B. K. Kanaujia, M. T. Beg, T. Khan, S. Kumar *et al.*, "A dual polarized multiband rectenna for RF energy harvesting," *AEU-Int. J. Electron. C.*, vol. 93, pp. 123–131, 2018.

[253] L. Breslau, Pei Cao, Li Fan, G. Phillips, and S. Shenker, "Web caching and Zipf-like distributions: evidence and implications," in *Proc. IEEE INFOCOM '99 (Cat. No.99CH36320)*, vol. 1, 1999, pp. 126–134 vol.1.

[254] J. Ji, K. Zhu, D. Niyato, and R. Wang, "Joint Cache Placement, Flight Trajectory, and Transmission Power Optimization for Multi-UAV Assisted Wireless Networks," *IEEE Trans. Wireless Commun.*, vol. 19, no. 8, pp. 5389–5403, 2020.

[255] N. Zhao, F. Cheng, F. R. Yu, J. Tang, Y. Chen, G. Gui, and H. Sari, "Caching UAV Assisted Secure Transmission in Hyper-Dense Networks Based on Interference Alignment," *IEEE Trans. Commun.*, vol. 66, no. 5, pp. 2281–2294, 2018.

[256] S. Gu, Y. Wang, N. Wang, and W. Wu, "Intelligent Optimization of Availability and Communication Cost in Satellite-UAV Mobile Edge Caching System with Fault-Tolerant Codes," *IEEE Trans. Cogn. Commun. Netw.*, pp. 1–1, 2020.

[257] J. Ji, K. Zhu, D. Niyato, and R. Wang, "Joint Trajectory Design and Resource Allocation for Secure Transmission in Cache-Enabled UAV-Relaying Networks With D2D Communications," *IEEE Internet of Things J.*, vol. 8, no. 3, pp. 1557–1571, 2021.

[258] T. X. Vu, S. Chatzinotas, B. Ottersten, and A. V. Trinh, "Full-duplex enabled mobile edge caching: From distributed to cooperative caching," *IEEE Trans. Wireless Commun.*, vol. 19, no. 2, pp. 1141–1153, 2020.

[259] Yuanyuan Jiang, S. J. Foti, A. Sambell, and D. Smith, "A low profile radiating element with nearly hemispheric coverage for satellite communications on-the-move hybrid array antenna," in *Proc. 2010 7th Inter. Symp. Commun. Sys., Net. Digital Signal Process. (CSNDSP 2010)*, 2010, pp. 123–127.

[260] R. Essaadali and A. Kouki, "A new simple unmanned aerial vehicle doppler effect rf reducing technique," in *Proc. MILCOM 2016*, 2016, pp. 1179–1183.

[261] U. Naeem, Z. Jawaid, and S. Sadruddin, "Doppler shift compensation techniques for leo satellite on-board receivers," in *Proc. 2012 9th Inter. Bhurban Conf. Applied Sciences Technology (IBCAST)*, 2012, pp. 391–393.

[262] A. S. Academy, "LOW EARTH CIRCULAR ORBITS," *http://www.spaceacademy.net.au/watch/track/leopars.htm*, 2020.

[263] I. S. Gradshteyn and I. M. Ryzhik, *Table of integrals, series, and products*. Academic press, 2014.

[264] T. Wang and L. Vandendorpe, "Successive convex approximation based methods for dynamic spectrum management," in *2012 IEEE Inter. Conf. Commun. (ICC)*, 2012, pp. 4061–4065.

[265] B. Ashok, B. S. Mysore, S. Chatzinotas, and B. Ottersten, "A joint solution for scheduling and precoding in multiuser MISO downlink channels," *IEEE Trans. Wireless Commun.*, vol. 19, no. 1, pp. 475–490, Jan. 2019.

[266] W. Murray and K.-M. Ng, "An Algorithm for Nonlinear Optimization Problems with Binary Variables," *Comput. Optim. Appl.*, vol. 47, no. 2, pp. 257–288, 2010.

[267] B. Kalantari and J. B. Rosen, "Penalty for Zero-One Integer Equivalent Problem," *Math. Program.*, vol. 24, no. 1, pp. 229–232, 1982.

[268] J.-C. Liou and N. L. Johnson, "Instability of the present LEO satellite populations," *Adv. Space Res.*, vol. 41, no. 7, pp. 1046–1053, 2008.

[269] S. Boyd, "Advances in Convex Optimization: Interior-point Methods, Cone Programming, and Applications," 2002.